

Alma Mater Studiorum- Università di Bologna

---

DOTTORATO DI RICERCA  
IN BIOINGEGNERIA

Ciclo XXVIII

SETTORE CONCORSUALE DI AFFERENZA: 09/G2- BIOINGEGNERIA

SETTORE SCIENTIFICO DISCIPLINARE: BIOINGEGNERIA INDUSTRIALE ING-IND/34

TITOLO TESI

IN VITRO MECHANICAL CHARACTERIZATION  
OF THE HUMAN NATURAL AND TREATED  
VERTEBRAE

Presentata da: Ing. Valentina Danesi

Coordinatore Dottorato:  
Prof. Elisa Magosso

Relatore:  
Prof. Luca Cristofolini

Co-Relatore:  
Gianluca Tozzi

---

Esame finale anno 2016

*A Pietro,*

## **Acknowledgement**

I would like to thank my supervisor Prof. Luca Cristofolini for the opportunity and guidance throughout this PhD and even before. Thanks are extended to Dr Gianluca Tozzi, who gave me the opportunity to use powerful tools for my research.

I am grateful to all the friends and colleagues within the Laboratory of Biomechanics, in particular Eng. Marco Palanca and Eng. Kavin Morellato for the helpful discussions and constructive criticism.

I am grateful to Serena, because mentioning her favourite television series “ you are my person”.

Finally, I am grateful to my family for their unconditional support and understanding, I want to dedicate this work to them. My immense gratitude goes to my mother who took care of my son when I was far from him. The greatest acknowledgement for anything goes to Cecca, thank you for loving me.

# Content

<b>Content</b> .....	2
<b>Sommario</b> .....	6
<b>Summary</b> .....	8
<b>Chapter 1: Introduction</b> .....	10
1.1 Bone.....	10
1.1.1 Bone: The human skeleton.....	10
1.1.2 Bone composition.....	11
1.1.3 Bone tissue architecture.....	12
1.1.4 Cortical bone.....	13
1.1.5 Trabecular bone.....	14
1.2 Spinal anatomy and biomechanics.....	16
1.2.1 Vertebral anatomy and biomechanics.....	18
1.2.2 The intervertebral disc.....	22
1.2.3 The facet joints.....	23
1.2.4 Spinal ligaments and musculature.....	24
1.2.5 Spinal loads.....	25
1.3 Osteoporosis.....	27
1.4 Vertebral fracture.....	28
1.4.1 Vertebral compression fracture.....	28
1.5 Vertebroplasty.....	30
1.5.1 The biomechanics of vertebroplasty.....	31
1.6 Biomechanical investigation of spine.....	34
1.6.1 In vitro testing of spine.....	34

1.6.2	In situ testing.....	39
1.6.3	Strain distribution measurement.....	39
1.7	Study aim.....	41
1.8	References.....	42

**Chapter 2: Reproducible reference frame for in vitro testing of the human vertebrae.....54**

2.1	Abstract.....	55
2.2	Introduction.....	56
2.3	Materials and methods.....	58
2.3.1	Definitions.....	58
2.3.2	Guidelines for implementing an anatomical reference frame.....	59
2.3.3	Testing the intra-operator and inter-operator repeatability in vitro.....	61
2.3.4	Testing the repeatability in vitro.....	61
2.3.5	Statistics.....	62
2.4	Results.....	63
2.5	Discussion.....	65
2.6	References.....	69

**Chapter 3: Effect of the in vitro boundary conditions on the surface strain experienced by the vertebral body in the elastic regime.....72**

3.1	Abstract.....	73
3.2	Introduction.....	74
3.3	Materials and methods.....	75
3.3.1	Overview.....	75
3.3.2	Bone specimen.....	78
3.3.3	Strain measurements.....	78
3.3.4	Loading conditions.....	79
3.3.5	Measured quantities and statistics.....	80

3.4 Results.....	82
3.5 Discussion.....	86
3.6 Supplementary materials.....	89
3.7 References.....	93

**Chapter 4: Elastic full-field strain analysis and microdamage progression in the vertebral body from digital volume correlation .....97**

4.1 Abstract.....	98
4.2 Introduction.....	99
4.3 Materials and methods.....	101
4.3.1 Materials and experimental procedures.....	101
4.3.2 Digital Volume Correlation (DVC).....	103
4.4 Results.....	104
4.5 Discussion.....	109
4.5 Conclusion.....	111
4.6 References.....	112

**Chapter 5: Application of Digital Volume Correlation (DVC) to investigate the strain distribution in the augmented vertebrae.....115**

5.1 Abstract.....	116
5.2 Introduction.....	117
5.3 Materials and methods.....	119
5.3.1 Specimens and prophylactic augmentation.....	119
5.3.3 Compression testing and Micro-CT scanning.....	120
5.3.3 Digital volume correlation (DVC).....	121
5.5 Results.....	124
5.6 Discussion.....	133
5.7 Supplementary Materials.....	135
5.8 References.....	137

<b>Conclusion</b> .....	143
<b>Appendix A: Strain distribution in the lumbar vertebrae under different loading conditions</b> .....	148
<b>Appendix B: Biomechanical effectiveness of prophylactic augmentation: an in vitro study</b> .....	178
<b>Appendix C: Strain uncertainties from two Digital Volume Correlation approach in natural and augmented vertebrae</b> .....	209

# Sommario

La presente tesi descrive i risultati delle ricerche svolte durante il mio Dottorato in Bioingegneria. L'obiettivo della ricerca era quello di investigare le proprietà biomeccaniche *in vitro* del corpo vertebrale di vertebre toraco-lombari naturali e trattate, sottoposte a vertebroplastica in via profilattica. La tesi fornisce un'analisi completa sulla distribuzione delle sollecitazioni e sulla meccanica del processo di frattura sia delle vertebre naturali che di quelle aumentate ottenendo indicazioni sulle prestazioni del trattamento stesso. La ricerca è stata effettuata principalmente presso il Laboratorio di Biomeccanica del Dipartimento di Ingegneria Industriale dell'Università di Bologna e in parte presso il Laboratorio di Tecnologia Medica (LTM) dell'Istituto Ortopedico Rizzoli (Bologna).

La vertebra è il principale argomento di tutti gli studi presentati in questa tesi. I risultati che verranno riportati riguardano solo gli aspetti della vertebra studiati a livello di organo. Il rachide e le vertebre sono state ampiamente investigate in passato, tuttavia vista la complessità biomeccanica di tali strutture possiamo dire che lo studio del rachide e delle vertebre rappresenta una sfida ancora aperta all'interno della Comunità Scientifica. Le fratture vertebrali da compressione sono il tipo più comune di frattura correlata all'osteoporosi, ogni anno all'incirca 1,4 milioni di nuove fratture si verificano in tutto il mondo. Queste fratture sono associate a dolore, diminuzione della qualità della vita ed a elevati costi sanitari. L'approccio più promettente per ridurre le conseguenze dell'osteoporosi, è quello di diagnosticare la perdita di massa ossea precocemente ed iniziare strategie di trattamento prima che si verifichi la frattura. Negli ultimi anni la vertebroplastica in via profilattica è stata proposta come alternativa ai trattamenti farmacologici per ridurre il rischio di frattura nelle vertebre gravemente osteoporotiche o nelle vertebre adiacenti a quelle che hanno subito la vertebroplastica per limitare il rischio di ulteriori collassi. Questo trattamento ha lo scopo di aumentare la resistenza e il supporto strutturale delle vertebre patologicamente indebolite, mediante iniezione di un cemento acrilico all'interno del corpo vertebrale. I rischi associati (fuoriuscita di cemento e conseguente danno neuronale; necrosi dei tessuti a causa del monomero residuo e della reazione esotermica; aumento del rischio di fratture nelle vertebre adiacenti) hanno sollevato domande circa l'efficacia e la sicurezza della vertebroplastica in generale. Inoltre, è ancora oggetto di dibattito se la vertebroplastica in realtà rafforzi la vertebra trattata. E' necessario quindi comprendere meglio i costi e i benefici di questo trattamento. Alla luce di questo dibattito, conoscere in modo approfondito il comportamento biomeccanico e i meccanismi di frattura delle

vertebra aumentata in via profilattica è di fondamentale importanza per migliorare la diagnosi e il trattamento. L'obiettivo principale di questo lavoro è stato quello di investigare il comportamento biomeccanico in termini di resistenza meccanica e di distribuzione delle sollecitazioni delle vertebre umane naturali e trattate in campo elastico ed effettuare un'analisi completa sulla meccanica del processo di frattura delle vertebre trattate per ottenere indicazioni sull'efficienza del trattamento.

Per superare alcune limitazioni degli attuali studi *in vitro* sono state sviluppate e/o migliorate alcune metodologie in grado di garantire un'elevata ripetibilità e riproducibilità degli esperimenti.

E' stato definito e validato per la prima volta un sistema di riferimento anatomico *in vitro* per vertebre. L'adozione di tale riferimento anatomico ha permesso un'allineamento del provino maggiormente accurato durante i test in campo elastico e a rottura.

E' stato effettuato uno studio simulando le condizioni al contorno più comunemente impiegate in letteratura nei test *in vitro*, per chiarire come variano le proprietà del corpo vertebrale in termini di distribuzione delle sollecitazioni quando la vertebra viene testata come singola o nella configurazione di tripletta.

Queste metodologie sperimentali sono state impiegate nei successivi test *in vitro* per la caratterizzazione biomeccanica delle vertebre umane naturali e trattate. Lo studio sulla distribuzione delle sollecitazioni delle vertebre è stato condotto attraverso un'approccio integrato, che incorpora differenti tecniche di misura, dalle tecniche tradizionali come quella estensimetrica a tecniche più recenti come la Digital Volume Correlation (DVC). Attraverso la tecnica estensimetrica sono state ottenute informazioni sulle sollecitazioni molto precise e puntuali ma esclusivamente a livello dell'osso corticale, mentre la tecnica della DVC ha permesso di investigare la distribuzione delle sollecitazioni all'interno del corpo vertebrale a livello dell'osso trabecolare. In conclusione questa tesi rappresenta un'approfondita analisi sulle proprietà biomeccaniche di vertebre umane naturali e aumentate allo scopo di fornire un'analisi biomeccanica completa sulla distribuzione delle componenti di sollecitazione (sia a livello corticale che trabecolare), sulla meccanica della frattura e sull'efficienza del trattamento della vertebroplastica in via profilattica.

# Summary

The present thesis illustrates the research carried out during PhD studies in Bioengineering. The research objective was to investigate the *in vitro* biomechanical properties of human thoracolumbar natural and treated vertebral body, underwent to prophylactic vertebroplasty, to provide a comprehensive analysis on the stress/strain distribution and the failure mechanics of natural and augmented vertebrae and to obtain indications on the performance of the treatment itself. The research was carried out mainly at the Biomechanics Laboratory of the Department of Industrial Engineering at the University of Bologna and partially at the Laboratory of Medical Technology (LTM) Rizzoli Orthopaedic Institute (Bologna).

Vertebra is the main topic of the studies reported in this thesis. The results are related to vertebra as organ level. Spine and vertebrae have been widely investigated in the past, however, given the complexity of such structures a deep understanding of biomechanical properties is necessary to improve treatments and reduce the negative outcome of spine pathologies. Therefore, investigation of the spine and vertebrae is still an open challenge within the scientific community. Vertebral compression fractures are the most common fracture type related to osteoporosis, with an estimated 1.4 million new fractures occurred worldwide every year. These fractures are associated with pain, decreased quality of life and large health care costs. The most promising approach to reduce the consequences of osteoporosis, is to diagnose the bone loss early and begin treatment strategies before fractures occur. In the last years prophylactic augmentation has been proposed as an alternative to pharmacological treatments in order to reduce the fracture risk of osteoporotic vertebrae or to prevent adjacent fractures after augmentation. This treatment is meant to increase the strength and the structural support of weak vertebrae, by injection of an augmentation material into the vertebral body. The associated risks (cement leakage and subsequent neural damage; tissue necrosis due to residual monomer and to the exothermal reaction; increased risk of fracture in the adjacent vertebrae) have raised questions about the efficacy and safety of the vertebroplasty in general. Furthermore, it is still debated whether prophylactic augmentation actually strengthens the treated vertebra. Therefore, there is a need for a clearer understanding on the cost-benefit trade-off. In the light of this debate, in-depth knowledge of the mechanical behaviour and failure of prophylactic-augmented vertebra is of fundamental importance to understand vertebral biomechanics and improve diagnosis and prophylactic treatments.

The main objective of this work was to investigate the biomechanical behavior of the natural and augmented human vertebrae in terms of mechanical properties and strain distribution in the elastic regime up to failure to obtain indications about the efficacy of the treatment.

To overcome some limitations of the current *in vitro* test, some methodological studies were developed to improve and make more accurate *in vitro* biomechanical test on vertebrae.

To obtain a greater reproducibility and repeatability of test, an *in vitro* anatomical reference frame for human vertebrae was defined and validated for the first time.

An investigation was developed to examine the effect of different experimental boundary conditions (with and without discs) in the human vertebra and to elucidate if testing a single-vertebra specimen (which provides a number of practical advantages) is an acceptable alternative to a three-adjacent-vertebrae-segment (which can be assumed closer to physiological), when measuring the principal strains (magnitude and direction) on the surface of the vertebral body, in the elastic regime.

The experimental methods developed were implemented during *in vitro* destructive e non-destructive test to investigate the biomechanical behaviour of human natural and augmented vertebrae. Studies about the vertebral strain distribution were based on an integrated approach, which combined different measurement methods (strain gauges and digital volume correlation) for a more comprehensive investigation. Through the strain gauge technique, very precise and punctual strain information was collected but only at the cortical bone level, while the technique of DVC allowed to capture the internal full-field strain distribution and quantify internal microdamage initiation/evolution under loading.

In conclusion this thesis is a comprehensive investigation of the biomechanical properties of natural and treated human in terms of strain distribution (both in the cortex and trabecular bone), and failure mechanics to obtain indication of the efficacy of prophylactic vertebroplasty.

# Chapter 1:

## Introduction

The mechanical behavior of vertebral bodies, their failure and their response to treatments rely on the complex relations that exist between the mechanics of bone tissue and its structure. The following section describes the bone tissue constituents and its structural micro organization and macro anatomy. An additional section describes the main constituent and the biomechanics of the human spine, with a focus on the vertebral body, the occurrence of vertebral compression fractures, and an emerging but still controversial treatment called vertebroplasty. Moreover an additional section is a review of *in vitro* and *in situ* studies that have been developed to investigate the structural behavior of human health and treated vertebral. It is then completed with an overview of the traditional experimental techniques used to investigate strain distribution, such as strain gauges and of a recent approach Digital Volume Correlation for the measurement of 3D deformation fields throughout entire volumes. The last one section describes the study aim and the related objectives.

### 1.1 Bone

#### 1.1.1 Biomechanical of the human skeleton

The skeletal system (Fig.1-1) includes individual bones and the soft tissues that connect them [1, 2]. The main component of the skeleton is bone and differs from the connective tissues (i.e. cartilage, ligaments and tendons) in rigidity and hardness. Bones are important both biomechanically and metabolically. In fact, the skeletal tissue performs three main functions: support, protection and homeostasis of calcium. The skeleton ensures that the shape of the body is maintained, it transmits muscular forces to create a movement, it protects the soft tissues of the cranial, thoracic and pelvic cavities, and it supplies the framework for the bone marrow. Furthermore, the mineral content of bone serves as a reservoir for ions, particularly calcium, and also contributes to the regulation of extracellular fluid composition. Bone is a self-repairing material, able to adapt its mass, shape and properties to the mechanical requirements during life.

## 1.1.2 Bone compositions

Bone matrix is composed of approximately 28% by weight of organic matter, from 60% of inorganic substance and the remaining 12% of water (38.4% in volume organic matter, 37.7% mineral and 23.9% water [3].

The mineral is largely impure hydroxyapatite  $\text{Ca}_6(\text{PO}_4)_6(\text{OH})_2$ , containing carbonate, citrate fluoride and strontium. The organic matrix consists of 90% collagen and about 10% noncollagenous proteins. From a mechanical point of view, the bone matrix is comparable to a composite material: the organic matrix is responsible to give toughness to the bone, while the inorganic one has the function to stiffen and strengthen the bone [1].

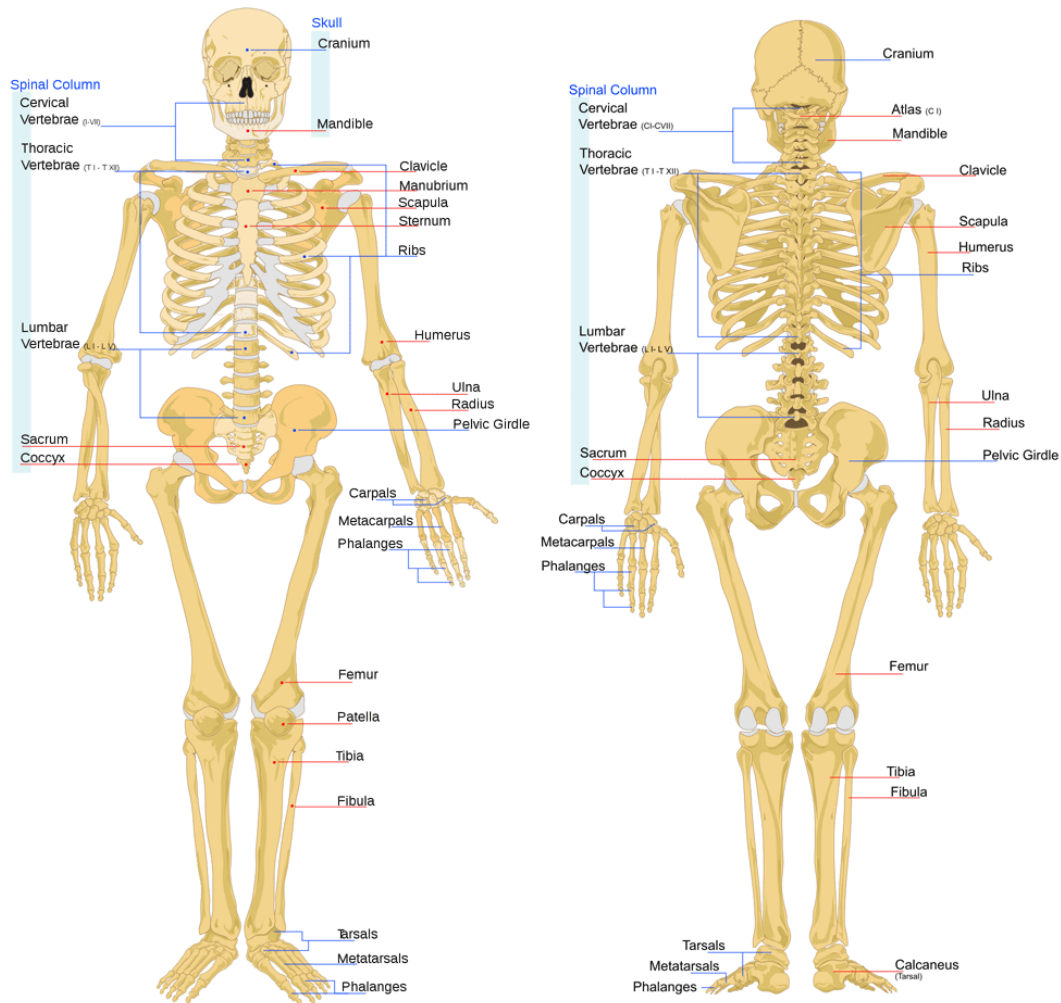


*Fig.1-1: Anterior and posterior view of a human adult male skeleton. Source from <http://www.innerbody.com>.*

### 1.1.3 Bone tissue architectures

Adult bones are composed of two basic structures [1], i.e. cortical (or compact) and trabecular (or cancellous or spongy) bone (Fig. 1-2). Cortical bone is a solid and compact material, with the exception of microscopic channels. Approximately 80% of the skeletal mass in the adult skeleton is cortical bone. It forms the outer wall of all bones, being largely responsible for the supportive and protective function of the skeleton. The remaining 20% of the bone mass is trabecular bone, a lattice of plates and rods having typical mean thicknesses ranging from 50  $\mu\text{m}$  to 300  $\mu\text{m}$  known as trabeculae, found in the inner parts of the skeleton. The trabecular bone is compliant and less strong than cortical bone, because of its discontinuous structure. Consequently it gives a smaller contribute to the rigidity of the bone. Moreover, it shows a greater variability in mechanical behaviour than cortical bone, due to its greater structural irregularity. However, it plays several important roles:

- 1 stiffens the structure by connecting the outer shell of cortical bone;
- 2 supports the cortex layer and distributes loads;
- 3 protects the hollows of bone from phenomena of instability (buckling).

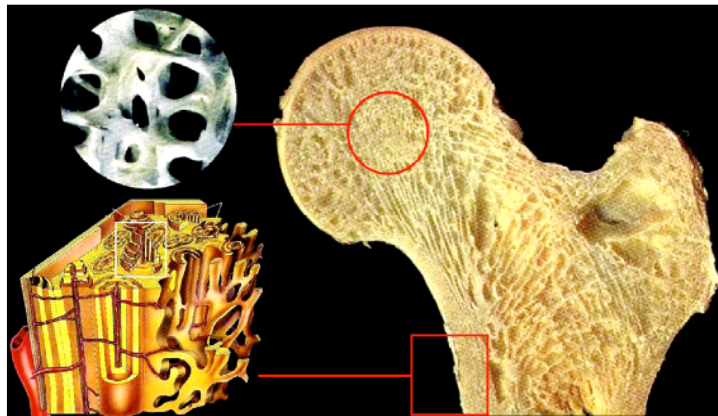


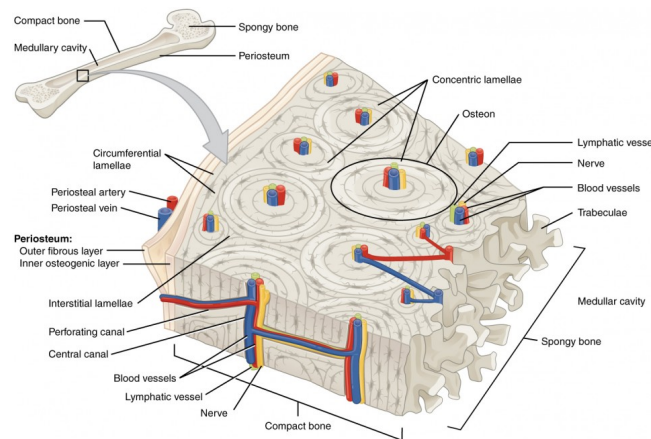
*Fig.1-2: Scheme showing cortical and trabecular bone. Source from [www.orthobullets.com](http://www.orthobullets.com).*

The diaphysis is composed mainly of cortical bone. Conversely, the epiphysis and metaphysis contain mostly trabecular bone, with a thin outer shell of cortical bone. During growing, the epiphysis is separated from the metaphysis by a plate of hyaline cartilage, known as the epiphyseal plate or growth plate. The growth plate and the adjacent trabecular bone of the metaphysis constitute a region where trabecular bone production and elongation of the cortex

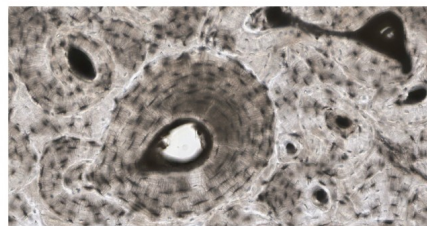
occurs. In the adult, the cartilaginous growth plate is replaced by trabecular bone, which causes the epiphysis to become fused to the metaphysis.

### 1.1.4 Cortical bone

Adult cortical bone is composed of 3- to 7- $\mu\text{m}$ -thick unit layers (called lamellae) which contain collagen fibers that run parallel to each other [1]. The main structural unit of cortical bone is given by the osteon or Haversian system (Fig. 1-3). A typical osteon is a cylinder about 200  $\mu\text{m}$  in diameter, consisting of a central canal (Haversian canal) surrounded by about 20-30 concentric lamellae. The external surface of every bone is surrounded by several layers of lamellae, immediately underneath the periosteum and on the internal surface adjacent to the endosteum. These lamellae are called circumferential lamellae. In the gaps between Haversian systems can be found interstitial lamellae, as angular fragments of previous concentric and circumferential lamellae. Within the Haversian canals run blood and lymphatics vessels, and nerves.



(a)



(b)

*Fig. 1-3: Diagram of cortical bone: (a) Cross-sectional view of cortical bone shows the basic structural unit, the osteon. (b) Histological cross-section of cortical bone, showing osteon with its Haversian canals, lacunae and capillary canaliculi. In this micrograph of the osteon, you can clearly see the concentric lamellae and central canals. Source from <https://courses.candelalearning.com/ap2x1/chapter/bone-structure>.*

The Haversian canals are interconnected by transverse canals, also called the Volkmann canals, which also allow the communication with the periosteum and bone marrow. The outer border of each osteon is surrounded by a cement line, which is a 1- to 2- $\mu\text{m}$ -thick layer of mineralized matrix, deficient in collagen fibers. Throughout the bone, small cavities (lacunae) containing entrapped bone cells (osteocytes) are found. Microscopic tubular canals (canaliculi) connect the lacunae to each other and to the Haversian canal.

### 1.1.5 Trabecular bone

The trabecular bone has not Havers systems, but consists of an array of interconnected beams (trabecule), of a thickness less than 0.2 mm and variable in shape (Figure 1-4). Each trabecula is constituted by a packages of parallel lamellae. Usually a package of lamellae is up to 1 mm long and 50-60 microns in section.

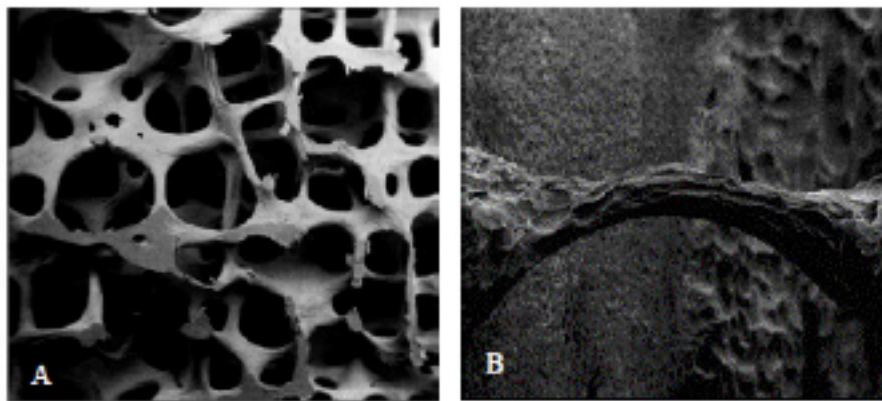


*Fig. 1-4: A: vertical section of trabecular bone from lumbar vertebra. B: single trabecula leaving from the endosteal surface. Source from [3].*

According to the site of analysis is possible to find trabecular bone with different characteristics. The quantity of trabecular bone can widely vary within different anatomical sites. This leads to great differences in bone density. Moreover the orientation of the trabecular structure is tightly bonded to the anatomical site and its mechanical role. In fact the correlation between the trabecular orientation and the load direction was already showed in literature [4]; trabecular structure result to be mainly oriented along the primary load direction. However load direction depends by the motion, therefore trabecular structure can became very complex.

The trabecular bone is compliant and less strong than cortical bone, generally because of its discontinuous structure. Consequently it gives a smaller contribute to the rigidity of the bone.

Most mechanical properties of trabecular bone depend to a large degree on the apparent density, which is defined as the mass of bone tissue present in a unit volume of bone [5]. Volume fraction typically ranges from 0.6 for dense trabecular bone to 0.05 for porous trabecular bone [6, 7]. The (wet) tissue density for human trabecular bone is fairly constant and is in the approximate range 1.6-2.0 g/cm<sup>3</sup> [8] By contrast, the (wet) apparent density varies substantially and is typically in the range 0.05-1.0 g/cm<sup>3</sup> [8].

The cancellous bone tissue mechanical behaviour can be qualitatively represented as in Figure 1-5.

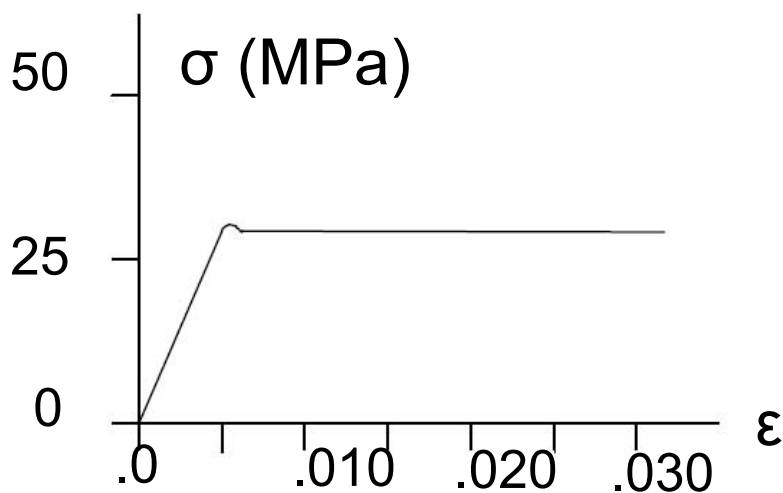


*Fig.1-5: Compression stress-strain curve for trabecular bone.*

The compressive stress-strain curves of cancellous bone show an initial linear elastic region up to a strain of about 0.05. The material yielding occurs as the trabeculae begin to fracture. A plateau region of almost constant stress follows this initial elastic region until fracture, exhibiting a ductile material behaviour. After yielding, it can sustain large deformations (up to 50% strain) while still maintaining its load-carrying capacity. Thus, trabecular bone can absorb substantial energy before mechanical failure. By contrast, cancellous bone fractures abruptly under tensile forces, showing a brittle material behaviour. The energy absorption capacity is considerably higher under compressive loads than under tensile loads.

Being a heterogeneous open cell porous solid, trabecular bone has anisotropic mechanical properties that depend on the porosity of the specimen as well as the architectural arrangement of the individual trabeculae. In order to specify its mechanical properties, one must therefore specify factors such as the anatomical site, loading direction with respect to the principal orientation of the trabeculae, age and health of the donor. Young's module can vary 100-fold within a single epiphysis [9] and can vary on average by factor of three depending on loading direction [9, 10]. Pathologies such as osteoporosis, osteoarthritis and bone cancer are known to affect mechanical properties [11, 12]. Typically the modulus of human trabecular bone is in the range 0.010-2 GPa depending on the above factors. Strength, which is linearly and strongly correlated with modulus [9], is typically in the range 0.1-30 MPa [8].

## **1.2 Spinal anatomy and biomechanics**

The human spine is an articulated multi-segment structure responsible for bearing the loads acting on the upper body as well as allowing its physiological range of motion (ROM) (Fig.1-6). In addition, the physical protection of the spinal cord depends on the integrity of the whole structure [13]. The spine is composed of 24 articulated vertebrae: seven cervical, twelve thoracic and five lumbar, therefore dividing the spine into three main regions. There are four main curvatures on the sagittal plane of the spine: the cervical, thoracic, lumbar and sacral curve. The thoracic region presents a kyphosis that ranges from 18° to 51° whilst the lumbar region lordosis ranges from 42° to 74° [14]. The first cervical vertebra (also called the atlas) is jointed with the skull, whilst the last lumbar vertebra (L5) is jointed with the sacrum. The sacrum is fused with the coccyx and is located posteriorly within the pelvis. This is the most caudal region of the spine and made of nine fused vertebrae. Each vertebra is articulated with its adjacent one through an intervertebral disc and a pair of facet joints. In addition, thoracic vertebrae present an additional joint, the costovertebral joint, where the ribs articulate. The additional stiffness provided by the rib cage increases strength and energy-absorbing capability in traumatic events [15]. Several muscle groups and ligaments run along the spine, exerting a complex set of forces and moments to achieve motion as well as cooperate with the other spinal structure to provide stability. Spinal stability is indeed a fundamental concept in spinal biomechanics which White et al. defines as “the ability of the spine under physiological loads to limit patterns of displacement in order not to damage or irritate the spinal cord and nerve roots and to prevent incapacitating deformity or pain caused by structural changes” [15].

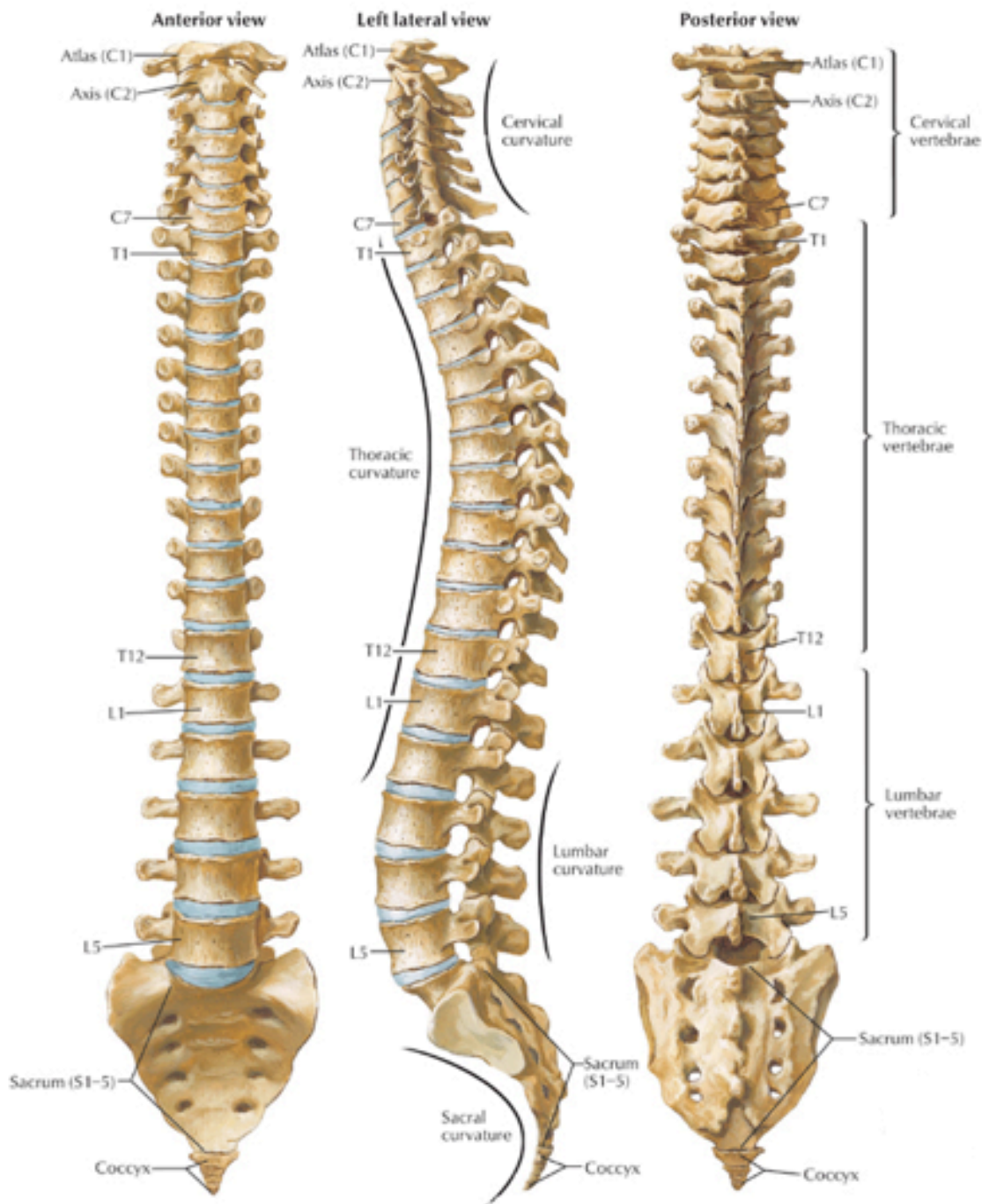
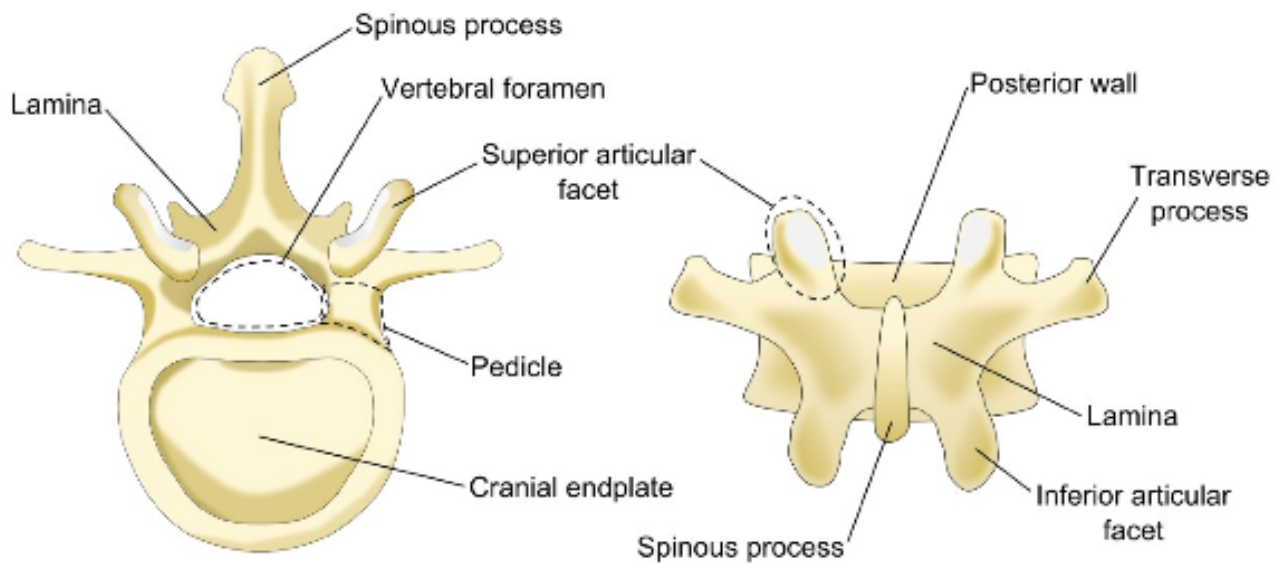


Fig. 1-6: Anterior, lateral and posterior view of spine. Source from

<http://www.backpain-guide.com>

## 1.2.1 Vertebral anatomy and biomechanics

The vertebra is a bone consisting of two main anatomical regions: vertebral body and neural arch. The neural arch originates at the end of the pedicles, which protrude from the posterior-lateral surface of the upper part of the vertebral body. The hollow region confined within the posterior wall of the vertebral body, the pedicles and the neural arch is the vertebral foramen, which encloses the spinal cord [15]. The posterior processes (transverse and spinous) are bony structures emerging from the neural arch and are site of insertion of numerous muscle and ligaments (Fig. 1-7).



*Fig.1-7: General anatomy of the vertebral body.*

The vertebral body can be roughly approximated to an elliptical cylinder, principally composed by trabecular bone, surrounded by a shell of cortical bone. The strength of the vertebral body has been typically associated with its bone mineral density (BMD) and overall geometry [13, 16]. However, these two factors alone have been shown not to be enough to fully describe the mechanical properties of the vertebra. The resultant structural behaviour is in fact the result of a complex interaction between the quality of the tissue and the architecture in which the bone is organized [17, 18]. It has been shown that the combination of BMD, micro-architecture and its heterogeneity can explain up to 86 % of variability in vertebral failure load whilst BMD alone can explain only up to 44 % [19]. The trabecular bone core is a network of rod and plate shaped struts [20, 21] which has been estimated to bear 76 to 89 % of the total load [22]. The thickness (Tb.Th)

and spacing (Tb.Sp) of the trabecular network have been measured by several authors using micro computed tomography (micro CT) and some indicative dimensions are reported below in Table 1-1. It is possible to note how measurements of micro-architecture vary among studies due to age and bone quality [20]

*Table 1-1: Trabecular thickness (Tb.Th) and spacing (Tb.Sp) for the vertebral body (mean±standard deviation).*

	Wegrzn et al., 2011 [19]	Roux et al., 2010 [23]	Fields et al., [18]	Lochmüller et al., 2008 [24]	Hulme et al., 2007 [25]
Tb.Th	0.31mm ± 0.04	0.24 mm ±0.44	0.16 mm ±0.02	0.15 mm ±0.02	0.22 mm ±0.02
Tb.Sp	1.34 mm ±0.33	–	0.98 mm ±0.11	0.96 mm ±0.18	1.11mm ±0.11

The trabeculae within the vertebral body are organized according to load paths [4] and micro-scale finite element (FE) modelling suggests that the majority of the load is transmitted through parallel columns of vertically oriented trabeculae [26]. Furthermore, the trabecular structure extends from the vertebral body into the posterior elements through the pedicles following typical pathways, both on the sagittal and transverse plane (Fig.1-8), to counteract the forces and deformations to which the posterior processes undergo [27]. The geometry of the pedicles also varies significantly along the cranio-caudal direction, with a peculiar transition at the thoracolumbar junction. The thoracolumbar junction is an anatomical region spanning T11 to L1, where the thoracic spine joints the lumbar spine. The average cross sectional area (CSA) of the pedicle ranges from ~32 to ~65 mm<sup>2</sup> in the thoracic vertebra and from ~83 to ~160 mm<sup>2</sup> in the lumbar [28, 29]. In addition, the micro-structural properties of trabecular bone within the pedicle are different to those of the vertebral body. Trabeculae within the pedicles are more numerous, plate-like, and tend to be more densely packed, with a mean Tb.Th and Tb.Sp of  $0.20 \pm 0.04$  and  $0.93 \pm 0.12$ , respectively [30].

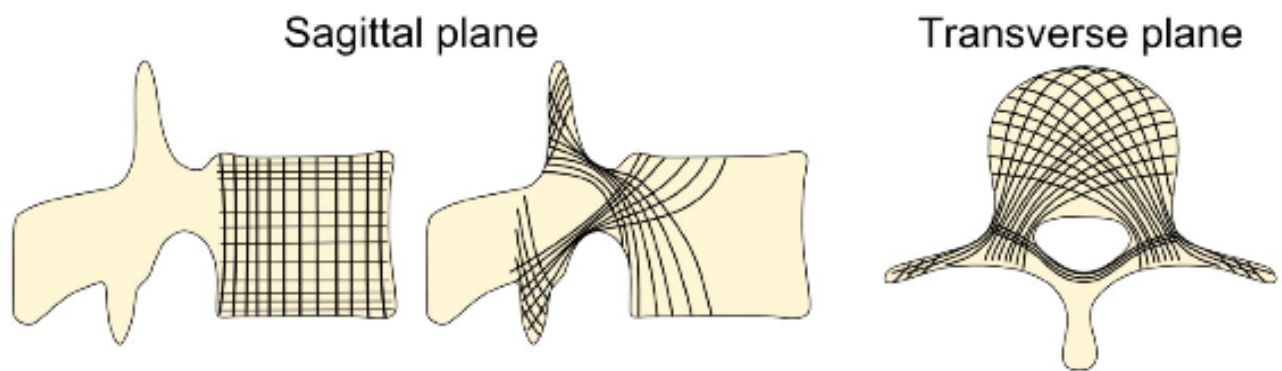


*Fig.1-8: Principal orientation of the trabeculae architecture in the vertebra. Adapted from [27].*

Although the overall anatomy of the vertebrae in the different regions remains the same, the actual bony features adapt to the functional changes along the spine, with the vertebral body being optimized to bear axial loads [31]. In fact, the size and mass of the vertebra, as well as the endplate area, increase downwards to withstand the increase in compressive forces [32] (Fig.1-9). The shape of the vertebral foramen also significantly changes along the spine, becoming more elliptical in the lumbar spine. This is mostly related to an increase of the spinal canal width (SCW), which can also be considered equivalent the interpedicular space distance (Fig.1-10).

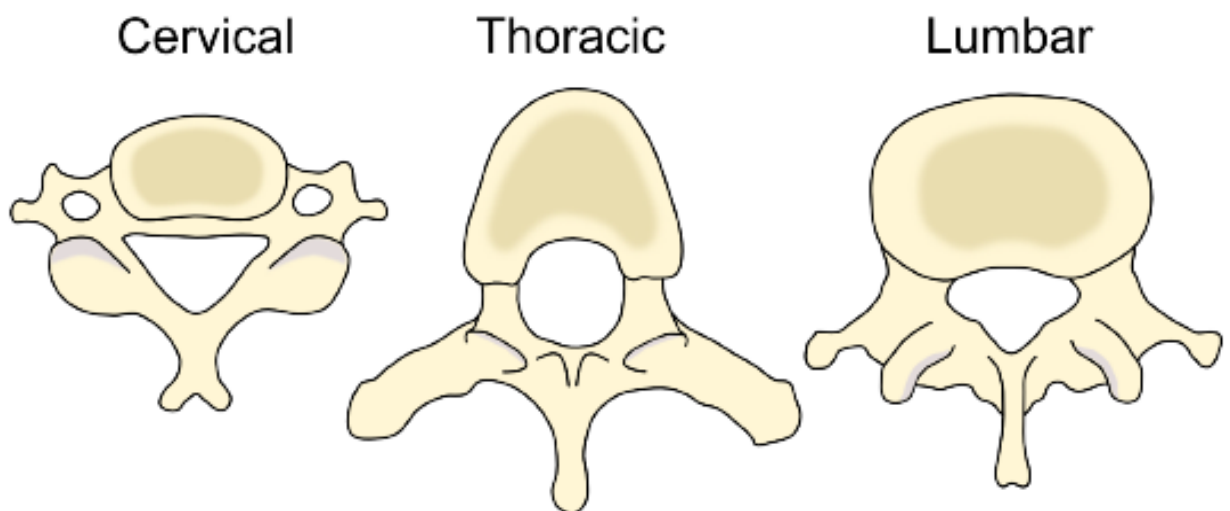


*Fig.1-9: Gross anatomical differences amongst cervical, thoracic and lumbar vertebrae.*

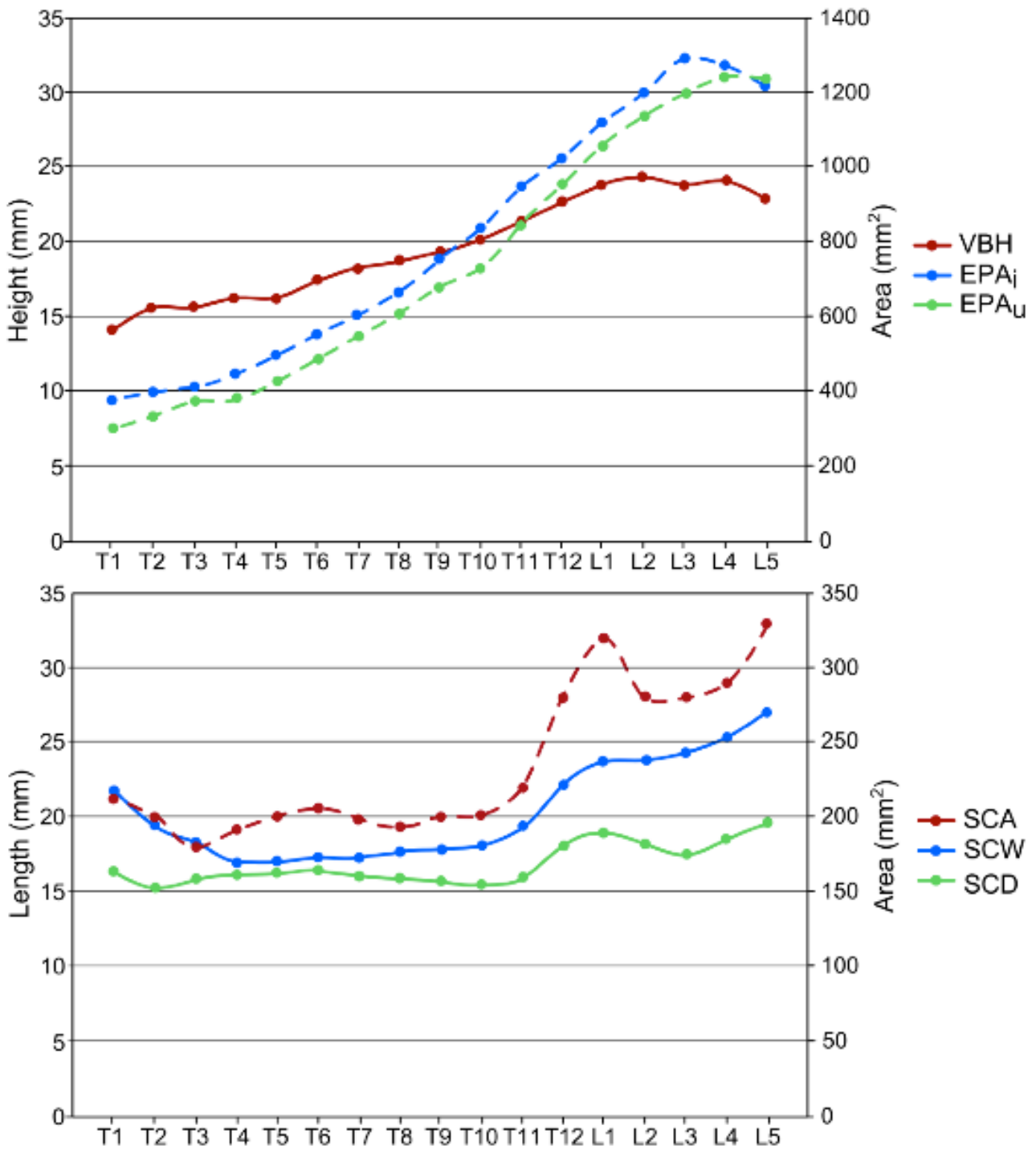
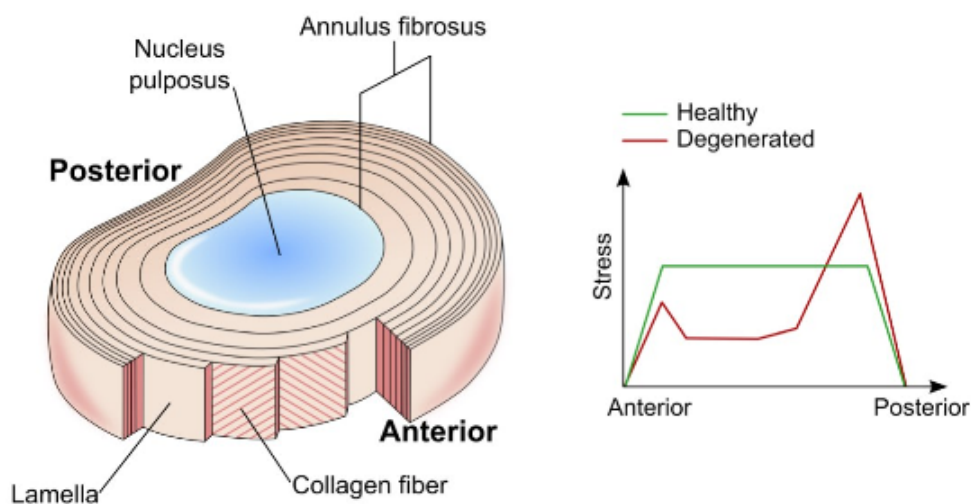


Fig.1-10: Anatomical variation of the vertebra across levels. VBH: vertebral body height; EPA endplate area (EPA<sub>i</sub> and EPA<sub>u</sub> stand for inferior and upper endplate, respectively); SCA: spinal canal area; SCW: spinal canal width; SCD: spinal canal depth. Data from [28, 29]

## 1.2.2 The intervertebral disc

Each vertebral body articulates with the adjacent one through an avascular soft tissue called intervertebral disc. The intervertebral disc is limited superiorly and inferiorly by the endplate (often considered as part of the intervertebral disc too [33]) and is divided in two main regions: the nucleus pulposus and the annulus fibrosus (Fig. 1-11). The nucleus pulposus is located centrally and composed of a loose network of fibres within a mucoprotein gel which has a water content ranging from 70-90 % [15]. An additional ~ 0.8 mm thick layer of hyaline cartilage separates the bony endplate and the nucleus. Such layer is called cartilaginous endplate and is responsible for the exchange of nutrients from the blood vessels within the vertebra to the nucleus [33]. The nucleus is confined radially within the annulus fibrosus which is organized in 15 to 25 concentric layers called lamellae. The main component of each lamella is collagen, arranged in thick fibers running parallel to each other and anchored to the endplate [34]. The fibers are oriented at about  $60^\circ$  to the vertical axis and they run in opposite direction to each adjacent lamella (i.e. there is a  $120^\circ$  angle between fibers in adjacent lamellae) [15]. When loaded, the nucleus generates a hydrostatic pressure towards the annulus and the endplates [35]. Such pressure makes the endplate deflect [36] whilst the annulus bulges, hence putting the collagen fibers in tension. In fact, a 500 N compressive load induces a 0.7 mm bulge which results in the fibers undergoing a 2.7 % strain [37].



*Fig.1-11: The intervertebral disc: anatomy and schematic stress profiles within the disc. Adapted from Adams et al. [38].*

### 1.2.3 The facet joints

The facet joints (or zygapophysial joints) are two synovial joints located between the neural arches of each pair of adjacent vertebrae. The facet is a bony process that originates laterally on the neural arch; each vertebra has two superior and inferior facets. A layer of hyaline cartilage (~1 mm thick) is present onto the mating surface of each facet to allow articular motion with minimum friction. The synovium and ligamentous capsule extend from the superior and inferior margin of the joint providing, respectively, lubrication for the cartilage and mechanical reaction against separation of the joint [39] (Fig. 1-12). The shape of the facet is what actually dictates the kinematics of the joint and therefore that of the functional spinal unit [15]. The facets of the thoracic spine have a flat geometry whilst in the lumbar spine they have significantly curved mating surfaces to constrain axial rotation [15]. In the thoracic region the articular surface has a typical inclination of approximately  $20^\circ$  with the transverse plane and  $60^\circ$  with the sagittal. Conversely, in the lumbar region, the facet surface becomes almost orthogonal to the transverse plane whilst their orientation increases in the caudal direction up to  $\sim 50^\circ$  (i.e. the facets splay) [15].

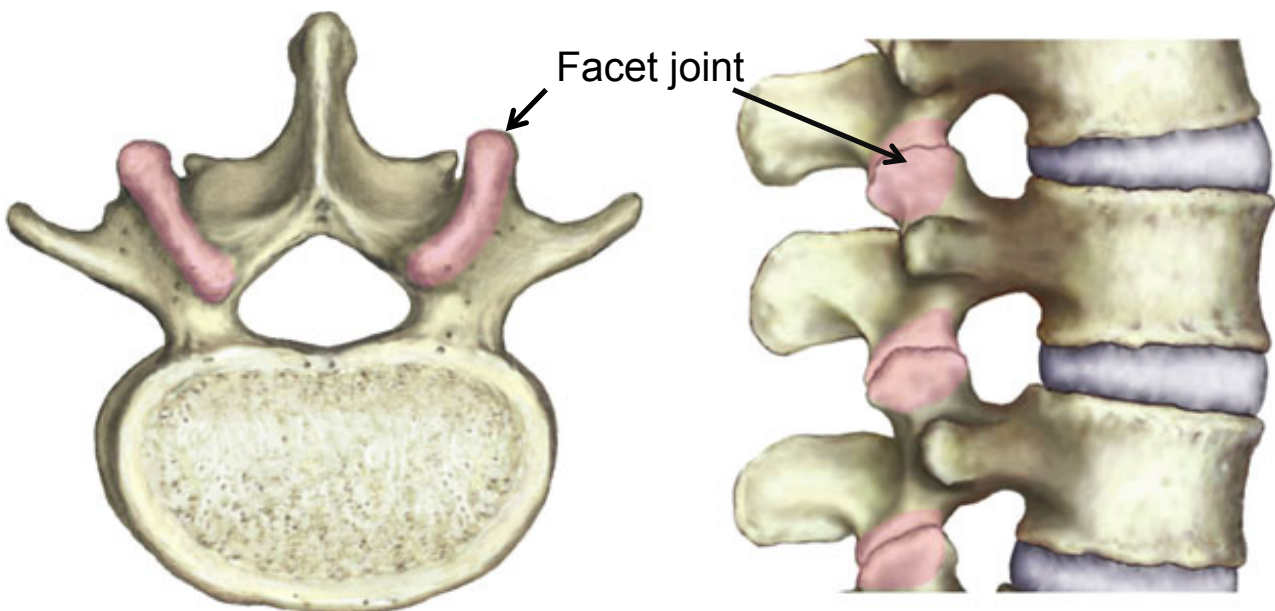
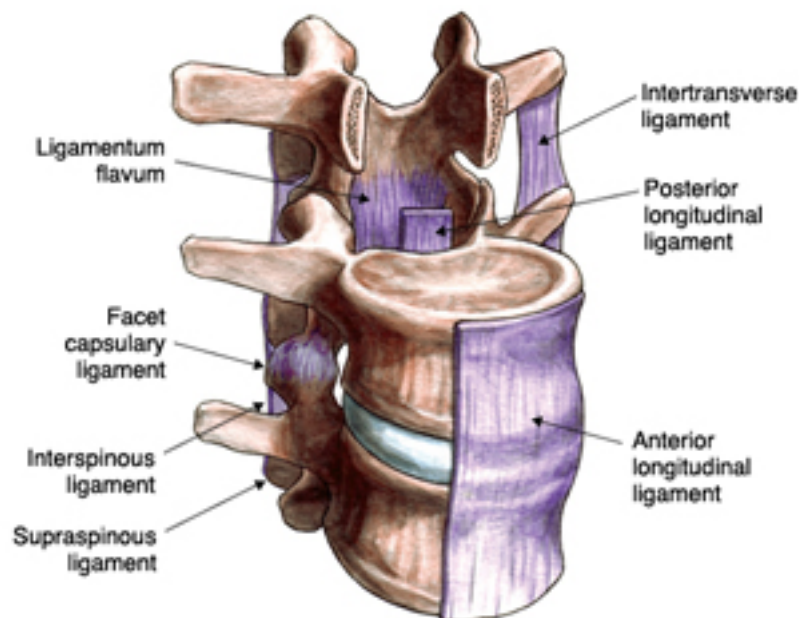


Fig.1-12: The facet joint. Source from <http://corewalking.com/spinal-movement-facet-joints/>

## 1.2.4 Spinal ligaments and musculature

The spine is surrounded by a complex ligamentous structure that runs in several layers along it (Figure 1-13). Ligaments are mainly made of collagen and elastin fibers arranged in fascicles to provide uniaxial resistance. Furthermore, ligaments can respond only to tensile forces as they buckle in compression. This behaviour is due to the fibrous nature of the tissue itself. At low strains the elastin takes on the majority of the load as the collagen fibers are still crimped. Although being highly linear, the stiffness of the elastin is significantly lower than that of collagen. As the strain increases the collagen fibers uncrimp providing the actual stiffness required to withstand significant loads. Mechanical testing reflects this behaviour. There is an initial tract with low stiffness (neutral zone, NZ), followed by a higher stiffness tract (elastic zone, EZ). NZ and EZ are the physiological working regions. Exceeding EZ injures the ligament (plastic zone) and may result in its failure [15]. Ligaments provide a passive component of stabilization by restricting motion of the vertebrae, therefore also protecting the spinal cord [40]. They have a fundamental role in traumatic events to provide quick reaction forces against deviation from the physiological posture [15]. There are two main longitudinal ligaments running down the whole spine which have insertions on the surface of the vertebral body and disc: the anterior longitudinal ligament (ALL) and the posterior longitudinal ligament (PLL). ALL provides stability mainly against extension as it covers the anterior aspects of the spine. Conversely, the PLL stabilizes mainly against flexion since it runs between the posterior wall and the spinal cord. The deposition of the fibers can originate from one vertebra and then span several levels whilst bulging of the disc contributes to their pre-tensioning [15]. This complex arrangement allows distributing the reaction force over several consecutive joints [41]. The posterior processes are connected via a set of multiple ligaments. The ligamentum flavum bridges the laminae of adjacent vertebrae and is located posteriorly to the spinal cord. This ligament is designed not to buckle (in physiological conditions) and recoil promptly in extension to avoid spinal cord impingement. Thus, the fibers of the ligamentum flavum are pre-tensioned also in the neutral position, whilst linearity of the response at low strains is given by the high content of elastin [15]. The interspinous ligament appears as a band connecting the superior ridge of the spinous process to the inferior of the adjacent one and is connected anteriorly to the ligamentum flavum. The fibers appear not to be organized as in other ligaments, thus the resistance provided in flexion is inferior [41]. The supraspinous ligament lies on the mid line of the most posterior aspect of the spinous process and bridges the interspinous spaces. The structure of the ligament is ambiguous as the deep layer is made up of tendinous fibres originating from the adjacent muscles [41]. The spinal

musculature is the only active component of the spine and their function is to contribute to stabilization and produce movements [15]. The aim of the muscles is to counteract the external loads through the modification of the shape of the spine [39]. From a functional point of view, the muscles can be generalized into four categories: superficial and deep flexors; superficial and deep extensors. Superficial muscles are usually longer, spanning several levels, and their activation controls gross movements. On the other hand, deep muscles are usually shorter and closer to the vertebral rotation axes and thus can act directly on the position of the vertebrae [40]. Preserving muscle integrity in surgery is paramount since dissection or excessive retraction of the tissue may lead to subsequent pain or disability [42].



*Fig.1-13: Ligaments of spine.*

### **1.2.5 Spinal loads**

Daily activities induce complex loading scenarios on the spine. Understanding those loads is important not only from a strictly clinical point of view, but also for the design of valid in vitro experiments. Several approaches have been developed to estimate spinal loads, exploiting both in vitro and in vivo measures, as well as numerical simulations. However, given the complexity of spinal biomechanics, it is difficult to provide accurate estimations, whilst each method has different advantages and disadvantages [43]. In vivo measures are perhaps the most representative source, although they can be invasive and affected by natural

inter-subject variability [43]. Bergmann et al. [44] has provided a series of in vivo studies using instrumented vertebral body replacements and spinal fixators. Measurements from vertebral body replacements have shown that the resultant force exerted during level walking can reach about 170 % of that measured when standing (ranging 100 - 300 N between two subjects). Loads increase when performing activities involving upper body flexion (e.g. ascending/descending stairs), during which the resultant can exceed 250 % of the standing force [45]. The direction of the resultant force acting on the vertebral body replacement during common daily activities can be approximated to span a cone with an aperture of 15°. This angle was estimated in a previous work [46], using data available from [44]. Measures over 10 patients with instrumented spinal fixators have shown that walking, as well as ascending/descending stairs, induces a peak bending moment of ~110 % of standing value [47]. Similar trends have been found also in another study where walking has induced a maximum bending moment ranging from 2 - 9 Nm and a maximum resultant force ranging from 50 - 400 N on the fixator rods [48]. However, it must be borne in mind that those in vivo measurements are not representative of a physiological condition and that instrumented implants share loads with other spinal structures (e.g. bone grafts, facet joints) [45].

An alternative site of measure is the intervertebral disc. Wilke et al. [49] has provided in vivo measurements by inserting a pressure transducer within the nucleus, showing an increase from 0.5 MPa when standing, to 2.3 MPa when lifting a 20 kg weight. McNally et al. [50] developed an in vitro stress profilometry technique, which was extensively used by Adams and his group [51-53]. The stress profile is obtained by inserting a transducer (continuously recording pressure) through the disc and then sliding it to the opposite side whilst the spine undergoes a constant load. Results showed that, in a healthy disc, the internal stress increases from the outer annulus towards the nucleus, where a plateau is reached (i.e. hydrostatic pressure condition). Conversely, a degenerated disc showed an altered load transfer, with stress concentration in the middle annulus and reduced stress within the nucleus [35](Fig.1-11). Such technique may also be used to estimate the force transmitted to the endplate. If the geometry of the disc is known, the integral of the pressure over the CSA will provide the force borne by the disc itself [54], although correction factors may be required [55]. In vivo data were then used to estimate forces of about 400–600 N when standing, which may reach 1200–1500 N when bending forward [56-58]. Together with the intervertebral disc, the facet joints are responsible for transmitting the whole load between two adjacent vertebrae,

with the facets bearing about 2–7 % of the force in axial compression [59]. Furthermore, the load sharing between the disc and the facet joints depends on posture: the more the extension the more load sharing shifts posteriorly [59]. In addition, the facet joints have a substantial role in resisting anterior shear, by bearing 55–65 % of such loading component [60]. Numerical modelling has the great advantage of being non invasive whilst allowing replicating several loading conditions, although requiring a thorough validation process to achieve sufficient accuracy [43]. Dreischarf et al. developed an FE model of the disc, which was validated using force estimations from intradiscal pressure measurements [55]. Results predicted forces ranging 430–600 N when standing, with an error below 4 %. An alternative numerical approach is multibody dynamics, where bones are typically modelled as rigid segments undergoing forces exerted by multiple muscle groups (i.e. output of the model). External forces and kinematic can be measured in vivo non invasively (e.g. gait analysis) and then used as input for the model, as boundary conditions or for its validation. This method has allowed generating complex spinal models with up to 18 degrees of freedom and 154 muscles, estimating up to 238 Nm occurring at L5–S1 in extension [61]. The same approach was exploited to estimate a moment of 8 Nm acting on L1 when standing with both arms elevated, which increased by 5 Nm per additional kg of weight held in the hands [62].

### **1.3 Osteoporosis**

Osteoporosis is a metabolic disease which results in loss of bone mass and deterioration of the bone micro-architecture, is a major cause of fractures in the elderly. It mostly affects the bony structures where the trabecular bone is prevalent, such as the femoral neck, wrist and vertebral body. Therefore, the weakened structure becomes susceptible to fracture. The incidence and associated socio-economic costs of these fractures are very high and their health impact is far reaching: about 440,000 and 700,000 new cases per year in the European Union (EU) countries and in the United States, respectively [63]; direct annual costs estimated to be about US\$440 million and US\$750 million in the EU countries and in the United States, respectively [64].

The pathology mostly affects women as the post-menopausal oestrogens deficiency enhances the bone resorption activity of osteoclasts [65]. Vertebral compression fractures, the most common type of osteoporotic fractures, are associated with pain, increased mortality and a 5-fold increased risk of additional vertebral fractures [66]. What makes the situation even worse is that vertebral compression fractures can be clinically elusive: about half of them are thought to be

asymptomatic and remain clinically undetected [67]. Better tools are therefore needed to better diagnose and prevent the occurrence of vertebral fractures.

## **1.4 Vertebral fracture**

Vertebral fractures occur when the loading conditions exceed the strength of the vertebrae [17]. However, the mechanism and outcome of that event is an extremely complex topic which involves several factors. Bone quality is a fundamental discriminant in the mechanics of traumatic and pathological fractures. Pathological conditions hinder bone quality and physiological loads may become too demanding for the vertebral structure. Therefore, daily activities may induce a micro-damage whose continuous accumulation causes back pain and may lead to fracture [67]. Conversely, traumatic fractures arise when the spine undergoes non physiological and extreme/impact loading conditions. Dissipation of such a high amount of energy may result in the fracture of the vertebra and/or damage to spinal soft tissue [15].

For the purpose of this work the candidate have focused on vertebral compression fracture.

### **1.4.1 Vertebral compression fractures**

Vertebral compression fractures are a severe cause of morbidity and disability as well as a significant burden for healthcare systems. However, the biomechanics underlying fracture onset and success of its treatment raises research questions which are still far from being answered. In simple terms, a vertebral compression fracture (VCF) is a fracture in which the vertebral body partially collapses. VCF are radiographically demonstrated deformities defined as a decrease of 15% to 20% of the vertebral height, measured by comparison with adjacent vertebrae. They typically occur when the combined axial and bending loads on the spine exceed the strength of the vertebral body [68]. This usually occurs in the anterior part of the vertebral body, involving the anterior cortex and occasionally one or both endplates, and may also spreads to the lateral cortex. When the posterior cortical shell is fractured, retropulsed fragments bursting out from the posterior cortex can create compression of the spinal cord (Fig.1-14).

The cause of the vertebral fracture may be either pathological or traumatic. The main pathological conditions are osteoporosis and cancer, whose metabolic alterations result in bone weakening [69, 70]. Osteoporosis has been estimated to afflict up to 30 % of post-menopausal

women [71] causing about 1.4 million new vertebral fractures every year [72]. Metastatic infiltration, primary spinal tumours and multiple myeloma usually induce gross osteolytic lesions, leading to painful vertebral fractures and severe back pain [73, 74]. Understanding the mechanics of those fractures is then fundamental to develop effective treatments, also considering the little time available to mend the life quality of patients (metastatic infiltration may occur at a terminal stage of the cancer). Spinal traumatic fractures are present in more than 20 % of trauma cases [75] and they occur when the spine undergoes accidental high-energy loading conditions, hence exceeding its own strength. The majority of spinal traumas arise from motor vehicle accidents (~66 %) and fall from heights (~13 %) [75], which are events where the main force component is axial. Compression fractures indeed account for about 66 % of all spinal fractures with a 14 % incidence of neurological deficit [76]. Burst fractures are a sub-type of compression fractures, and they account for about 30 % of all spinal injuries [76] whilst approximately 47 % of cases present with a degree of neurological deficit at the time of admission [77]. The main features of the fracture are the spinal canal occlusion (SCO), comminution of the endplates and interpedicular widening (IPW).

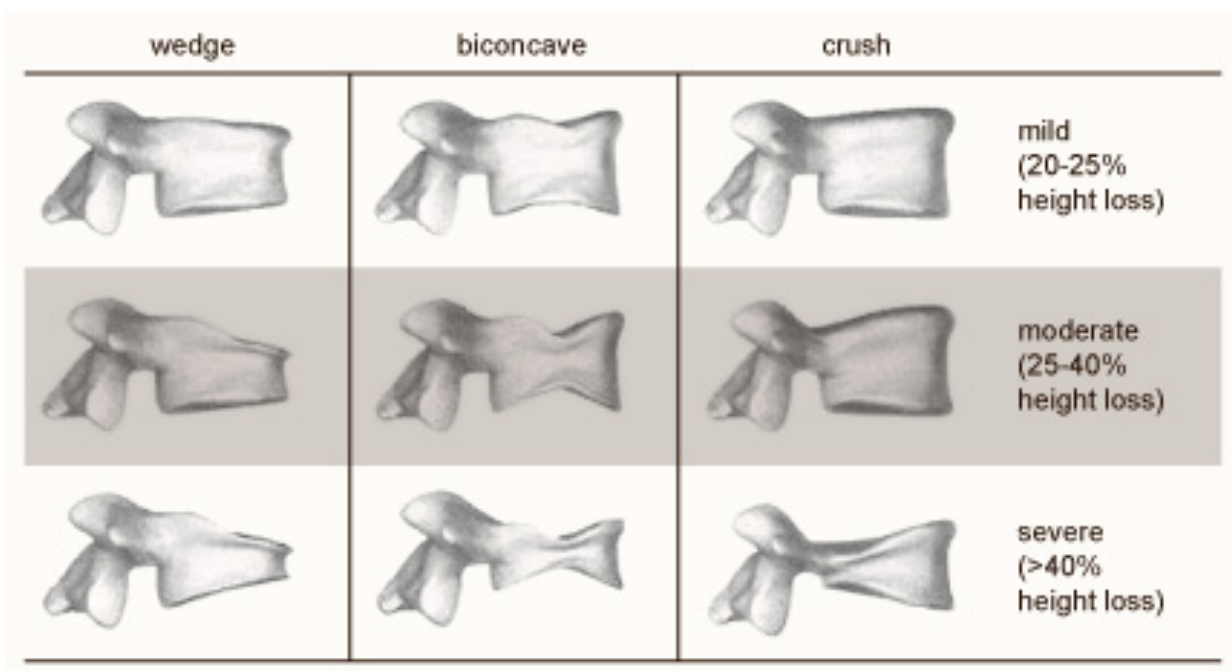


*Fig.1-14: Classification of vertebral compression fractures according to Genant [78].*

While most compression fractures from trauma will heal within 8 to 10 weeks with conservative treatment consisting of bed rest, bracing, and pain medications, in some cases excessive deformity require surgical procedures to correct and reverse the damage caused by the VCF.

A minimally-invasive method called vertebroplasty is used to treat VCF in cases where vertebral collapse doesn't exceed 65% [79]. More severe trauma necessitates more complex surgical procedures and the use of instrumentation that might present a greater risk and precipitation of associated medical complications for elderly patients [80]. This is indicated when there is spinal cord compression leading to neurological deficit, or a progressive deformity (kyphosis or scoliosis) leading to pulmonary compromise or imbalance of the trunk. In some cases, spinal instrumentation consisting of spinal rods, hooks and screws can be attached to the posterior part of the spine to act as a splint, with the aim to improve support and halt progression of deformity

## **1.5 Vertebroplasty**

Vertebroplasty is a minimally-invasive approach which consists in injecting low viscosity cement, typically polymethylmethacrylate (PMMA), directly into the collapsed vertebral body, with the goal of stabilizing the fracture and relieving the associated pain. After the cement has polymerized and hardened, it can prevent further collapse of the vertebra and further deformity such as spine curvature and/or loss of height. Successful repair of the collapsed vertebrae is commonly said to be achieved when strength is restored to pre-fracture values [81].

Vertebroplasty is considered a minimally invasive surgical procedure because takes about 1 hour to complete and patients usually go home the same or next day as the procedure. The main steps of this procedure are: The patient is treated with local anesthesia and light sedation, usually in a x-ray suite or operating room on an outpatient basis.

1. A biopsy needle is guided into the fractured vertebra under fluoroscopic x-ray guidance through a small puncture in the patient's skin (Fig.1.15).
2. Specially formulated acrylic bone cement (most commonly PMMA) is injected under pressure directly into the fractured vertebra, filling the spaces within the bone, with the goal of creating a type of internal cast (a cast within the vertebra) to stabilize the vertebral bone (Fig.1.15).
3. The needle is removed and the cement hardens quickly (few minutes) and forms a support structure inside the vertebra that provide stabilization and strength.

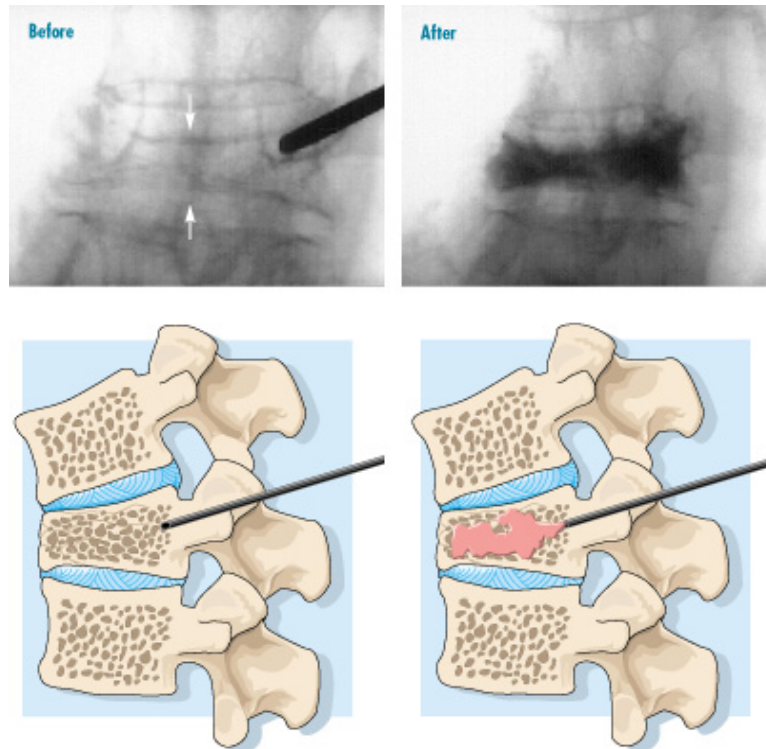


*Fig.1-15: Illustration of the vertebroplasty procedure, consisting in the injection of cement with cannulae placed through the pedicles ( Modified from Medical Encyclopedia: [www.nlm.nih.gov](http://www.nlm.nih.gov)).*

In the last years vertebroplasty has also been successfully used as a prophylactic treatment, with the objective to reinforce osteoporotic vertebral bodies which are at risk of failure, thus preventing fracture [82].

### **1.5.1 The biomechanics of vertebroplasty**

Vertebroplasty procedure was first performed in 1984 in France by Galibert and Deramond [83] and has been gradually introduced in Europe and in the United States [84]. Efficacy of vertebroplasty on the pain relief and quality of life [80], was reported in 73% to 90% of patients [85]. This immediate pain alleviation resulting from cement augmentation is associated with inhibition of painful micro movement at the fracture site [86]. This has mainly contributed to make vertebroplasty an attractive option to more conservative and surgically-invasive treatments related to tumors and osteoporotic vertebral compression fractures.

Despite the potential advantage of vertebroplasty, this procedure has several drawbacks. It is clinically performed under fluoroscopy to control the amount of injected cement, and avoid cement leakage. Cement leakage has been reported as cause of temporal or permanent paralysis and at

worth patient death, due to a reaction to the toxicity of cement. These circumstances are rare and mostly due to a mistaken placement of needle or an altered cement mixtures that increase their fluidity and leaking risks [70]. It has been hypothesized that the cement filling of the intertrabecular spaces prevent the supply of bone nutrients coming from marrow lead to bone necrosis in the neighbor tissues as much as the heat of polymerization [87, 88]. Moreover, an altered biomechanical stress and load transfer after procedure may affect the risk of failure of the adjacent vertebral bodies. In fact, more than 20% of patients undergoing to vertebroplasty suffer to further fractures [89], and in 67% of the cases, these fractures occur within 30 days post-operatively. An example of such a case is shown in Figure 1.16 [90]. Due to the stiff nature of PMMA, most of these new fractures occur in the vertebrae adjacent to the one that has been reinforced with cement. The stress shielding effects due to the stiff cement, is known to cause undesirable of bone resorption [91].

The effects of injected cement volume and distribution are still debated. *In vivo* studies have shown that only small amounts of cement (from 2 ml to 8 ml) are required for strength and stiffness restoration [92] [93]. Volume fill also correlated with strength and stiffness restoration [84]. A general agreement is that although very low amounts could restore strength in a fractured vertebra, larger volumes are required to restore stiffness [92]. Clinically, the distribution and volume of injected cement is influenced to the injection method (uni- or bi-pedicular approach) and to the anatomy of the vertebral body (angle of needle insertion and placement).

Moreover, the mechanical properties of the polymerized cement might also affect the outcomes of the procedure. The presence of a quantity of very stiff cement, typically PMMA, which is one order of magnitude stiffer than trabecular bone, is believed to promote the failure of the already weak osteoporotic bone of the adjacent vertebrae. Finite element analyses as well as *in vivo* studies have been shown that even relatively low volumes of PMMA may increase the risk of adjacent vertebrae failure at lower loads than if the fracture vertebra had been left untreated [89].

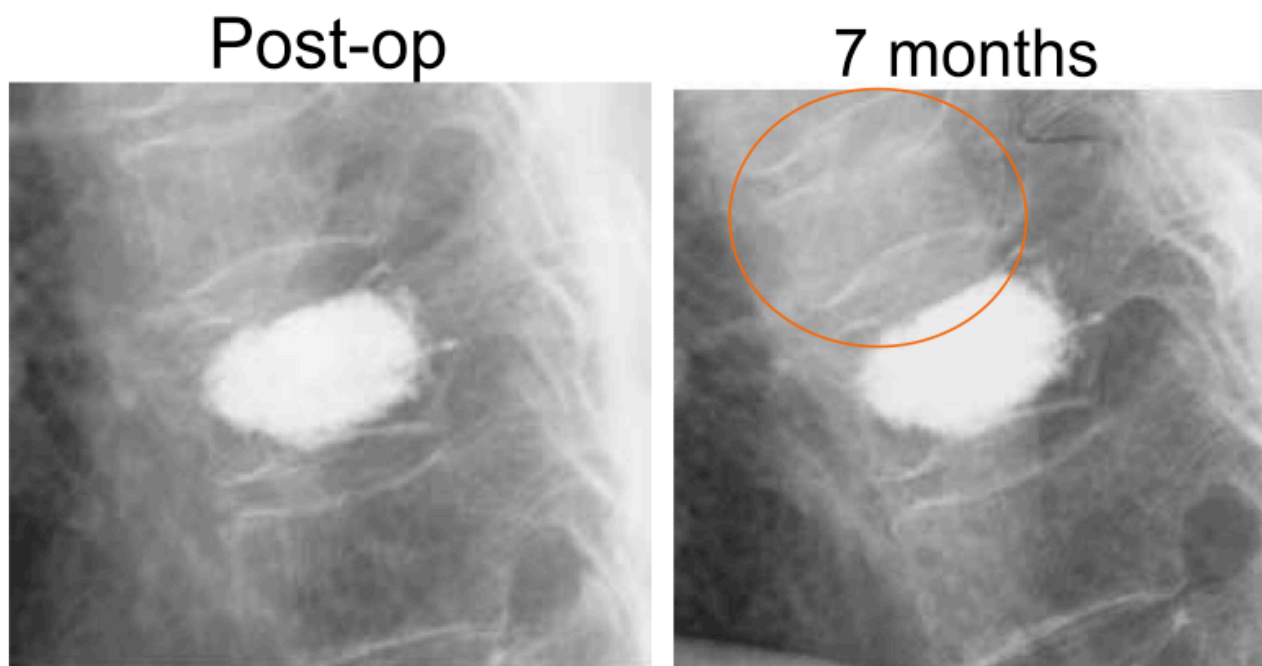


*Fig.1-16: Radiographic evidence of adjacent vertebral fracture (color circle) 6 months after vertebroplasty (Source from Tanigawa et al. [90])*

This might be related to the so-called "pillar effect", demonstrated by a few studies of 2 or more spine levels [94-96]. The pillar effect of injected cement is hypothesized to decrease the endplate bulge in the augmented vertebra causing an increase in adjacent disc pressure that is communicated to the adjacent vertebra [94].

In the last years prophylactic vertebroplasty has been proposed as an option to reduce the fracture risk of metastatic and osteoporotic vertebrae [69, 81, 97-99], or to prevent adjacent fractures after vertebroplasty [100, 101].

The risks affiliate with vertebroplasty has raised many questions about the safety of the procedure, moreover prophylactic augmentation (treatment of nonfractured vertebra) exposes the patients to additional risk ,for this reason there is a need for a clearer understanding on the cost-benefit trade-off.

## 1.6 Biomechanical investigation of spine

Biomechanical investigations are paramount to gain a thorough understanding of spinal biomechanics and related treatments. The following section is meant to provide an overview of the literature relevant to the experiments carried out in this study.

### 1.6.1 *In vitro* testing of spine

Knowledge of the normal functional behavior and mechanical properties of the vertebral column is important to understand the pathogenesis of back lesions, to identify the clinical manifestations of back pain, and to ensure a rational approach to physical therapy.

Daily activity induces complex loading scenarios on the human vertebrae. Information about spinal loads can be derived from a combination of *in vivo* or *in vitro* measured, and mathematical models. Even if direct *in vivo* spine measurements provide the most reliable loading data [57, 102-104], *in vivo* studies are difficult to perform because of their methodological and ethics limitations. Conversely, biomechanical *in vitro* simulations have the advantage of being non-invasive and more effortless to carry out. For these reasons it is clear that *in vitro* mechanical testing is widespread performed to better understand the biomechanics of spine, fracture, and to test/optimize surgical treatment.

Since *in vitro* testing represents a simplified scenario, the simulated loading conditions follow different approaches, reflecting the complexity of the human musculoskeletal system. *In vitro* experiments aim at assessing [43]:

- Kinematics of the spine: these experimental protocols are usually designed to replicate simple motor tasks (i.e., by applying combinations of pure moments and forces), focusing on the relationship between motion and loads. Hence, results provide information about parameters such as range of motion (ROM), joint axes of rotation, neutral zone and elastic zone.
- Mechanical and structural properties of the vertebral body and discs: stiffness, strains, failure strength, mode of failure are investigated by applying simplified loading conditions (e.g., axial compression) to grant better control of the experimental scenario.

- Comparison with healthy and pathological conditions (e.g., disc degeneration, spinal instability, osteoporosis, malignant infiltration): these experiments are also performed to assess the effects of clinical treatments (e.g. cement augmentation, spinal implants).

The experimental approach performed in this study, is based on the study of mechanical and structural properties of human natural and treated vertebral body.

*In vivo* measurements and numerical modelling of the spine only record/predict compressive forces in the vertebral body (Table 1-2). Tensile forces measured *in vivo* and predicted by numerical models are 1-2 orders of magnitude smaller than the compressive ones. This was recently confirmed by two large EU-funded international consortia investigating the spine biomechanics [105], and vertebral treatments [106]. Moreover, recent *in vitro* studies [31, 46, 107] have shown that the structure of the vertebral body is optimized to withstand pure compressive forces (as opposed to tensile, oblique or torsional). This confirms that in nature the vertebral body is not subjected to tension.

In fact, all *in vitro* tests and numeric models aiming at replicating relevant physiological conditions apply a pure compressive force (possibly including a bending component associated with an anterior offset of the load or an eccentric load, Table 1-2). Recently, a study was published [46] where eight thoracolumbar vertebrae instrumented with eight triaxial strain gauges. The vertebrae were loaded through their disks and were subjected to a variety of loading conditions that included the cone spanned by the resultant force during physiological motor tasks, but also other load components such as torsion and traction [44].

*In vitro* experiments are also performed to assess the outcomes of clinical treatments, such as cement augmentation (Table1-3). The increasing interest in the use of vertebroplasty as a treatment for vertebral compression fractures has led to a number of studies on the biomechanical aspects of the technique using both experimental and computational models. In both experimental and computational modelling of the vertebroplasty process, studies have generally concentrated on examining the effects of the cement type and volume.

It must be noted that most studies focused on the overall failure strength of the natural and treated vertebral body, without analyzing the strain distribution.

Table 1-2: Examples of *in vitro* and numerical studies where the vertebral body is subjected to compression

Number & type of cycles	Method of estimation	References
Destructive axial compression (burst fracture)	<i>In vitro</i> study	[108]
Increasing cyclic compressive fatigue test (from 10000 to 80000 cycles) under escalating load to the patient's Body Weight (BW) (1 to 3.5 BW)	<i>In vitro</i> study	[109]
Compression cycles loading until failure	<i>In vitro</i> study	[110]
Simulation of axial compression up to 1000 N	Numerical study	[111]
Destructive axial compression (burst fracture)	<i>In vitro</i> and numerical study	[112]
Destructive axial compression	<i>In vitro</i> and numerical study	[113]
Creep analysis during static compressive loading	<i>In vitro</i> study	[114]
Compressive loading along the follower load path (tangent to the curve of spine)	<i>In vitro</i> study	[115]
Destructive testing under eccentric compression	<i>In vitro</i> studies	[100]; [116]
Eccentric compression	<i>In vitro</i> study	[117]
Creep analysis during static compressive loading	<i>In vitro</i> study	[118]
Destructive testing under compressive loading tilted in 6°-10° of flexion	<i>In vitro</i> study	[119]
Destructive testing under unconstrained compressive loading by using a 6-degree-of-freedom robotic arm	<i>In vitro</i> study	[120]
Destructive axial compression	<i>In vitro</i> study	[121]
No destructive testing under compressive loading and tilted of 15° in each direction	<i>In vitro</i> study	[46]
No destructive axial compression	<i>In vitro</i> study	[122]
No destructive testing under axial compressive loading and tilted of 15° in each direction	<i>In vitro</i> study	[107]
The body of the thoraco-lumbar vertebrae is optimized to resist to a load applied strictly in an axial direction	<i>In vitro</i> study	[31]
Destructive axial compression	<i>In vitro</i> study	[123]
Destructive axial compression	<i>In vitro</i> study	[124]
Destructive axial compression	<i>In vitro</i> study	[125]
Destructive axial compression	<i>In vitro</i> study	[126]
Destructive axial compression	<i>In vitro</i> study	[127]
Destructive axial compression	<i>In vitro</i> study	[128]
Destructive axial compression	<i>In vitro</i> and numerical study	[129]
Destructive axial compression	<i>In vitro</i> and numerical study	[130]
Destructive axial compression	<i>In vitro</i> study	[131]
Destructive axial compression	<i>In vitro</i> and numerical study	[132]
Destructive axial compression	<i>In vitro</i> study	[133]
Destructive axial compression	<i>In vitro</i> and numerical study	[18]
Destructive axial compression	<i>In vitro</i> and numerical study	[26]
Destructive axial compression	<i>In vitro</i> study	[134]
Destructive axial compression	<i>In vitro</i> study	[135]
Destructive axial compression	<i>In vitro</i> study	[67]
Destructive axial compression	<i>In vitro</i> and numerical study	[136]
Destructive axial compression	<i>In vitro</i> study	[137]
Destructive axial compression	<i>In vitro</i> study	[23]
Destructive axial compression	<i>In vitro</i> study	[138]
Eccentric compression	<i>In vitro</i> study	[139]
Anterior bending	<i>In vitro</i> study	[140]
Anterior bending	<i>In vitro</i> and numerical study	[141]

Table 1-3: Examples of in vitro studies on augmented vertebrae

Type of treatment	Applied force and number of cycles	Type of cement	References
Post-fracture vertebroplasty	Static destructive test Failure load= 2857 N	Acrylic cement	[142]
Prophylactic augmentation	Static destructive test: Failure force=2019±979 N for controls Failure force = 6407 ± 6336 N augmented	Acrylic or brushite cement	[143]
Prophylactic augmentation	Static destructive test Failure force= 11936±1985 N <sup>1</sup>	Calcium phosphate (CP) cement	[144]
Post-fracture vertebroplasty	Destructive fatigue loading (flexion-compression force) and a stepwise increasing applied peak force (no detail about number of cycles) Fatigue fracture force: PMMA group 2854±648 N PMMA modified group 1980±786 N	A variety of modified acrylic formulations	[145]
Post-fracture vertebroplasty	Increasing cyclic compressive fatigue test (from 10000 to 80000) under escalating load to the patient's Body Weight (BW) (1 to 3.5 BW) Failure force 2280±890 N	Acrylic cement	[109]
Post-fracture kyphoplasty	Non destructive dynamic compressive fatigue test (10000 cycles 100 or 200-600 N) Destructive static compression test for both techniques: Failure force= 4709±1953 N Failure force= 4779±1068 N	Acrylic cement injected with two different technique	[146] [147]
Synthetic vertebral body augmentation model for Balloon Kyphoplasty	Three series of destructive compression fatigue life testing: 0-2300 N 100% of PMMA run out (one million loading cycles) 0-2300 N 28% of CP run out 0-1150 N 100% of CP run out (one million loading cycles)	Acrylic bone cement and Calcium Phosphate (CP) bone substitute This study uses a polyurethane foam vertebral body model.	[148]
Prophylactic augmentation and kyphoplasty	Compressive fatigue test 100000 cycles of eccentric loading (100-600 N)	Acrylic bone cement and Calcium Phosphate (CP)	[149]
Post-fracture vertebroplasty	Destructive anterior wedge fracture Failure force=1114±325 N for specimens augmented endplate to endplate Failure force=767±257 N for specimens partially augmented	Acrylic bone cement	[150]
Prophylactic augmentation and post-fracture vertebroplasty	Destructive compression test Failure force 5000-8000 N	Acrylic and Calcium Phosphate (CP) bone cements	[151]

<sup>1</sup> The values reported by (Ikeuchi et al., 2001) are significantly higher than any other study, and refer to formalin-fixed vertebrae completely filled with cement.

Type of treatment	Applied force and number of cycles	Type of cement	References
Post-fracture vertebroplasty	Destructive static compression. For central and lateral 3.5 ml injection cement: Failure force= 2175±295 N Failure force= 2027±335 N For central and lateral 7.0 ml injection cement: Failure force= 3396±295 N (central) Failure force= 3311±295 N (lateral)	Acrylic bone cement	[152]
Prophylactic augmentation	Destructive static compression Failure force 7807±2650 N (4309-12431 N)	Acrylic bone cement	[153]
Post-fracture vertebroplasty	Destructive static compression. Failure force for lumbar 1788-2336 N Failure force for thoracic 1362-3310 N	Acrylic bone cement	[93]
Post-fracture vertebroplasty	Destructive static compressive test. Results of the different cements for lumbar vertebrae: Failure load 4208±364 N Failure load 3134±364 N Failure load 2450±364 N and for thoracic vertebrae: Failure load 4058±347 N Failure load 4146±330 N Failure load 2476±330 N	Three different hydroxyapatite cements	[154]
Prophylactic augmentation and post-fracture vertebroplasty	Compressive wedge fracture Failure strength: Prophylactic 2230±620 N Vertebroplasty 2630±850 N	Acrylic bone cement	[117]
Post-fracture kyphoplasty	Destructive static compressive test: Failure load 1122±993 N (T1-T5) Failure load 2906±1008 N (T1-T5)	Acrylic bone cement	[98]
Post-fracture kyphoplasty	Destructive static compressive test: Failure load 5092±2543 N (T1-T5)	Acrylic bone cement	[137]
Post-fracture vertebroplasty	Destructive static compressive test: Failure load 4200 N (uni-pedicular) Failure load 6800 N (bi-pedicular)	Acrylic bone cement	[155]
Prophylactic augmentation	In vitro and numerical study. Destructive static compressive test: Failure load range 2000 N -7000 N	Acrylic bone cement standard and with low-modulus	[156]
Prophylactic augmentation	Destructive static compressive test Failure load omitted	Acrylic bone cement standard and with low-modulus	[157]

### **1.6.2 *In situ* testing**

In situ testing is an experimental paradigm where stepwise loading is integrated with CT scanning, hence allowing the investigator to perform high-resolution scanning of the sample under load. Therefore, the testing cell is designed to deliver a known force to the sample as well as satisfy the requirements for CT scanning. One of the firstly developed protocols allowed axial compression of a 9 x 22 mm specimen within a micro CT with a resolution of 34  $\mu\text{m}$  [158]. However, that testing cell required loading through a universal testing machine, with obvious issues to consistently maintain the applied strain when the rig was fitted into the scanner. Subsequently, the in situ protocol has been used with synchrotron radiation source CT to achieve resolution up to a few nm [159, 160]. Despite the high resolution, micro CT typically has a limited field of view and sealed scanning chamber. High-resolution peripheral quantitative CT (HR-pQCT) has provided a viable alternative for whole bone scanning since it allows a cylindrical first instance of an in situ investigation with HR-pQCT is from Hulme et al. [36]. The authors developed a rig to be fitted within the scanner where the axial compression could be applied manually by means of a screw-driven actuator. Load and displacement were recorded throughout the test as the rig was equipped with a load cell and displacement transducer. The authors tested functional spinal units which underwent scan 1500–200 N). Image processing based on rigid registration of the two datasets was used to compute the deflection of the endplates.

### **1.6.3 Strain distribution measurements**

One of the first studies on the strain distribution in the vertebral body was carried out by means of brittle coating, photoelasticity [161] and 17 strain gauges [162], for different compressive loads. They reported strains of the order of 500–1500 microstrains for a 1470 N compressive force. The effect of an inclined load (2800 N at 161) has been investigated on functional spinal units using 3 to 4 strain gauges, where compressive strain of about 650 microstrain were measured [163]. Strains induced by compression and shear loads were quantified with three triaxial strain gauges on the vertebral rim, and one on the endplate surface [164]. Fracture risk was assessed by Kayanja et al. [165], but the most stressed region could not be identified as only one gauge was applied on each vertebral body. The principal strains were generally aligned as expected: axially/circumferentially for all loading configurations implying a compressive force, and roughly at 45° for torsion. Recent studies [166-168] has been successfully implemented digital image correlation (DIC) to understand the biomechanics of the vertebra.

However, these traditional experimental techniques such as strain gauges are restricted to the surface of specimens, where no internal strain distribution could be interrogated [169]. Alternative approaches have been exploited to overcome this limitation. With the advent of high-resolution micro-CT imaging ( $\mu$ CT) in conjunction with *in situ* mechanical testing, digital volume correlation (DVC) techniques emerged as a novel tool for the measurement of 3D deformation fields throughout entire volumes. DVC is based on tracking the displacement of micro-structural features observed within image volumes, by optimizing an objective function used to compare small subsets of image data from two subsequent scans of a sample, in both an unloaded and a loaded state [170]. Strain fields are calculated from the displacement fields by gradient estimation technique. For bones such as the vertebra, the use of DVC allows the detection of the onset and progression of failure. Application of DVC to whole bones was recently exploited to examine yield and post-yield deformations in vertebral compression experiments [171].

## 1.7 Study aim

The main aim of this thesis was to investigate the mechanical properties of human natural and augmented thoraco-lumbar vertebrae in term of strain distribution. Moreover, the ultimate goal of the candidate was to provide a comprehensive biomechanical analysis to gain further insight on the mechanics of the failure process in prophylactic augmented vertebrae as well as the performance of the treatments. To elucidate the mechanical properties of the natural (either healthy, or osteoporotic) and augmented vertebrae, an integrated approach is presented, which incorporates different experimental measurement methods (strain gauges and digital volume correlation).

1. To improve and make more reproducible *in vitro* biomechanical test of natural and treated vertebrae the following methods were validated and implemented by the candidate:

- Definition of a reproducible anatomical reference frame for the human vertebrae, suitable for *in vitro* and numerical applications
- Provide comprehensive *in vitro* investigation on different boundary condition experienced by vertebrae, assessing the surface strain distribution between vertebra tested in physiological condition (i.e. through its adjacent discs and vertebrae) and the same vertebra tested as isolated vertebra body

1. The methods described above, were applied in the following applications. These objectives were pursued by the candidate to satisfy the aim of this study:

- To provide comprehensive *in vitro* investigation about prophylactic augmentation
- To develop an *in situ* testing protocol for use with natural and augmented vertebrae
- To provide for the first time experimental data on augmented vertebrae using DVC analysis
- To provide comprehensive investigation of the internal strain distribution, both in the elastic regime and up to failure in the natural and augmented vertebrae
- To better evaluate biomechanical efficacy of prophylactic augmentation, using two commercial biomaterials, in preventing fracture of non-fractured vertebral body.

## 1.8 References

- [1] Cowin, S. C., 2001, Bone Mechanics Handbook, CRC Press.
- [2] Williams, P. L., 1995: Churchill Livingstone, London, UK., Gray's anatomy. 38th edition.
- [3] Black, J. a. G. H., "Handbook of biomaterial properties, : Chapman & Hall.."
- [4] Cowin, S. C., 1986, "Wolff's law of trabecular architecture at remodeling equilibrium," J Biomech Eng, 108(1), pp. 83-88.
- [5] Keaveny, T. M., Morgan, E. F., Niebur, G. L., and Yeh, O. C., 2001, "Biomechanics of trabecular bone," Annual Review of Biomedical Engineering, 3(1), pp. 307-333.
- [6] Kuhn, J. L., Goldstein, S. A., Feldkamp, L. A., Goulet, R. W., and Jesion, G., 1990, "Evaluation of a microcomputed tomography system to study trabecular bone structure," J Orthop Res, 8(6), pp. 833-842.
- [7] Mosekilde, L., Bentzen, S. M., Ortoft, G., and Jorgensen, J., 1989, "The predictive value of quantitative computed tomography for vertebral body compressive strength and ash density," Bone, 10(6), pp. 465-470.
- [8] Keaveny, T., 1998, "Cancellous Bone," in Handbook of Biomaterial Properties, J Black and G Hastings, Editors. 1998, Chapman&Hall: London, UK.15-23.
- [9] Goldstein, S. A., Wilson, D. L., Sonstegard, D. A., and Matthews, L. S., 1983, "The mechanical properties of human tibial trabecular bone as a function of metaphyseal location," J Biomech, 16(12), pp. 965-969.
- [10] Linde, F., Pongsoipetch, B., Frich, L. H., and Hvid, I., 1990, "Three-axial strain controlled testing applied to bone specimens from the proximal tibial epiphysis," J Biomech, 23(11), pp. 1167-1172.
- [11] Hipp, J. A., Rosenberg, A. E., and Hayes, W. C., 1992, "Mechanical properties of trabecular bone within and adjacent to osseous metastases," J Bone Miner Res, 7(10), pp. 1165-1171.
- [12] Pugh, J. W., Radin, E. L., and Rose, R. M., 1974, "Quantitative studies of human subchondral cancellous bone. Its relationship to the state of its overlying cartilage," J Bone Joint Surg Am, 56(2), pp. 313-321.
- [13] Brinckmann, P., Biggemann, M., and Hilweg, D., 1989, "Prediction of the compressive strength of human lumbar vertebrae," Spine (Phila Pa 1976), 14(6), pp. 606-610.
- [14] Stagnara, P., De Mauroy, J. C., Dran, G., Gonon, G. P., Costanzo, G., Dimnet, J., and Pasquet, A., 1982, "Reciprocal angulation of vertebral bodies in a sagittal plane: approach to references for the evaluation of kyphosis and lordosis," Spine (Phila Pa 1976), 7(4), pp. 335-342.
- [15] White, A. A., and Panjabi, M.M. Clinical biomechanics of the spine. 2nd ed. Philadelphia: Lippincott, 1990., 1990, "Clinical biomechanics of the spine. 2nd ed. Philadelphia: Lippincott, 1990.."
- [16] Tabensky, A. D., Williams, J., DeLuca, V., Briganti, E., and Seeman, E., 1996, "Bone mass, areal, and volumetric bone density are equally accurate, sensitive, and specific surrogates of the breaking strength of the vertebral body: an in vitro study," J Bone Miner Res, 11(12), pp. 1981-1988.

- [17] Bouxsein, M. L., 2003, "Bone quality: where do we go from here?," *Osteoporos Int*, 14 Suppl 5, pp. S118-127.
- [18] Fields, A. J., Eswaran, S. K., Jekir, M. G., and Keaveny, T. M., 2009, "Role of Trabecular Microarchitecture in Whole-Vertebral Body Biomechanical Behavior," *Journal of Bone and Mineral Research*, 24(9), pp. 1523-1530.
- [19] Wegrzyn, J., Roux, J. P., Arlot, M. E., Boutroy, S., Vilayphiou, N., Guyen, O., Delmas, P. D., Chapurlat, R., and Bouxsein, M. L., 2010, "Role of trabecular microarchitecture and its heterogeneity parameters in the mechanical behavior of ex vivo human L3 vertebrae," *J Bone Miner Res*, 25(11), pp. 2324-2331.
- [20] Stauber, M., and Muller, R., 2006, "Age-related changes in trabecular bone microstructures: global and local morphometry," *Osteoporos Int*, 17(4), pp. 616-626.
- [21] Wang, J., Zhou, B., Liu, X. S., Fields, A. J., Sanyal, A., Shi, X., Adams, M., Keaveny, T. M., and Guo, X. E., 2015, "Trabecular plates and rods determine elastic modulus and yield strength of human trabecular bone," *Bone*, 72, pp. 71-80.
- [22] Eswaran, S. K., Gupta, A., Adams, M. F., and Keaveny, T. M., 2006, "Cortical and trabecular load sharing in the human vertebral body," *J Bone Miner Res*, 21(2), pp. 307-314.
- [23] Roux, J. P., Wegrzyn, J., Arlot, M. E., Guyen, O., Delmas, P. D., Chapurlat, R., and Bouxsein, M. L., 2010, "Contribution of trabecular and cortical components to biomechanical behavior of human vertebrae: an ex vivo study," *J Bone Miner Res*, 25(2), pp. 356-361.
- [24] Lochmüller, E. M., Poschl, K., Wurstlin, L., Matsuura, M., Muller, R., Link, T. M., and Eckstein, F., 2008, "Does thoracic or lumbar spine bone architecture predict vertebral failure strength more accurately than density?," *Osteoporos Int*, 19, pp. 537-545.
- [25] Hulme, P. A., Boyd, S. K., and Ferguson, S. J., 2007, "Regional variation in vertebral bone morphology and its contribution to vertebral fracture strength," *Bone*, 41(6), pp. 946-957.
- [26] Fields, A. J., Lee, G. L., Liu, X. S., Jekir, M. G., Guo, X. E., and Keaveny, T. M., 2011, "Influence of vertical trabeculae on the compressive strength of the human vertebra," *Journal of Bone & Mineral Research*, 26(2), pp. 263-269.
- [27] Bogduk, N., 2005, "Clinical anatomy of the lumbar spine and sacrum. 4th ed. London: Elsevier Churchill Livingstone,."
- [28] Panjabi, M. M., Goel, V., Oxland, T., Takata, K., Duranceau, J., Krag, M., and Price, M., 1992, "Human lumbar vertebrae. Quantitative three-dimensional anatomy," *Spine (Phila Pa 1976)*, 17(3), pp. 299-306.
- [29] Panjabi, M. M., Takata, K., Goel, V., Federico, D., Oxland, T., Duranceau, J., and Krag, M., 1991, "Thoracic human vertebrae. Quantitative three-dimensional anatomy," *Spine (Phila Pa 1976)*, 16(8), pp. 888-901.
- [30] Inceoglu, S., Burghardt, A., Akbay, A., Majumdar, S., and McLain, R. F., 2005, "Trabecular architecture of lumbar vertebral pedicle," *Spine (Phila Pa 1976)*, 30(13), pp. 1485-1490.
- [31] Cristofolini, L., 2015, "In vitro evidence of the structural optimization of the human skeletal bones," *J Biomech*, 48(5), pp. 787-796.
- [32] White III, A. A., and Panjabi, M. M., 1990, *Clinical Biomechanics of the Spine*, Lippincott Williams & Wilkins.

- [33] Moon, S. M., Yoder, J. H., Wright, A. C., Smith, L. J., Vresilovic, E. J., and Elliott, D. M., 2013, "Evaluation of intervertebral disc cartilaginous endplate structure using magnetic resonance imaging," *Eur Spine J*, 22(8), pp. 1820-1828.
- [34] Raj, P. P., 2008, "Intervertebral disc: anatomy-physiology-pathophysiology-treatment," *Pain practice : the official journal of World Institute of Pain*, 8(1), pp. 18-44.
- [35] Adams, M. A., Dolan, P., and McNally, D. S., 2009, "The internal mechanical functioning of intervertebral discs and articular cartilage, and its relevance to matrix biology," *Matrix biology : journal of the International Society for Matrix Biology*, 28(7), pp. 384-389.
- [36] Hulme, P. A., Ferguson, S. J., and Boyd, S. K., 2008, "Determination of vertebral endplate deformation under load using micro-computed tomography," *J Biomech*, 41(1), pp. 78-85.
- [37] Heuer, F., Schmidt, H., and Wilke, H. J., 2008, "The relation between intervertebral disc bulging and annular fiber associated strains for simple and complex loading," *J Biomech*, 41(5), pp. 1086-1094.
- [38] Adams, M. A., Phillip, P., Jon, H. T., Glenn, K. W., and Patricia, D., 2006, "Intervertebral Disc Degeneration Can Predispose to Anterior Vertebral Fractures in the Thoracolumbar Spine," *Journal of Bone and Mineral Research*, 21(9), pp. 1409-1416.
- [39] Jaumard, N. V., Welch, W. C., and Winkelstein, B. A., 2011, "Spinal facet joint biomechanics and mechanotransduction in normal, injury and degenerative conditions," *J Biomech Eng*, 133(7), p. 071010.
- [40] Izzo, R., Guarnieri, G., Guglielmi, G., and Muto, M., 2013, "Biomechanics of the spine. Part I: spinal stability," *European journal of radiology*, 82(1), pp. 118-126.
- [41] Bogduk, N., 2005, *Clinical anatomy of the lumbar spine and sacrum*, Elsevier.
- [42] Datta, G., Gnanalingham, K. K., Peterson, D., Mendoza, N., O'Neill, K., Van Dellen, J., McGregor, A., and Hughes, S. P., 2004, "Back pain and disability after lumbar laminectomy: is there a relationship to muscle retraction?," *Neurosurgery*, 54(6), pp. 1413-1420; discussion 1420.
- [43] Brandolini, N., Cristofolini, L., and Viceconti, M., 2014, "Experimental methods for the biomechanical investigation of the human spine: a review " *Journal of Mechanics in Medicine and Biology*, 14(1), p. 1430002 (1430033 pages).
- [44] Bergmann, G., 2011, " (ed.), Charite – Universitaetsmedizin Berlin "OrthoLoad". Retrieved July 1, 2011. <<http://www.OrthoLoad.com>>."
- [45] Rohlmann, A., Dreischarf, M., Zander, T., Graichen, F., and Bergmann, G., 2014, "Loads on a vertebral body replacement during locomotion measured in vivo," *Gait Posture*, 39(2), pp. 750-755.
- [46] Cristofolini, L., Brandolini, N., Danesi, V., Juszczyk, M. M., Erani, P., and Viceconti, M., 2013, "Strain distribution in the lumbar vertebrae under different loading configurations," *The Spine Journal*, 13(10), pp. 1281-1292.
- [47] Rohlmann, A., Claes, L. E., Bergmann, G., Graichen, F., Neef, P., and Wilke, H. J., 2001, "Comparison of intradiscal pressures and spinal fixator loads for different body positions and exercises," *Ergonomics*, 44(8), pp. 781-794.
- [48] Rohlmann, A., Bergmann, G., Graichen, F., and Neff, G., 1999, "Braces do not reduce loads on internal spinal fixation devices," *Clin Biomech (Bristol, Avon)*, 14(2), pp. 97-102.

- [49] Wilke, H., Neef, P., Hinz, B., Seidel, H., and Claes, L., 2001, "Intradiscal pressure together with anthropometric data--a data set for the validation of models," *Clin Biomech (Bristol, Avon)*, 2001, 16(S1), pp. S111-126.
- [50] McNally, D. S., and Adams, M. A., 1992, "Internal intervertebral disc mechanics as revealed by stress profilometry," *Spine (Phila Pa 1976)*, 17(1), pp. 66-73.
- [51] Adams, M. A., and Dolan, P., 2005, "Spine biomechanics," *J Biomech*, 38(10), pp. 1972-1983.
- [52] Pollintine, P., van Tunen, M. S., Luo, J., Brown, M. D., Dolan, P., and Adams, M. A., 2010, "Time-dependent compressive deformation of the ageing spine: relevance to spinal stenosis," *Spine (Phila Pa 1976)*, 35(4), pp. 386-394.
- [53] Skrzypiec, D. M., Pollintine, P., Przybyla, A., Dolan, P., and Adams, M. A., 2007, "The internal mechanical properties of cervical intervertebral discs as revealed by stress profilometry," *Eur Spine J*, 16(10), pp. 1701-1709.
- [54] McMillan, D. W., McNally, D. S., Garbutt, G., and Adams, M. A., 1996, "Stress distributions inside intervertebral discs: the validity of experimental 'stress profilometry'," *Proc Inst Mech Eng H*, 210(2), pp. 81-87.
- [55] Dreischarf, M., Rohlmann, A., Zhu, R., Schmidt, H., and Zander, T., 2013, "Is it possible to estimate the compressive force in the lumbar spine from intradiscal pressure measurements? A finite element evaluation," *Med Eng Phys*, 35(9), pp. 1385-1390.
- [56] Nachemson, A. L., 1981, "Disc pressure measurements," *Spine (Phila Pa 1976)*, 6(1), pp. 93-97.
- [57] Sato, K., Kikuchi, S., and Yonezawa, T., 1999, "In vivo intradiscal pressure measurement in healthy individuals and in patients with ongoing back problems," *Spine (Phila Pa 1976)*, 24(23), pp. 2468-2474.
- [58] Takahashi, I., Kikuchi, S., Sato, K., and Sato, N., 2006, "Mechanical load of the lumbar spine during forward bending motion of the trunk-a biomechanical study," *Spine (Phila Pa 1976)*, 31(1), pp. 18-23.
- [59] Ivicsics, M. F., Bishop, N. E., Puschel, K., Morlock, M. M., and Huber, G., 2014, "Increase in facet joint loading after nucleotomy in the human lumbar spine," *J Biomech*, 47(7), pp. 1712-1717.
- [60] Skrzypiec, D. M., Bishop, N. E., Klein, A., Puschel, K., Morlock, M. M., and Huber, G., 2013, "Estimation of shear load sharing in moderately degenerated human lumbar spine," *J Biomech*, 46(4), pp. 651-657.
- [61] de Zee, M., Hansen, L., Wong, C., Rasmussen, J., and Simonsen, E. B., 2007, "A generic detailed rigid-body lumbar spine model," *J Biomech*, 40(6), pp. 1219-1227.
- [62] Zander, T., Dreischarf, M., Schmidt, H., Bergmann, G., and Rohlmann, A., 2015, "Spinal loads as influenced by external loads: a combined in vivo and in silico investigation," *J Biomech*, 48(4), pp. 578-584.
- [63] WHO, 1994, "Assessment of fracture risk and its application to screening for postmenopausal osteoporosis. Report of a WHO study group. WHO Technical Report Series, World Health Organization, Geneva, Switzerland, 843: 1-130."

- [64] Johnell, O., 2003, "Economic implication of osteoporotic spine disease: cost to society," *Eur Spine J*, 12 Suppl 2, pp. S168-169.
- [65] McDonnell, P., McHugh, P. E., and O'Mahoney, D., 2007, "Vertebral osteoporosis and trabecular bone quality," *Ann Biomed Eng*, 35(2), pp. 170-189.
- [66] Whealan, K. M., Kwak, S. D., Tedrow, J. R., Inoue, K., and Snyder, B. D., 2000, "Noninvasive imaging predicts failure load of the spine with simulated osteolytic defects," *J Bone Joint Surg Am*, 82(9), pp. 1240-1251.
- [67] Kopperdahl, D. L., Pearlman, J. L., and Keaveny, T. M., 2000, "Biomechanical consequences of an isolated overload on the human vertebral body," *Journal of Orthopaedic Research*, 18(5), pp. 685-690.
- [68] Mathis, J. M., Barr, J. D., Belkoff, S. M., Barr, M. S., Jensen, M. E., and Deramond, H., 2001, "Percutaneous vertebroplasty: a developing standard of care for vertebral compression fractures," *AJNR Am J Neuroradiol*, 22(2), pp. 373-381.
- [69] Tancioni, F., Lorenzetti, M. A., Navarra, P., Pessina, F., Draghi, R., Pedrazzoli, P., Scorsetti, M., Alloisio, M., Santoro, A., and Rodriguez y Baena, R., 2011, "Percutaneous vertebral augmentation in metastatic disease: state of the art," *J Support Oncol*, 9(1), pp. 4-10.
- [70] Uppin, A. A., Hirsch, J. A., Centenera, L. V., Pfiefer, B. A., Pazianos, A. G., and Choi, I. S., 2003, "Occurrence of new vertebral body fracture after percutaneous vertebroplasty in patients with osteoporosis," *Radiology*, 226(1), pp. 119-124.
- [71] Kanis, J., Alexandre, J.-M., Bone, H., Abadie, E., Brasseur, D., Chassany, O., Durrleman, S., Lekkerkerker, J., and Caulin, F., 2003, "Study Design in Osteoporosis: A European Perspective," *Journal of Bone and Mineral Research*, 18(6), pp. 1133-1138.
- [72] Klazen, C. A., Lohle, P. N., de Vries, J., Jansen, F. H., Tielbeek, A. V., Blonk, M. C., Venmans, A., van Rooij, W. J., Schoemaker, M. C., Juttmann, J. R., Lo, T. H., Verhaar, H. J., van der Graaf, Y., van Everdingen, K. J., Muller, A. F., Elgersma, O. E., Halkema, D. R., Fransen, H., Janssens, X., Buskens, E., and Mali, W. P., 2010, "Vertebroplasty versus conservative treatment in acute osteoporotic vertebral compression fractures (Vertos II): an open-label randomised trial," *Lancet (London, England)*, 376(9746), pp. 1085-1092.
- [73] Pingali, S. R., Haddad, R. Y., and Saad, A., 2012, "Current concepts of clinical management of multiple myeloma," *Disease-a-month : DM*, 58(4), pp. 195-207.
- [74] Whyne, C. M., 2014, "Biomechanics of metastatic disease in the vertebral column," *Neurological research*, 36(6), pp. 493-501.
- [75] Pirouzmand, F., 2010, "Epidemiological trends of spine and spinal cord injuries in the largest Canadian adult trauma center from 1986 to 2006," *J Neurosurg Spine*, 12(2), pp. 131-140.
- [76] Magerl, F., Aebi, M., Gertzbein, S. D., Harms, J., and Nazarian, S., 1994, "A comprehensive classification of thoracic and lumbar injuries," *Eur Spine J*, 3(4), pp. 184-201.
- [77] Denis, F., 1983, "The three column spine and its significance in the classification of acute thoracolumbar spinal injuries," *Spine (Phila Pa 1976)*, 8(8), pp. 817-831.
- [78] Genant, H. K., Jergas, M., Palermo, L., Nevitt, M., Valentin, R. S., Black, D., and Cummings, S. R., 1996, "Comparison of semiquantitative visual and quantitative morphometric assessment of prevalent and incident vertebral fractures in osteoporosis The Study of Osteoporotic Fractures Research Group," *J Bone Miner Res*, 11(7), pp. 984-996.

- [79] J. M. Mathis, M. P., and N. Naff., 1998, " Percutaneous vertebroplasty treatment of steroid-induced osteoporotic compression fractures.," *Arthritis Rheum*, 41(1), pp. 171-175.
- [80] Belkoff, S. M., Maroney, M., Fenton, D. C., and Mathis, J. M., 1999, "An in vitro biomechanical evaluation of bone cements used in percutaneous vertebroplasty," *Bone*, 25(2 Suppl), pp. 23s-26s.
- [81] Sun, K., and Liebschner, M. A., 2004, "Biomechanics of prophylactic vertebral reinforcement," *Spine (Phila Pa 1976)*, 29(13), pp. 1428-1435; discussion 1435.
- [82] Kallmes, D. F., and Jensen, M. E., 2003, "Percutaneous vertebroplasty," *Radiology*, 229(1), pp. 27-36.
- [83] Galibert, P., Deramond, H., Rosat, P., and Le Gars, D., 1987, "[Preliminary note on the treatment of vertebral angioma by percutaneous acrylic vertebroplasty]," *Neuro-Chirurgie*, 33(2), pp. 166-168.
- [84] Jensen, M. E., Evans, A. J., Mathis, J. M., Kallmes, D. F., Cloft, H. J., and Dion, J. E., 1997, "Percutaneous polymethylmethacrylate vertebroplasty in the treatment of osteoporotic vertebral body compression fractures: technical aspects," *AJNR Am J Neuroradiol*, 18(10), pp. 1897-1904.
- [85] Predey, T. A., Sewall, L. E., and Smith, S. J., 2002, "Percutaneous vertebroplasty: new treatment for vertebral compression fractures," *American family physician*, 66(4), pp. 611-615.
- [86] Avery J Evans, M. E. J., Kevin E Kip, Andrew J DeNardo, Gregory J Lawler, Geoffrey A Negin, Kent B Remley, Selene M Boutin, and Steven A Dunnagan., 2003, "Vertebral compression fractures: pain reduction and improvement in functional mobility after percutaneous polymethylmethacrylate vertebroplasty retrospective report of 245 cases. ," *Radiology*, 226(2):366-372, Feb 2003., 226(2), pp. 366-372.
- [87] Carrodeguas, R. G., Lasa, B. V., and Del Barrio, J. S., 2004, "Injectable acrylic bone cements for vertebroplasty with improved properties," *Journal of biomedical materials research. Part B, Applied biomaterials*, 68(1), pp. 94-104.
- [88] Lewis, G., 2006, "Injectable bone cements for use in vertebroplasty and kyphoplasty: state-of-the-art review," *Journal of biomedical materials research. Part B, Applied biomaterials*, 76(2), pp. 456-468.
- [89] Berlemann, U., Ferguson, S. J., Nolte, L. P., and Heini, P. F., 2002, "Adjacent vertebral failure after vertebroplasty. A biomechanical investigation," *J Bone Joint Surg Br*, 84(5), pp. 748-752.
- [90] Tanigawa, N., Komemushi, A., Kariya, S., Kojima, H., Shomura, Y., and Sawada, S., 2006, "Radiological follow-up of new compression fractures following percutaneous vertebroplasty," *Cardiovascular and interventional radiology*, 29(1), pp. 92-96.
- [91] Huiskes, R., Weinans, H., and van Rietbergen, B., 1992, "The relationship between stress shielding and bone resorption around total hip stems and the effects of flexible materials," *Clin Orthop Relat Res*(274), pp. 124-134.
- [92] Belkoff, S. M., Mathis, J. M., Jasper, L. E., and Deramond, H., 2001, "The biomechanics of vertebroplasty. The effect of cement volume on mechanical behavior," *Spine (Phila Pa 1976)*, 26(14), pp. 1537-1541.

- [93] Molloy, S., Mathis, J. M., and Belkoff, S. M., 2003, "The effect of vertebral body percentage fill on mechanical behavior during percutaneous vertebroplasty," *Spine (Phila Pa 1976)*, 28(14), pp. 1549-1554.
- [94] Baroud, G., Nemes, J., Heini, P., and Steffen, T., 2003, "Load shift of the intervertebral disc after a vertebroplasty: a finite-element study," *Eur Spine J*, 12(4), pp. 421-426.
- [95] Farooq, N., Park, J. C., Pollintine, P., Annesley-Williams, D. J., and Dolan, P., 2005, "Can vertebroplasty restore normal load-bearing to fractured vertebrae?," *Spine (Phila Pa 1976)*, 30(15), pp. 1723-1730.
- [96] Polikeit, A., Nolte, L. P., and Ferguson, S. J., 2003, "The effect of cement augmentation on the load transfer in an osteoporotic functional spinal unit: finite-element analysis," *Spine (Phila Pa 1976)*, 28(10), pp. 991-996.
- [97] Chiang, C. K., Wang, Y. H., Yang, C. Y., Yang, B. D., and Wang, J. L., 2009, "Prophylactic vertebroplasty may reduce the risk of adjacent intact vertebra from fatigue injury: an ex vivo biomechanical study," *Spine (Phila Pa 1976)*, 34(4), pp. 356-364.
- [98] Kayanja, M. M., Togawa, D., and Lieberman, I. H., 2005, "Biomechanical changes after the augmentation of experimental osteoporotic vertebral compression fractures in the cadaveric thoracic spine," *Spine J*, 5(1), pp. 55-63.
- [99] Langdon, J., Way, A., Heaton, S., Bernard, J., and Molloy, S., 2009, "The management of spinal metastases from renal cell carcinoma," *Annals of the Royal College of Surgeons of England*, 91(8), pp. 649-652.
- [100] Aquarius, R., Homminga, J., Hosman, A. J., Verdonschot, N., and Tanck, E., 2014, "Prophylactic vertebroplasty can decrease the fracture risk of adjacent vertebrae: an in vitro cadaveric study," *Med Eng Phys*, 36(7), pp. 944-948.
- [101] Kobayashi, N., Numaguchi, Y., Fuwa, S., Uemura, A., Matsusako, M., Okajima, Y., Ishiyama, M., and Takahashi, O., 2009, "Prophylactic vertebroplasty: cement injection into non-fractured vertebral bodies during percutaneous vertebroplasty," *Academic radiology*, 16(2), pp. 136-143.
- [102] Rohlmann, A., Consmuller, T., Dreischarf, M., Bashkuev, M., Disch, A., Pries, E., Duda, G. N., and Schmidt, H., 2014, "Measurement of the number of lumbar spinal movements in the sagittal plane in a 24-hour period," *Eur Spine J*, 23(11), pp. 2375-2384.
- [103] Rohlmann, A. F., Bergmann, G. F.-G., F., Graichen F Fau - Weber, U., and Weber, U., 1995, "In vivo measurement of implant loads in a patient with a fractured vertebral body," *European spine journal*, 4 (6)(0940-6719 (Print)), pp. 347-353.
- [104] Wilke, H. J., Neef, P., Caimi, M., Hoogland, T., and Claes, L. E., 1999, "New in vivo measurements of pressures in the intervertebral disc in daily life," *Spine (Phila Pa 1976)*, 24(8), pp. 755-762.
- [105] MySpine\_A\_NEW\_PREDICTIVE\_TOOL\_FOR\_LUMBAR\_SPINE\_SURGERY, "Lacroix Damien , <http://www.myspineproject.eu/>."
- [106] SpineFX\_training\_network, "Hall, R. M., <http://www.spinefx.eu/>."
- [107] Cristofolini, L., Brandolini, N., Danesi, V., and Viceconti, M., 2012, "Sensitivity of strain in the vertebral body to loading direction," *Journal of Biomechanics*, pp. pp. 616-616.

- [108] Hongo, M., Abe, E., Shimada, Y., Murai, H., Ishikawa, N., and Sato, K., 1999, "Surface Strain Distribution on Thoracic and Lumbar Vertebrae Under Axial Compression: The Role in Burst Fractures," *Spine*, 24(12), p. 1197.
- [109] Oakland, R. J., Furtado, N. R., Wilcox, R. K., Timothy, J., and Hall, R. M., 2009, "Preliminary biomechanical evaluation of prophylactic vertebral reinforcement adjacent to vertebroplasty under cyclic loading," *The Spine Journal*, 9(2), pp. 174-181.
- [110] Lochmüller, E. M., Eckstein, F., Kaiser, D., Zeller, J. B., Landgraf, J., Putz, R., and Steldinger, R., 1998, "Prediction of vertebral failure loads from spinal and femoral dual-energy x-ray absorptiometry, and calcaneal ultrasound: an in situ analysis with intact soft tissues," *Bone*, 23(5), pp. 417-424.
- [111] Dreischarf, M., Zander, T., Shirazi-Adl, A., Puttlitz, C. M., Adam, C. J., Chen, C. S., Goel, V. K., Kiapour, A., Kim, Y. H., Labus, K. M., Little, J. P., Park, W. M., Wang, Y. H., Wilke, H. J., Rohlmann, A., and Schmidt, H., 2014, "Comparison of eight published static finite element models of the intact lumbar spine: predictive power of models improves when combined together," *J Biomech*, 47(8), pp. 1757-1766.
- [112] Wilcox, R. K., Allen, D. J., Hall, R. M., Limb, D., Barton, D. C., and Dickson, R. A., 2004, "A dynamic investigation of the burst fracture process using a combined experimental and finite element approach," *Eur Spine J*, 13(6), pp. 481-488.
- [113] Chevalier, Y., Pahr, D., and Zysset, P. K., 2009, "The role of cortical shell and trabecular fabric in finite element analysis of the human vertebral body," *J Biomech Eng*, 131(11), p. 111003.
- [114] Keller, T. S., Spengler, D. F., and Hansson, T. H., 1987, "Mechanical behavior of the human lumbar spine. I. Creep analysis during static compressive loading," *J Orthop Res*, 5, pp. 467-478.
- [115] Patwardhan, A. G., Havey, R. M., Meade, K. P., Lee, B., and Dunlap, B., 1999, "A follower load increases the load-carrying capacity of the lumbar spine in compression," *Spine (Phila Pa 1976)*, 24(10), pp. 1003-1009.
- [116] Aquarius, R., Homminga, J., Verdonschot, N., and Tanck, E., 2011, "The fracture risk of adjacent vertebrae is increased by the changed loading direction after a wedge fracture," *Spine (Phila Pa 1976)*, 36(6), pp. E408-412.
- [117] Furtado, N., Oakland, R. J., Wilcox, R. K., and Hall, R. M., 2007, "A Biomechanical Investigation of Vertebroplasty in Osteoporotic Compression Fractures and in Prophylactic Vertebral Reinforcement," *Spine*, 32(17), pp. E480-E487  
410.1097/BRS.1090b1013e31811ea31812ee.
- [118] Pollintine, P., Luo, J., Offa-Jones, B., Dolan, P., and Adams, M. A., 2009, "Bone creep can cause progressive vertebral deformity," *Bone*, 45(3), pp. 466-472.
- [119] Jiang, G., Luo, J., Pollintine, P., Dolan, P., Adams, M. A., and Eastell, R., 2010, "Vertebral fractures in the elderly may not always be "osteoporotic"," *Bone*, 47(1), pp. 111-116.
- [120] Fahim, D. K., Sun, K., Tawackoli, W., Mendel, E., Rhines, L. D., Burton, A. W., Kim, D. H., Ehni, B. L., and Liebschner, M. A., 2011, "Premature adjacent vertebral fracture after vertebroplasty: a biomechanical study," *Neurosurgery*, 69(3), pp. 733-744.
- [121] Dean, J. R., Ison, K. T., and Gishen, P., 2000, "The strengthening effect of percutaneous vertebroplasty," *Clinical radiology*, 55(6), pp. 471-476.

- [122] Danesi V., Erani P., Brandolini N., Mateusz M Juszczyk, and L., C., 2015, "Effect of the in vitro boundary conditions on the strain experienced by the vertebral body," submitted to Journal of Biomechanical Engineering.
- [123] Bürklein, D., Lochmüller, E. M., Kuhn, V., Grimm, J., Barkmann, R., Müller, R., and Eckstein, F., 2001, "Correlation of thoracic and lumbar vertebral failure loads with in situ vs. ex situ dual energy X-ray absorptiometry," *Journal of Biomechanics*, 34(5), pp. 579-587.
- [124] Lochmüller, E. M., Bürklein, D., Kuhn, V., Glaser, C., Müller, R., Gluer, C. C., and Eckstein, F., 2002, "Mechanical strength of the thoracolumbar spine in the elderly: prediction from in situ dual-energy X-ray absorptiometry, quantitative computed tomography (QCT), upper and lower limb peripheral QCT, and quantitative ultrasound," *Bone*, 31(1), pp. 77-84.
- [125] Luo, J., Bertram, W., Sangar, D., Adams, M. A., Annesley-Williams, D. J., and Dolan, P., 2010, "Is kyphoplasty better than vertebroplasty in restoring normal mechanical function to an injured spine?," *Bone*, 46(4), pp. 1050-1057.
- [126] Moro, M., Hecker, A. T., Bouxsein, M. L., and Myers, E. R., 1995, "Failure load of thoracic vertebrae correlates with lumbar bone mineral density measured by DXA," *Calcif Tissue Int*, 56(3), pp. 206-209.
- [127] Przybyla, A. S., Skrzypiec, D., Pollintine, P., Dolan, P., and Adams, M. A., 2007, "Strength of the cervical spine in compression and bending," *Spine (Phila Pa 1976)*, 32(15), pp. 1612-1620.
- [128] Skrzypiec, D., Tarala, M., Pollintine, P., Dolan, P., and Adams, M. A., 2007, "When Are Intervertebral Discs Stronger Than Their Adjacent Vertebrae?," *Spine*, 32(22), pp. 2455-2461  
2410.1097/BRS.2450b2013e3181573b3181587.
- [129] Andresen, R., Werner, H., and Schober, H., 1998, "Contribution of the cortical shell of vertebrae to mechanical behaviour of the lumbar vertebrae with implications for predicting fracture risk," *Br J Radiol*, 71(847), pp. 759-765.
- [130] Buckley, J. M., Loo, K., and Motherway, J., 2007, "Comparison of quantitative computed tomography-based measures in predicting vertebral compressive strength," *Bone*, 40(3), pp. 767-774.
- [131] Cheng, X. G., Nicholson, P. H., Boonen, S., Lowet, G., Brys, P., Aerssens, J., Van der Perre, G., and Dequeker, J., 1997, "Prediction of vertebral strength in vitro by spinal bone densitometry and calcaneal ultrasound," *J Bone Miner Res*, 12(10), pp. 1721-1728.
- [132] Dall'Ara, E., Schmidt, R., Pahr, D., Varga, P., Chevalier, Y., Patsch, J., Kainberger, F., and Zysset, P., 2010, "A nonlinear finite element model validation study based on a novel experimental technique for inducing anterior wedge-shape fractures in human vertebral bodies in vitro," *Journal of Biomechanics*, 43(12), pp. 2374-2380.
- [133] Eriksson, S. A., Isberg, B. O., and Lindgren, J. U., 1989, "Prediction of vertebral strength by dual photon absorptiometry and quantitative computed tomography," *Calcif Tissue Int*, 44(4), pp. 243-250.
- [134] Hansson, T., Roos, B., and Nachemson, A., 1980, "The bone mineral content and ultimate compressive strength of lumbar vertebrae," *Spine (Phila Pa 1976)*, 5(1), pp. 46-55.
- [135] Haidekker, M. A., Andresen, R., and Werner, H. J., 1999, "Relationship Between Structural Parameters, Bone Mineral Density and Fracture Load in Lumbar Vertebrae, Based on High-Resolution Computed Tomography, Quantitative Computed Tomography and Compression Tests," *Osteoporosis International*, 9(5), pp. 433-440.

- [136] Mirzaei, M., Zeinali, A., Razmjoo, A., and Nazemi, M., 2009, "On prediction of the strength levels and failure patterns of human vertebrae using quantitative computed tomography (QCT)-based finite element method," *Journal of Biomechanics*, 42(11), pp. 1584-1591.
- [137] Rotter, R., Martin, H., Fuerderer, S., Gabl, M., Roeder, C., Heini, P., and Mittlmeier, T., 2010, "Vertebral body stenting: a new method for vertebral augmentation versus kyphoplasty," *European spine journal*, 19(6), pp. 916-923.
- [138] Singer, K., Edmondston, S., Day, R., Breidahl, P., and Price, R., 1995, "Prediction of thoracic and lumbar vertebral body compressive strength: correlations with bone mineral density and vertebral region," *Bone*, 17(2), pp. 167-174.
- [139] Teo, E. C., Paul, J. P., Evans, J. H., and Ng, H. W., 2001, "Experimental investigation of failure load and fracture patterns of C2 (axis)," *J Biomech*, 34(8), pp. 1005-1010.
- [140] Granhed, H., Jonson, R., and Hansson, T., 1989, "Mineral content and strength of lumbar vertebrae. A cadaver study," *Acta orthopaedica Scandinavica*, 60(1), pp. 105-109.
- [141] Buckley, J. M., Cheng, L., Loo, K., Slyfield, C., and Xu, Z., 2007, "Quantitative Computed Tomography-Based Predictions of Vertebral Strength in Anterior Bending," *Spine*, 32(9), pp. 1019-1027.
- [142] Aquarius, R., van der Zijden, A. M., Homminga, J., Verdonschot, N., and Tanck, E., 2013, "Does bone cement in percutaneous vertebroplasty act as a stress riser?," *Spine (Phila Pa 1976)*, 38(24), pp. 2092-2097.
- [143] Heini, P. F., Berlemann, U., Kaufmann, M., Lippuner, K., Fankhauser, C., and van Landuyt, P., 2001, "Augmentation of mechanical properties in osteoporotic vertebral bones--a biomechanical investigation of vertebroplasty efficacy with different bone cements," *Eur Spine J*, 10(2), pp. 164-171.
- [144] Ikeuchi, M., Yamamoto, H., Shibata, T., and Otani, M., 2001, "Mechanical augmentation of the vertebral body by calcium phosphate cement injection," *Journal of orthopaedic science : official journal of the Japanese Orthopaedic Association*, 6(1), pp. 39-45.
- [145] Kolb, J. P., Kueny, R. A., Puschel, K., Boger, A., Rueger, J. M., Morlock, M. M., Huber, G., and Lehmann, W., 2013, "Does the cement stiffness affect fatigue fracture strength of vertebrae after cement augmentation in osteoporotic patients?," *Eur Spine J*, 22(7), pp. 1650-1656.
- [146] Rotter, R., Schmitt, L., Gierer, P., Schmitz, K. P., Noriega, D., Mittlmeier, T., Meeder, P. J., and Martin, H., 2015, "Minimum cement volume required in vertebral body augmentation--A biomechanical study comparing the permanent SpineJack device and balloon kyphoplasty in traumatic fracture," *Clin Biomech (Bristol, Avon)*, 30(7), pp. 720-725.
- [147] Kruger, A., Baroud, G., Noriega, D., Figiel, J., Dorschel, C., Ruchholtz, S., and Oberkircher, L., 2013, "Height restoration and maintenance after treating unstable osteoporotic vertebral compression fractures by cement augmentation is dependent on the cement volume used," *Clin Biomech (Bristol, Avon)*, 28(7), pp. 725-730.
- [148] Lewis, G., Schwardt, J. D., Slater, T. A., and Janna, S., 2008, "Evaluation of a synthetic vertebral body augmentation model for rapid and reliable cyclic compression life testing of materials for balloon kyphoplasty," *Journal of biomedical materials research. Part B, Applied biomaterials*, 87(1), pp. 179-188.
- [149] Wilke, H. J., Mehnert, U., Claes, L. E., Bierschneider, M. M., Jaksche, H., and Boszczyk, B. M., 2006, "Biomechanical evaluation of vertebroplasty and kyphoplasty with polymethyl

- methacrylate or calcium phosphate cement under cyclic loading," *Spine (Phila Pa 1976)*, 31(25), pp. 2934-2941.
- [150] Steens, J., Verdonshot, N., Aalsma, A. M., and Hosman, A. J., 2007, "The influence of endplate-to-endplate cement augmentation on vertebral strength and stiffness in vertebroplasty," *Spine (Phila Pa 1976)*, 32(15), pp. E419-422.
- [151] Lim, T. H., Brebach, G. T., Renner, S. M., Kim, W. J., Kim, J. G., Lee, R. E., Andersson, G. B., and An, H. S., 2002, "Biomechanical evaluation of an injectable calcium phosphate cement for vertebroplasty," *Spine (Phila Pa 1976)*, 27(12), pp. 1297-1302.
- [152] Molloy, S., Riley, L. H., 3rd, and Belkoff, S. M., 2005, "Effect of cement volume and placement on mechanical-property restoration resulting from vertebroplasty," *AJNR Am J Neuroradiol*, 26(2), pp. 401-404.
- [153] Cristofolini, L., Ferguson, S. J., Danesi, V., Erani, P., Viceconti, M., and Brandolini, N., IN PRESS, "A preliminary in vitro biomechanical evaluation of prophylactic cement augmentation of the thoracolumbar vertebrae," *Journal of Mechanics in Medicine and Biology* in press.
- [154] Belkoff, S. M., Mathis, J. M., Jasper, L. E., and Deramond, H., 2001, "An ex vivo biomechanical evaluation of a hydroxyapatite cement for use with vertebroplasty," *Spine (Phila Pa 1976)*, 26(14), pp. 1542-1546.
- [155] Tohmeh, A. G., Mathis, J. M., Fenton, D. C., Levine, A. M., and Belkoff, S. M., 1999, "Biomechanical efficacy of unipedicular versus bipedicular vertebroplasty for the management of osteoporotic compression fractures," *Spine (Phila Pa 1976)*, 24(17), pp. 1772-1776.
- [156] Kinzl, M., Schwiedrzik, J., Zysset, P. K., and Pahr, D. H., 2013, "An experimentally validated finite element method for augmented vertebral bodies," *Clin Biomech (Bristol, Avon)*, 28(1), pp. 15-22.
- [157] Kinzl, M., Benneker, L. M., Boger, A., Zysset, P. K., and Pahr, D. H., 2012, "The effect of standard and low-modulus cement augmentation on the stiffness, strength, and endplate pressure distribution in vertebroplasty," *Eur Spine J*, 21(5), pp. 920-929.
- [158] Muller, R., Gerber, S. C., and Hayes, W. C., 1998, "Micro-compression: a novel technique for the nondestructive assessment of local bone failure," *Technology and health care : official journal of the European Society for Engineering and Medicine*, 6(5-6), pp. 433-444.
- [159] Christen, D., Levchuk, A., Schori, S., Schneider, P., Boyd, S. K., and Muller, R., 2012, "Deformable image registration and 3D strain mapping for the quantitative assessment of cortical bone microdamage," *Journal of Mechanical Behavior of Biomedical Materials*, 8, pp. 184-193.
- [160] Thurner, P. J., Wyss, P., Voide, R., Stauber, M., Stampanoni, M., Sennhauser, U., and Muller, R., 2006, "Time-lapsed investigation of three-dimensional failure and damage accumulation in trabecular bone using synchrotron light," *Bone*, 39(2), pp. 289-299.
- [161] Shah, J. S., Coggins, J., Rogers, R., Jayson, M. I., and Hampson, W. G., 1976, "Surface strain distribution in isolated single lumbar vertebrae," *Ann Rheum Dis*, 35(1), pp. 51-55.
- [162] Shah, J., Hampson, W., and Jayson, M., 1978, "The distribution of surface strain in the cadaveric lumbar spine," *J Bone Joint Surg Br*, 60-B(2), pp. 246-251.
- [163] Lin, H. S., Liu, Y. K., and Adams, K. H., 1978, "Mechanical response of the lumbar intervertebral joint under physiological (complex) loading," *J Bone Joint Surg Am*, 60(1), pp. 41-55.

- [164] Frei, H., Oxland, T. R., and Nolte, L. P., 2002, "Thoracolumbar spine mechanics contrasted under compression and shear loading," *J Orthop Res.*, 20(6), pp. 1333-1338.
- [165] Kayanja, M. M., Ferrara, L. A., and Lieberman, I. H., 2004, "Distribution of anterior cortical shear strain after a thoracic wedge compression fracture," *The Spine Journal*, 4(1), pp. 76-87.
- [166] Campos-Lopez, J. P., Fuerte-Hernandez, A., Hernandez-Gomez, L. H., Martinez-Garcia, A., Beltran-Fernandez, J. A., and Urriolagoitia-Calderon, G., 2015, "Determination of the mechanical properties of lumbar porcine vertebrae with 2D digital image correlation," *Journal of applied biomaterials & functional materials*, 13(3), pp. e195-200.
- [167] Giambini, H. W., H; Nassr, A; An, K; Dragomir-Daescu, D, 2013, "Surface Strain Analysis Using Digital Image Correlation in Induced Vertebral Wedge Fracture," *ORS 2013 Annual Meeting*.
- [168] Palanca M, B. T., Cristofolini L. , 2015, "Use of digital image correlation to understand the biomechanics of the vertebra," *J Mech Med Biol*, 15:1540001-1540010.
- [169] Grassi, L., and Isaksson, H., 2015, "Extracting accurate strain measurements in bone mechanics: A critical review of current methods," *Journal of the mechanical behavior of biomedical materials*, 50, pp. 43-54.
- [170] Roberts, B. C., Perilli, E., and Reynolds, K. J., 2014, "Application of the digital volume correlation technique for the measurement of displacement and strain fields in bone: a literature review," *J Biomech*, 47(5), pp. 923-934.
- [171] Hussein, A. I., Barbone, P. E., and Morgan, E. F., 2012, "Digital Volume Correlation for Study of the Mechanics of Whole Bones," *Procedia IUTAM*, 4, pp. 116-125.

# **Chapter 2: Reproducible reference frame for *in vitro* testing of the human vertebrae**

Valentina Danesi MEng<sup>1,2</sup>, Lorenzo Zani BEng<sup>1</sup>, Axel Scheele, BSc<sup>3</sup>,  
Francesco Berra MEng<sup>2</sup>, Luca Cristofolini, PhD<sup>2</sup>

<sup>1</sup> Laboratory for Medical Technology, Rizzoli Orthopaedic Institute, Bologna, Italy

<sup>2</sup> Department of Industrial Engineering, School of Engineering and Architecture, University  
of Bologna, Italy

<sup>3</sup> Department of Biomedical Engineering, Delft University of Technology, Delft, The  
Netherlands

*The candidate was the main investigator of the present study. This paper was published on  
Journal of Biomechanics*

## 2.1 Abstract

Definition of an anatomical reference frame is necessary for *in vitro* biomechanical testing. Nevertheless, there is neither a clear recommendation, nor consensus in the literature concerning an anatomical reference frame for *in vitro* testing of the human vertebrae. The scope of this work is to define a reference frame for the human vertebrae for *in vitro* applications. The proposed anatomical reference frame relies on alignment of well-defined points on the endplates, and on two landmarks on the posterior wall. The repeatability of the proposed alignment procedure has been tested *in vitro* by 5 operators, on 7 specimens. Furthermore, the feasibility and repeatability of the proposed procedure was assessed *in silico*, using CT-scans of the same specimens.

Variations between operators were slightly larger than between repetitions by the same operator. The intra-operator *in vitro* repeatability was better than 3° for all angles. The inter-operator *in vitro* repeatability was better than 9° for all angles. The lateral tilt was the most repeatable angle, while anterior-posterior tilt was least repeatable. The repeatability when alignment was performed *in silico* on CT-scans was comparable to that obtained *in vitro*, on the physical specimens.

This is the first time than an anatomical reference frame is formally defined and validated for the human vertebrae.

The adoption of this reference frame will provide more reproducible alignment of the specimens and of the test load. This will enable better *in vitro* biomechanical tests, and comparisons with numerical models.

**Keywords:** Human vertebrae, Thoraco-lumbar spine, Vertebral body, Anatomical Reference frame, Mechanical *in vitro* testing, *In vitro* landmarks

## 2.2 Introduction

There is a consensus within the biomechanics community (e.g. International Society of Biomechanics, ISB) about the need to standardize reference frames [1-3]. Univocal definition of reference frames is extremely important to allow comparisons of data-sets from different studies [4-7]. *In vitro* reference frames enable the correct alignment of the specimens and the applied loads, and the definition of reproducible testing conditions [2, 8]. While *in vivo* a reference frame is based on anatomical landmarks that need to be palpable non-invasively [9] an *in vitro* reference can rely on landmarks that are accessed invasively (e.g. when soft tissues are removed).

Nevertheless, there is still some lack of consensus about the definition of reference frames for *in vitro* biomechanical testing, especially for the vertebrae [2] (Table 2-1). This makes comparisons between various studies difficult, if not impossible.

In most of the previous works, details on the procedures to align the vertebra are missing: single vertebrae [10, 11] or functional spinal units (FSU) [12, 13] had their extremities embedded in bone cement to provide parallel planes for mechanical loading, but information about the alignment procedure is not reported.

When some kind of alignment is indicated, the procedure usually refers to horizontal alignment of anatomical structures such as the endplates or intervertebral disks, but little anatomical detail is given [14-16]. Alternatively, a steel rod was clamped in the medullary canal, against the posterior wall of the vertebral body to align a single vertebra [17], or three-adjacent-vertebra segments [18]. This procedure seems able to firmly hold the specimens, but cannot guarantee consistent anatomical alignment. A robust reference frame for single vertebrae is based upon CT scans: the centre of mass (CoM) of the vertebra was computed, while projections of the frontal and sagittal planes containing the CoM were used to align the specimen in the testing machine [19].

The group of Panjabi probably performed the most extensive anatomical study to provide a quantitative vertebral geometric database [20-23]. The reference frame proposed by Panjabi et al. is based on the identification of four landmarks (right and left, superior and inferior edges of the posterior wall of the vertebral body). The digitized coordinates of these four points are used to define the reference planes, using a least-squares method. However, this procedure is difficult to implement for two reasons: (i) the need of digitizing the landmarks; and (ii) the complex procedure for aligning the physical specimen with a reference frame which is numerically derived from such

digitized coordinates. In fact, the reference frame of Panjabi *et al* was conceived to perform anatomical measurements, not for *in vitro* tests.

Table 2-1: Overview of the *in vitro* anatomical reference frames proposed in the literature for testing the human vertebrae.

	Type of specimen	Anterior-Posterior Tilt	Lateral Tilt	Axial Rotation
[21-23]	Whole vertebra	Alignment of anatomical landmarks	Alignment of anatomical landmarks	Alignment of anatomical landmarks
[15]	Three-adjacent-vertebrae segment	Parallelism of endplates	Posterior wall of the central vertebra vertical respect to the ground	Not specified
[10]	Isolated vertebral body	Not specified	Not specified	Not specified
[14]	Functional Spinal Unit (FSU)	Align intervertebral disk horizontally	Align intervertebral disk horizontally	Not specified
[17]	Whole vertebra	Insertion of a rod through the spinal canal against the posterior wall of the vertebral body		
[18]	Three –adjacent-vertebrae segment	Insertion of a rod through the spinal canal against the posterior wall of the vertebral bodies		
[11]	Isolated vertebral body	Not specified	Not specified	Not specified
[13]	Functional Spinal Unit (FSU)	Not specified	Not specified	Not specified
[12]	Functional Spinal Unit (FSU)	Not specified	Not specified	Not specified
[19]	Isolated vertebral body without endplates	No alignment of anatomic landmarks but of points recognizable in CT scan and in the FE model		
[16]	Whole vertebra	Endplates perpendicular to the level of fixation pot carrying the bone cement	Endplates perpendicular to the level of fixation pot carrying the bone cement	Not specified

The main aim of this study was to provide a portable definition for a reproducible anatomical reference frame for the human vertebrae, suitable for *in vitro* applications. Such a reference frame must rely on robust anatomical landmarks, and needs to be implemented, consistently, by different operators. Consequently, the intra-operator and inter-operator repeatability of the proposed reference frame have been measured.

## **2.3 Material and Methods**

### **2.3.1 Definitions**

To leverage on past experience, the proposed reference frame adopted some part of the alignment commonly found in the literature (orientation of the endplates), and the most robust definition available for axial rotation (based on the posterior wall of the vertebral body). The reference frame was developed to be applicable both to isolated vertebrae, and to three-adjacent-vertebrae segments, where the central vertebra is investigated. In this work the reference frame was validated for the three-adjacent-vertebrae segment, which is the most critical case because of the limited visibility of the endplates.

The anatomical planes were defined as follows (Fig.2-1):

- The transverse plane is parallel to the endplates (if the endplates are not parallel to each other, the bisector of the two endplates is considered).
- The frontal plane is perpendicular to the transverse plane, and goes through points LL and LR. The landmarks LL and LR correspond to the left and right upper edges of the posterior wall of the central vertebra [21-23].
- The sagittal plane is perpendicular to the previous two planes.

The rotations were defined as follows:

- Lateral tilt is a rotation in the frontal plane (i.e. about an antero-posterior axis).
- Anterior-posterior tilt is a rotation in the sagittal plane (i.e. about a right-left axis).
- Axial rotation occurs in a transverse plane (i.e. about a cranio-caudal axis).

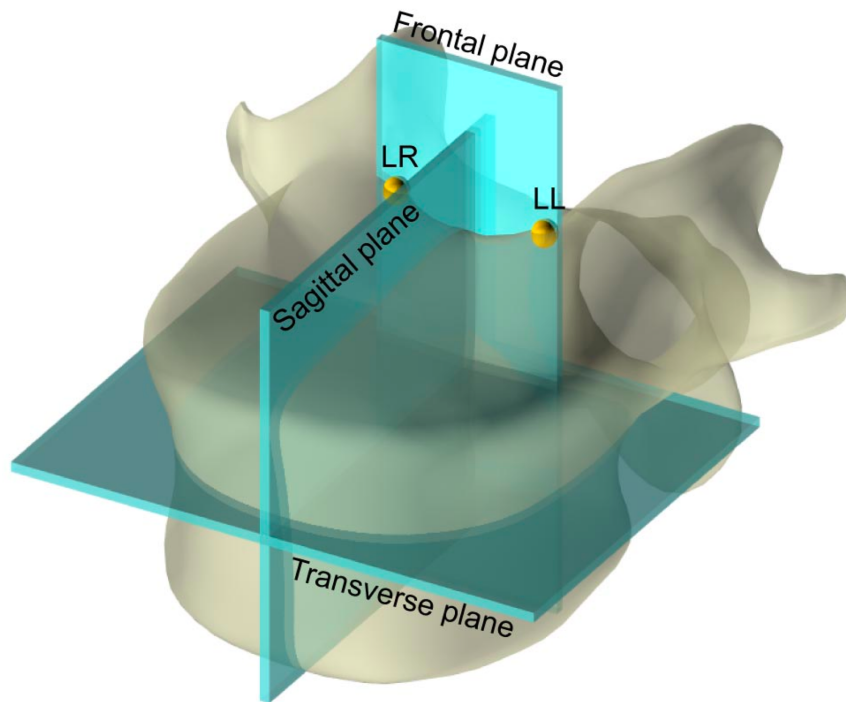


*Fig. 2-1 – Definition of the proposed anatomical reference frame for the vertebral body. The transverse plane is parallel to the endplates. The frontal plane is perpendicular to the transverse plane, and goes through points LL and LR. The landmarks LL and LR correspond to the left and right upper edges of the posterior wall of the central vertebra. The sagittal plane is perpendicular to the previous two planes.*

### **2.3.2 Guidelines for implementing an anatomical reference frame *in vitro***

All the surrounding tissues, with exception of the intervertebral disks, must be removed, including the ligaments. Special attention must be paid to the cavity between the vertebral body and the posterior element, because this is used for alignment. The posterior elements of the adjacent vertebrae must be removed using a saw, to remove excess material.

The posterior process of the central vertebra must be clamped in a 6-degree-of-freedom (6 DOF) clamp, which allows rotational adjustment about three axes. The 6 DOF clamp (which is mounted on a reference table) can be replaced by modelling clay as an adjustable support for the bone specimen, similar to [24]. First, a visual unaided preliminary alignment must be performed:

the peripheral portion of the endplates must be horizontal in the anterior and lateral view, and the posterior wall of the vertebral body parallel to the edge of the reference table in a cranial view.

Then, fine alignment must be carried out using a 6 DOF clamp in this sequence:

A. To align the vertebra in the frontal plane, the endplates must be aligned horizontally from an anterior point of view, using adjustable horizontal rulers. The specimen is correctly aligned when the right- and left-most points of both endplates are at the same height (Fig. 2-2A).

B. To align the vertebra in the sagittal plane the endplates must aligned horizontally from a lateral view using adjustable horizontal rulers. The specimen is correctly aligned when the most anterior and most posterior points of both endplates are at the same height (Fig. 2-2B).

C. To align the vertebra in the transverse plane the landmarks LL and LR at the upper corners of the posterior wall are aligned from a superior view, using a smaller engineering square (Fig. 2-2C).

If the landmarks for steps A) and B) are not recognizable because of the presence of osteophytes, the visible part of the endplates must be used for alignment. If the endplates are not parallel to each other, the bisector of the two endplates must be horizontal.

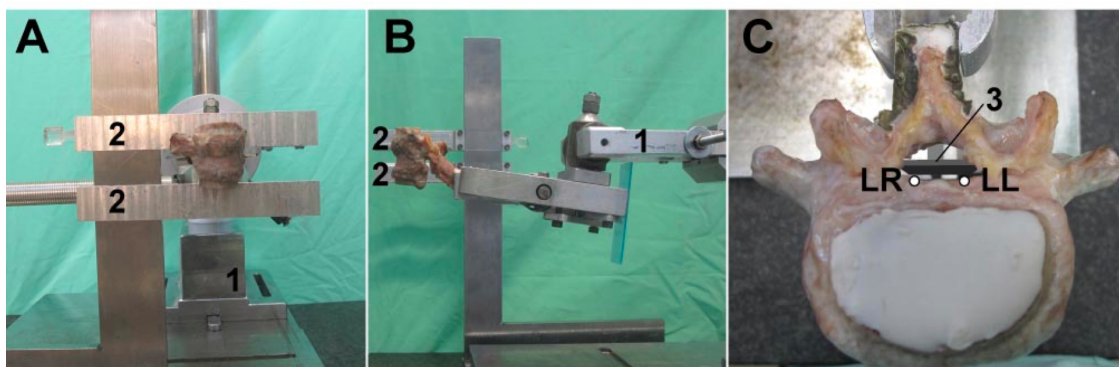


*Fig. 2-2 – Steps for aligning the vertebra, which is held in the 6DOF clamp (partially shown, (1)):* (A) alignment in the frontal plane using adjustable horizontal rulers (2). (B) Lateral view for the alignment in the sagittal plane using the adjustable horizontal rulers (2). (C) Top view of the vertebra. A vertical ruler (3) is co-planar with landmarks LL and LR (defined in Fig. 1) inside the

*spinal canal, to obtain the correct alignment in the transverse plane. In this picture, the distal vertebra was partially resected as part of a different study.*

### **2.3.3 Testing the intra-operator and inter-operator repeatability *in vitro***

Thoraco-lumbar specimens (Table 2-2), consisting of three-adjacent-vertebra segments were obtained through an ethically-approved program (IIAM, [www.iiam.org](http://www.iiam.org)) from donors free of musculoskeletal pathologies. The first 6 specimens (4 donors, 1female, 3males, age 49-84y.o.) were the training set, to optimize the alignment procedure (section 2.3.2). Other 7 specimens (different from the ones above: 2 donors, males, age 70-88y.o.) were the test set, to validate the procedure.

The spines were visually inspected and CT-scanned while submersed in saline solution (multislice BrightSpeed, GE Medical Systems, Waukesha, USA: tube current 160mA, 120kVp voltage, helical mode with 0.195 mm pixel in the transverse plane and 0.625 mm slice thickness).

To assess the intra-operator repeatability (i.e. when the same operator repeatedly aligns the same specimen) and the inter-operator repeatability (i.e. when different operators align the same specimen), five experienced operators aligned each specimen three times. To avoid any bias, the specimen orientation was modified between repetitions, so that the operator could not recognize previous alignments. For each repetition, the absolute orientation was measured using a goniometer (Mitutoyo, Tokyo, Japan; precision: 0.1degrees).

### **2.3.4 Testing the repeatability *in silico***

The CT-scans of the specimens used to test the repeatability *in vitro* were imported in dedicated software (LHPBuilder, B3C, Bologna, Italy). LHPBuilder supports handling of medical images, automatic segmentation, virtual palpation, and definition of customized reference frames [25, 26]. The same landmarks as for the *in vitro* alignment were identified by an experienced operator, three times for each specimen.

Table 2-2: Details of the specimen used in this study as a test set to validate the alignment procedure. In the first five columns, the details of the donors are listed. In the following three columns, the biomechanical dimensions are reported. The vertebral body height was measured between the centre of the upper endplate and the centre of the lower endplate. The antero-posterior depth was measured between the most anterior and the most posterior point at mid-height of the vertebral body. The vertebral body right-left width was measured between the most lateral points at mid-height of the vertebral body. The presence/absence of significant osteophytes is reported in the last column.

Specimen ID	Three-vertebra segment	Donor's details					Vertebral body details			
		Gender	Age at death (years)	Height (cm)	Weight (kg)	Cause of death	Height (mm)	Antero-posterior length (mm)	Right-left width (mm)	Presence of Osteophytes
T3-a	T2-T3-T4	M	70	168	86	Cardiac dysrhythmia	11.6	22.9	26.9	yes
T5-a	T4-T5-T6	M	70	168	86	Cardiac dysrhythmia	11.2	24.4	28.4	no
T7-a	T6-T7-T8	M	70	168	86	Cardiac dysrhythmia	17.6	30.5	25.9	yes
T9-a	T8-T9-T10	M	70	168	86	Cardiac dysrhythmia	15.5	33.2	29.8	yes
L3-a	L2-L3-L4	M	70	168	86	Cardiac dysrhythmia	24.7	32.1	42.9	no
L3-b	L2-L3-L4	M	88	180	77	Congestive heart failure	25.8	34.7	45.0	yes
L5-a	L4-L5-S1	M	70	168	86	Cardiac dysrhythmia	17.5	50.1	34.3	yes

### 2.3.5 Statistics

The intra-operator repeatability was quantified as follows:

- For each of the five operators, and each specimen, the standard deviation between the three repetitions was computed for each angle defining the specimen's orientation.
- The root-mean-square-average between specimens was computed, for each operator.

The inter-operator repeatability was quantified as follows:

- For each of the five operators, and each specimen, the average orientation (out of three repetitions) was computed.
- The reference orientation of each specimen was computed as the average between the five operators.

All analyses were performed using MatLab (2009Edition, MathWorks, Natick, MA, USA).

## 2.4 Results

The variation between *in vitro* repetitions performed by the same operator was less than 3° for all angles, with the exception of four outliers (Fig.2-3).

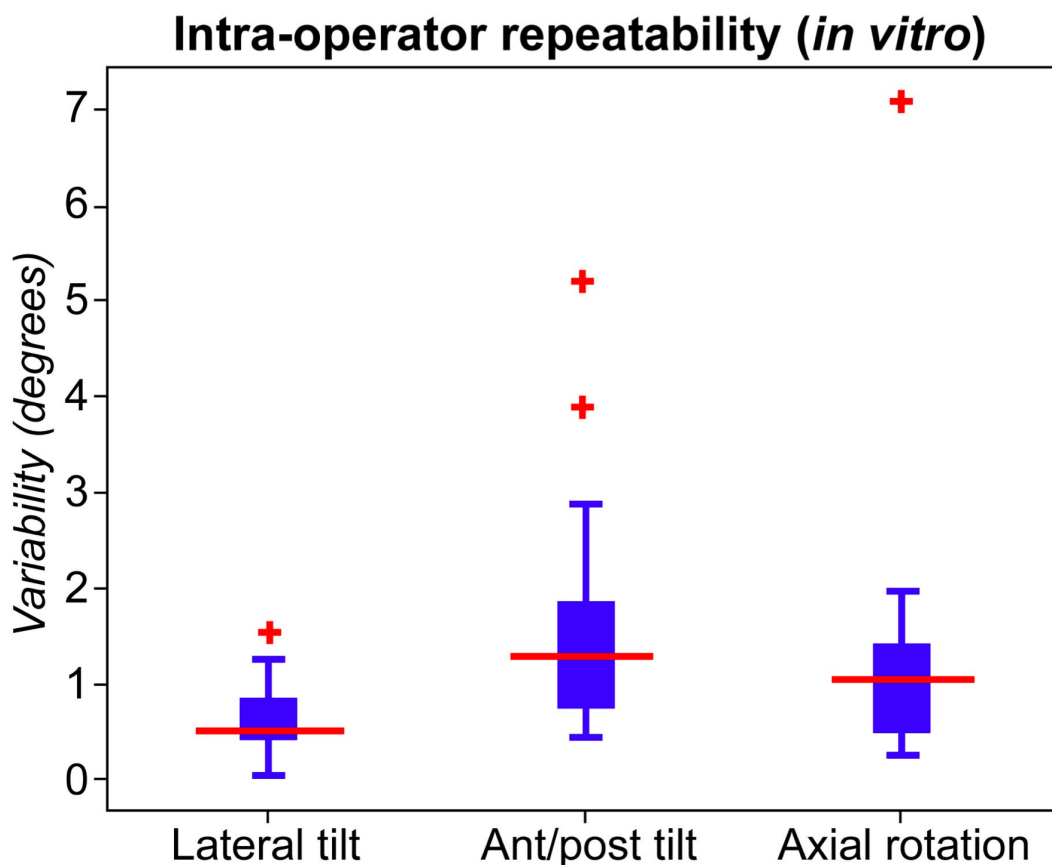


Fig.2-3 – *In vitro* intra-operator repeatability for the three angles defining the specimen's orientation (lateral tilt, anterior-posterior tilt, and axial rotation) reported in terms of standard

deviation between repetitions, for all operators. The central red mark indicates the median of the 5 operators over 7 specimens; the blue boxes includes the 25<sup>th</sup> to the 75<sup>th</sup> percentile; the whiskers extend to the most extreme data points. The outliers (i.e. those data points exceeding the 99% coverage range) are marked with red crosses, and were excluded from the analysis.

The lateral tilt was the most repeatable angle, while the anterior-posterior tilt was least repeatable. The orientation identified *in vitro* by the five operators fell within a range of 9° for all angles, with the exception of two outliers (Fig.2-4).

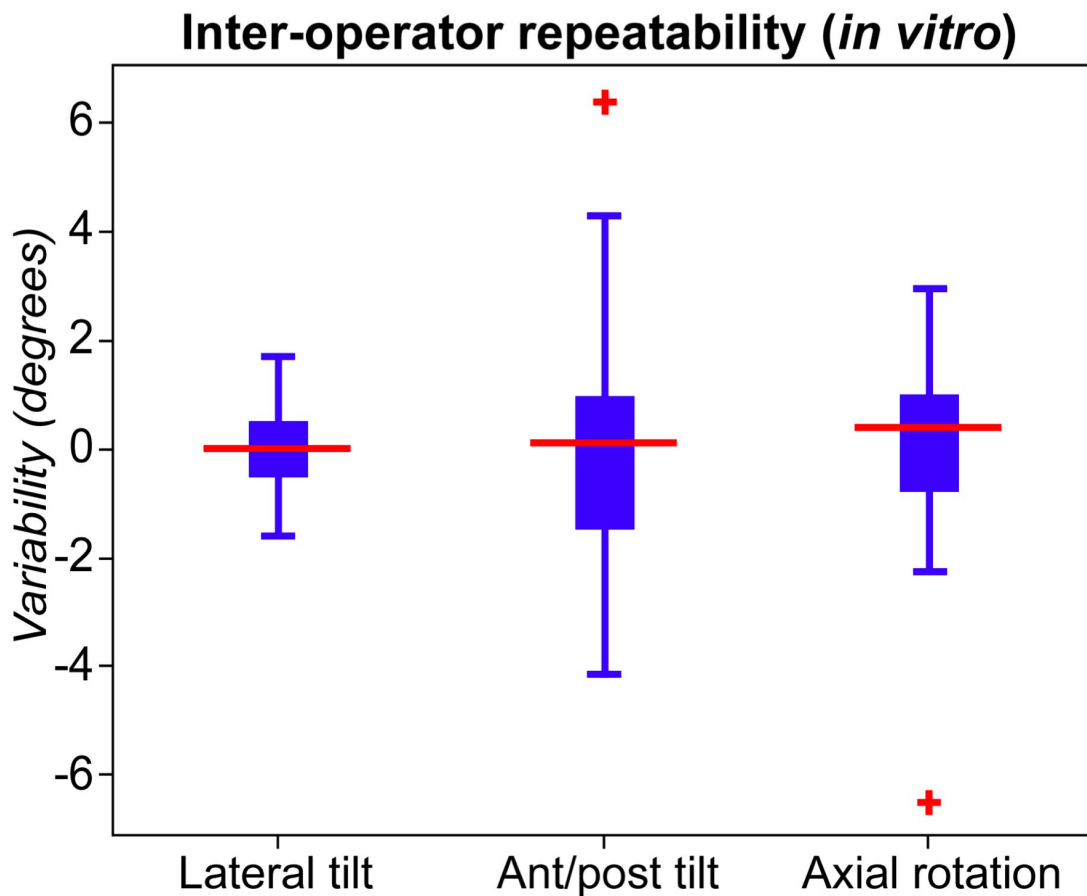


Fig. 2-4 – *In vitro* inter-operator repeatability for the three angles defining the specimen’s orientation reported in terms of mean variation between 5 operators (a positive angle corresponds respectively to: lateral tilt towards left; anterior tilt; axial rotation towards right). The central red mark indicates the median of the 5 operators; the blue boxes includes the 25<sup>th</sup> to the 75<sup>th</sup> percentile; the whiskers extend to the most extreme data points. The outliers (i.e. those data points exceeding the 99% coverage range) are marked with red crosses, and were excluded from the analysis.

Also the inter-operator test confirmed that the lateral tilt was most repeatable, while the anterior-posterior tilt was least repeatable. Variation between operators was slightly larger than between repetitions by the same operator (Fig.2-3 - 2-4). The intra-operator repeatability *in silico* was comparable to the *in vitro* one (Fig.2-5).

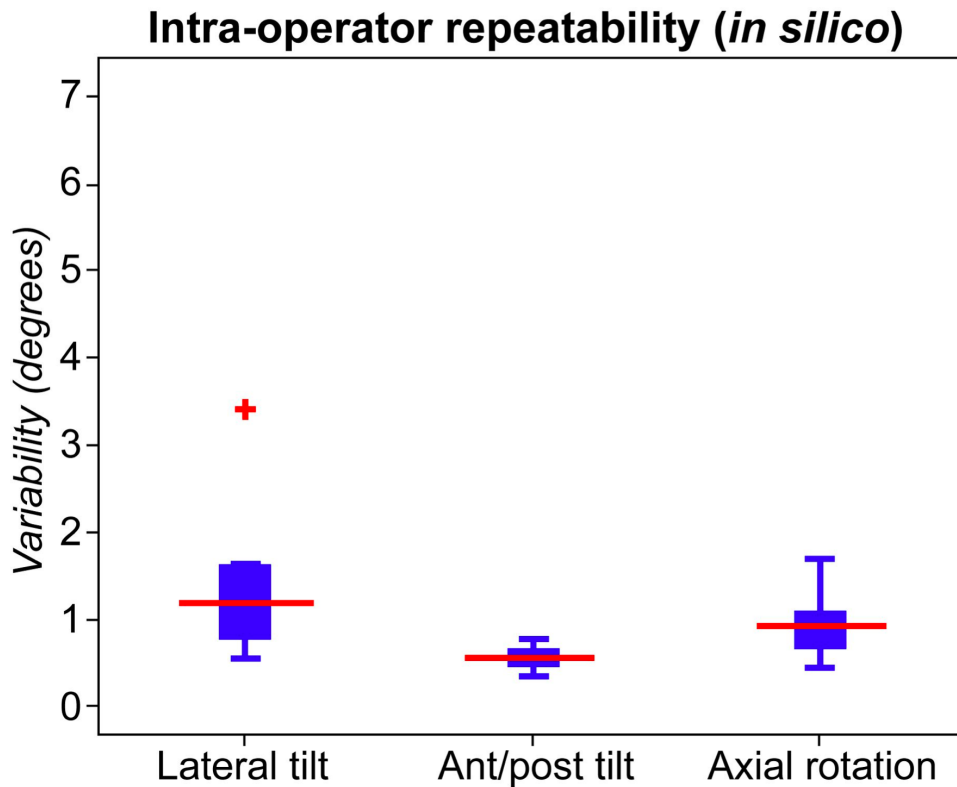


Fig. 2-5 – *In silico* intra-operator repeatability for the three angles defining the specimen’s orientation (lateral tilt, anterior-posterior tilt, and axial rotation) reported in terms of standard deviation between repetitions. The central red mark indicates the median of the specimens, the blue boxes includes the 25<sup>th</sup> to the 75<sup>th</sup> percentile, the whiskers extend to the most extreme data points. The outliers (i.e. those data points exceeding the 99% coverage range) are marked with red crosses, and were excluded from the analysis.

## 2.5 Discussion

While *in vitro* mechanical testing of the human vertebrae is regularly performed (e.g. [10-19]), no clear definition has been proposed for an anatomical reference frame for *in vitro* purposes.

The aim of this study was to formalize a proposal for a reference frame for the human thoracolumbar vertebrae.

The importance of alignment of trabecular bone is known: the Young's modulus and ultimate stress decrease by about 40% for a misalignment of 20° between the testing direction and the trabecular main direction [27]. Thus, since most of the vertebral body structure is trabecular, misalignment will result in a significant alteration of the vertebral strength.

To the Authors' knowledge, the current study defines and validates, for the first time, a reproducible reference frame of the human vertebrae for *in vitro* applications. The proposed reference frame relies on robust anatomical landmarks and can be consistently applied by different operators.

*In vitro*, lateral tilt was most repeatable, both for the same operator, and between operators. Conversely, the anterior-posterior tilt was least repeatable *in vitro*, both for the same operator, and between operators (Figs. 2-3 and 2-4). The main *in vitro* problem reported by the 5 operators was the identification of the most anterior and posterior landmarks, because of the ambiguity associated with observing the vertebra (which has some degree of asymmetry) from both right and left sides: this affects the anterior-posterior tilt. *In vitro*, lateral tilt was best repeatable, possibly because of the larger distance separating the most lateral points of the vertebral body (if the same error affects identification of a landmark, this propagates less heavily to the identification of a plane if the "lever arm" is longer).

*In silico* identification of the landmarks was somewhat easier, thanks to the LHPBuilder tools that enable adjustable thresholding, etc. [25, 26]. For this reason, comparable uncertainty was found for the alignment in all planes.

The outliers (Figs. 2-3 and 2-5) were associated with those specimens that were small in dimension (thoracic vertebrae).

Despite the presence of osteophytes in most specimens (Table 2-2), the *in vitro* alignment repeatability remained satisfactory. Landmarks LL and LR on the posterior wall of the vertebra were highly repeatable, because the posterior wall is seldom affected by deformity or osteophytes [20-23]. For this reason, the axial rotation is affected by limited uncertainty. Similar to most studies, the proposed reference frame does not rely on the posterior process, because this structure

is often affected by deformity and large inter-subject variations (inter-subject variations of about 10° [23]).

Direct comparison with other studies is not possible, as for no other vertebral reference frame the intra- and inter-operator repeatability have been published. Repeatability has not been quantified even for the reference frame by [21-23].

In the past, however, anatomical reference frames for the long bones have been investigated [2, 28, 29]:

- The alignment repeatability of the vertebrae is one order of magnitude worse than for long bones (tibia, femur, humerus) in the sagittal and frontal planes. In fact, long bones are one order of magnitude longer than the vertebra.
- Conversely, the alignment repeatability of the vertebra is comparable to that of the long bones about their long axis (their transverse dimension is of the same order of magnitude as the vertebra).
- Alignment repeatability of the vertebra was of the same order of magnitude as that for short bones such as the metatarsal bones (they have comparable dimensions).

This study has some limitations. First, after being optimized on a training set, this reference frame was tested on a limited sample size (7 specimens), obtained from 2 donors, reducing the variability in the dimension and shape of the vertebrae. Moreover the proposed reference frame was tested only on the thoracolumbar vertebrae. The reference frame is intended only for *in vitro* use; in fact the vertebra surface can only be accessed invasively (e.g. when soft tissue are removed). However, we have shown that it can be implemented also *in silico*, on CT-scans.

A further limitation is associated with the practical problems encountered while performing alignment. The *in vitro* problems reported by the operators were: bad visibility of the bone surface, the asymmetry in the vertebral structure, anatomical differences among specimens, and the presence of deformities (e.g. osteophytes, scoliosis, calcifications etc). Also the limited dimensions of the specimens played an important role in the alignment procedure, especially for the thoracic vertebrae.

Our methodology incorporated relatively simple and inexpensive equipment, while achieving high repeatability. If the 6DOF clamp used in our study is not available, it can easily be replaced by modelling clay as an adjustable support for the bone specimen, similar to [24].

The proposed reference frame relies on bony prominences and landmarks (as opposed to anatomical planes and axes) for more robust alignment. The adoption of this anatomical reference frame provides more reproducible specimen alignment, making *in vitro* biomechanical tests more accurate. The use of this reference frame can also be useful for the development of accurate numerical models, and for numerical-experimental comparison.

## 2.6 References

- [1] Wu, G., Siegler, S., Allard, P., Kirtley, C., Leardini, A., Rosenbaum, D., Whittle, M., D'Lima, D. D., Cristofolini, L., Witte, H., Schmid, O., and Stokes, I., 2002, "ISB recommendation on definitions of joint coordinate system of various joints for the reporting of human joint motion--part I: ankle, hip, and spine," *Journal of Biomechanics*, 35(4), pp. 543-548.
- [2] Cristofolini, L., 2011, "Anatomical reference frames for long bones: biomechanical applications," *Handbook of Anthropometry: Physical Measures of Human Form in Health and Disease*, Springer, New York.
- [3] Wu, G., and Cavanagh, P. R., 1995, "ISB recommendations for standardization in the reporting of kinematic data," *Journal of Biomechanics*, 28(10), pp. 1257-1261.
- [4] Cristofolini, L., 2011, "Anatomical reference frames for long bones: biomechanical applications. ," In :*Handbook of Anthropometry: Physical Measures of Human Form in Health and Disease*, Preedy, V.R.(Eds), Springer, New York.
- [5] Currey, J. D., 1982, "Bone as mechanical structure. In: Huijskes, R., van Campen, D.H., de Wijn, J.R.(Eds.), *Biomechanics—Principles and Applications*. Martinus Nijhoff Publishers, pp.75–85.."
- [6] Fung, Y. C., "1980. Bone and cartilage. In: *Biomechanics—Mechanical Properties of Living Tissues*. Springer, New York, pp.383–415.."
- [7] Van Sint Jan, S., and Della Croce, U., 2005, "Identifying the location of human skeletal landmarks: why standardized definitions are necessary--a proposal," *Clin Biomech (Bristol, Avon)*, 20(6), pp. 659-660.
- [8] O'Connor, J. J., 1992, "Load simulation problems in model testing," *Strain measurement in biomechanics*, A. W. Miles, and K. E. Tanner, eds., Chapman & Hall, London, pp. 14-38.
- [9] Cappozzo, A., Catani, F., Croce, U. D., and Leardini, A., 1995, "Position and orientation in space of bones during movement: anatomical frame definition and determination," *Clin Biomech (Bristol, Avon)*, 10(4), pp. 171-178.
- [10] Kopperdahl, D. L., Pearlman, J. L., and Keaveny, T. M., 2000, "Biomechanical consequences of an isolated overload on the human vertebral body," *Journal of Orthopaedic Research*, 18(5), pp. 685-690.
- [11] Buckley, J. M., Parmeshwar, R., Deviren, V., and Ames, C. P., 2009, "An improved metric for quantifying the stiffnesses of intact human vertebrae," *Proc Inst Mech Eng H*, 223(5), pp. 537-543.
- [12] Jiang, G., Luo, J., Pollintine, P., Dolan, P., Adams, M. A., and Eastell, R., 2010, "Vertebral fractures in the elderly may not always be "osteoporotic"," *Bone*, 47(1), pp. 111-116.
- [13] Pollintine, P., Luo, J., Offa-Jones, B., Dolan, P., and Adams, M. A., 2009, "Bone creep can cause progressive vertebral deformity," *Bone*, 45(3), pp. 466-472.
- [14] Frei, H., Oxland, T. R., and Nolte, L. P., 2002, "Thoracolumbar spine mechanics contrasted under compression and shear loading," *J Orthop Res.*, 20(6), pp. 1333-1338.
- [15] Hongo, M., Abe, E., Shimada, Y., Murai, H., Ishikawa, N., and Sato, K., 1999, "Surface Strain Distribution on Thoracic and Lumbar Vertebrae Under Axial Compression: The Role in Burst Fractures," *Spine*, 24(12), p. 1197.

- [16] Koller, H., Zenner, J., Hitzl, W., Resch, H., Stephan, D., Augat, P., Penzkofer, R., Korn, G., Kendell, A., Meier, O., and Mayer, M., 2013, "The impact of a distal expansion mechanism added to a standard pedicle screw on pullout resistance. A biomechanical study," *Spine J*, 13(5), pp. 532-541.
- [17] Furtado, N., Oakland, R. J., Wilcox, R. K., and Hall, R. M., 2007, "A Biomechanical Investigation of Vertebroplasty in Osteoporotic Compression Fractures and in Prophylactic Vertebral Reinforcement," *Spine*, 32(17), pp. E480-E487  
410.1097/BRS.1090b1013e31811ea31812ee.
- [18] Oakland, R. J., Furtado, N. R., Wilcox, R. K., Timothy, J., and Hall, R. M., 2009, "Preliminary biomechanical evaluation of prophylactic vertebral reinforcement adjacent to vertebroplasty under cyclic loading," *The Spine Journal*, 9(2), pp. 174-181.
- [19] Dall'Ara, E., Schmidt, R., Pahr, D., Varga, P., Chevalier, Y., Patsch, J., Kainberger, F., and Zysset, P., 2010, "A nonlinear finite element model validation study based on a novel experimental technique for inducing anterior wedge-shape fractures in human vertebral bodies in vitro," *Journal of Biomechanics*, 43(12), pp. 2374-2380.
- [20] Panjabi, M. M., Krag, M. H., and Goel, V. K., 1981, "A technique for measurement and description of three-dimensional six degree-of-freedom motion of a body joint with an application to the human spine," *Journal of Biomechanics*, 14(7), pp. 447-449, 451-460.
- [21] Panjabi, M. M., Duranceau, J., Goel, V., Oxland, T., and Takata, K., 1991, "Cervical human vertebrae. Quantitative three-dimensional anatomy of the middle and lower regions," *Spine (Phila Pa 1976)*, 16(8), pp. 861-869.
- [22] Panjabi, M. M., Takata, K., Goel, V., Federico, D., Oxland, T., Duranceau, J., and Krag, M., 1991, "Thoracic human vertebrae. Quantitative three-dimensional anatomy," *Spine (Phila Pa 1976)*, 16(8), pp. 888-901.
- [23] Panjabi, M. M., Goel, V., Oxland, T., Takata, K., Duranceau, J., Krag, M., and Price, M., 1992, "Human lumbar vertebrae. Quantitative three-dimensional anatomy," *Spine (Phila Pa 1976)*, 17(3), pp. 299-306.
- [24] Ruff, C. B., and Hayes, W. C., 1983, "Cross-sectional geometry of Pecos Pueblo femora and tibiae--a biomechanical investigation: II. Sex, age, side differences," *American journal of physical anthropology*, 60(3), pp. 383-400.
- [25] Taddei, F., Ansaloni, M., Testi, D., and Viceconti, M., 2007, "Virtual palpation of skeletal landmarks with multimodal display interfaces," *Medical informatics and the Internet in medicine*, 32(3), pp. 191-198.
- [26] Viceconti, M., Taddei, F., Montanari, L., Testi, D., Leardini, A., Clapworthy, G., and Van Sint Jan, S., 2007, "Multimod Data Manager: a tool for data fusion," *Computer methods and programs in biomedicine*, 87(2), pp. 148-159.
- [27] Öhman, C., Baleani, M., Perilli, E., Dall'Ara, E., Tassani, S., Baruffaldi, F., and Viceconti, M., 2007, "Mechanical testing of cancellous bone from the femoral head: Experimental errors due to off-axis measurements," *Journal of Biomechanics*, 40(11), pp. 2426-2433.
- [28] Conti, G., Cristofolini, L., Juszczak, M., Leardini, A., and Viceconti, M., 2008, "Comparison of three standard anatomical reference frames for the tibia-fibula complex," *J Biomech*, 41(16), pp. 3384-3389.

[29] Cristofolini, L., 1997, "A critical analysis of stress shielding evaluation of hip prostheses," *Crit Rev Biomed Eng*, 25(4-5), pp. 409-483.

## CHAPTER 3:

# Effect of the *in vitro* boundary conditions on the surface strain experienced by the vertebral body in the elastic regime

Valentina Danesi, MEng<sup>1</sup>, Paolo Erani, BEng<sup>2</sup>, Nicola Brandolini, PhD<sup>2,3</sup>,  
Mateusz M. Juszczak, PhD<sup>1,2</sup>, Luca Cristofolini, PhD<sup>1</sup>

<sup>1</sup> Department of Industrial Engineering, University of Bologna, Italy

<sup>2</sup> Laboratorio di Tecnologia Medica, Istituto Ortopedico Rizzoli, Bologna, Italy

<sup>3</sup> School of Mechanical Engineering, University of Leeds, Woodhouse Lane, Leeds, UK

*The candidate was the first investigator of this study. This paper was submitted to Journal of Biomechanical Engineering.*

### 3.1 Abstract

The strength of natural and treated vertebrae can be assessed through *in vitro* mechanical tests both on isolated vertebral bodies, and on sets of three-adjacent-vertebrae (where the central one, under investigation, is loaded through the adjacent intervertebral discs). The goal of this *in vitro* study was to determine if testing the human vertebral body in a single-vertebra configuration provides different results from three-adjacent-vertebrae-segment. Twelve sets of three-adjacent-vertebrae were extracted from fresh-frozen thoracolumbar human spines. To measure the magnitude and direction of surface principal strains, the central vertebra of each three-adjacent-vertebrae-segment was prepared with eight strain-gauges. They were tested *in vitro*, allowing comparison of the surface strain distribution when the same vertebral body was loaded through the intervertebral discs (three-adjacent-vertebrae-segment), and with the endplates embedded in acrylic cement (single-vertebra). They were subjected to four non-destructive loading conditions (axial-compression, axial-traction, torsion-clockwise, torsion-counter-clockwise) first as a three-adjacent-vertebrae-segment, then as single-vertebra. The magnitude of measured principal strains differed significantly between the two boundary conditions. For axial loading, the largest principal strains on the surface (along the cranio-caudal axis of the vertebra) were significantly higher when the same vertebra was tested isolated, as opposed to a three-adjacent-vertebrae-segment. Conversely, the circumferential strains decreased significantly in the single-vertebra compared to the three-adjacent-vertebrae. In some cases, variations exceeded 100% of the strain magnitude, including changes from tension to compression. For torsional loads, the differences between the two boundary conditions were smaller. This study shows that when the vertebral body is loaded through a cement pot, load is transferred in a different way from the physiological one (through the intervertebral discs). Therefore, when single vertebrae are tested, results on the bone surface should be taken with caution.

**Keywords:** *in vitro* biomechanical testing; human vertebral body; single vertebra; intervertebral disc; spine segment; principal strains.

## 3.2 Introduction

*In vitro* mechanical testing of the vertebra is essential to investigate fracture risk [1, 2], spinal disease [3, 4], the effects of aging [5], surgical treatments [6], and in general to investigate the biomechanics of the spine [7]. Different *in vitro* methods to characterize the mechanical behaviour of the vertebral body are present in the literature [8]. The most common types of test specimen are:

- Spine segments composed of a series of adjacent vertebrae, including the surrounding soft tissues [2, 6, 9-13]: this boundary condition allows physiological load transfer to the endplates through the adjacent intervertebral discs. The main disadvantage is that failure can occur in the vertebral body under investigation, but also in the adjacent discs and/or vertebrae, adding complexity to the experiment.
- Isolated vertebrae, after removal of the adjacent intervertebral discs: this simplified approach facilitates control of the loading conditions, and allows focusing exclusively on the vertebra under investigation. The most frequent type of isolated vertebra consists of a vertebral body (with or without the neural arch) loaded through its endplates. In some cases the endplates have been simply placed in contact with the platens of the testing machine (which is associated with undesirable point-wise load application [14-17]). A better option consists in embedding the endplates in bone cement, enabling a rather uniform load transfer [18-28]. To generate a highly-reproducible test condition, the endplates can be removed to obtain flat-parallel loading surfaces [15, 29].

Testing single vertebrae is appealing. First of all, it requires shorter (more cost-effective) specimens. Secondly, when a single-vertebra is tested, failure surely initiates within the vertebral body (as opposed to the adjacent discs/vertebrae). However, this simplified boundary condition may limit the physiological relevance of results. In fact, loading the endplates through a cement pot, rather than through the discs, may result in a non-physiological loading mechanism, and a different distribution of stress/strain inside the vertebral body.

The strain distribution for different boundary conditions was investigated *in vitro* [30]: three-adjacent-vertebrae, single-vertebra loaded through intervertebral discs, and single vertebra (without discs) embedded in bone cement. Measurements were made using a texture-correlation

technique on a sagittal slice of trabecular bone. Although at that time such measurement technique was not fully-developed, distinctly different strain patterns were observed for the different boundary conditions. A study using micro-computed-tomography and digital volume correlation (DVC) [31] showed that testing vertebral bodies from young rabbits with or without intervertebral discs did not affect the strength, but only the strain distribution inside the vertebra, and the failure mechanism. A finite element (FE) study showed that the strength for a three-adjacent-vertebrae-segment (with the intervertebral discs) was approximately 34% lower than for a single vertebra (loaded through cement pots) [13]. The biomechanical role of the cortical shell in the vertebral body can be substantial, being about 45% at the mid-height; but a better understanding of the structural role of the cortical and trabecular bone is needed [32].

The effect of different boundary conditions (with and without discs) on the strain distribution in the human vertebra has never been measured experimentally. A better understanding is needed about the effect of the different experimental boundary conditions, when investigating the biomechanics of the vertebral body.

Our research question was whether a single-vertebra configuration is an acceptable alternative to a three-adjacent-vertebrae-segment, when measuring the principal strains (magnitude and direction) on the surface of the vertebral body, in the elastic regime.

### **3.3 Materials and Methods**

#### **3.3.1 Overview**

Non-destructive tests were performed on twelve specimens (Table 3-1), under two different boundary conditions (Fig.3-1):

- Three-adjacent-vertebrae: the central vertebra was loaded through its adjacent vertebrae and intervertebral discs.
- Single-vertebra: the central vertebra of each three-adjacent-vertebrae-segment was isolated and tested again, after having been potted in bone cement.

The strain distribution on the bone surface was investigated by means of strain-gauges. Different loading configurations (axial-compression, axial-traction and torsion) were performed in order to assess the mechanical behaviour for different loading scenarios.

*Table 3- 1: Details of specimen investigated.*

Specimen: three-adjacent-vertebrae	Specimen: single-vertebra	Donor's details						Vertebral body dimensions		
		Donor	Gender	Age at death (years)	Height (cm)	Weight (kg)	Cause of death	Height (mm)	Antero-posterior length (mm)	Right-left width (mm)
half T2 - T3 - half T4	T3	#1	M	70	168	86	Cardiac dysrhythmia	11.6	22.9	26.9
half T4 - T5 - half T6	T5	#1	M	70	168	86	Cardiac dysrhythmia	11.2	24.4	28.4
half T6 - T7 - half T8	T7	#1	M	70	168	86	Cardiac dysrhythmia	17.6	30.5	25.9
half T8 - T9 - T10	T9	#1	M	70	168	86	Cardiac dysrhythmia	15.5	33.2	29.8
half T12 - L1 -half L2	L1	#2	M	49	182	181	Pneumonia	25.7	23.7	37.2
half T12 - L1 - half L2	L1	#3	M	66	177	59	Infarct	25.7	27	37.4
half L2 - L3 - half L4	L3	#2	M	49	182	181	Pneumonia	25.5	35	43
half L2 - L3 - half L4	L3	#4	F	78	171	64	Euthanasia	26.3	23	38.2
half L2 - L3 - half L4	L3	#5	M	88	180	77	Congestive heart failure	25.8	34.7	45
half L2 - L3 - half L4	L3	#1	M	70	168	86	Cardiac dysrhythmia	24.7	32.1	42.9
half L4 - L5 - S1	L5	#2	M	49	182	181	Pneumonia	23.2	27.9	42.2
half L4 - L5 - S1	L5	#6	M	84	178	82	Dementia	28.8	31.9	43.1
<b>Average</b>	-	-	-	67	178	114	-	<b>25.7</b>	<b>29.4</b>	<b>41.4</b>
<b>Standard deviation</b>	-	-	-	16	5	56	-	<b>1.5</b>	<b>4.4</b>	<b>2.8</b>

*Note. — The first two columns describe the specimen in the three-adjacent-vertebrae configuration (the test vertebra was connected to the intervertebral discs and at least half of each adjacent vertebrae), and in the single-vertebra condition (the same test vertebra as before). In the last three columns, the biomechanical dimensions are reported, which were measured as in [33]. The vertebral body height was measured between the centers of the two endplates from a lateral view.*

The antero-posterior length was measured between the most anterior and most posterior point at mid-height of the vertebral body. The vertebral body width was measured between the two most lateral points at mid-height of the vertebral body.

Note. — To maximize the number of test specimens, in most cases, the adjacent vertebrae (which served only to transfer load to the intervertebral discs) were sectioned transversally, so as to leave half of the adjacent vertebra attached to each intervertebral disc.

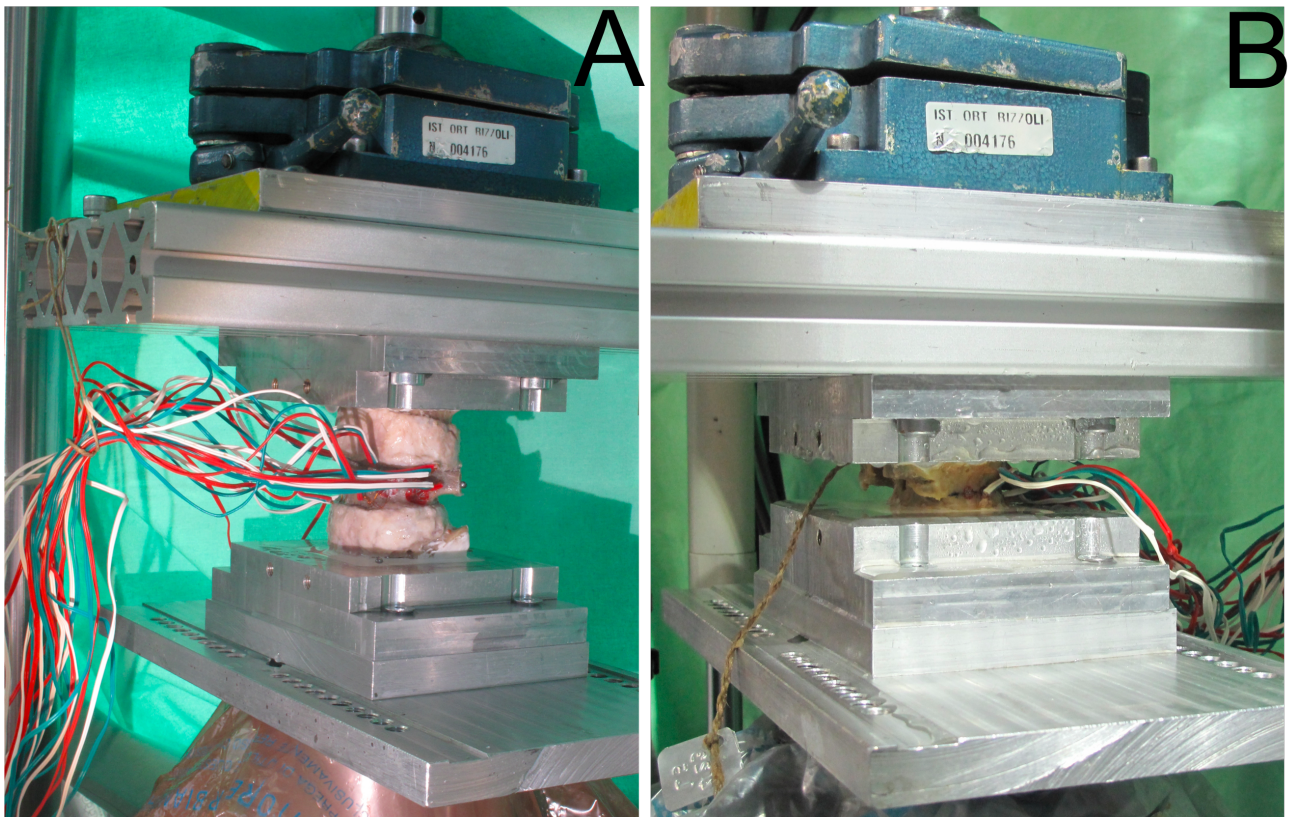


Fig. 3-1: Two different boundary conditions were applied to the same vertebrae: (A) three-adjacent-vertebrae (the central vertebra was loaded through its adjacent intervertebral discs); (B) single-vertebra (the same central vertebra of three-adjacent-vertebrae specimen was loaded through its endplates embedded in bone cement). (C) Schematic of a vertebra showing the position of the eight triaxial strain-gauges. The strain-gauges were equally spaced around the vertebral body, at mid-height. The actual position of the strain-gauges was sometimes adjusted by up to 4 mm from the theoretical location due to small defects of the bone surface (pores, ridges, or grooves). One grid of each strain-gauge was aligned parallel to the cranio-caudal axis

### **3.3.2 Bone specimen**

Twelve test specimens were obtained from six fresh-frozen thoraco-lumbar spines, through an ethically-approved donation program (IIAM, <http://www.iiam.org>). Donors did not suffer from cancer nor musculoskeletal pathologies, with the exception of osteoporosis (Table 3-1). The spines were computed-tomography scanned to exclude the internal defects or previous fractures. The specimens were sealed in bags at -28°C when not in use. They were thawed in physiological saline solution for at least 6 hours prior to each test, and kept hydrated with saline solution during testing.

All the surrounding soft tissues were removed, including the ligaments. A reproducible reference frame was adopted [33]. The two extremes of the three-adjacent-vertebrae specimens were potted in acrylic bone cement (Restray, Salmoiraghi, Mulazzano, Italy). In order to isolate the mechanical behaviour of the vertebral body from the surrounding structures, the neural arches were removed. The three-adjacent-vertebrae specimens were tested non-destructively (see below).

The single-vertebra specimens were dissected from the three-adjacent-vertebrae specimens. Both intervertebral discs were completely removed. The endplates of each single-vertebra were potted in acrylic cement. Dedicated procedures were adopted to ensure that the alignment of the single-vertebra was the same as when it was tested in the three-adjacent-vertebrae-segment (removal of one disc at a time, immediate potting of the cleaned endplate of the single-vertebra). The same non-destructive tests were performed again on each single-vertebra.

### **3.3.3 Strain measurement**

Eight strain-gauges were equally spaced at mid-height of the body of the test vertebra (the central one of the three-adjacent-vertebrae-segment, Fig.3-1). Triaxial-stacked rosettes strain-gauges (FRA-1-11-3L, TML Tokyo-Sokki-Kenkyujo, Japan, 1mm grid, 120 Ohm) were bonded following an established procedure for wet cadaveric specimens [34], which included removal of soft tissues, degreasing with ethanol, and a cocktail of acetone and 2-propanol, bonding with cyanoacrylate glue (CN-Adhesive, TML), and waterproofing with polyurethane (M-COAT-A, Vishay-MicroMeasurements, Raleigh, NC, USA). To avoid overheating, a grid excitation of 1Volt was selected. The same strain-gauges were used when the same vertebra was tested in the three-adjacent-vertebrae and single-vertebra conditions. In 15 cases out of 96, a strain-gauge was

damaged during dissection to isolate the single-vertebra from the three-adjacent-vertebrae-segment: an identical strain-gauge was placed in the original location.

Strains were recorded at 5000Hz using a multi-channel data-logger (System-6000, Vishay-MicroMeasurements), together with force/torsion and displacement/rotation signals from the testing machine.

### **3.3.4 Loading conditions**

In order to obtain a comprehensive characterization of the strain distribution, multiple loading configurations were applied to each specimen. The same conditions were applied both to the three-adjacent-vertebrae-segment, and the single-vertebra:

- To replicate a scenario close to physiological loading, a compressive axial force was applied (axial-compression), as frequently found in the literature (e.g. [2]).
- To understand if traction induces a symmetric strain distribution respect to compression, a tensile axial force was similarly applied (axial-traction).
- To gather information about a completely different (yet physiological) loading scenario, torsion about the cranio-caudal axis was applied in both directions (clockwise and counter-clockwise) [10].

These loading conditions were selected as they could be replicated identically for the two boundary conditions.

Tests were performed on an axial-torsional testing machine (858-MiniBionix, MTS, Minneapolis, USA, Fig.1). Specimens were over-constrained: all components of rotation and translation were constrained at both extremities. A lockable ball-joint was placed between the actuator and the upper loading plate to ensure correct alignment. During the tests the ball-joint was locked, avoiding any further rotation [10, 35, 36]. To monitor all components of loading during testing, an additional six-components load-cell (FDC-011, Metior, Dongo, Italy) was used.

The loading protocol was similar to [6, 10, 34, 37]. The testing machine operated in position control (axial-displacement, or rotation). A trapezoidal waveform was implemented for each loading configuration. The actuator displacement/rotation was adjusted for each specimen,

and each loading configuration, so that principal strains in the most stressed strain-gauge did not exceed  $\pm 2000$  microstrain (such displacement/rotation was determined in a pre-test where the testing machine was manually-operated). This is a physiological value [38], and is approximately 20% of the failure strain for cortical bone [39]. For this reason, the applied force (N) and moment (Nm) were different among specimens, and also for the same specimen tested as a three-adjacent-vertebrae-specimen and as a single-vertebra. Because of the compliance of the discs, such displacement/rotation were one order of magnitude larger for the three-adjacent-vertebrae-segment than the single-vertebra. The actuator speed was tuned to reach the maximum displacement/rotation in 0.2seconds, which is comparable to many motor tasks [40, 41]. The maximum displacement/rotation was held for 2seconds. To overcome variations due to viscoelasticity, strain readout was averaged over the first 0.1seconds (500points) after the maximum displacement/rotation was reached.

Each configuration was repeated six times for each specimen, with 4 minutes recovery similar to [10], as in such recovery time bone strains returns close to zero [42].

### **3.3.5 Measured quantities and statistics**

For each strain-gauge the principal strain magnitude ( $\epsilon_1, \epsilon_2$ ) and direction ( $\theta_p$ , counter-clockwise from the cranio-caudal axis) were computed for each test repetition. A high linearity existed between applied load and strain ( $R^2 > 0.98$  for all the gauges where strain exceeded 50 microstrain). Small intra-specimen variability existed in the load applied among test repetitions, while larger variability existed among different specimens for the same loading condition. Before doing any further analysis, the strain magnitude for each test repetition was scaled to the body weight, BW (axial-compression, axial-traction) and to 0.5% BW\*m (torsion).

Intra-specimen test repeatability was good. For axial-compression, the magnitude of principal strains ( $\epsilon_1, \epsilon_2$ ) varied by 1.86% among repetitions; the principal direction ( $\theta_p$ ) by 0.60°. For axial-traction, the principal strains ( $\epsilon_1, \epsilon_2$ ) and direction ( $\theta_p$ ) varied respectively by 3.11% and 0.64° among repetitions. For torsion, the principal strains ( $\epsilon_1, \epsilon_2$ ) and direction ( $\theta_p$ ) varied by 1.06% and 0.06° among repetitions.

To exclude outliers, Peirce's criterion was applied [43]. Suspect data were checked among repetitions, for each specimen: approximately 6% of the repetitions had to be excluded. To obtain a

single output for each specimen and each loading configuration, the average of the principal strain ( $\epsilon_1, \epsilon_2$ , which follow a normal distribution) and the median of the principal direction ( $\theta_p$ , does not follow a normal distribution) were calculated among the six repetitions.

To quantify the variations of principal strains between the two boundary conditions, the ratio between the magnitude in the single-vertebra and in the three-adjacent-vertebra configuration (assumed as a reference) was calculated for the principal strains:

$$\epsilon_{1\_RATIO} = \frac{\epsilon_{1\_SINGLE-VERTEBRA}}{\epsilon_{1\_THREE-VERTEBRAE-SPECIMEN}} \quad (\text{Eq. 1})$$

$$\epsilon_{2\_RATIO} = \frac{\epsilon_{2\_SINGLE-VERTEBRA}}{\epsilon_{2\_THREE-VERTEBRAE-SPECIMEN}} \quad (\text{Eq. 2})$$

Similarly, the variation of principal strain direction ( $\theta_p$ ) was computed as the difference between the angle in the single-vertebra and three-adjacent-vertebrae configurations:

$$\Delta\theta_p = \theta_{P\_SINGLE-VERTEBRA} - \theta_{P\_THREE-VERTEBRAE-SPECIMEN} \quad (\text{Eq. 3})$$

Such comparisons were performed separately for each specimen, each loading configuration, and each strain-gauge. To exclude points where such a ratio is poorly significant, measurements below 50 microstrain were excluded.

For each loading condition, the significance of the differences between the two boundary conditions was assessed with the paired t-test for the principal strains ( $\epsilon_{1\_SINGLE-VERTEBRA}$  vs  $\epsilon_{1\_THREE-VERTEBRAE-SPECIMEN}$ , and  $\epsilon_{2\_SINGLE-VERTEBRA}$  vs  $\epsilon_{2\_THREE-VERTEBRAE-SPECIMEN}$ ), and with the Wilcoxon paired-sample non-parametric test for the principal direction ( $\theta_{P\_SINGLE-VERTEBRA}$  vs  $\theta_{P\_THREE-VERTEBRAE-SPECIMEN}$ ). To assess if the strain distribution for the two boundary conditions ( $\epsilon_{1\_SINGLE-VERTEBRA}$  vs  $\epsilon_{1\_THREE-VERTEBRAE-SPECIMEN}$ , and  $\epsilon_{2\_SINGLE-VERTEBRA}$  vs  $\epsilon_{2\_THREE-VERTEBRAE-SPECIMEN}$ ) had similar trends, the Pearson product-moment correlation coefficient ( $r_{Pearson}$ ) was computed. Statistics were performed with SPSS-16.0 (SPSS, Chicago, USA).

### 3.4 Results

For axial-compression, the largest principal strain (absolute value) was always compressive ( $\epsilon_2$ ), and roughly aligned to the cranio-caudal axis (median: within  $6^\circ$  for the single-vertebra,  $13^\circ$  for the three-adjacent-vertebrae). This strain component in the single-vertebra was 79% larger (average of 8 strain measurement locations) than in the three-adjacent-vertebrae specimen. However, such a difference was statistically significant only at 6 out of 8 locations (Fig.3-2). The other principal strain component ( $\epsilon_1$ , nearly circumferential) was one order of magnitude lower in the single-vertebra than in the three-adjacent-vertebrae (Fig.3-2). In some strain-gauges (mainly anteriorly) the circumferential principal strain switched from tensile (three-adjacent-vertebrae) to compressive (single-vertebra). Such difference was statistically significant for 7 of 8 measurements locations. The angles of principal strain differed little between the two boundary conditions, when the median of all specimens was considered (maximum difference  $12^\circ$ , with limited statistical significance, Fig.3-2). However, in some specimens the principal strain direction varied by over  $30^\circ$  between the two boundary conditions.

For axial-traction, the largest principal strain (absolute value) was always tensile ( $\epsilon_1$ ), and roughly aligned with the cranio-caudal axis (median: within  $21^\circ$  for the single-vertebra,  $29^\circ$  for the three-adjacent-vertebrae). This strain component in the single-vertebra was on average 61% larger than in the three-adjacent-vertebrae: such a difference was larger and statistically significant in the two posterior strain-gauges (Fig.3-3). The other principal strain component ( $\epsilon_2$ , nearly circumferential) was one order of magnitude lower in the single-vertebra than in the three-adjacent-vertebrae (Fig.3-3). In some strain-gauges the circumferential principal strain switched from compressive to tensile or vice-versa (statistically significant only at one location). The angles of principal strain differed little between the two boundary conditions, when the median of all specimens was considered (maximum difference  $24^\circ$ , statistically not-significant, Fig.3-3). However, in some individual specimen the principal strain direction varied by over  $45^\circ$  between the two boundary conditions.

For torsion, the two principal strain components ( $\epsilon_1, \epsilon_2$ ) had similar magnitude and were within  $5^\circ$  from being at  $\pm 45^\circ$  from the cranio-caudal axis. On average, the principal tensile ( $\epsilon_1$ ) and compressive ( $\epsilon_2$ ) strains in the single-vertebra were 12% lower than in the three-adjacent-vertebrae-segment. However, the effect was not uniform over the vertebral body (Fig.3-4). In the posterior region both principal strain components slightly increased in the single-vertebra compared



vertebra). (The detailed strain distribution in absolute terms for the two boundary conditions is reported as Supplementary material).

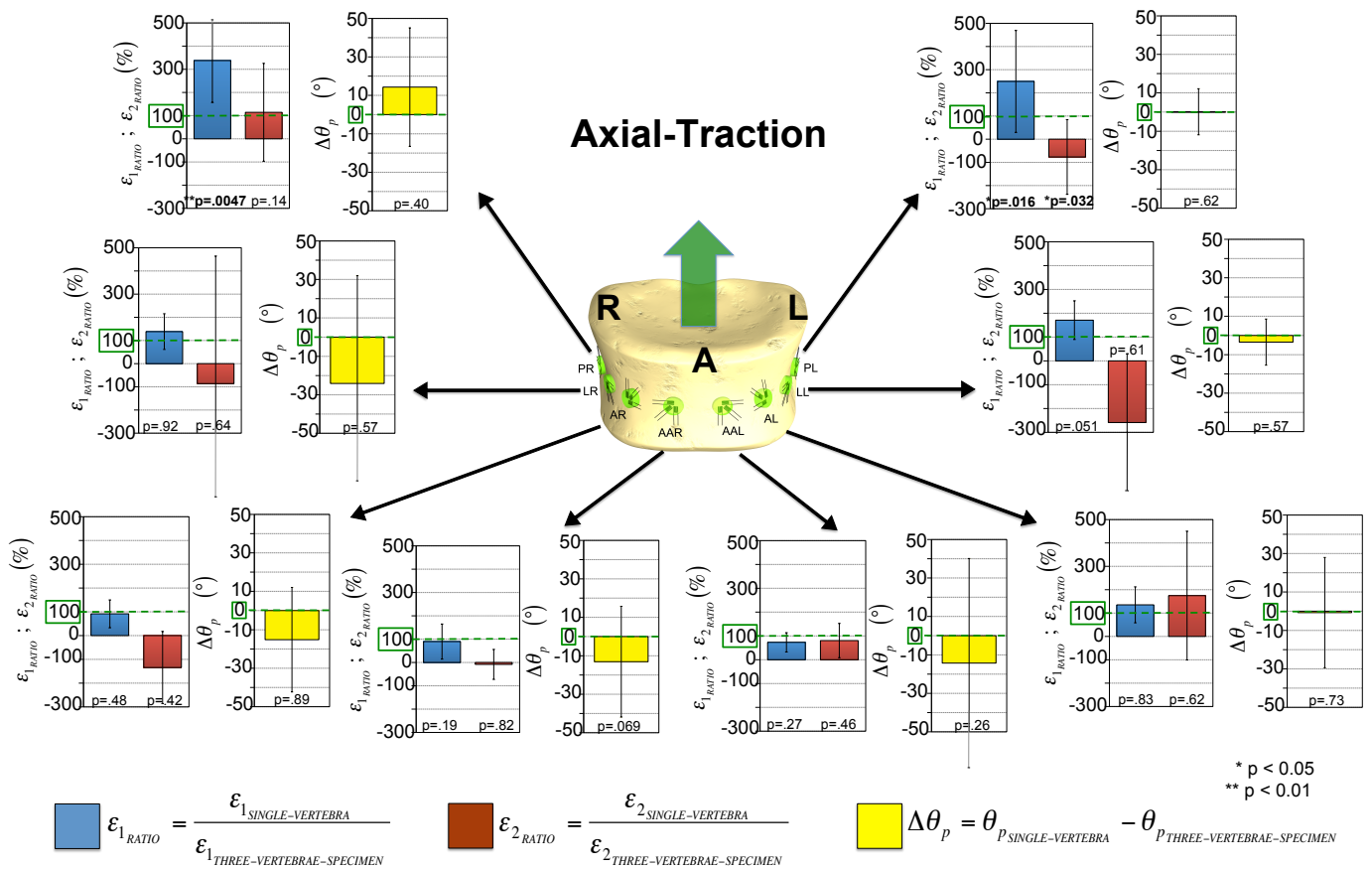


Fig. 3-3: Axial-traction. The principal strain magnitude ( $\epsilon_1$ ,  $\epsilon_2$ ) in the single-vertebra is expressed as a fraction of the three-adjacent-vertebrae condition (average and SD: 100% indicates no difference between the two conditions; greater than 100% means that the single-vertebra experienced an increase of strain compared to the three-adjacent-vertebrae; a negative value indicates a change of sign). The variation of principal direction ( $\theta_p$ ) is the difference between the three-adjacent-vertebrae and the single-vertebra (median and SD:  $0^\circ$  indicates no variation; a positive sign indicates a clockwise difference from the three-adjacent-vertebrae to the single-vertebra). (The detailed strain distribution in absolute terms for the two boundary conditions is reported as Supplementary material).

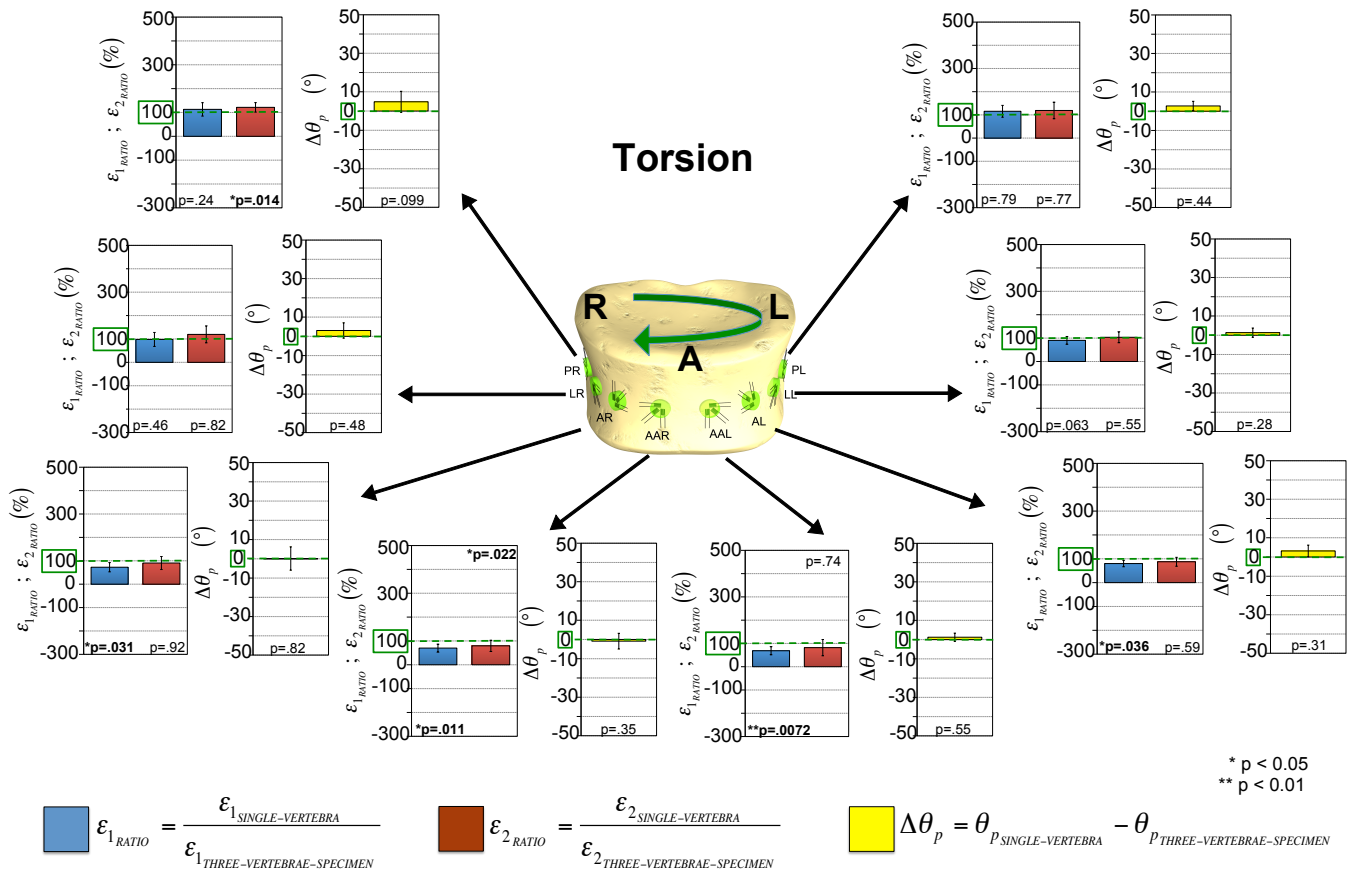


Fig. 3-4: Torsion. The principal strain magnitude ( $\epsilon_1$ ,  $\epsilon_2$ ) in the single-vertebra is expressed as a fraction of the three-adjacent-vertebrae condition (average and SD: 100% indicates no difference between the two conditions; greater than 100% means that the single-vertebra experienced an increase of strain compared to the three-adjacent-vertebrae). The variation of principal direction ( $\theta_p$ ) is the difference between the three-adjacent-vertebrae and the single-vertebra (median and SD:  $0^\circ$  indicates no variation; a positive sign indicates a clockwise difference from the three-adjacent-vertebrae to the single-vertebra). (The detailed strain distribution in absolute terms for the two boundary conditions is reported as Supplementary materials).

The strain magnitudes in the single-vertebra and three-adjacent-vertebrae-segment were poorly correlated for axial-compression and axial-traction (Table 3-2); rPearson was negative for the tensile principal strain ( $\epsilon_1$ ), and positive for the compressive one ( $\epsilon_2$ ). Correlation was higher for torsion, with positive rPearson.

Table 3-2: For each loading condition, the Pearson product-moment correlation coefficient ( $r_{Pearson}$ ) was computed between the strain magnitude measured in the single-vertebra and in the three-adjacent-vertebrae condition, separately for the two principal components of strain ( $\epsilon_1$ ,  $\epsilon_2$ ).

	<b>Axial-compression</b>	<b>Axial-traction</b>	<b>Torsion</b>
Principal tensile strain ( $\epsilon_1$ )	-0.226	-0.103	0.809
Principal compressive strain ( $\epsilon_2$ )	0.351	0.238	0.829

### 3.5 Discussion

While *in vitro* mechanical tests are regularly performed on the vertebral body, it remains unclear how the mechanical behaviour is affected by the experimental boundary conditions. In fact, studies involving both sets of three-adjacent-vertebrae [2, 6, 10-13, 44, 45] and single-vertebrae [18-28] can be found. The goal of this study was to elucidate if testing a single-vertebra specimen (which provides a number of practical advantages) provides similar results to a three-adjacent-vertebrae-segment (which can be assumed closer to physiological).

Our findings suggest that direct application of load to the endplates leads to some differences in the strain distribution (magnitude and direction) on the bone surface, compared to a three-adjacent-vertebrae-segment. The differences in strain magnitude were larger when an axial force (compressive or tensile) was applied. Compared with the three-adjacent-vertebrae configuration, the single-vertebra condition was associated with a marked and uniform increase of the strains along the cranio-caudal axis of the vertebra, and a decrease of the circumferential ones, both for axial-compression and axial-traction. Such differences were less pronounced in torsion.

The principal strain direction was slightly affected by the boundary conditions. The largest differences were observed for axial-compression and axial-traction. This effect varied greatly between specimens (no statistical significance), and measurement locations. This could be explained by the fact that the spine is mainly optimized to withstand axial compression, and other modes of loading may result in unpredictable load transfer [46].

Such findings might be related to the biomechanical conditions experienced by the vertebrae and the adjacent discs. When a vertebra is axially loaded through the adjacent discs, the pressure existing in the nucleus pulposus generates a state of tensile stress in the annulus fibrosus. This tension tends to shield the compressive stress transferred to the cortical shell (while enhancing the amount of load transferred to the center of the vertebra) [47]. In fact, a common failure mechanism consists in a partial rupture of the endplate, when the nucleus partially herniates within the vertebral body (Schmorl's node [48]). This load transfer mechanism is completely modified when a single vertebra is loaded through two cement pots, which provide a rather uniform stress to the endplates, without distinction between the edges (cortical shell) and the central region (trabecular core). Such alteration was more pronounced when an axial force was applied, and was less visible in torsion.

Our findings are in agreement with another *in vitro* study [30]. Their results on sagittal slices of spine segments loaded in compression showed distinctly different strain patterns for different boundary conditions. They found that the principal compressive strain in the trabecular bone was 20-30% larger when the same vertebra was loaded through a cement pot, than when it was loaded through its discs. However, their results cannot be directly compared to ours, as they focused on the trabecular core, while we measured cortical strains.

A recent DVC study [31] showed that testing vertebral bodies with or without intervertebral discs affected the load transfer and failure mechanism, but not the magnitude of the failure force. Direct comparisons are not possible as our study focused on cortical strain in the elastic regime. However, the fact that strains are generally larger in the single-vertebra suggests that this condition is more critical for the vertebral body. The differences between their and our findings can be explained by their use of vertebrae from growing rabbits (with open growth plates), with a different anatomy and tissue architecture from humans [49].

An experimental-numerical study [13] showed that the failure force predicted by an FE model for a single vertebra loaded through cement pots overestimated by 34% the strength of the same vertebra loaded through its discs. They suggested that cement embedding would provide a higher vertebral strength because this way the cortex carries a larger portion of the load [13]. However, such effect may depend on the way the thin cortical shell was modelled.

Some limitations of this study should be considered. First of all, the specimens were obtained from different donors, and from the thoracic and lumbar regions. While specimens were

carefully screened (visually and from CT-images) to exclude defective specimens, the bone quality was not quantitatively assessed. Furthermore, our specimens were obtained from elderly donors (Table 3-1): although the discs did not have obvious lesions, they possibly had some degree of degeneration. The variability of the intervertebral discs might affect the load distribution across the endplate and the mechanical response of the vertebral body [50-52]. All these factors might have concurred to the scatter of our results, and to the lack of statistical significance for some observations.

The soft tissues and posterior elements were removed from our specimens. Such elements are important to the biomechanics of the spine segments, but are not essential to investigate the biomechanical competence of the vertebral body, and are often removed in similar studies [14-29].

The same specimens were tested first as a three-adjacent-vertebrae-segment and then as a single-vertebra. As the tests were well within the elastic regime, no damage or conditioning should be expected between the two boundary conditions.

Strain measurement was affected by systematic error: the actual strain was underestimated by 3-9% because of the reinforcement effect of the strain-gauges [10]. While the absolute strain value is affected by such error, this artifact was compensated when the ratio was computed between the three-adjacent-vertebrae and single-vertebra conditions, for the same strain-gauge.

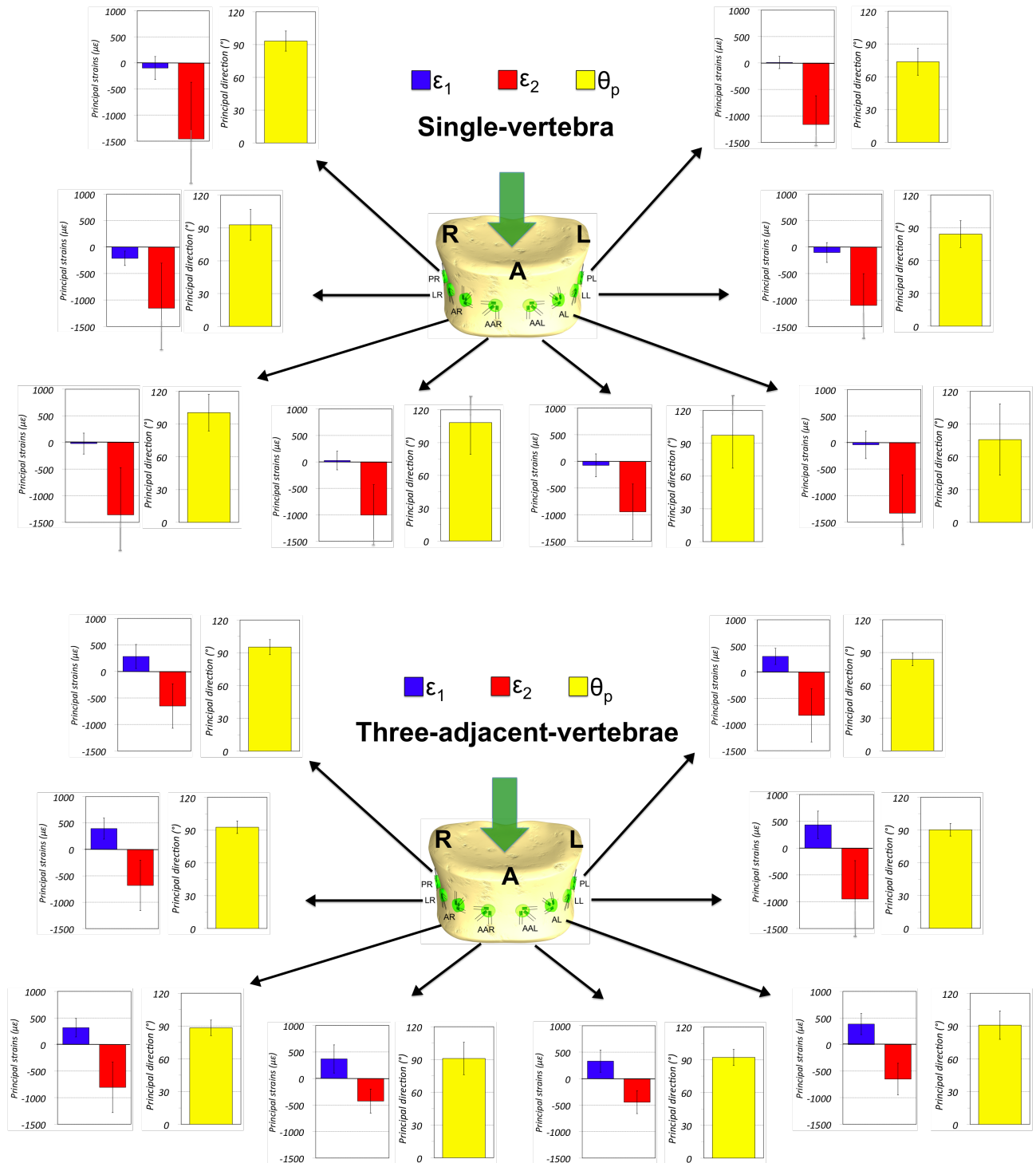
In this study only the strain on the surface of the cortical shell was investigated, and does not provide any insight about the stress/strain distribution within the trabecular structure. An alternative tool for investigating internal strains is DVC [53-56].

In summary, this study supports the idea that the magnitude of the principal strains on the vertebral surface is significantly different between boundary condition (three-adjacent-vertebrae and single vertebra). Even if testing the single-vertebra is advantageous from several points of view, the strain distribution for this boundary condition presents some difference from the case where the vertebra is loaded through its adjacent discs, especially when axial compression is investigated.

### 3.6 Supplementary Materials

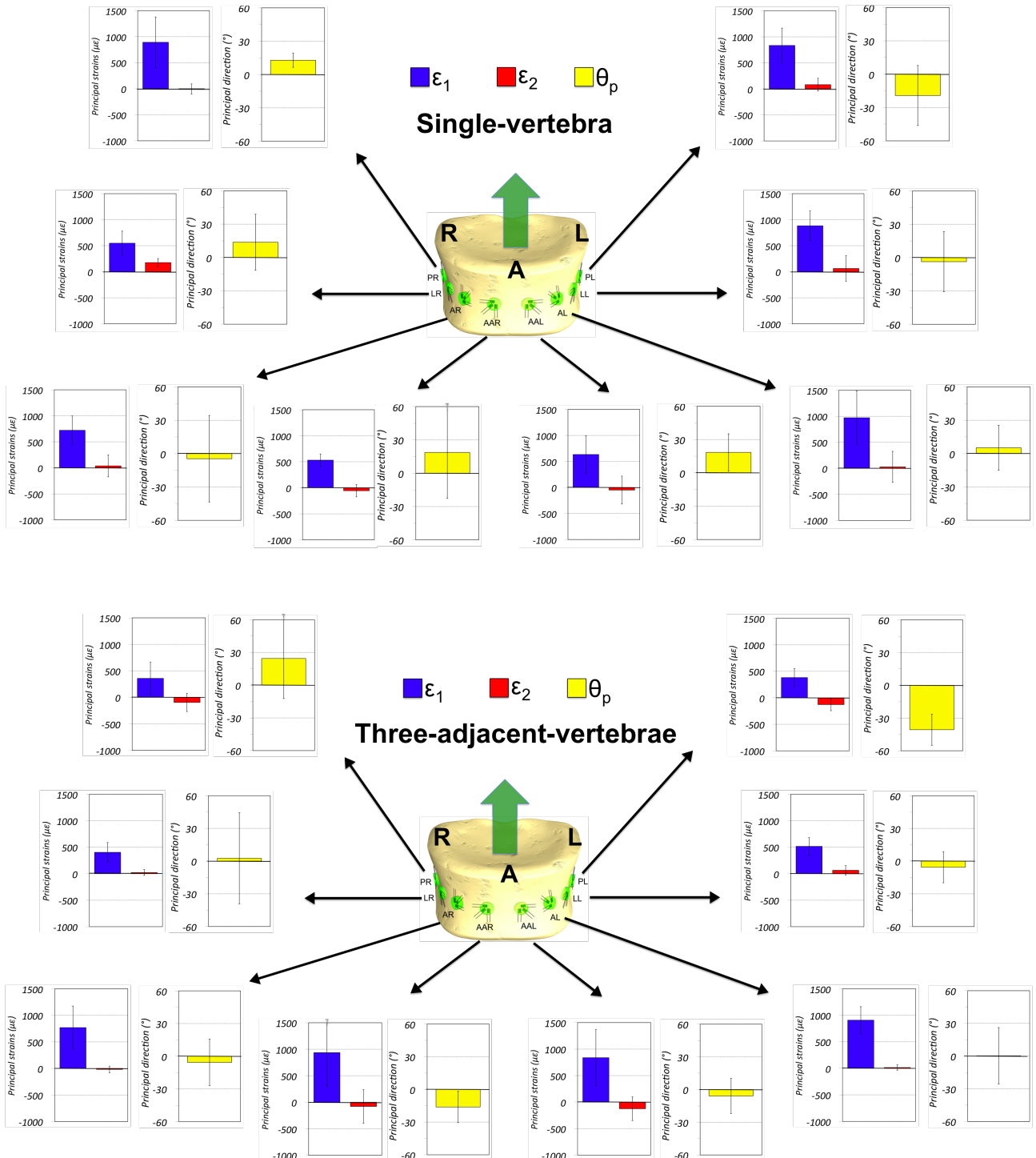
#### A. AXIAL-COMPRESSION

The charts below compare the strain distribution in the three-adjacent-vertebrae and the single-vertebra conditions. The magnitude ( $\epsilon_1$ ,  $\epsilon_2$ ) and the direction ( $\theta_p$ , measured counter-clockwise from the cranio-caudal axis) of principal strains are reported at the eight measurement locations (average and standard deviation of 12 specimens). Peirce's criterion was applied to exclude outliers.



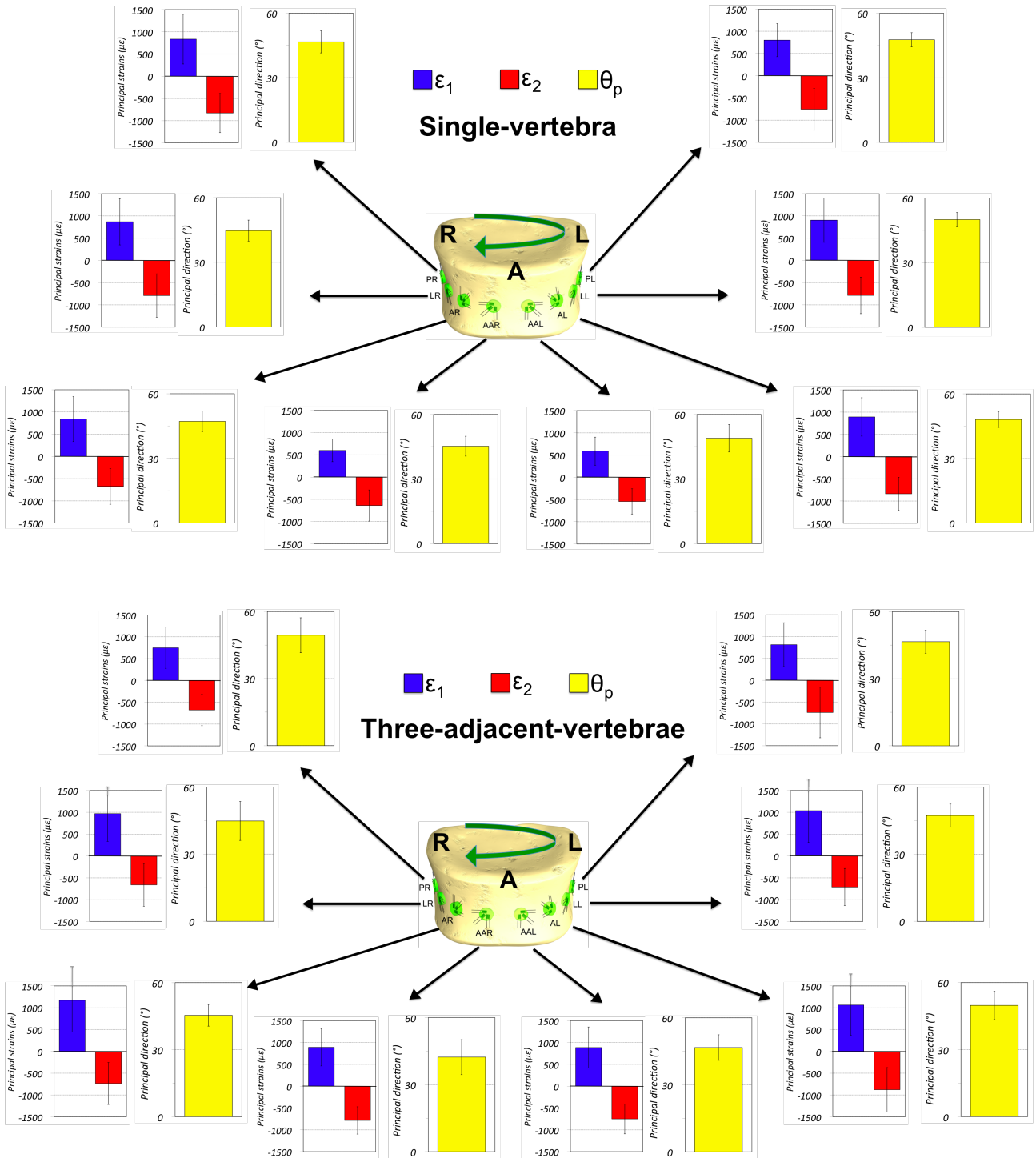
## B. AXIAL-TRACTION

The charts below compare the strain distribution in the three-adjacent-vertebrae and the single-vertebra conditions. The magnitude ( $\epsilon_1$ ,  $\epsilon_2$ ) and the direction ( $\theta_p$ , measured counter-clockwise from the cranio-caudal axis) of principal strains are reported at the eight measurement locations (average and standard deviation of 12 specimens). Peirce's criterion was applied to exclude outliers.



### C. TORSION

The charts below compare the strain distribution in the three-adjacent-vertebrae and the single-vertebra conditions. The magnitude ( $\epsilon_1$ ,  $\epsilon_2$ ) and the direction ( $\theta_p$ , measured counter-clockwise from the cranio-caudal axis) of principal strains are reported at the eight measurement locations (average and standard deviation of 12 specimens). The plots are referred to a clockwise torque. Results with a counter-clockwise torque were quite similar. Peirce's criterion was applied to exclude outliers



#### **D. REMARK ABOUT COMPARISONS BETWEEN THESE CHARTS AND FIG. 3-2, 3-3, 3-4**

The plots in the Supplementary Material are relatively easy to understand: the average between specimens was computed to for the principal strains (the median was computed for the principal direction). - Fig. 3-2, 3-3 and 3-4 report the average of the ratio between the strain in the single-vertebra and threevertebra-specimen. - For this reason, the values in Fig. 3-2, 3-3, 3-4 cannot be directly obtained by simply computing the ratio of the average strain values in the Supplementary material. - For instance it can happen that the actual principal strain is small in magnitude with some positive and some negative values in the different specimens. The result is a close-to-zero average strain in the charts in the Supplementary material (possibly with the same sign in the singlevertebra and three-vertebra-specimen). However, as the ratio between the single-vertebra and the three-vertebra is computed for each specimen, this may result in negative (or positive) average values of the ratio.

### 3.7 References

- [1] Brandolini, N., Kapur, N., and Hall, R. M., 2014, "Dynamics of interpedicular widening in spinal burst fractures: an in vitro investigation," *Spine J.*
- [2] Hongo, M., Abe, E., Shimada, Y., Murai, H., Ishikawa, N., and Sato, K., 1999, "Surface Strain Distribution on Thoracic and Lumbar Vertebrae Under Axial Compression: The Role in Burst Fractures," *Spine*, 24(12), p. 1197.
- [3] Whyne, C. M., Hu, S. S., and Lotz, J. C., 2003, "Burst fracture in the metastatically involved spine: development, validation, and parametric analysis of a three-dimensional poroelastic finite-element model," *Spine (Phila Pa 1976)*, 28(7), pp. 652-660.
- [4] Zirbel, S. A., Stolworthy, D. K., Howell, L. L., and Bowden, A. E., 2013, "Intervertebral disc degeneration alters lumbar spine segmental stiffness in all modes of loading under a compressive follower load," *Spine J.*, 13(9), pp. 1134-1147.
- [5] Jiang, G., Luo, J., Pollintine, P., Dolan, P., Adams, M. A., and Eastell, R., 2010, "Vertebral fractures in the elderly may not always be "osteoporotic"," *Bone*, 47(1), pp. 111-116.
- [6] Cristofolini, L., Ferguson, S. J., Danesi, V., Erani, P., Viceconti, M., and Brandolini, N., IN PRESS, "A preliminary in vitro biomechanical evaluation of prophylactic cement augmentation of the thoracolumbar vertebrae," *Journal of Mechanics in Medicine and Biology* in press.
- [7] White, A. A., 3rd, and Panjabi, M. M., 1978, "The basic kinematics of the human spine. A review of past and current knowledge," *Spine (Phila Pa 1976)*, 3(1), pp. 12-20.
- [8] Brandolini, N., Cristofolini, L., and Viceconti, M., 2014, "Experimental methods for the biomechanical investigation of the human spine: a review " *Journal of Mechanics in Medicine and Biology*, 14(1), p. 1430002 (1430033 pages).
- [9] Lochmüller, E. M., Burklein, D., Kuhn, V., Glaser, C., Muller, R., Gluer, C. C., and Eckstein, F., 2002, "Mechanical strength of the thoracolumbar spine in the elderly: prediction from in situ dual-energy X-ray absorptiometry, quantitative computed tomography (QCT), upper and lower limb peripheral QCT, and quantitative ultrasound," *Bone*, 31(1), pp. 77-84.
- [10] Cristofolini, L., Brandolini, N., Danesi, V., Juszczak, M. M., Erani, P., and Viceconti, M., 2013, "Strain distribution in the lumbar vertebrae under different loading configurations," *The Spine Journal*, 13(10), pp. 1281-1292.
- [11] Kayanja, M. M., Ferrara, L. A., and Lieberman, I. H., 2004, "Distribution of anterior cortical shear strain after a thoracic wedge compression fracture," *The Spine Journal*, 4(1), pp. 76-87.
- [12] Ananthakrishnan, D., Berven, S., Deviren, V., Cheng, K., Lotz, J. C., Xu, Z., and Puttitz, C. M., 2005, "The effect on anterior column loading due to different vertebral augmentation techniques," *Clin Biomech (Bristol, Avon)*, 20(1), pp. 25-31.
- [13] Lu, Y., Maquer, G., Museyko, O., Puschel, K., Engelke, K., Zysset, P., Morlock, M., and Huber, G., 2014, "Finite element analyses of human vertebral bodies embedded in polymethylmethacrylate or loaded via the hyperelastic intervertebral disc models provide equivalent predictions of experimental strength," *J Biomech*, 47(10), pp. 2512-2516.
- [14] Andresen, R., Werner, H., and Schober, H., 1998, "Contribution of the cortical shell of vertebrae to mechanical behaviour of the lumbar vertebrae with implications for predicting fracture risk," *Br J Radiol*, 71(847), pp. 759-765.

- [15] Ebbesen, E. N., Thomsen, J. S., Beck-Nielsen, H., Nepper-Rasmussen, H. J., and Mosekilde, L., 1999, "Lumbar vertebral body compressive strength evaluated by dual-energy X-ray absorptiometry, quantitative computed tomography, and ashing," *Bone*, 25(6), pp. 713-724.
- [16] Perilli, E., Briggs, A. M., Kantor, S., Codrington, J., Wark, J. D., Parkinson, I. H., and Fazzalari, N. L., 2012, "Failure strength of human vertebrae: prediction using bone mineral density measured by DXA and bone volume by micro-CT," *Bone*, 50(6), pp. 1416-1425.
- [17] Fields, A. J., Eswaran, S. K., Jekir, M. G., and Keaveny, T. M., 2009, "Role of Trabecular Microarchitecture in Whole-Vertebral Body Biomechanical Behavior," *Journal of Bone and Mineral Research*, 24(9), pp. 1523-1530.
- [18] Chevalier, Y., Pahr, D., Charlebois, M., Heini, P., Schneider, E., and Zysset, P., 2008, "Cement distribution, volume, and compliance in vertebroplasty: some answers from an anatomy-based nonlinear finite element study," *Spine (Phila Pa 1976)*, 33(16), pp. 1722-1730.
- [19] Aquarius, R., van der Zijden, A. M., Homminga, J., Verdonschot, N., and Tanck, E., 2013, "Does bone cement in percutaneous vertebroplasty act as a stress riser?," *Spine (Phila Pa 1976)*, 38(24), pp. 2092-2097.
- [20] Belkoff, S. M., Mathis, J. M., Fenton, D. C., Scribner, R. M., Reiley, M. E., and Talmadge, K., 2001, "An ex vivo biomechanical evaluation of an inflatable bone tamp used in the treatment of compression fracture," *Spine (Phila Pa 1976)*, 26(2), pp. 151-156.
- [21] Heini, P. F., Berlemann, U., Kaufmann, M., Lippuner, K., Fankhauser, C., and van Landuyt, P., 2001, "Augmentation of mechanical properties in osteoporotic vertebral bones--a biomechanical investigation of vertebroplasty efficacy with different bone cements," *Eur Spine J*, 10(2), pp. 164-171.
- [22] Higgins, K. B., Harten, R. D., Langrana, N. A., and Reiter, M. F., 2003, "Biomechanical effects of unipedicular vertebroplasty on intact vertebrae," *Spine (Phila Pa 1976)*, 28(14), pp. 1540-1547; discussion 1548.
- [23] Ikeuchi, M., Yamamoto, H., Shibata, T., and Otani, M., 2001, "Mechanical augmentation of the vertebral body by calcium phosphate cement injection," *Journal of orthopaedic science : official journal of the Japanese Orthopaedic Association*, 6(1), pp. 39-45.
- [24] Buckley, J. M., Cheng, L., Loo, K., Slyfield, C., and Xu, Z., 2007, "Quantitative Computed Tomography-Based Predictions of Vertebral Strength in Anterior Bending," *Spine*, 32(9), pp. 1019-1027.
- [25] Buckley, J. M., Kuo, C. C., Cheng, L. C., Loo, K., Motherway, J., Slyfield, C., Deviren, V., and Ames, C., 2009, "Relative strength of thoracic vertebrae in axial compression versus flexion," *The Spine Journal*, 9(6), pp. 478-485.
- [26] Edmondston, S. J., Singer, K. P., Day, R. E., Price, R. I., and Breidahl, P. D., 1997, "Ex vivo estimation of thoracolumbar vertebral body compressive strength: The relative contributions of bone densitometry and vertebral morphometry," *Osteoporosis International*, 7(2), pp. 142-148.
- [27] Furtado, N., Oakland, R. J., Wilcox, R. K., and Hall, R. M., 2007, "A Biomechanical Investigation of Vertebroplasty in Osteoporotic Compression Fractures and in Prophylactic Vertebral Reinforcement," *Spine*, 32(17), pp. E480-E487  
410.1097/BRS.1090b1013e31811ea31812ee.
- [28] Imai, K., Ohnishi, I., Bessho, M., and Nakamura, K., 2006, "Nonlinear finite element model predicts vertebral bone strength and fracture site," *Spine (Phila Pa 1976)*, 31(16), pp. 1789-1794.

- [29] Dall'Ara, E., Schmidt, R., Pahr, D., Varga, P., Chevalier, Y., Patsch, J., Kainberger, F., and Zysset, P., 2010, "A nonlinear finite element model validation study based on a novel experimental technique for inducing anterior wedge-shape fractures in human vertebral bodies in vitro," *Journal of Biomechanics*, 43(12), pp. 2374-2380.
- [30] Yerby, S. A., Bay, B. K., Toh, E., McLain, R. F., and Drews, M. J., 1998, "The effect of boundary conditions on experimentally measured trabecular strain in the thoracic spine," *J Biomech*, 31(10), pp. 891-897.
- [31] Hussein, A. I., Mason, Z. D., and Morgan, E. F., 2013, "Presence of intervertebral discs alters observed stiffness and failure mechanisms in the vertebra," *J Biomech*, 46(10), pp. 1683-1688.
- [32] Eswaran, S. K., Gupta, A., Adams, M. F., and Keaveny, T. M., 2006, "Cortical and trabecular load sharing in the human vertebral body," *J Bone Miner Res*, 21(2), pp. 307-314.
- [33] Danesi, V., Zani, L., Scheele, A., Berra, F., and Cristofolini, L., 2014, "Reproducible reference frame for in vitro testing of the human vertebrae," *Journal of biomechanics*, 47(1), pp. 313-318.
- [34] Cristofolini, L., Conti, G., Juszczak, M., Cremonini, S., Van Sint Jan, S., and Viceconti, M., 2010, "Structural behaviour and strain distribution of the long bones of the human lower limbs," *J Biomech*, 43(5), pp. 826-835.
- [35] Liebschner, M. A., Kopperdahl, D. L., Rosenberg, W. S., and Keaveny, T. M., 2003, "Finite element modeling of the human thoracolumbar spine," *Spine (Phila Pa 1976)*, 28(6), pp. 559-565.
- [36] Kopperdahl, D. L., Pearlman, J. L., and Keaveny, T. M., 2000, "Biomechanical consequences of an isolated overload on the human vertebral body," *Journal of Orthopaedic Research*, 18(5), pp. 685-690.
- [37] Cristofolini, L., Juszczak, M., Taddei, F., and Viceconti, M., 2009, "Strain distribution in the proximal human femoral metaphysis," *Proc Inst Mech Eng H*, 223(3), pp. 273-288.
- [38] Lanyon, I. E., 1980, "Bone remodelling, mechanical stress, and osteoporosis," *Osteoporosis*, H. F. De Luca, ed., University Park Press, Baltimore, pp. 129-138.
- [39] Bayraktar, H. H., Morgan, E. F., Niebur, G. L., Morris, G. E., Wong, E. K., and Keaveny, T. M., 2004, "Comparison of the elastic and yield properties of human femoral trabecular and cortical bone tissue," *J Biomech*, 37(1), pp. 27-35.
- [40] Rohlmann, A., Graichen, F., Bender, A., Kayser, R., and Bergmann, G., 2008, "Loads on a telemeterized vertebral body replacement measured in three patients within the first postoperative month," *Clinical Biomechanics*, 23(2), pp. 147-158.
- [41] Bergmann, G., 2011, " (ed.), Charite – Universitaetsmedizin Berlin "OrthoLoad". Retrieved July 1, 2011. <<http://www.OrthoLoad.com>>."
- [42] Cristofolini, L., Pallini, F., Schileo, E., Juszczak, M., Varini, E., Martelli, S., and Taddei, F., 2006, ""Biomechanical testing of the proximal femoral epiphysis: intact and implanted condition,"" *Proceedings of 8th Biennial ASME Conference CD*, Profumo F: ed., ASME Publ.: 95187.
- [43] Ross, S. M., 2003, "Peirce's criterion for the elimination of suspect experimental data," *J. Engineering Technology*, 2003(Fall), pp. 1-12.

- [44] Fahim, D. K., Sun, K., Tawackoli, W., Mendel, E., Rhines, L. D., Burton, A. W., Kim, D. H., Ehni, B. L., and Liebschner, M. A., 2011, "Premature adjacent vertebral fracture after vertebroplasty: a biomechanical study," *Neurosurgery*, 69(3), pp. 733-744.
- [45] Oakland, R. J., Furtado, N. R., Wilcox, R. K., Timothy, J., and Hall, R. M., 2009, "Preliminary biomechanical evaluation of prophylactic vertebral reinforcement adjacent to vertebroplasty under cyclic loading," *The Spine Journal*, 9(2), pp. 174-181.
- [46] Cristofolini, L., 2015, "In vitro evidence of the structural optimization of the human skeletal bones," *J Biomech*, 48(5), pp. 787-796.
- [47] Adams, M. A., Dolan, P., and McNally, D. S., 2009, "The internal mechanical functioning of intervertebral discs and articular cartilage, and its relevance to matrix biology," *Matrix biology : journal of the International Society for Matrix Biology*, 28(7), pp. 384-389.
- [48] Kyere, K. A., Than, K. D., Wang, A. C., Rahman, S. U., Valdivia-Valdivia, J. M., La Marca, F., and Park, P., 2012, "Schmorl's nodes," *Eur Spine J*, 21(11), pp. 2115-2121.
- [49] McLain, R. F., Yerby, S. A., and Moseley, T. A., 2002, "Comparative morphometry of L4 vertebrae: comparison of large animal models for the human lumbar spine," *Spine (Phila Pa 1976)*, 27(8), pp. E200-206.
- [50] Pollintine, P., Dolan, P., Tobias, J. H., and Adams, M. A., 2004, "Intervertebral disc degeneration can lead to "stress-shielding" of the anterior vertebral body: a cause of osteoporotic vertebral fracture?," *Spine (Phila Pa 1976)*, 29(7), pp. 774-782.
- [51] Hansson, T., Roos, B., and Nachemson, A., 1980, "The bone mineral content and ultimate compressive strength of lumbar vertebrae," *Spine (Phila Pa 1976)*, 5(1), pp. 46-55.
- [52] Hulme, P. A., Boyd, S. K., and Ferguson, S. J., 2007, "Regional variation in vertebral bone morphology and its contribution to vertebral fracture strength," *Bone*, 41(6), pp. 946-957.
- [53] Hussein, A. I., Barbone, P. E., and Morgan, E. F., 2012, "Digital Volume Correlation for Study of the Mechanics of Whole Bones," *Procedia IUTAM*, 4, pp. 116-125.
- [54] Roberts, B. C., Perilli, E., and Reynolds, K. J., 2014, "Application of the digital volume correlation technique for the measurement of displacement and strain fields in bone: a literature review," *J Biomech*, 47(5), pp. 923-934.
- [55] Freddi, A., Olmi, G., and Cristofolini, L., 2015, *Experimental Stress Analysis for Materials and Structures: Stress Analysis Models for Developing Design Methodologies*, Springer, Cham (Switzerland).
- [56] Palanca, M., Tozzi, G., Cristofolini, L., Viceconti, M., and Dall'Ara, E., 2015, "Three-dimensional local measurements of bone strain and displacement: comparison of three digital volume correlation approaches," *J Biomech Eng*, 137(7).

# **CHAPTER 4:**

## **Elastic full-field strain analysis and microdamage progression in the vertebral body from digital volume correlation**

Gianluca Tozzi<sup>1</sup>, Valentina Danesi<sup>2</sup>, Marco Palanca<sup>2</sup>, Luca Cristofolini<sup>2</sup>

<sup>1</sup>School of Engineering, University of Portsmouth, UK

<sup>2</sup> Department of Industrial Engineering, Alma Mater Studiorum – Università di Bologna, Italy

*The candidate was one of the main investigator of the present work, taking care of imaging acquisition, in vitro testing and DVC analysis. This paper was submitted to Strain.*

## 4.1 Abstract

The strain distribution in vertebral body has been measured *in vitro* in the elastic regime, but only on the bone surface by means of strain gauges and digital image correlation (DIC). Micro-CT based digital volume correlation (DVC) allowed measurements of the internal strain distribution in bone at both tissue (trabecular and cortical bone) and organ (vertebra) level. However, DVC has been mainly employed to investigate failure of the vertebral body, but hasn't yet been deployed to investigate the internal strain distribution in the elastic regime. In this sense, recent methodological studies on DVC helped in improving its accuracy and precision, so that even relatively low strain can be reliably measured. The aim of this study was to investigate elastic strain and failure inside the vertebral body, including analysis of strain in all directions. Three porcine thoracic vertebrae were micro-CT scanned in a step-wise fashion at increasing steps of compression (5%, 10%, 15%). Micro-CT images successfully identified regions of failure initiation and progression, which were well quantified by DVC-computed strains. Interestingly, the same regions where failure eventually occurred experienced the largest strain magnitude also for the lowest degrees of compression (yet in the elastic regime).

**Keywords:** digital volume correlation, micro-CT, bone, vertebral body, microdamage, full-field strain, elastic strain.

## 4.2 Introduction

Pathologies such as osteoporosis and bone metastases are the major causes of vertebral fractures, often in combination with trauma or para-physiological overloading. These vertebrae are weak because their micro- and/or macro-structure are pathologically compromised. If untreated, they might fracture, causing severe disabilities and in some cases even mortality [1, 2]. For this reason, knowledge of the failure mechanism in the vertebra is of fundamental importance to understand vertebral biomechanics [3], improve diagnosis and prophylactic treatments [4, 5].

*In vitro* testing of the vertebral body has been extensively carried out in the past [6]. The strain distribution in the vertebral body was investigated using different experimental techniques but mainly with strain gauges [7], where the full-field strain distribution was not investigated. Furthermore, strain gauges are associated with a reinforcement effect that in the case of a thin shell of cortical bone cannot be neglected [8].

More recently, digital image correlation (DIC) was adopted to investigate the full-field strain distribution on the cortical surface of vertebrae, in an attempt to avoid direct contact measurement (i.e. via strain gauges) that could potentially produce important artifacts in the local strain determination [9]. To this extent, [10] presented a comparison of strain rosettes and DIC to measure the vertebral body strain. In that study porcine vertebrae were prepared with a strain rosette plus a speckled paint pattern for DIC and loaded in compression. However, it must be pointed out that also the specimen preparation for an appropriate DIC measurement (i.e. speckle pattern distribution) must be planned carefully if reliable results are to be achieved [9, 11]. When measuring strain in bone one must consider the magnitude of strain experienced during physiological tasks (1000-2000 microstrain, [12]), and the failure strain of bone tissue (7000-10000 microstrain, [13]). The overall precision that can be obtained with strain gauges when applied to bone is of the order of 1-2% of the readout [8, 14], which corresponds to 10-20 microstrain when physiological strains are applied *in vitro*. The overall precision that can be obtained with DIC (which is mainly limited by noise) is of the order of 100-300 microstrain [8-10].

In any case, for all the above studies with strain gauges and DIC the main limitation is represented by the inability to capture and quantify internal microdamage evolution and full-field strain distribution under load. As the internal trabecular bone of the vertebral body plays a

fundamental structural role [3] it would be extremely important to measure the internal strain distribution. In fact, a number of studies have shown that in several cases failure starts inside the vertebral body itself [15, 16]. In this perspective, digital volume correlation (DVC) is ideal to investigate the internal strain distribution and the local damage inside the vertebra. In recent years, DVC has become a powerful tool to examine full-field internal deformations mainly in trabecular [17-21] and cortical bone [19, 21, 22]. The use of DVC to investigate the strain distribution in vertebrae has been firstly introduced by Hardisty et al. [23]. In that study a new image registration algorithm was developed to spatially resolve strain in whole bones (rat vertebrae) using micro-CT images. Since then, a number of studies investigated the full-field strain distribution in vertebral bodies without [24] and with the adjacent intervertebral discs [25], as well as entire vertebrae [26] under compressive loading. Hussein et al. [24] reported the highest strain magnitudes (minimum principal strain) distributed in the superior-inferior (axial) direction ranging between -20000 and -40000 microstrain, in human vertebral bodies. In a following study from the same Authors [25], a comparison between vertebral body (rabbits) without and with the presence of adjacent intervertebral discs highlighted a different minimum principal strain distribution in the two configurations for yield and failure conditions, with maximum differences of -10000 microstrain for the average strain magnitude in the two configurations (with and without discs). However, in both studies [24, 25] there is no information on the progression of strain levels from the elastic regime (more physiological), preceding the final failure event. Also, the influence of strain directionality and local levels of strain on microdamage evolution in the vertebra has not been investigated. [26] is the only study to date to report the microdamage in metastatic and healthy vertebrae (rat models) associated with full-field strain from DVC, but only for the axial strain. That work reported an average axial strain at failure of -27000 microstrain for the healthy group (5 specimens), but no information of the critical strain values in different locations of the vertebrae. Another important aspect to be considered is the level of uncertainty of the DVC-computed strain distribution, that can be associated to imaging conditions, bone type, image preparation, computation sub-volume size and nature of the DVC approach (i.e. local vs global). Very recently, an in-depth methodological investigation of all those aspects for natural and augmented vertebral bodies (porcine models) was carried out [27, 28]. Those studies reported that strain uncertainties can be reduced below 300 microstrain for both local and global approaches if the images are adequately prepared (excluding the non-tissue background), and with an appropriate choice of the computation sub-volume size (i.e. 48 voxel for a 39 micrometers voxel size image).

In this study, full-field strain distributions inside porcine vertebral bodies were obtained through DVC under compressive load. Specifically, the main aims of this paper were:

- 1) to measure the internal strain, both in the elastic regime and up to failure;
- 2) to analyze the distribution of the different components of strain (axial, antero-posterior and lateral-lateral) for each specimen;
- 3) to identify microdamage initiation/progression during loading, and to correlate it with the distribution of the three components of strain.

## **4.3 Materials and Methods**

### **4.3.1 Materials and experimental procedures**

Three thoracic vertebrae (specimens T1, T2, T3) were harvested from animals that were bred and slaughtered for alimentary purposes. All the surrounding soft tissues were removed, including the ligaments and discs. The vertebrae were obtained from young animals, where the growth plates were still fully open. To avoid the presence of soft tissue and prevent viscoelastic phenomena (which might compromise image acquisition under load), the growth plates were removed together with the adjacent endplates (due to the young age of the animals at sacrifice, this could be performed with little manual effort). The endplate areas of the vertebrae were aligned and potted in poly-methyl-methacrylate (PMMA) following a procedure adapted from Danesi et al. [29]. The spinous process was used to center the specimen in the transverse plane and align it about its vertical axis. The posterior arch was subsequently removed.

Step-wise compression testing of the vertebrae in combination with time-lapsed micro-CT imaging was performed. *In situ* testing was conducted by means of a loading device (CT5000, Deben Ltd, UK), equipped with a 5kN load cell and a custom-designed environmental chamber which was filled with physiological saline solution (Fig. 4-1). The specimens were constrained against rotation inside the loading device with sandpaper discs applied to the bottom compressive platen. A preload of 50 N was applied. Each specimen was compressed axially under displacement control in a step-wise fashion. The compression steps were adjusted for each specimen based on its height, so that at each step the free height was compressed by 5% (this corresponded to actuator steps of 0.54-0.66 mm, depending on the specimen's size). All tests were carried out at a constant

actuator speed of 0.1 mm/sec. At each compression step the specimens were allowed to relaxate to reach a steady state for 15 minutes before imaging.

Micro-CT imaging (XTH225, Nikon Metrology, UK) was carried out at each step (0% with 50N preload, 5%, 10% and 15% compression). The micro-CT scanner was set to a voltage of 88-89 kV, a current of 115-116 microA and exposure time of 2 s. The image acquisition was performed at a rotational step of  $0.23^\circ$  over  $360^\circ$  for a scanning time of approximately 90 min at each compression step. The reconstructed micro-CT images had an isotropic voxel size of 38.8 micrometers.

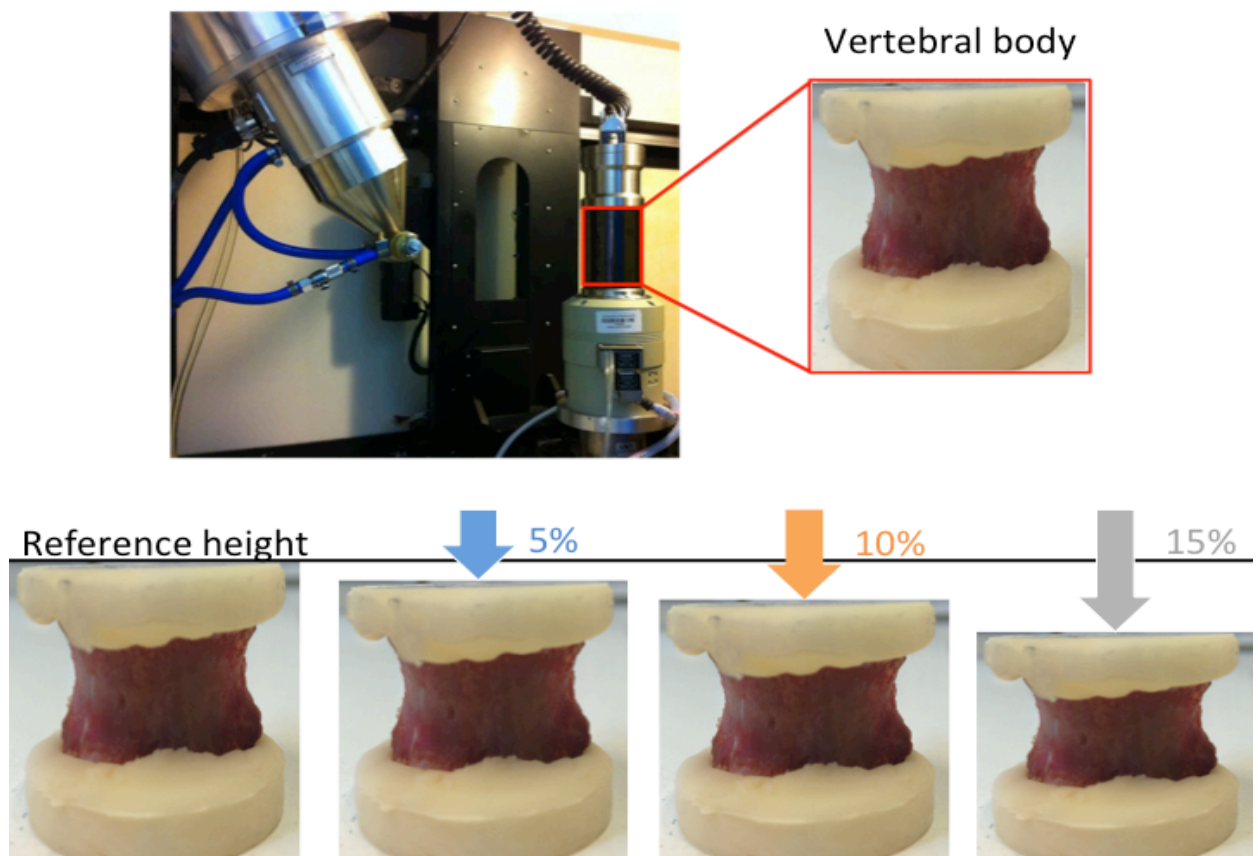


*Fig. 4-1: The mechanical loading device inside the micro-CT chamber (top-left). The specimen was potted in PMMA and aligned to the rotation axis of the micro-CT (top-right). At the bottom, the reference and compressive steps are shown.*

### 4.3.2 Digital volume correlation (DVC)

DaVis DVC software (v8.3, LaVision, Germany) was used to compute the full-field strains in the vertebra along the axial, antero-posterior and lateral-lateral directions. The operating principle of the DaVis DVC has been detailed elsewhere [21, 30]. Briefly, DaVis sub-divides the 3D images into smaller sub-volumes that can be correlated independently (local approach) as a discrete function of grey-levels. The matching between the sub-volumes corresponding to the different stages of loading is achieved via a direct correlation function (DaVis-DC). Additionally, a piece-wise linear shape function and a third-order spline interpolation in the image reconstruction are employed to help correlation of the pattern information contained in the reference and deformed images. The displacement vector field is obtained at the center of each sub-volume. The strain field is subsequently computed using a centered finite differences (CFD) scheme. The original micro-CT images were masked in order to remove the background areas where no bone was present. In fact, it was shown that regions that do not contain useful feature for the correlation algorithm are associated with large strain artifacts [27, 28]. A user-defined polygon mask was created, which corresponded to the contour shape of each vertebral body. The mask was defined in the transverse plane of the vertebral body and sequentially adapted in the cranial-caudal direction to follow the shape of the vertebra. The geometric mask enabled the DVC software to include only to voxels inside the mask (vertebral body area).

The DVC computation relied on final sub-volumes of 48 voxels, reached after successive (predictor) passes using sub-volumes of 128 voxels, 112 voxels, 96 voxels, 80 voxels and 64 voxels, with a 0% overlap. This multipass sequence was found to produce the lowest strain error in DaVis-DC for such type of specimens, with the same imaging and environmental settings [27, 28]. Given the voxel size of the acquired micro-CT images, the final computation sub-volume size corresponded to 1862 micrometers.

In order to evaluate the strain distribution in the vertebra and to associate local high-strains with visible microdamage, dedicated Matlab (v2014a, MathWorks, US) scripts were developed. This allowed visualization of the 3D strain maps for the three components of normal strain. Moreover, for each compression step, the average within each slice was computed for each component of strains (axial, antero-posterior and lateral-lateral strain), following a procedure reported in [21].

## 4.4 Results

The force-displacement curves showed a monotonic trend for all specimens while load was increased (Fig.4-2). Specimen failure (clearly visible as a plateau and decrease in the force-displacement plots) occurred at 10% or 15% steps in all specimens. The loads applied onto the three specimens for each loading steps are reported in Table 4-1. Relaxation was also visible at the end of each step of compression, when the actuator was stopped to allow micro-CT scanning.

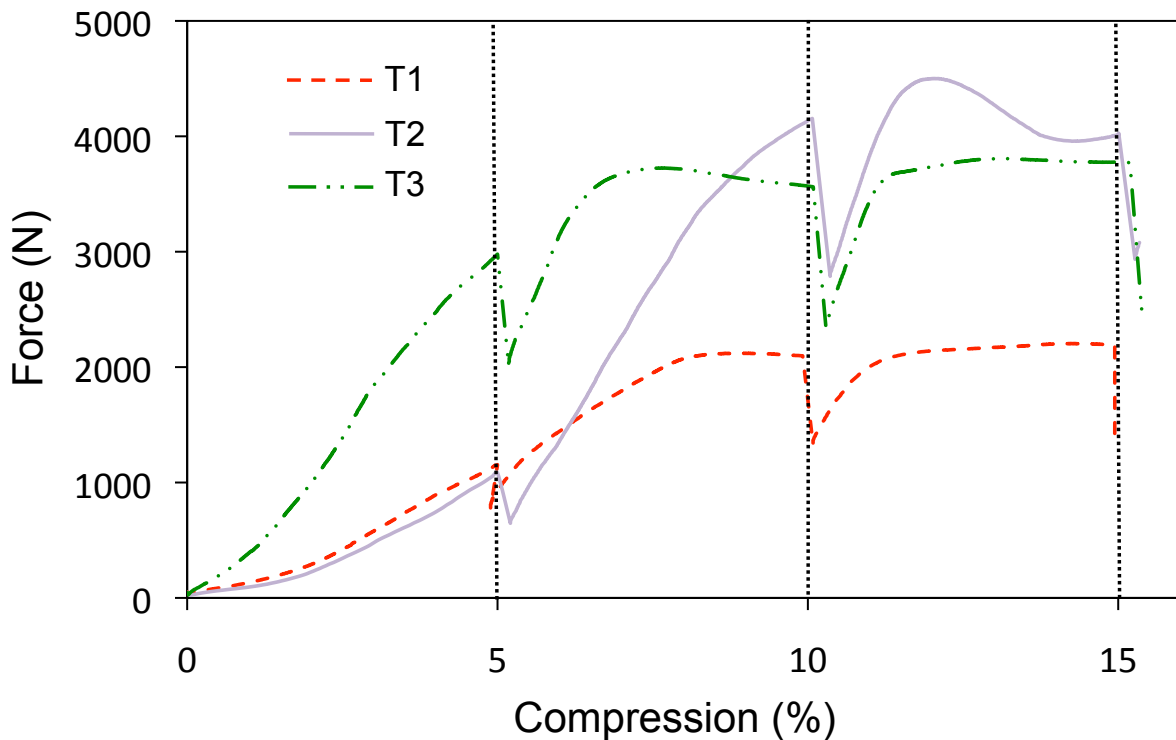


*Fig.4- 2: Force-compression curves for the three specimens. The load shows a drop at the end of each step of compression: this corresponds to relaxation while the specimen was allowed to settle (15 minutes) before the micro-CT scan took place (90 minutes).*

The internal strain distributions (axial, antero-posterior and lateral-lateral components of strain) for the three compression steps (5%, 10% and 15%) on the sagittal section of the three specimens are reported in Figures 4-3 4-4 and 4-5.

The micro-CT images of specimen T1 showed a main microdamage localized in the trabecular bone (caudal region), which started to appear at the 10% compressive step, and degenerated into a trabecular collapse at 15% (Fig. 4-3).

Table 4-1: Loads experienced by the three specimens (T1, T2, T3) at each step of compression (applied in displacement control).

Loading step	Specimen T1	Specimen T2	Specimen T3	Average and standard deviation of 3 specimens
Force at 5% compression	1115 N	1025 N	2917 N	1686 ± 1067N
Force at 10% compression	2104 N	4118 N	3576 N	3266 ± 1042 N
Force at 15% compression	2198 N	3994 N	3777 N	3323 ± 980 N

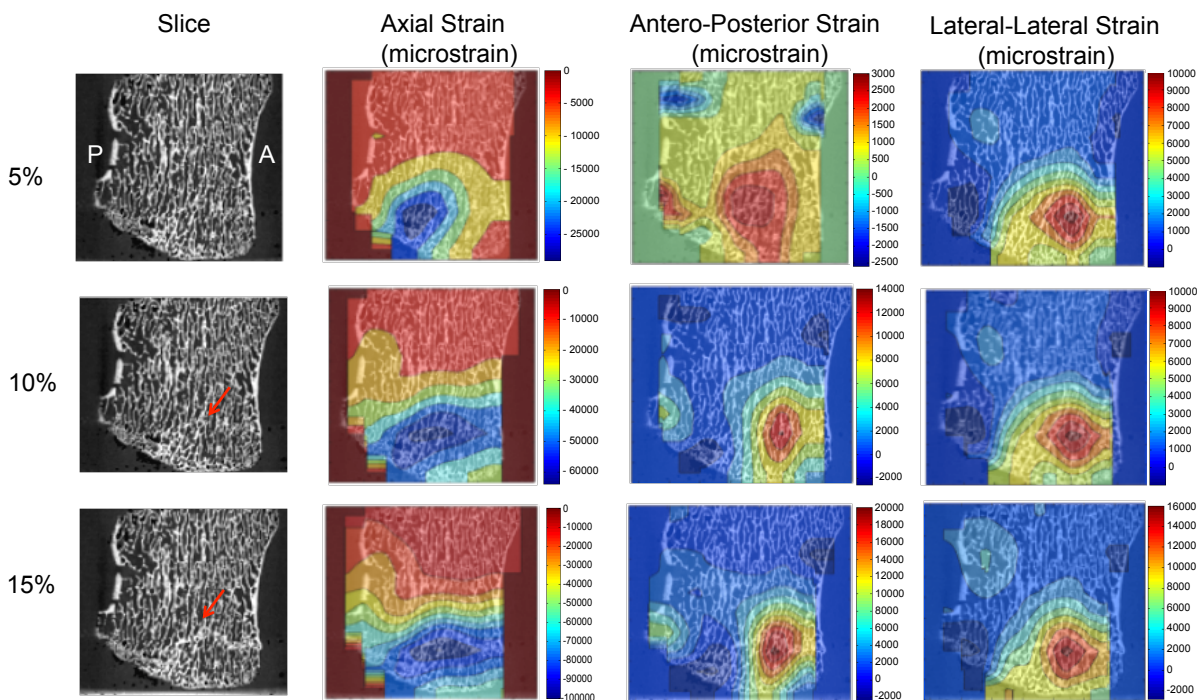


Fig. 4-3: Specimen T1: Internal strain distribution for the three steps of compression. Left: Sagittal micro-CT slice taken at each compression step (the antero (A) and posterior (P) regions are also indicated). The crushed zone of specimen T1 is visible in the images at 10% and 15% compression steps (red arrows). The distribution of the Axial, Antero-Posterior and Lateral-Lateral components of strain are plotted over the same sagittal slice in the colored plots. The most strained region

corresponded to the damaged area, which gradually progressed in a collapse propagating across the vertebral body, in an approximately transverse plane.

Such a collapse gradually led to a weakening of the vertebral body in the transverse plane, with damage extending to the cortical bone anteriorly. The distribution of the three components of strain well described the damage events, with the maximum strains located in regions adjacent to the crushed zone; away from the crushed zone the strains were significantly lower (Fig. 4-3).

A similar agreement between the damage (visible in the micro-CT images) and the distribution of strain (computed by means of DVC) was found in the other two specimens, although the damage pattern was different (Fig. 4-4 and 4-5). In specimen T2 the microdamage seemed to be localized in the trabecular structure as a gradual collapse that initiated (10%) and then propagated (15%) posteriorly, along the caudal-cranial direction (Fig. 4-4), similarly to specimen T1. In specimen T3 damage initiated in the cranial region (10% compression) and progressively extended as a collapse in a transverse plane (15% compression) (Fig. 4-5).

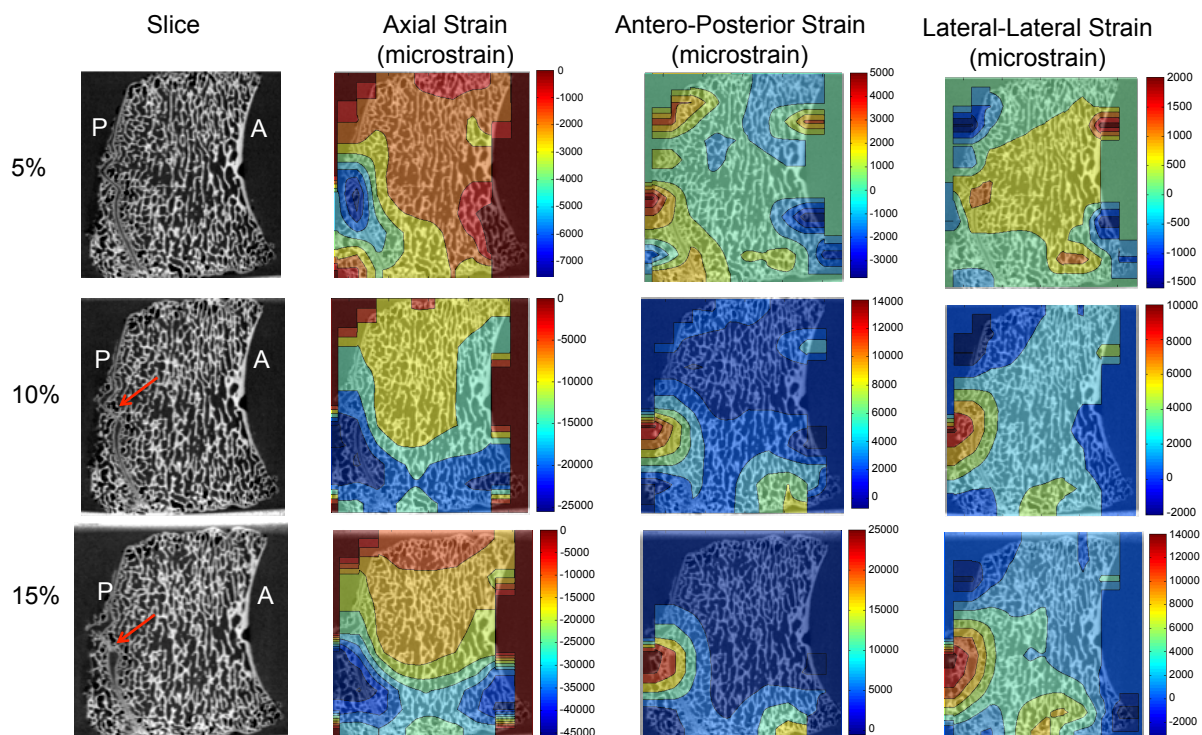


Fig. 4-4: Specimen T2: Internal strain distribution for the three steps of compression. Left: Sagittal micro-CT slice taken at each compression step (the antero (A) and posterior (P) regions are also indicated). The crushed zone of specimen T2 is visible in the images at 10% and 15% compression steps (red arrows). The distribution of the Axial, Antero-Posterior and Lateral-Lateral components

of strain are plotted over the same sagittal slice in the colored plots. The most strained region corresponded to the damaged area, which gradually progressed in a collapse propagating across the vertebral body, in an approximately caudal-cranial direction.

In general, for all specimens the increase of strain was larger from 10% to 15% compression, than from 5% to 10% compression, both for the axial component of strain (compressive), and the antero-posterior and lateral-lateral ones (tensile).

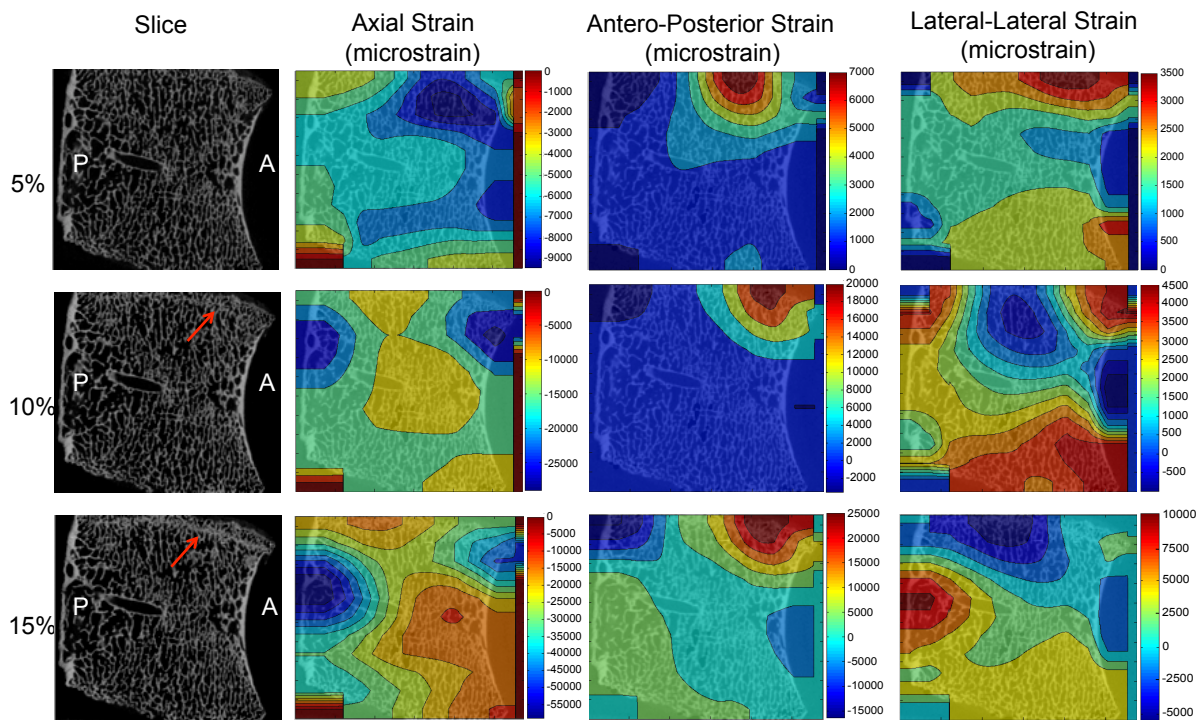


Fig. 4-5: Specimen T3: Internal strain distribution for the three steps of compression. Left: Sagittal micro-CT slice taken at each compression step (the antero (A) and posterior (P) regions are also indicated). The crushed zone of specimen T3 is visible in the images at 10% and 15% compression steps (red arrows). The distribution of the Axial, Antero-Posterior and Lateral-Lateral components of strain are plotted over the same sagittal slice in the colored plots. The most strained region corresponded to the damaged area, which gradually progressed in a collapse propagating across the vertebral body, in an approximately transverse plane.

For all specimens, the strain distribution in the elastic regime (first step of loading, 5%) showed a non-uniform strain distribution, which seemed to predict the location of damage initiation before it actually became identifiable (Fig. 4-3; 4-4; 4-5).

The progression of strain (axial, antero-posterior and lateral-lateral components of strain) during compression for the three specimens is shown in Figure 4-6 in terms of average strain at each cross-section.

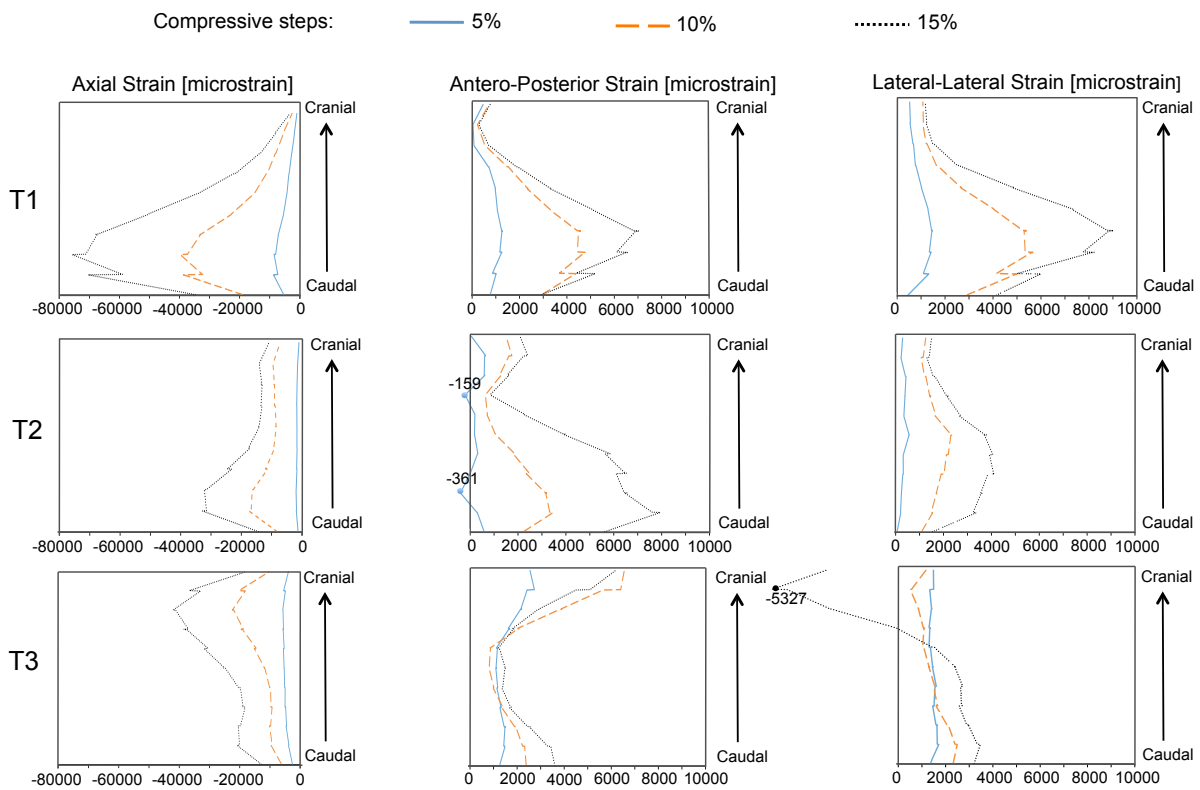


Fig. 4-6: Progression of strain as compression was increased (5%, 10% and 15% steps). The average strains were computed for each transverse slice of the DVC-computed 3D strain map for the Axial, Antero-Posterior and Lateral-Lateral components of strain. In general, an incremental strain pattern among the consecutive compression steps was observed in all specimens (T1, T2 and T3). The slices where the largest strains were observed corresponded to the areas where collapse was localized (Fig. 4-3;4-4;4-5).

Specimen T1 experienced the highest axial compressive strain (-75689 microstrain, average over the most strained cross-section), followed by specimen T3 (-42005 microstrain) and specimen T2 (-32859 microstrain). For the antero-posterior component of strain, the most strained regions experienced a strain between 6161 and 7940 microstrain (average over the most strained cross-section), in all specimens. For the lateral-lateral component of strain, the most strained regions experienced a strain between 3430 and 9013 microstrain (average over the most strained cross-section), in all specimens. The strain pattern along the caudal-cranial direction was similar for

specimens T1 and T2, with the largest deformation localized in correspondence of the first quarter caudal. In specimen T3 the highest axial strain magnitudes were found where the cortical shell was mostly curved (first quarter cranial); the largest antero-posterior and lateral-lateral strains were observed in correspondence of the cranial and caudal endplates. The cranial-posterior portion of this specimen was in a compressive state, with the largest strain (-5327 microstrain) at 15% loading step.

## 4.5 Discussion

The first aim of this paper was to evaluate the internal strain distribution (axial, antero-posterior and lateral-lateral components of strain) from DVC in porcine vertebral body, under applied compressive load. A deeper understanding of the internal elastic full-field strain distribution was achieved. In fact, despite a number of studies used DVC to investigate the vertebral global fracture under compression [24-26], the elastic strain distribution is still unexplored. The results clearly showed how local strain built up from the elastic regime, and highlighted those internal weaker regions that could result in microdamage initiation and progression up to vertebral failure (Fig. 4-3; 4-4; 4-5). When a compression of 5% was applied, all specimens experienced levels of internal tensile and compressive strains above or close to the typical values of bone tissue failure (i.e. 7000 microstrain for tensile and -10000 microstrain for compression as reported in [3]). For two specimens (T1 and T2) rather regular strain maps were identified for each component of strain, and for the steps of applied Compression. Conversely, the third specimen (T3) exhibited a more irregular strain distribution, possibly associated with the superimposition of compression and some degree of bending.

The benefit of using DVC compared to surface strain measurement techniques (i.e. strain gauges or DIC) is particularly evident in specimen T1. In fact, surface strain measurement in the 5% compression step (load of 1115 N) would have only provided information on the strain distribution on the cortical shell that was mostly below the yield values for bone in both compression and tension (Fig. 4-3 and 4-6). In fact, strains of the order of 500 to 1500 microstrain were found in the cortical shell of vertebral bodies using strain gauges for a 1470 N compressive load [31] and average compressive and tensile strains (minimum and maximum principal strains) from DIC were found to be -2587 microstrain and 678 microstrain for a compressive load equal to 2050 N [10]. These values would have therefore obscured the real nature of internal strain distribution and made impossible to predict where the damage in the vertebral body would initiate.

In this context the ability of DVC in identifying internal strain represents an invaluable resource, despite its lower strain precision (of the order of 100-300 microstrains) [27, 28] when compared to DIC (of the order of 10-50 of microstrains) [9, 32] or strain gauges (few microstrains)[10].

Another important advantage of DVC relies in its ability to quantify internal microdamage in the bone microstructures. The use of micro-CT image-guided failure assessment [33, 34] has allowed three-dimensional analysis of microdamage in bone tissue, allowing the assessment of damage onset and progression under load. In trabecular bone the microdamage is mainly characterised by bending and buckling of the trabeculae at different locations [34, 35]. The use of DVC allowed a successful coupling of a qualitative microdamage inspection (from micro-CT images), to quantitative information about the strain fields (from DVC), throughout the entire volume of the specimens [30]. Interestingly, the use of DVC in vertebral mechanics rarely focused on the coupling of microdamage with strain distribution in the failure region. When this was done, it mainly involved the axial strain [26], which is surely important in a compression loading but provides only incomplete physiological information. Conversely, when the main physiological directions (axial, antero-posterior and lateral-lateral components of strain) were considered, the microdamage development associated to that specific strain condition was not analyzed [24, 25]. Moreover, only scattered information on the average strains at the different levels along the vertebral body are reported [25]. Hussein et al. presented an average compressive strain (minimum principal strain) in six vertebral bodies at three locations; namely superior ( $-44000 \pm 53000$  microstrain), central ( $-49000 \pm 76000$  microstrain) and inferior ( $-50000 \pm 65000$  microstrain) regions. However, no details on the single vertebral bodies were reported and, as indicated by the large scatter in the results, a number of different damage patterns are to be expected. Our findings are in agreement with the results of Hussein et al. [25], where the most important compressive strains were found in caudal direction (or inferior) for both specimen T1 ( $-75689$  microstrain) and specimen T2 ( $-32859$  microstrain). Dissimilarly, the third specimen (T3) experienced highest compressive strains ( $-42005$  microstrain) in the cranial region, confirming the high standard deviations reported by Hussein et al. [25].

The current study has two main limitations. Firstly, the use of three specimens could not provide enough statistical power to identify consistent trends. However, this sample was sufficient to demonstrate the feasibility of measuring internal strain in the elastic regime, to correlate such elastic strain with the final failure mechanism and to understand the basic strain distribution

associated with microdamage in vertebral bodies. A second limitation relates to the use of animal vertebrae (which are certainly different from the human ones [7]). This choice was is justified by easier tissue availability compared to human, and by the possibility of fitting the entire vertebral body in the micro-CT scanner and its loading device. Additionally, animal tissue was also used in similar studies [23, 25, 26] and is fully justified for explorative *in vitro* testing of vertebrae [36].

## 4.6 Conclusions

In this paper building up of internal full-field strain from DVC in the elastic regime and progression up to failure was measured in vertebral bodies loaded under step-wise compression. Regions of internal microdamage were successfully matched with the distribution of strains, where axial, antero-posterior and lateral-lateral strains were monitored for all specimens at all levels of compression. The results obtained in this study clearly show how different vertebral bodies may be subjected to different stress/strain distribution. Thus, consequent microdamage can develop and progress in different ways towards the final failure of the vertebra. Interestingly, DVC-computed strains in the elastic regime have the ability to predict high-strain concentration and therefore damage before failure actually occurs. This has the potential to be implemented in clinical CT assessment of vertebrae, given controlled loading conditions during imaging.

## 4.7 References

1. Ferrar L., Jiang G., Adams J. and Eastell R. (2005) Identification of vertebral fractures: An update. *Osteoporosis International* **16**: 717-728.
2. Tancioni F., Lorenzetti M.A., Navarria P., Pessina F., Draghi R., Pedrazzoli P., Scorsetti M., Alloisio M., Santoro A. and Rodriguez y Baena R. (2011) Percutaneous vertebral augmentation in metastatic disease: state of the art. *J Support Oncol* **9**: 4-10.
3. Cristofolini L. (2015) In vitro evidence of the structural optimization of the human skeletal bones. *Journal of biomechanics* **48**: 787-796.
4. Goel V.K., Panjabi M.M., Patwardhan A.G., Dooris A.P. and Serhan H. (2006) Test Protocols for Evaluation of Spinal Implants. *Journal of Bone and Joint Surgery* **88**: 103-109.
5. Pollintine P., van Tunen M.S., Luo J., Brown M.D., Dolan P. and Adams M.A. (2010) Time-dependent compressive deformation of the ageing spine: relevance to spinal stenosis. *Spine (Phila Pa 1976)* **35**: 386-394.
6. Brandolini N., Cristofolini L. and Viceconti M. (2014) Experimental Method for the Biomechanical Investigation of Human Spine: a Review *Journal Of Mechanics in Medicine and Biology* **14**: 1430002.
7. Cristofolini L., Brandolini N., Danesi V., Juszczak M.M., Erani P. and Viceconti M. (2013) Strain distribution in the lumbar vertebrae under different loading configurations. *The spine journal : official journal of the North American Spine Society* **13**: 1281-1292.
8. Freddi A., Olmi G. and Cristofolini L. (2015) *Experimental Stress Analysis for Materials and Structures: Stress Analysis Models for Developing Design Methodologies* Springer.
9. Palanca M., Brugo T.M. and Cristofolini L. (2015) Use of Digital Image Correlation to Understand the Biomechanics of the Vertebra. *Journal Of Mechanics in Medicine and Biology* **15**: 1540004-1540001/1540004-1540010.
10. Gustafson H., Siegmund G. and Cripton P. (2016) Comparison of Strain Rosettes and Digital Image Correlation for Measuring Vertebral Body Strain. *Journal of biomechanical engineering* **Accepted**.
11. Lionello G. and Cristofolini L. (2014) A practical approach to optimizing the preparation of speckle patterns for digital-image correlation. *Measurement Science and Technology* **25**: 107001.
12. Lanyon I.E. (1980) Bone remodelling, mechanical stress, and osteoporosis. In: Osteoporosis, H.F. De Luca (Ed). University Park Press, Baltimore: 129-138.
13. Bayraktar H.H., Morgan E.F., Niebur G.L., Morris G.E., Wong E.K. and Keaveny T.M. (2004) Comparison of the elastic and yield properties of human femoral trabecular and cortical bone tissue. *Journal of biomechanics* **37**: 27-35.
14. Cristofolini L. and Viceconti M. (1997) Comparison of Uniaxial and Triaxial Rosette Gages for Strain Measurement in the Femur. *Experimental Mechanics* **37**: 350 - 354.

15. Silva M.J., Keaveny T.M. and Hayes W.C. (1997) Load sharing between the shell and centrum in the lumbar vertebral body. *Spine (Phila Pa 1976)* **22**: 140-150.
16. Wang X.-Y., Dai L.-Y., Xu H.-Z. and Chi Y.-L. (2007) The Load-Sharing Classification of Thoracolumbar Fractures: An In Vitro Biomechanical Validation. *Spine* **32**: 1214-1219  
1210.1097/BRS.1210b1013e318053ec318069.
17. Liu L. and Morgan E.F. (2007) Accuracy and precision of digital volume correlation in quantifying displacements and strains in trabecular bone. *Journal of biomechanics* **40**: 3516-3520.
18. Gillard F., Boardman R., Mavrogordato M., Hollis D., Sinclair I., Pierron F. and Browne M. (2014) The application of digital volume correlation (DVC) to study the microstructural behaviour of trabecular bone during compression. *J Mech Behav Biomed Mater* **29**: 480-499.
19. Dall'Ara E., Barber D. and Viceconti M. (2014) About the inevitable compromise between spatial resolution and accuracy of strain measurement for bone tissue: A 3D zero-strain study. *Journal of biomechanics* **47**: 2956 - 2963.
20. Roberts B.C., Perilli E. and Reynolds K.J. (2014) Application of the digital volume correlation technique for the measurement of displacement and strain fields in bone: A literature review. *Journal of biomechanics* **47**: 923-934.
21. Palanca M., Tozzi G., Cristofolini L., Viceconti M. and Dall'Ara E. (2015) 3D Local Measurements of Bone Strain and Displacement: Comparison of Three Digital Volume Correlation Approaches. *J Biomech Eng (ASME)* **137**: 071006-071001/071006-071014.
22. Christen D., Levchuk A., Schori S., Schneider P., Boyd S.K. and Muller R. (2012) Deformable image registration and 3D strain mapping for the quantitative assessment of cortical bone microdamage. *Journal of Mechanical Behavior of Biomedical Materials* **8**: 184-193.
23. Hardisty M.R. and Whyne C.M. (2009) Whole bone strain quantification by image registration: a validation study. *Journal of biomechanical engineering* **131**: 064502.
24. Hussein A.I., Barbone P.E. and Morgan E.F. (2012) Digital Volume Correlation for Study of the Mechanics of Whole Bones. *Procedia IUTAM* **4**: 116-125.
25. Hussein A.I., Mason Z.D. and Morgan E.F. (2013) Presence of intervertebral discs alters observed stiffness and failure mechanisms in the vertebra. *Journal of biomechanics* **46**: 1683-1688.
26. Hardisty M., Akens M., Hojjat S., Yee A. and Whyne C. (2012) Quantification of the Effect of Osteolytic Metastases on Bone Strain within Whole Vertebrae Using Image Registration. *J Orthop Res* **30**: 1032-1039.
27. Palanca M., Tozzi G., Dall'Ara E., Curto M., Innocente F., Danesi V. and Cristofolini L. (2016) Strain uncertainties from two digital volume correlation approaches in natural and augmented vertebrae: an organ-level analysis. *J Mech Behav Biomed Mater* **Submitted**.
28. Tozzi G., Dall'Ara E., Palanca M., Curto M., Innocente F. and Cristofolini L. (2016) Strain uncertainties from two DVC approaches in prophylactically augmented vertebrae: local analysis on bone and bone-cement microstructures. *Journal of the Mechanical Behavior of Biomedical Materials* **Submitted**.

29. Danesi V., Zani L., Scheele A., Berra F. and Cristofolini L. (2014) Reproducible reference frame for in vitro testing of the human vertebrae. *Journal of biomechanics* **47**: 313-318.
30. Tozzi G., Zhang Q.H. and Tong J. (2014) Microdamage assessment of bone-cement interfaces under monotonic and cyclic compression. *Journal of biomechanics* **47**: 3466 - 3474.
31. Shah J., Hampson W. and Jayson M. (1978) The distribution of surface strain in the cadaveric lumbar spine. *J Bone Joint Surg Br* **60-B**: 246-251.
32. Grassi L. and Isaksson H. (2015) Extracting accurate strain measurements in bone mechanics: A critical review of current methods. *J Mech Behav Biomed Mater* **50**: 43-54.
33. Nazarian A. and Müller R. (2004) Time-lapsed microstructural imaging of bone failure behavior. *Journal of biomechanics* **37**: 55-65.
34. Tozzi G., Zhang Q.H. and Tong J. (2012) 3D real-time micromechanical compressive behaviour of bone-cement interface: experimental and finite element studies. *Journal of biomechanics* **45**: 356-363.
35. Tozzi G., Zhang Q.H., Lupton C., Tong J., Guillen T., Ohrndorf A. and Christ H.J. (2013) Characterisation of a metallic foam-cement composite under selected loading conditions. *J Mater Sci Mater Med* **24**: 2509-2518.
36. Brandolini N., Cristofolini L. and Viceconti M. (2014) Experimental Methods for the biomechanical investigation of the human spine: a review. *Journal Of Mechanics in Medicine and Biology* **14**: 1430002.

## **Chapter 5:**

# **Application of digital volume correlation to study the efficacy of prophylactic vertebral augmentation**

Valentina Danesi<sup>1</sup>, Gianluca Tozzi<sup>2</sup>, Luca Cristofolini<sup>3</sup>

<sup>1</sup>Department of Industrial Engineering, Alma Mater Studiorum – Università di Bologna, Italy

<sup>2</sup>School of Engineering, University of Portsmouth, UK

*The candidate was the first investigator of this study. This paper was submitted to Clinical Biomechanics.*

## 5.1 Abstract

While the biomechanical effects of vertebroplasty on fractured vertebrae have been thoroughly investigated, very little data exist regarding the effects of prophylactic augmentation on non-fractured vertebrae. Moreover, such studies on vertebroplasty and prophylactic augmentation mainly focused on the overall failure strength of the treated vertebral body, without analyzing the internal strain distributions. The aim of this study was, for the first time, to measure the full-field strain distributions by means of DVC inside prophylactically augmented vertebral bodies under compression. Specifically, we aimed at investigating the state of strain distribution inside the vertebral body, in the injected cement, and in the cement-bone interdigitated region of vertebrae that were prophylactically augmented with two different cements, including the elastic regime (axial, antero-posterior and lateral-lateral components of strain), but also the internal micro-failure mechanisms. Destructive tests were carried out on twelve porcine natural and prophylactically augmented vertebral bodies. Specimens were tested under axial-compression loading in a step-wise fashion. Micro-CT images were acquired after each loading step of compression (5%, 10%, 15%). Micro-CT images successfully identified regions of failure initiation and progression, which were well quantified by DVC-computed strains. Our findings showed that prophylactic augmentation increased the force required to induce damage only in some of the vertebrae and other specimens failed under a force that was lower than the one produced in the controls. Augmentation was not associated to an evident modification of the strain magnitude when compared to the control vertebrae, but rather to a different localization of highly strained regions due to the variable cement distribution. Such elevated strain concentration within the cement did not produce visible damage to the cement region itself, but affected the strength of the surrounded trabecular bone, resulting in an increased fracture risk at the cement-bone interdigitated region and of the surrounding trabecular bone regions just above or below the cement mass.

**Keywords:** Augmentation, Digital volume correlation, Micro-CT, Bone, Vertebral body, Fracture, Microdamage, full-field strain measurement, elastic strain.

## 5.2 Introduction

Vertebral fractures are a severe cause of morbidity and disability [1, 2], as well as a significant burden for healthcare systems [3]. The cause of the fracture may be pathological, traumatic, or a combination of the two. The main pathological conditions are osteoporosis [4] or metastatic lesion [5], whose metabolic alterations result in bone weakening. However, the biomechanics underlying fracture onset and development of post-fracture and prophylactic treatments raises research questions that are still far from being answered.

In the last years prophylactic augmentation has been proposed as an alternative to pharmacological treatments [6] in order to reduce the fracture risk of osteoporotic vertebrae [2, 7-10] or to prevent adjacent fractures after augmentation [11, 12]. This treatment is meant to increase the strength and the structural support of weak vertebrae, by the injection of an augmentation material into the vertebral body [7, 10, 11, 13-15].

The associated risks such as cement leakage and subsequent neural damage; tissue necrosis due to residual monomer and to the exothermal reaction; increased risk of fracture in the adjacent vertebrae, have raised questions about the efficacy and safety of the vertebroplasty [16-20]. Moreover, prophylactic augmentation (treatment of non-fractured vertebra) exposes the patients to additional risk, hence there is a need for a clearer understanding on the cost-benefit trade-off. For this reason, in-depth knowledge of the mechanical behaviour and failure of prophylactic-augmented vertebra is of fundamental importance to understand vertebral biomechanics and improve diagnosis and prophylactic treatments [14].

Furthermore, it is still debated whether prophylactic augmentation actually strengthens the treated vertebra. The increasing interest in the use of prophylactic augmentation, as a treatment for reduce the risk of fracture, has led to a number of experimental studies [13, 21-32]. Several in vitro studies showed that the strength of prophylactically augmented vertebrae was on average greater than that of non-augmented vertebrae [23, 27], however there were cases where single treated specimens were weaker than the untraded controls [16, 33]. Prophylactic augmentation has been found to strengthen [27, 34, 35], to provide no improvement [8], or even to weaken at least some specimens [16], in comparison to untreated controls. It must be noted that most of these studies focused on the overall failure strength of the natural and treated vertebral body, without analyzing the strain distribution.

The strain distribution has been partially assessed in the untreated vertebral body [36] (the most stressed region could not be identified as only one strain-gauge was applied on each vertebra). Recently, the strain distribution was measured for a variety of loading conditions using eight strain gauges [37]. While strain gauges provide pointwise measurements, digital image correlation (DIC) allows investigating the full-field strain distribution on the specimen's surface. In recent years, DIC has successfully been exploited to measure the strain distribution on the surface of untreated vertebrae [38-42]. The surface strain distribution was also measured in prophylactically augmented vertebrae *in vitro*, using eight strain gauges [13]. The measured principal strains were generally aligned as expected: axially/circumferentially for all loading conditions implying an axial force. That paper concluded that the variability of the weakening/strengthening effect of prophylactic augmentation depended on the quality of augmentation (amount, localization and distribution of the injected material). Even this study could not draw any conclusive information about the failure mechanisms associated to the internal state of the vertebra. However, strain gauges and DIC allow investigating only the surface of specimens, where the stress/strain distribution inside the bone and the augmentation material cannot be measured.

Numerical predictions through finite element (FE) models allowed the investigation of the internal strain distribution (e.g. [10, 43, 44]). However, one cannot take for granted the credibility of FE models of complex structures such as an augmented vertebra, which include thin cortical shell, cement-bone interdigitation, interfaces between different materials, tissue anisotropy, inhomogeneity and nonlinearity [45, 46].

For these reasons alternative approaches have been exploited to overcome this limitation. With the recent and rapid progress of high-resolution micro-CT imaging in conjunction with *in situ* mechanical testing [47, 48], digital volume correlation (DVC) emerged as a novel tool for the measurement of 3D deformation fields throughout entire bone volumes [49]. So far, DVC was successfully employed to examine full-field internal deformations in trabecular bone [50-55], cortical bone [51, 56, 57] and cement-bone interface [58]. Application of DVC to whole untreated vertebra was also exploited to examine yield and post-yield deformations [59, 60], and more recently also the strain field in the elastic regime [61]. DVC is an ideal tool to investigate the internal mechanism leading to onset and progression of failure of augmented vertebrae, and could potentially be used to elucidate under which conditions prophylactic augmentations can reinforce/weaken the vertebral body.

While DVC has been applied to characterize the mechanical performance of untreated vertebral body, so far it has not been applied to augmented vertebral bodies. Because of its high complexity, accuracy and precision of DVC cannot be taken for granted [54, 62]. Recently for the first time, 3D zero-strain studies demonstrated the suitability of DVC approach to investigate augmented bone both at organ-level [63] and tissue-level [64]. Those studies reported that strain uncertainties can be reduced below 300 microstrain if the images are adequately prepared (excluding the non-tissue background), and with an appropriate choice of the computation sub-volume size (i.e. 48 voxels for a 39 micrometers voxel size image).

The aim of this study was, for the first time, to measure the full-field strain distributions by means of DVC inside prophylactically augmented vertebral bodies under compression. Specifically, we aimed at investigating the state of strain distribution inside the vertebral body, in the injected cement, and in the cement-bone interdigitated region of vertebrae that were prophylactically augmented with two different cements, including the elastic regime (axial, antero-posterior and lateral-lateral components of strain), but also the internal micro-failure mechanisms.

### **5.3 Materials and Methods**

Destructive tests were carried out on twelve porcine natural and prophylactically augmented vertebral bodies. Specimens were tested under axial-compression loading in a step-wise fashion. Micro-CT images were acquired after each loading step. Starting from the reconstructed micro-CT volumes, the full-field strain distribution and the associated failure mechanisms were investigated inside the vertebral bodies by image-guided failure assessment (IGFA) and digital volume correlation (DVC).

#### **5.3.1 Specimens and prophylactic augmentation**

Four porcine thoracic spine segments (T1-T3) were obtained from animals, which were sacrificed for alimentary purposes. The animals were all female, of the same breed, approximately 9 months and 100kg at sacrifice. The single vertebrae were dissected from the spine segments, removing the soft tissues, including the intervertebral discs (Fig. 5-1). Within each spine segment, two vertebrae were assigned for prophylactic augmentation with two types of bone cement, and one vertebra was used as non-augmented control. Sampling was arranged so that the augmented and

control samples were well distributed within the spine segment, in order to have at least one T1, one T2 and one T3 per group:

- A sample of four vertebrae (Mendec-1, Mendec-2, Mendec-3 and Mendec-4) was prophylactically augmented with acrylic bone cement (Mendec-Spine, Tecres, Italy), using its proprietary mixing and delivery kit. Mendec contains 8% of BaSO<sub>4</sub> pellets with an average size of 300 micrometers, which grant adequate visibility during micro-CT imaging [63].
- Another sample of four vertebrae (Cal-CEMEX-1, Cal-CEMEX-2, Cal-CEMEX-3 and Cal-CEMEX-4) was treated with an experimental acrylic-based bone substitute, using a similar delivery device as for the Mendec specimens. This cement (Cal-CEMEX, Tecres, Italy, consisting of 40.4%poly-methyl-methacrylate (PMMA)), additivated with 6% of BaSO<sub>4</sub> pellets (average size: 300 micrometers) to make it suitable for vertebroplasty.
- The remaining four specimens served as untreated controls (hereafter referred to as Natural-1, Natural-2, Natural-3 and Natural-4). Three of these specimens were part of a different methodological study [61]. These specimens are included in the present paper as a blank control; more details about the natural specimens can be found in [61].

Augmentation was performed on the selected 8 specimens with the two types of bone cement with a uni-lateral approach (Fig.5-1). Injection was stopped at the first visible sign of leakage (injected volume: ~1-1.5 ml of cement). In order to facilitate a more realistic cement flow and polymerization, the vertebrae were heated for 1 hour before and 12 hours after augmentation, in saline solution at 44°C (the physiologic temperature in pigs is 38.5-40°C [65, 66]).

To avoid the presence of soft tissue and reduce viscoelastic effects and strain concentration, which would compromise micro-CT imaging and DVC analysis, the growth plates were removed from the augmented and natural vertebrae, together with the adjacent endplates (due to the young age of the animals, this could be performed with little manual effort) [67]. A reproducible reference frame was adapted [68], and the ends of each vertebra were potted in PMMA so that the cranio-caudal axis was consistently aligned with the loading direction within the micro-CT scanner (Fig.5-1). The neural arches were subsequently excised through resection of the pedicles.

### **5.3.2 Compression testing and micro-CT scanning**

Destructive tests were carried out on all prophylactically augmented and control vertebrae, under axial-compression with a customized-micro-mechanical loading device (CT5000, Deben Ltd,

UK), equipped with a 5kN load cell and environmental chamber filled with 0.9% saline solution (Fig. 5-1). To avoid translation and rotation of the specimens inside the chamber, a sandpaper disc was applied to the bottom loading platen. The force and displacement signals were acquired at 2 Hz (Microtest V6 2.67, Deben Ltd, UK).

A preload of 50 N was applied. Each specimen was compressed axially under displacement control in a step-wise fashion (Fig. 5-1). The compression steps were adjusted for each specimen based on its height, so that at each step the free height was compressed by 5% (this corresponded to actuator steps ranging between 0.47 and 0.67 mm, depending on the specimen's size). The actuator speed was 0.1 mm/sec. At each compression step, the specimens were allowed to settle for 15 minutes, to reach a steady state prior to scanning.

Micro-CT imaging (XTH225, Nikon Metrology, UK) was carried out at each step (0% with 50N preload, 5%, 10% and 15% compression) (Fig. 5-1). The micro-CT scanner was set to a voltage of 88-89 kV, a current of 110-116 microA and exposure time of 2 seconds. Images were collected at rotational steps of 0.23° over 360°, for a scanning time of approximately 90 min at each compression step. The reconstructed micro-CT images had an isotropic voxel size of 38.8 micrometers.

### **5.3.3 Digital volume correlation (DVC)**

DaVis DVC software (v8.3, LaVision, Germany) was used to investigate the full-field strains in both control and augmented vertebrae along the axial, antero-posterior and lateral-lateral directions. The operating principle of the DaVis DVC software has been detailed elsewhere [63]. Briefly, DVC discretizes the 3D volume into small sub-volumes, which are independent each other (local approach). Each sub-volume is represented as a discrete function of grey-level. A direct correlation function (DaVis-DC) is employed together with a piece-wise linear shape function and a third-order spline interpolation, to correlate the structural patterns contained in the reference and deformed sub-volumes. To achieve this, LaVision's software adopts a multi-pass approach that uses the displacement gradient from the previous pass to deform the sub-volume on the subsequent pass until the highest possible correlation is achieved [69]. The displacement vector field is obtained at the center of each sub-volume. The strain field is subsequently computed using a centered finite differences (CFD) scheme. The original micro-CT images were masked in correspondence to the contour shape of each vertebral body, in order to isolate the vertebra from noisy background areas

where no tissue was present [61]. In fact, it was shown that regions that do not contain useful pattern for the correlation algorithm are associated with large strain artifacts [63, 64]

DVC calculation settings utilized a final sub-volume of 48 voxels (0% overlapping), reached after prior passes of 128, 112, 96, 80 and 64 voxels. This multipass sequence was found to produce the lowest strain error in DaVis-DC for such type of specimens, under the same imaging and environmental [63, 64]. As for large deformations the local pattern experiences significant changes, the displacement field obtained was calculated not relative to the specimen in its undeformed state (preload of 50N, 0% compression), but using a ‘sum of differential’ approach between successive images (0%-5%; 5%-10%, 10%-15% compression) that were then summed in a Lagrangian coordinate system.

As LaVision’s software can only display 2D image views in the transverse plane, a dedicated Matlab (v2014a, MathWorks, US) script was developed to allow visualization of the 2D strain maps in sagittal and frontal planes. Moreover, for each compression step, the average strain within each transverse slice was computed for the strain components in axial, antero-posterior and lateral-lateral direction, following a procedure reported in [57].

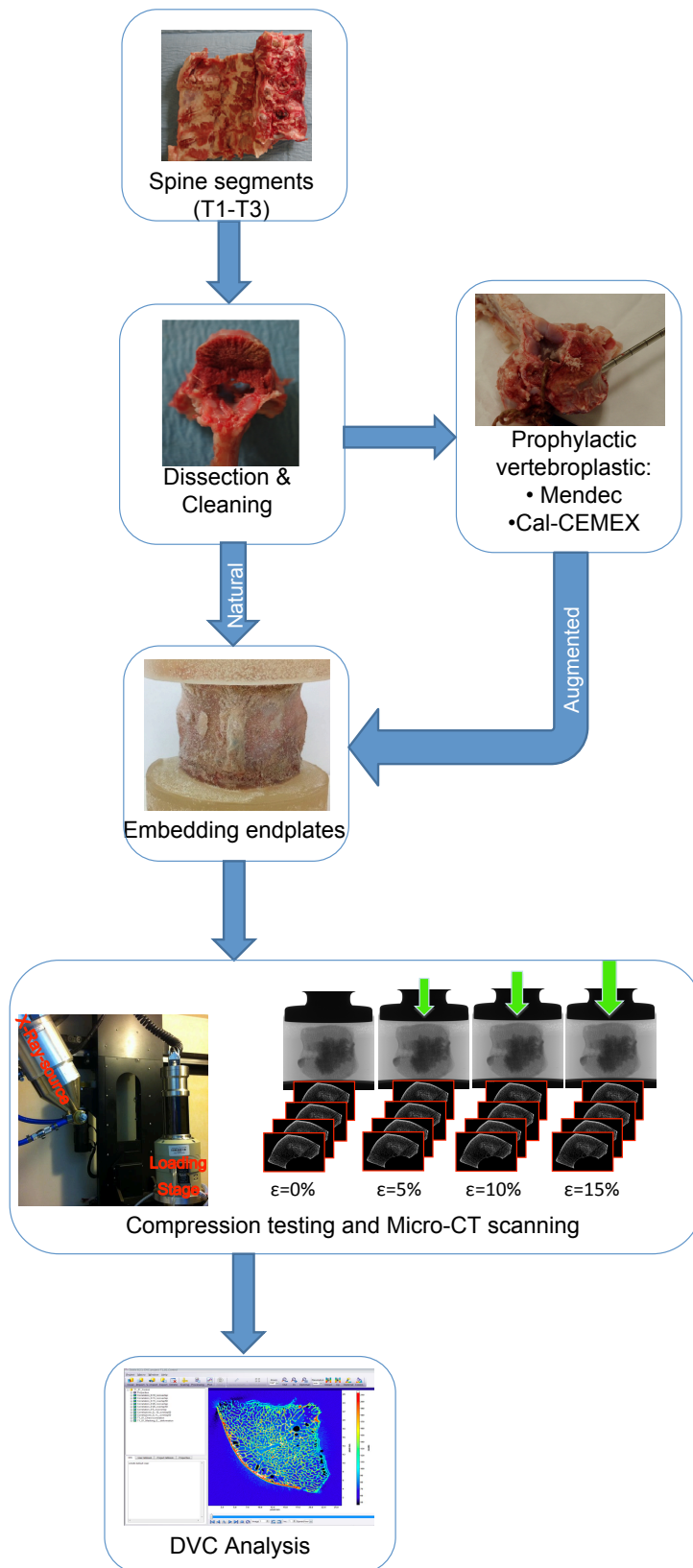


Fig.5-1: Overview of the experimental design. The vertebral bodies were dissected from the spine segments, removing all soft tissues. Prophylactic augmentation was performed on the selected

*specimens with two types of cements (Mendec and Cal-CEMEX). The remaining specimens were used as untreated controls. The ends of each vertebra were potted in PMMA. Then, destructive tests were carried out under axial-compression in a step-wise fashion. Micro-CT imaging was acquired at each loading step (0% with 50N preload, 5%, 10% and 15% compression). Finally, digital volume correlation (DVC) was performed to compute the internal full-field strains.*

## **5.4 Results**

The force-displacement curves for augmented specimens showed a monotonic trend for all specimens, while load was increased (Fig. 5-2 and 5-3). Specimen failure (in most cases clearly visible as the point was immediately followed by load drop) occurred either at 10% or 15% steps in all augmented specimens. The loads applied onto the augmented specimens for each loading steps are reported in Table 5-1. Relaxation was also visible at the end of each compression step, when the actuator was stopped to allow micro-CT imaging.

For both groups the force-displacement curves differed among specimens, according to the quality of augmentation [13] (Fig. 5-2 and 5-3). Comparing the force-displacement curves of augmented specimens to the controls reported in[61], both augmented groups exhibited different trends. In some cases the failure load of augmented vertebrae was higher than the respective control (Mendec-2, Mendec-3, Cal-CEMEX-2), conversely in other cases the failure load of augmented vertebrae was lower than the control.

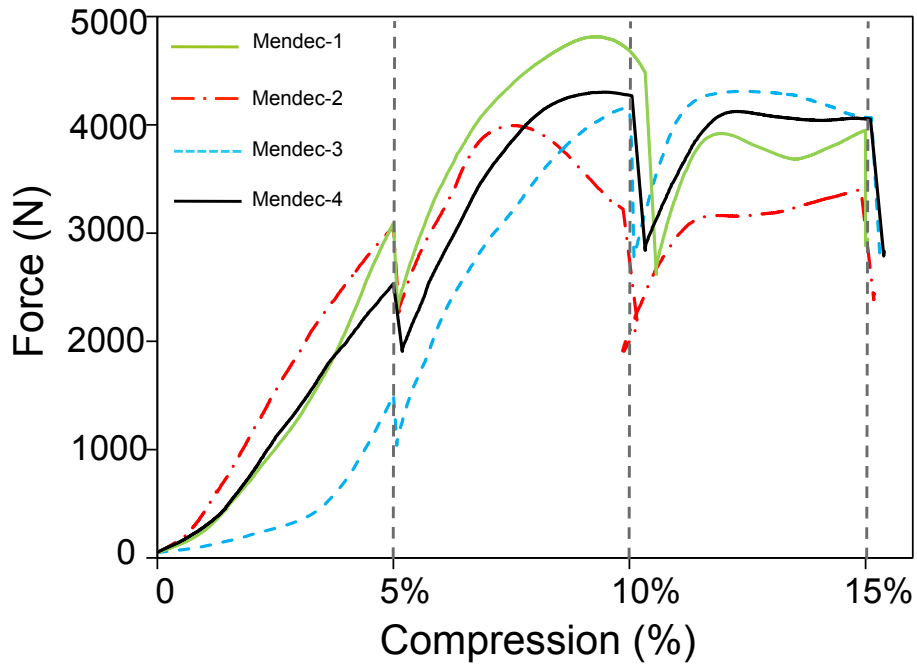


Fig. 5-2: Force-compression curves for the four specimens augmented with Mendec cement. The load showed a drop at the end of each step of compression: this corresponded to the stress relaxation while the specimen was allowed to settle (15 minutes), before the micro-CT scan took place (90 minutes).

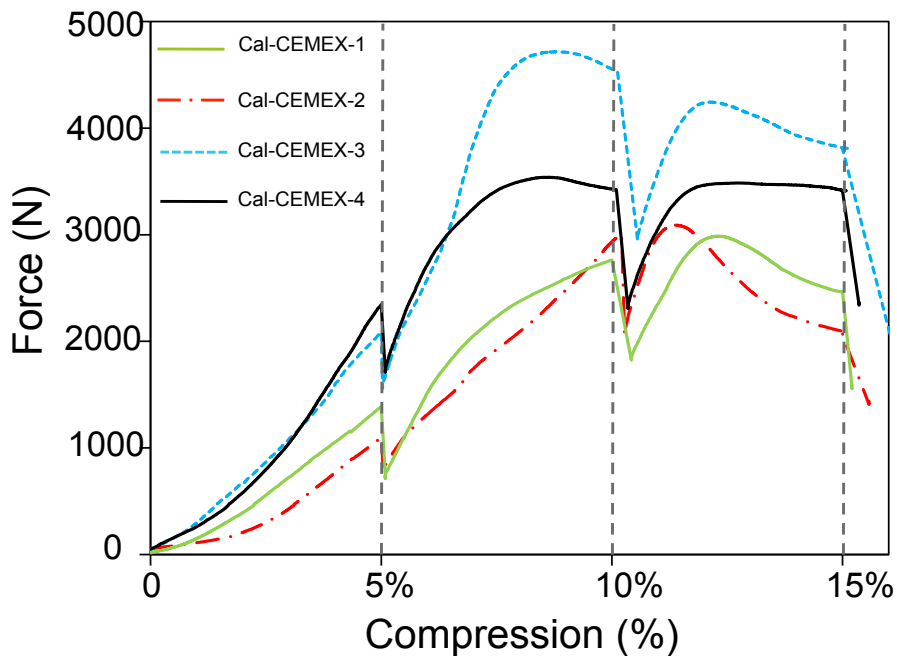


Fig. 5-3: Force-compression curves for the four specimens augmented with Cal-CEMEX cement. The load showed a drop at the end of each step of compression: this corresponded to stress

relaxation while the specimen was allowed to settle (15 minutes), before the micro-CT scan took place (90 minutes).

Table 5-1: Loads experienced by the eight augmented specimens at each step of compression (applied in displacement control).

<b>Augmented Specimens</b>	Force at 5% compression	Force at 10% compression	Force at 15% compression
Mendec-1	1502 N	4125 N	4064 N
Mendec-2	3089 N	4481 N	4036 N
Mendec-3	3058 N	3222 N	3403 N
Mende-4	2532 N	4267 N	4053 N
Cal-CEMEX-1	1388 N	2762 N	2463 N
Cal-CEMEX-2	1101 N	3007 N	2057 N
Cal-CEMEX-3	2088 N	4527 N	3802 N
Cal-CEMEX-4	2345 N	3423 N	3408 N

The micro-CT images for the three compression steps (5%, 10% and 15% compression) on the sagittal section of the specimens augmented with Mendec and Cal-CEMEX cements are reported in Figures 5-4 and 5-5, respectively.

In general, the micro-CT images of Mendec specimens showed a main microdamage, which started to be visible at the 10% compressive step, and degenerated into a trabecular collapse at 15% (Fig. 5-4). In the majority of cases, specimens showed a main microdamage localized in the trabecular bone at middle region in the transverse plane. Such collapses seemed to initiate from the cement-bone interface, then gradually spread across the trabecular bone anteriorly and finally in the transverse plane reaching the cortical bone. In addition, Mendec-3 showed a further microdamage just below the cement area (Fig. 5-4, 15% compression). Only the specimen Mendec-4 seemed to

show a vertebral collapse in the cranio-caudal direction (Fig. 5-4, 15% compression), which ended with a trabecular crushing in most of the caudal region, far away from the cement area. Conversely, in all specimens the cement region appeared to be unaffected even at the final loading stage (15% compression).

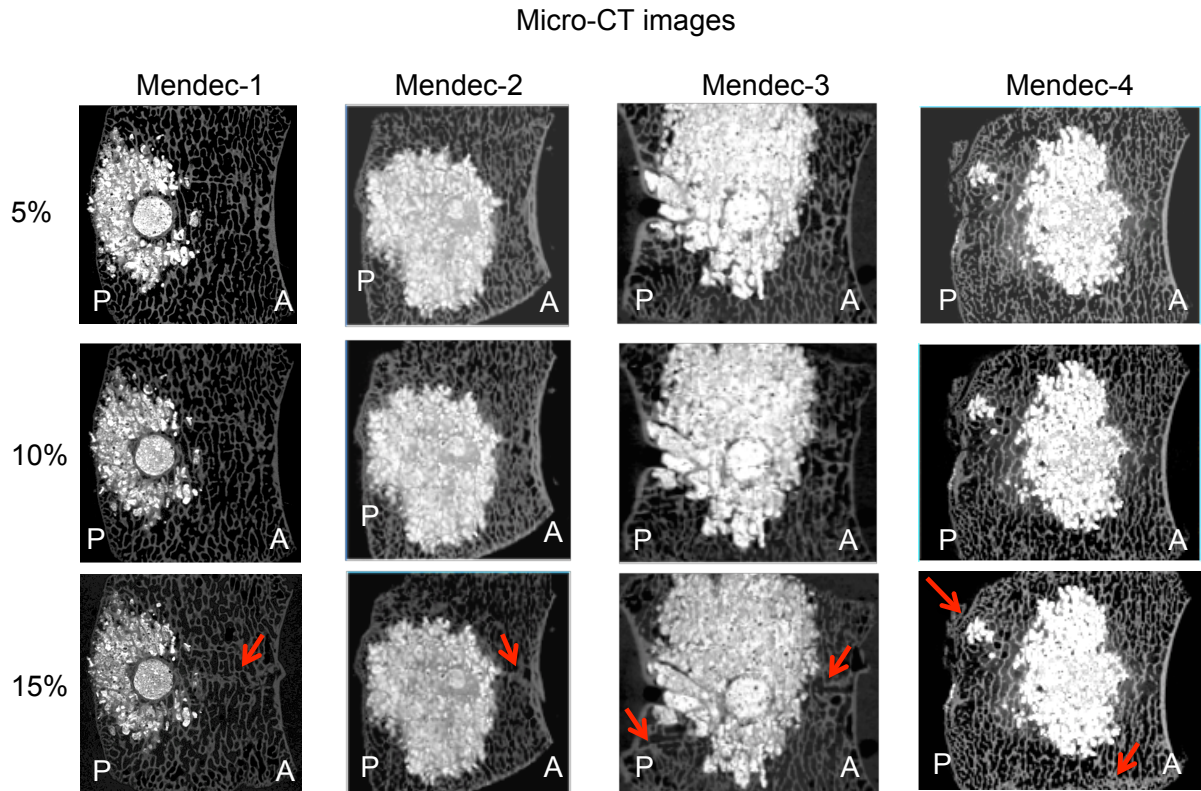


*Fig.5-4: Sagittal micro-CT slice taken at each compression step of specimens augmented with Mendec cement (the antero (A) and posterior (P) regions are also indicated). In the micro-CT images the microdamage started to be recognize at 10% stage, but only at the last step 15% their full extent was detected (red arrows). Conversely the microdamage was not detected in the early loading stage (5%) in any specimens.*

The specimens augmented with Cal-CEMEX showed a main microdamage localized in the trabecular bone region just above or below the cement mass (Fig. 5-5, 15% compression). Only in Cal-CEMEX-3 the microdamage was detected laterally respect to the cement mass (Fig. 5-4, 15% compression). As for the Mendec specimens, such collapses initiated from cement-bone interface and then gradually developed across the trabecular bone anteriorly or posteriorly in the transverse plane, affecting the cortical bone in some cases (Fig. 5-5; Cal-CEMEX-2 and Cal-CEMEX-3).

Once again, the cement region appeared to be unaffected even at the final stage (15% compression) for all specimens.

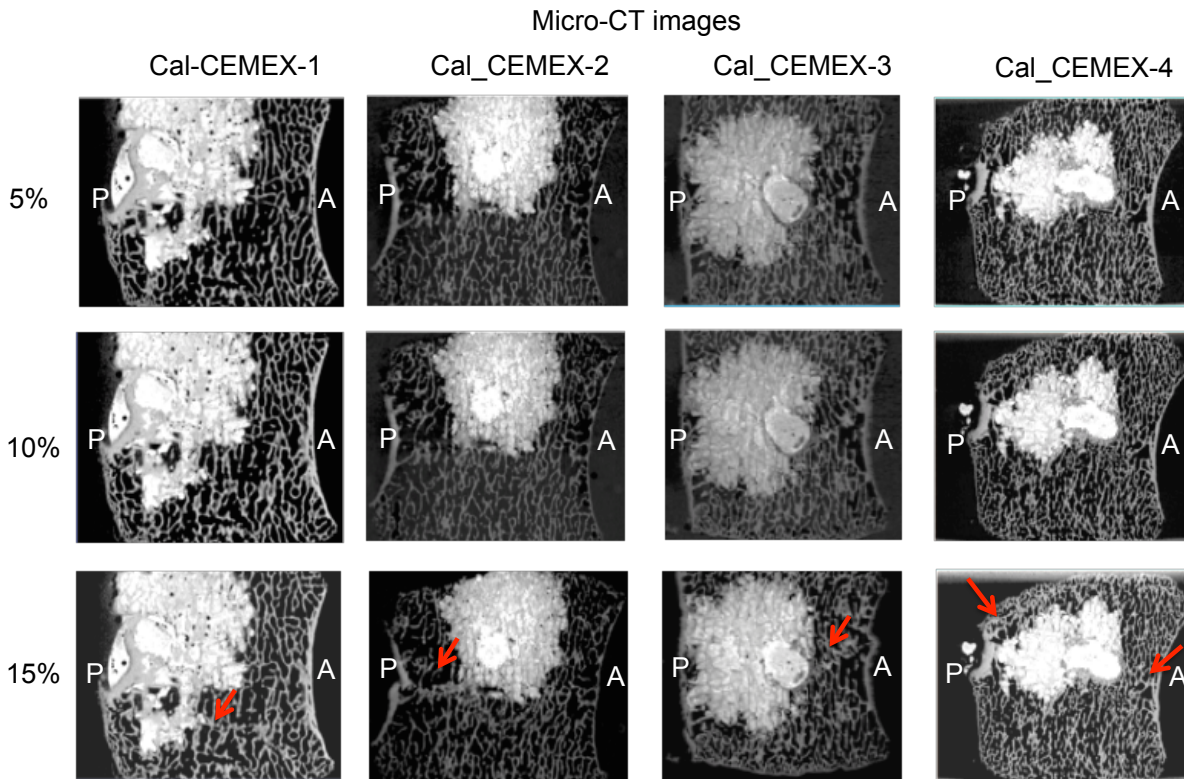


*Fig.5-5: Sagittal micro-CT slice taken at each compression step of specimens augmented with Cal-CEMEX cement (the antero (A) and posterior (P) regions are also indicated). In the micro-CT images the microdamage started to be recognize at 10% stage, but only at the last step 15% their full extent was detected (red arrows). Conversely the microdamage was not detected in the early loading stage (5%) in any specimens.*

The internal axial strain distributions for the three compression steps (5%, 10% and 15% compression) on the sagittal section of the specimens augmented with Mendec and Cal-CEMEX cement are reported in Figures 5-6 and 5-7, respectively.

For specimens augmented with Mendec cement, the regions of high compressive strains in the strain maps seemed to describe very well the microdamage visualized in the micro-CT. Elevated compressive strains were also present in the vicinity of the microdamage. The axial strain, which reflecting the compressive deformation was the dominating mode at microdamage and they were always compressive in all specimens. For the antero-posterior and lateral-lateral directions, the normal strains were mainly tensile (details of antero-posterior and lateral-lateral strain maps are

reported as supplementary material). In all cases, antero-posterior and lateral-lateral strain magnitudes were significantly lower than axial strain. The highest strains (compressive or tensile) were generally concentrated in the regions where the microdamage developed. Strains were significantly lower away from the damaged regions. In most of the specimens subjected to the first compression stage (5%), some parts of the cement regions experienced the largest axial-strain. Conversely in the final loading step (15%) the cement areas seemed to be the less strained regions in all specimens. The strain distribution in the elastic regime (5% compression) seemed being able to predict the location of the microdamage initiation before it actually became identifiable in the most of specimens (Fig. 5-6; Mendec-2, Mendec-3 and Mendec-4). Only the specimen Mendec-1 showed a relocation of the highest axial strain from the posterior (5% compression) to the anterior region (15% compression) (Fig. 5-6).

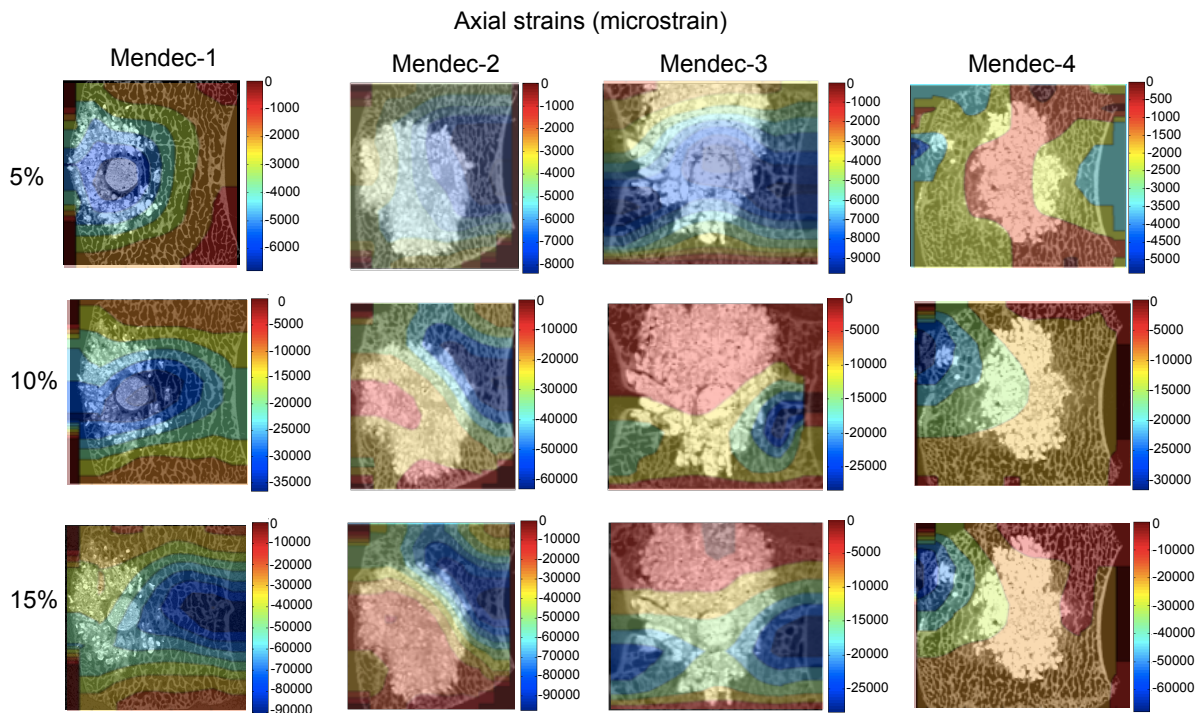


*Fig. 5-6: Internal strain distribution of specimens augmented with Mendec cement for the three steps of compression. The distribution of axial strains is showed for each specimen over the same sagittal slice as in Fig. 5-4. The most strained regions corresponded to the damaged area, which gradually progressed into a collapse propagating across the trabecular bone.*

A similar agreement between the damage (visible in the micro-CT images) and the distribution of strain (computed by means of DVC) was also found in specimens augmented with Cal-CEMEX (Fig. 5-5 and 5-7). In most of the cases, larger strains were localized and concentrated only in one region of the specimen, which was more or less extended. Only in Cal-CEMEX-4 the highest strain was detected in two different regions of the specimen that were quite far away from each other, but both close to the cement mass. For the normal strains in antero-posterior and lateral-lateral directions the highest strains were always tensile (details of antero-posterior and lateral-lateral strain maps are reported as supplementary material). Antero-posterior and lateral-lateral strains magnitudes were significantly lower than axial strain. However, in all directions the highest strains (compressive or tensile) were typically concentrated in the regions of the microdamage and significantly lower away from the damaged regions. In most of the specimens, the cement regions were partially affected by the largest axial strain at the first stage (5% compressive). Conversely, in the final step (15% compressive) the cement areas appeared to be the less strained regions in all specimens. Once again, the strain distribution in the elastic regime (5% compressive) seemed to predict quite well the location of damage initiation before it actually occurred (Fig. 5-7).

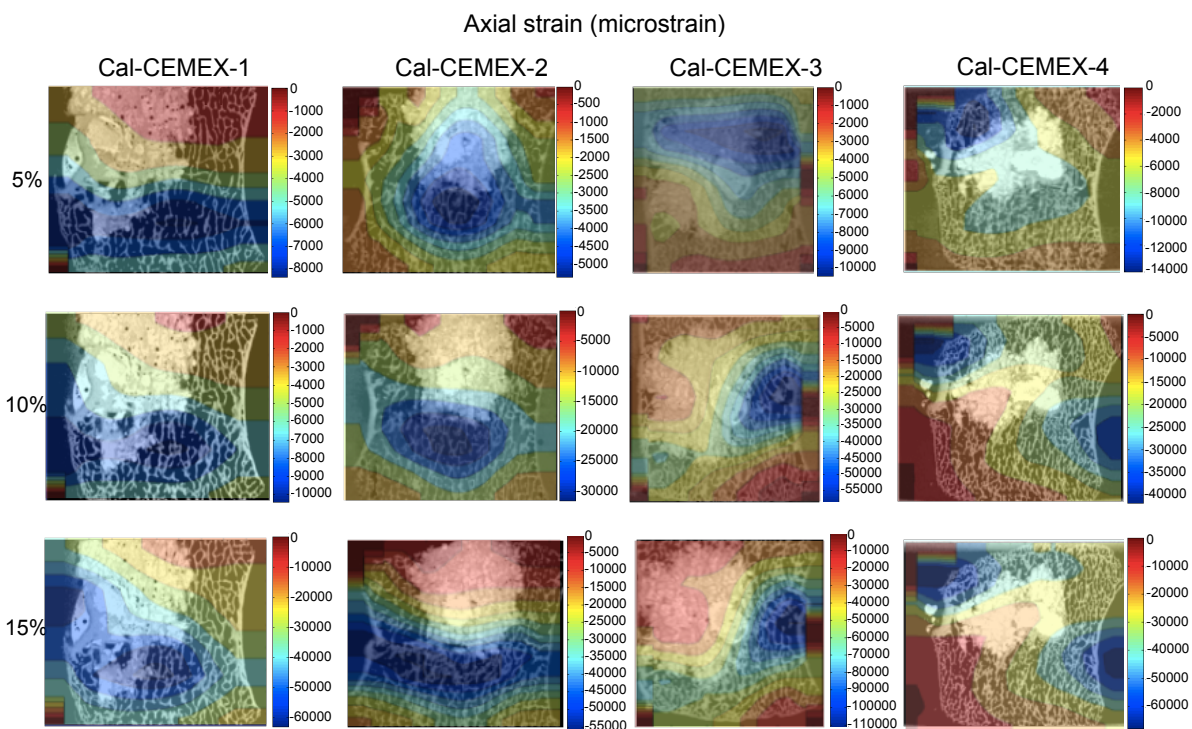


*Fig. 5-7: Internal strain distribution of specimen augmented with Cal-CEMEX cement for the three steps of compression. The distribution of axial strains is showed for each specimen over the same*

sagittal slice as in Fig. 5-5. The most strained regions corresponded to the damaged area, which gradually progressed into a collapse propagating across the trabecular bone.

In general, no apparent differences were observed between the values of strain experienced by augmented and control groups. Also in the most strained regions, where the microdamage developed, the value of strains between augmented and control specimen were similar.

The progression of axial strain during compression for the two augmented groups is shown in Figure 5-8 and 5-9, in terms of average strain calculated for each cross-section.

### Axial Strain (microstrain) of specimens augmented with Mendec cement

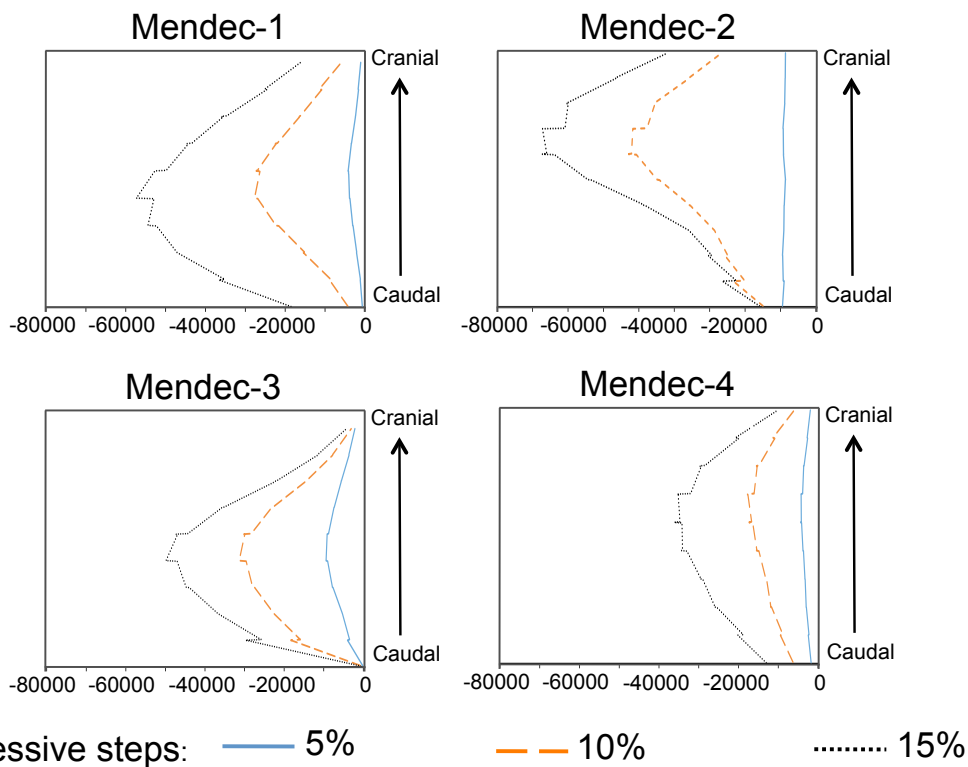
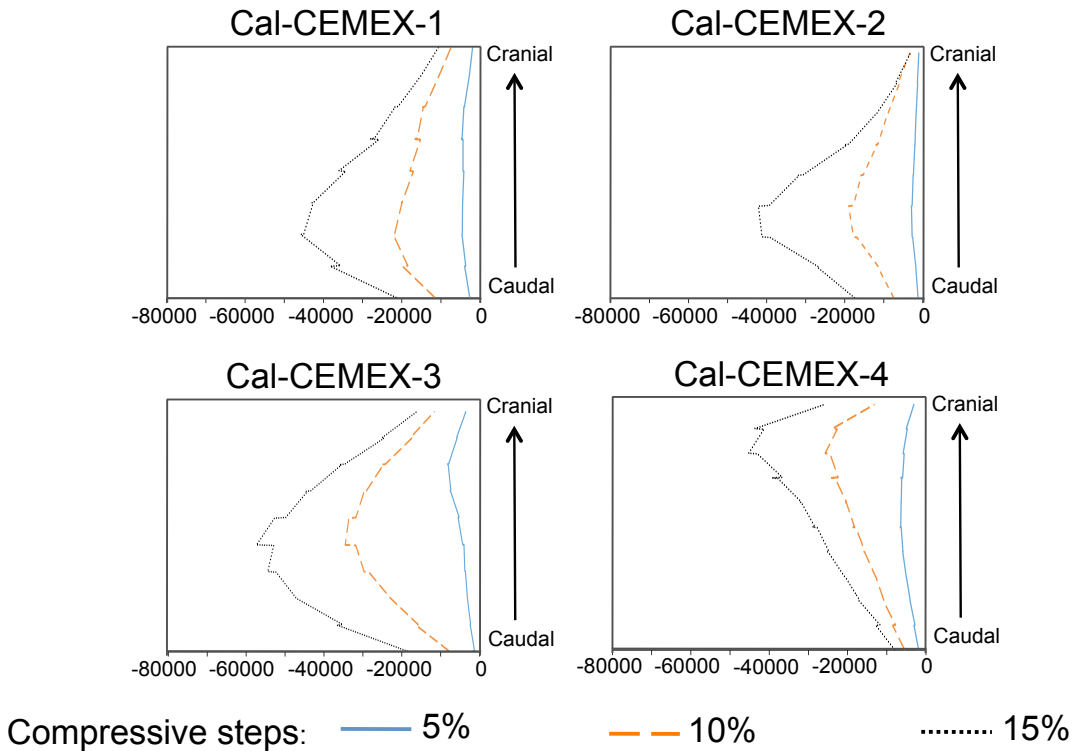


Fig. 5-8: Progression of strain with compression steps (5%, 10% and 15%). The average axial strains were computed for each transverse slice of the DVC-computed 3D strain maps. In general, an incremental strain pattern among the consecutive compression steps was observed in all specimens. The slices where the largest strains were observed corresponded to the areas where internal damage was localized in the vertebra (Fig. 5-4 and 5-6).

The strain pattern along the caudal-cranial direction was mostly similar, with the largest deformation localized in correspondence approximately of the specimen middle region or slightly moved toward cranial direction as for Mendec-2 (Fig. 5-8). This strain trend was different from the pattern of control specimens reported in [61], where the largest deformation was observed in correspondence of the cranial or caudal extremities of the specimen.

**Axial Strain (microstrain) of specimens augmented with Cal-CEMEX cement**



*Fig. 5-9: Progression of strain with compression steps (5%, 10% and 15%). The average axial strains were computed for each transverse slice of the DVC-computed 3D strain maps. In general, an incremental strain pattern among the consecutive compression steps was observed in all specimens. The slices where the largest strains were observed corresponded to the areas where internal damage was localized in the vertebra (Fig. 5-5 and 5-7).*

The strain pattern along the caudal-cranial direction of specimens augmented with Cal-CEMEX was pretty different from the pattern exhibited by the specimens augmented with Mendec, but more similar to the control specimens reported by Tozzi et al. [61], with the largest deformation localized in correspondence of the first quarter caudal or cranial of the specimen (Fig. 5-9).

## 5.5 Discussion

While the biomechanical effects of vertebroplasty on fractured vertebrae have been thoroughly investigated, very little data exist regarding the effects of prophylactic augmentation on non-fractured vertebrae. Moreover, such studies on vertebroplasty and prophylactic augmentation mainly focused on the overall failure strength of the treated vertebral body, without analyzing the internal strain distributions [21-32]. The aim of this study was, for the first time, to measure the full-field internal strain distributions by means of DVC in prophylactically augmented vertebral bodies under compression. Specifically, we aimed at investigating the strain localization (axial, antero-posterior and lateral-lateral components) in both fully augmented and cement-bone interdigitated regions of vertebrae with two different cements and to couple this information with the internal microdamage initiation and development under applied load.

Our findings showed that prophylactic augmentation increased the force required to induce damage only in some of the vertebrae and other specimens failed under a force that was lower than the one produced in the controls. These findings were consistent with previous studies, which reported cases where treated vertebrae were weaker than the untreated controls [13, 16, 33]. This variability of the weakening/strengthening effect of prophylactic augmentation seems to confirm a recent study [13], in which it has been hypothesized that the effect of augmentation depends on the quality of augmentation itself (i.e. amount, localization and distribution of the injected material).

This study confirmed for the first time the usefulness of the DVC technique in investigating the internal strain distribution of augmented vertebrae, from the elastic regime and up to failure. In fact, despite a number of studies used DVC to investigate the internal strain distribution of natural vertebrae under compression [59-61, 70], the internal strain distribution of augmented vertebrae is still unexplored. The results clearly showed that augmentation was not associated to an evident modification of the strain magnitude when compared to the control vertebrae, but rather to a different localization of highly strained regions due to the variable cement distribution. Hence, the higher strains were distributed within the cement region in the elastic regime (5% compression) and successively developed towards the surrounding trabecular bone during failure (10% and 15% compression steps). This suggests an alteration of the load sharing in the augmented structure where the load is mostly carried by the cement region, rather than the trabecular core in the vertebra. This would result in an altered load transferred to the endplates [71] and to the disc [72], and could easily

explain some of the clinically reported incidence of fracture in the adjacent (and untreated) vertebrae to the augmented one [20, 73-76].

Such elevated strain concentration within the cement did not produce visible damage to the cement region itself, but affected the strength of the surrounded trabecular bone, resulting in an increased fracture risk at the cement-bone interdigitated region and of the surrounding trabecular bone regions just above or below the cement mass. In conclusion the most critical region was found at the cement-bone interface, where the onset of the fracture was recognizable consistently with previous studies [58, 77]. Starting from the cement-bone interdigitated region the microdamage gradually spread under applied load across the trabecular bone, which provided a lower stiffness than the injected cement. In most of the cases, the microdamage developed in the trabecular bone was mainly characterized by bending and buckling of trabeculae in the transverse plane [77]. The failure mechanism did not seem to depend on the cement type.

There are some limitations in this study that must be considered. First of all, porcine specimens were used, which have a different anatomy and tissue properties than human tissues [78]. This choice was driven by the size of the specimens to fit inside the microCT-scanner and its loading device. For this reason, the current results cannot be entirely indicative from a clinical perspective, as both the failure force and the strain magnitude may differ from human vertebrae. However, comparisons between the natural and augmented specimens, and between different types of cement are possible. Furthermore, this study allowed, for the first time, a complete *in vitro* characterization of the internal failure mechanisms in the augmented vertebral body. Another limitation is the relatively small sample size: 4 specimens were tested for each group, making difficult any conclusive statistical comparison. Larger samples (from 30 to 66) were tested when only the failure force was measured [22, 27, 79], but as in our study we investigated in detail the internal strain distribution a smaller number of specimens could be considered. All these limitations are compensated by the fact that, to the author's knowledge, this is the first time that the internal strain distribution (in the elastic regime) through DVC was employed to investigate the internal failure mechanisms in prophylactically augmented vertebrae.

## 5.6 Supplementary Materials

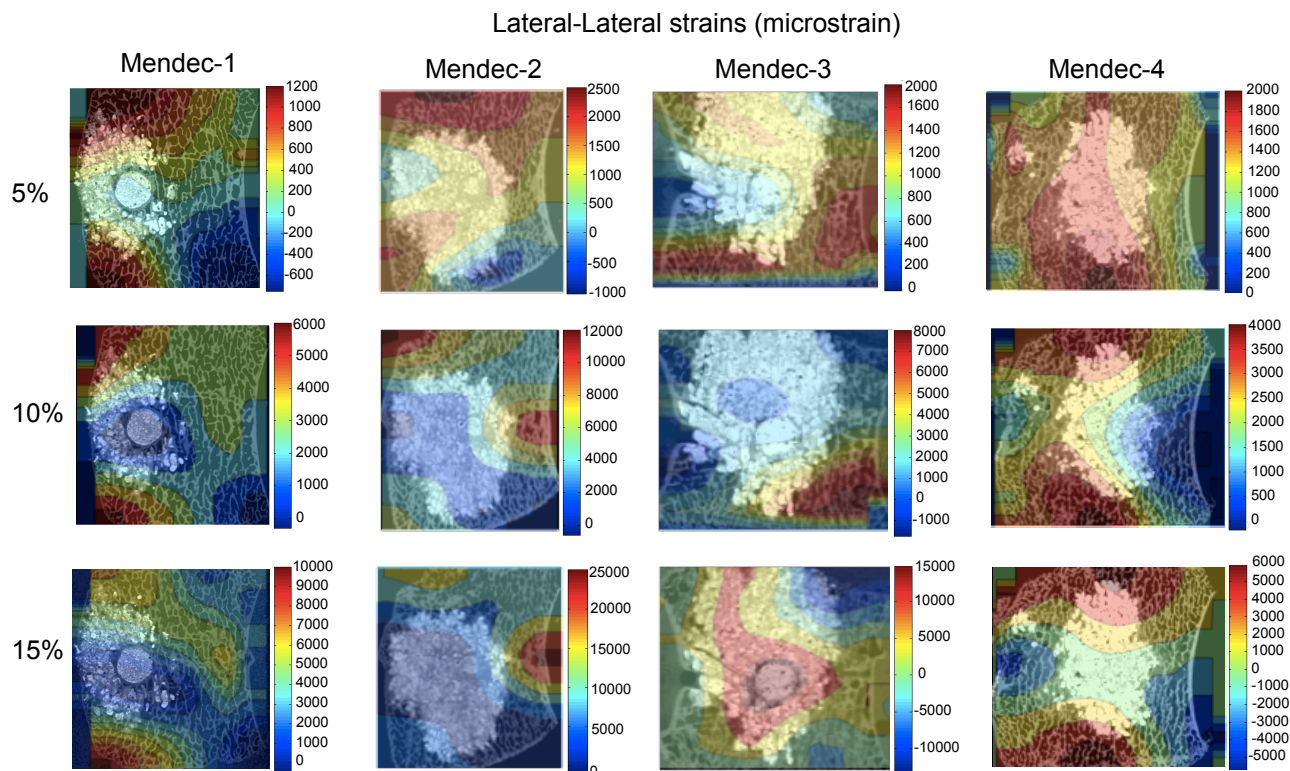


*Fig. A: Internal strain distribution of specimens augmented with Mendec cement for the three steps of compression. The distribution of lateral-lateral strains is shown for each specimen over the same sagittal slice as in Fig. 5-4. The most strained regions corresponded to the damaged area, which gradually progressed into a collapse propagating across the trabecular bone. The distribution of anterior-posterior strains showed a similar pattern.*

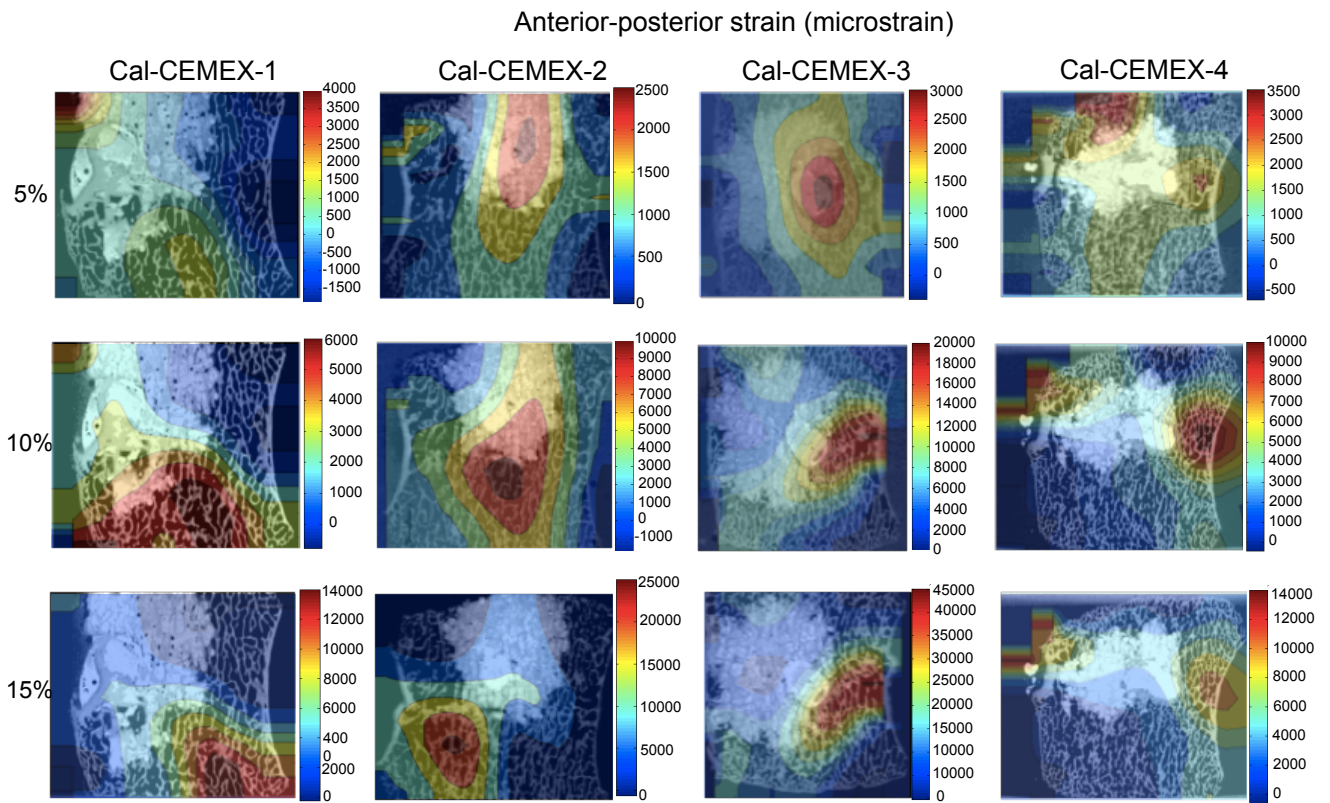


*Fig. B: Internal strain distribution of specimens augmented with Cal-CEMEX cement for the three steps of compression. The distribution of anterior-posterior strains is showed for each specimen over the same sagittal slice as in Fig. 5-5. The most strained regions corresponded to the damaged area, which gradually progressed into a collapse propagating across the trabecular bone. The distribution of lateral-lateral strains showed a similar pattern.*

## 5.7 References

- [1] Ferrar, L., Jiang, G., Adams, J., and Eastell, R., 2005, "Identification of vertebral fractures: An update," *Osteoporosis International*, 16(7), pp. 717-728.
- [2] Tancioni, F., Lorenzetti, M. A., Navarra, P., Pessina, F., Draghi, R., Pedrazzoli, P., Scorsetti, M., Alloisio, M., Santoro, A., and Rodriguez y Baena, R., 2011, "Percutaneous vertebral augmentation in metastatic disease: state of the art," *J Support Oncol*, 9(1), pp. 4-10.
- [3] Goldstein, C. L., Chutkan, N. B., Choma, T. J., and Orr, R. D., 2015, "Management of the Elderly With Vertebral Compression Fractures," *Neurosurgery*, 77 Suppl 4, pp. S33-45.
- [4] WHO, 2007, "WHO SCIENTIFIC GROUP ON THE ASSESSMENT OF OSTEOPOROSIS AT PRIMARY HEALTH CARE LEVEL " Summary Meeting Report of a WHO study group Brussels, Belgium, 5-7 May 2004, World Health Organization, Geneva, Switzerland, pp. pp. 1-13.
- [5] Sutcliffe, P., Connock, M., Shyangdan, D., Court, R., Kandala, N. B., and Clarke, A., 2013, "A systematic review of evidence on malignant spinal metastases: natural history and technologies for identifying patients at high risk of vertebral fracture and spinal cord compression," *Health technology assessment (Winchester, England)*, 17(42), pp. 1-274.
- [6] Diamond, T. H., Champion, B., and Clark, W. A., "Management of acute osteoporotic vertebral fractures: a nonrandomized trial comparing percutaneous vertebroplasty with conservative therapy," *The American Journal of Medicine*, 114(4), pp. 257-265.
- [7] Chiang, C. K., Wang, Y. H., Yang, C. Y., Yang, B. D., and Wang, J. L., 2009, "Prophylactic vertebroplasty may reduce the risk of adjacent intact vertebra from fatigue injury: an ex vivo biomechanical study," *Spine (Phila Pa 1976)*, 34(4), pp. 356-364.
- [8] Kayanja, M. M., Togawa, D., and Lieberman, I. H., 2005, "Biomechanical changes after the augmentation of experimental osteoporotic vertebral compression fractures in the cadaveric thoracic spine," *Spine J*, 5(1), pp. 55-63.
- [9] Langdon, J., Way, A., Heaton, S., Bernard, J., and Molloy, S., 2009, "The management of spinal metastases from renal cell carcinoma," *Annals of the Royal College of Surgeons of England*, 91(8), pp. 649-652.
- [10] Sun, K., and Liebschner, M. A., 2004, "Biomechanics of prophylactic vertebral reinforcement," *Spine (Phila Pa 1976)*, 29(13), pp. 1428-1435; discussion 1435.
- [11] Aquarius, R., Homminga, J., Hosman, A. J., Verdonschot, N., and Tanck, E., 2014, "Prophylactic vertebroplasty can decrease the fracture risk of adjacent vertebrae: an in vitro cadaveric study," *Med Eng Phys*, 36(7), pp. 944-948.
- [12] Kobayashi, N., Numaguchi, Y., Fuwa, S., Uemura, A., Matsusako, M., Okajima, Y., Ishiyama, M., and Takahashi, O., 2009, "Prophylactic vertebroplasty: cement injection into non-fractured vertebral bodies during percutaneous vertebroplasty," *Academic radiology*, 16(2), pp. 136-143.
- [13] Cristofolini, L., Ferguson, S. J., Danesi, V., Erani, P., Viceconti, M., and Brandolini, N., IN PRESS, "A preliminary in vitro biomechanical evaluation of prophylactic cement augmentation of the thoracolumbar vertebrae," *Journal of Mechanics in Medicine and Biology* in press.

- [14] Oakland, R. J., Furtado, N. R., Wilcox, R. K., Timothy, J., and Hall, R. M., 2008, "The biomechanical effectiveness of prophylactic vertebroplasty: a dynamic cadaveric study," *J Neurosurg Spine*, 8(5), pp. 442-449.
- [15] Oakland, R. J., Furtado, N. R., Wilcox, R. K., Timothy, J., and Hall, R. M., 2009, "Preliminary biomechanical evaluation of prophylactic vertebral reinforcement adjacent to vertebroplasty under cyclic loading," *The Spine Journal*, 9(2), pp. 174-181.
- [16] Berlemann, U., Ferguson, S. J., Nolte, L. P., and Heini, P. F., 2002, "Adjacent vertebral failure after vertebroplasty. A biomechanical investigation," *J Bone Joint Surg Br*, 84(5), pp. 748-752.
- [17] Carrodeguas, R. G., Lasa, B. V., and Del Barrio, J. S., 2004, "Injectable acrylic bone cements for vertebroplasty with improved properties," *Journal of biomedical materials research. Part B, Applied biomaterials*, 68(1), pp. 94-104.
- [18] Lewis, G., 2006, "Injectable bone cements for use in vertebroplasty and kyphoplasty: state-of-the-art review," *Journal of biomedical materials research. Part B, Applied biomaterials*, 76(2), pp. 456-468.
- [19] Tanigawa, N., Komemushi, A., Kariya, S., Kojima, H., Shomura, Y., and Sawada, S., 2006, "Radiological follow-up of new compression fractures following percutaneous vertebroplasty," *Cardiovascular and interventional radiology*, 29(1), pp. 92-96.
- [20] Uppin, A. A., Hirsch, J. A., Centenera, L. V., Pfiefer, B. A., Pazianos, A. G., and Choi, I. S., 2003, "Occurrence of new vertebral body fracture after percutaneous vertebroplasty in patients with osteoporosis," *Radiology*, 226(1), pp. 119-124.
- [21] Belkoff, S. M., Mathis, J. M., Jasper, L. E., and Deramond, H., 2001, "An ex vivo biomechanical evaluation of a hydroxyapatite cement for use with vertebroplasty," *Spine (Phila Pa 1976)*, 26(14), pp. 1542-1546.
- [22] Heini, P. F., Berlemann, U., Kaufmann, M., Lippuner, K., Fankhauser, C., and van Landuyt, P., 2001, "Augmentation of mechanical properties in osteoporotic vertebral bones--a biomechanical investigation of vertebroplasty efficacy with different bone cements," *Eur Spine J*, 10(2), pp. 164-171.
- [23] Ikeuchi, M., Yamamoto, H., Shibata, T., and Otani, M., 2001, "Mechanical augmentation of the vertebral body by calcium phosphate cement injection," *Journal of orthopaedic science : official journal of the Japanese Orthopaedic Association*, 6(1), pp. 39-45.
- [24] Kolb, J. P., Kueny, R. A., Puschel, K., Boger, A., Rueger, J. M., Morlock, M. M., Huber, G., and Lehmann, W., 2013, "Does the cement stiffness affect fatigue fracture strength of vertebrae after cement augmentation in osteoporotic patients?," *Eur Spine J*, 22(7), pp. 1650-1656.
- [25] Kruger, A., Baroud, G., Noriega, D., Figiel, J., Dorschel, C., Ruchholtz, S., and Oberkircher, L., 2013, "Height restoration and maintenance after treating unstable osteoporotic vertebral compression fractures by cement augmentation is dependent on the cement volume used," *Clin Biomech (Bristol, Avon)*, 28(7), pp. 725-730.
- [26] Lewis, G., Schwardt, J. D., Slater, T. A., and Janna, S., 2008, "Evaluation of a synthetic vertebral body augmentation model for rapid and reliable cyclic compression life testing of materials for balloon kyphoplasty," *Journal of biomedical materials research. Part B, Applied biomaterials*, 87(1), pp. 179-188.

- [27] Lim, T. H., Brebach, G. T., Renner, S. M., Kim, W. J., Kim, J. G., Lee, R. E., Andersson, G. B., and An, H. S., 2002, "Biomechanical evaluation of an injectable calcium phosphate cement for vertebroplasty," *Spine (Phila Pa 1976)*, 27(12), pp. 1297-1302.
- [28] Molloy, S., Riley, L. H., 3rd, and Belkoff, S. M., 2005, "Effect of cement volume and placement on mechanical-property restoration resulting from vertebroplasty," *AJNR Am J Neuroradiol*, 26(2), pp. 401-404.
- [29] Rotter, R., Schmitt, L., Gierer, P., Schmitz, K. P., Noriega, D., Mittlmeier, T., Meeder, P. J., and Martin, H., 2015, "Minimum cement volume required in vertebral body augmentation--A biomechanical study comparing the permanent SpineJack device and balloon kyphoplasty in traumatic fracture," *Clin Biomech (Bristol, Avon)*, 30(7), pp. 720-725.
- [30] Steens, J., Verdonshot, N., Aalsma, A. M., and Hosman, A. J., 2007, "The influence of endplate-to-endplate cement augmentation on vertebral strength and stiffness in vertebroplasty," *Spine (Phila Pa 1976)*, 32(15), pp. E419-422.
- [31] Tohmeh, A. G., Mathis, J. M., Fenton, D. C., Levine, A. M., and Belkoff, S. M., 1999, "Biomechanical efficacy of unipedicular versus bipedicular vertebroplasty for the management of osteoporotic compression fractures," *Spine (Phila Pa 1976)*, 24(17), pp. 1772-1776.
- [32] Wilke, H. J., Mehnert, U., Claes, L. E., Bierschneider, M. M., Jaksche, H., and Boszczyk, B. M., 2006, "Biomechanical evaluation of vertebroplasty and kyphoplasty with polymethyl methacrylate or calcium phosphate cement under cyclic loading," *Spine (Phila Pa 1976)*, 31(25), pp. 2934-2941.
- [33] Dean, J. R., Ison, K. T., and Gishen, P., 2000, "The strengthening effect of percutaneous vertebroplasty," *Clinical radiology*, 55(6), pp. 471-476.
- [34] Higgins, K. B., Harten, R. D., Langrana, N. A., and Reiter, M. F., 2003, "Biomechanical effects of unipedicular vertebroplasty on intact vertebrae," *Spine (Phila Pa 1976)*, 28(14), pp. 1540-1547; discussion 1548.
- [35] Bai, B., Jazrawi, L., Kummer, F., and Spivak, J., 1999, "The use of an injectable, biodegradable calcium phosphate bone substitute for the prophylactic augmentation of osteoporotic vertebrae and the management of vertebral compression fracture," *Spine*, 24(15), pp. 1521-1526.
- [36] Kayanja, M. M., Ferrara, L. A., and Lieberman, I. H., 2004, "Distribution of anterior cortical shear strain after a thoracic wedge compression fracture," *The Spine Journal*, 4(1), pp. 76-87.
- [37] Cristofolini, L., Brandolini, N., Danesi, V., Juszczyk, M. M., Erani, P., and Viceconti, M., 2013, "Strain distribution in the lumbar vertebrae under different loading configurations," *The Spine Journal*, 13(10), pp. 1281-1292.
- [38] Campos-Lopez, J. P., Fuerte-Hernandez, A., Hernandez-Gomez, L. H., Martinez-Garcia, A., Beltran-Fernandez, J. A., and Urriolagoitia-Calderon, G., 2015, "Determination of the mechanical properties of lumbar porcine vertebrae with 2D digital image correlation," *Journal of applied biomaterials & functional materials*, 13(3), pp. e195-200.
- [39] Giambini, H. W., H; Nassr, A; An, K; Dragomir-Daescu, D, 2013, "Surface Strain Analysis Using Digital Image Correlation in Induced Vertebral Wedge Fracture," *ORS 2013 Annual Meeting*.
- [40] Palanca M, B. T., Cristofolini L. , 2015, "Use of digital image correlation to understand the biomechanics of the vertebra," *J Mech Med Biol*, 15:1540001-1540010.

- [41] Palanca M, T. G., Cristofolini L., 2016, "The use of digital image correlation in the biomechanical area: a review," *International Biomechanics*, 3(1).
- [42] Grassi, L., and Isaksson, H., 2015, "Extracting accurate strain measurements in bone mechanics: A critical review of current methods," *Journal of the mechanical behavior of biomedical materials*, 50, pp. 43-54.
- [43] Wilcox, R. K., 2006, "The biomechanical effect of vertebroplasty on the adjacent vertebral body: a finite element study," *Proc Inst Mech Eng H*, 220(4), pp. 565-572.
- [44] Kinzl, M., Schwiedrzik, J., Zysset, P. K., and Pahr, D. H., 2013, "An experimentally validated finite element method for augmented vertebral bodies," *Clin Biomech (Bristol, Avon)*, 28(1), pp. 15-22.
- [45] Cristofolini, L., Schileo, E., Juszczak, M., Taddei, F., Martelli, S., and Viceconti, M., 2010, "Mechanical testing of bones: the positive synergy of finite-element models and in vitro experiments," *Philosophical transactions. Series A, Mathematical, physical, and engineering sciences*, 368(1920), pp. 2725-2763.
- [46] Henninger, H. B., Reese, S. P., Anderson, A. E., and Weiss, J. A., 2010, "Validation of computational models in biomechanics," *Proc Inst Mech Eng H*, 224(7), pp. 801-812.
- [47] Buffière, J. Y., Maire, E., Adrien, J., Masse, J. P., and Boller, E., 2010, "In Situ Experiments with X ray Tomography: an Attractive Tool for Experimental Mechanics," *Experimental Mechanics*, 50(3), pp. 289-295.
- [48] Nazarian, A., and Muller, R., 2004, "Time-lapsed microstructural imaging of bone failure behavior," *J Biomech*, 37(1), pp. 55-65.
- [49] Roberts, B. C., Perilli, E., and Reynolds, K. J., 2014, "Application of the digital volume correlation technique for the measurement of displacement and strain fields in bone: a literature review," *J Biomech*, 47(5), pp. 923-934.
- [50] Bay, B. K., Smith, T. S., Fyhrie, D. P., and Saad, M., 1999, "Digital Volume Correlation: Three-dimensional Strain Mapping Using X-ray Tomography," *Experimental Mechanics*, 39(3), pp. 217 - 226.
- [51] Dall'Ara, E., Barber, D., and Viceconti, M., 2014, "About the inevitable compromise between spatial resolution and accuracy of strain measurement for bone tissue: A 3D zero-strain study," *J Biomech*, 47(12), pp. 2956-2963.
- [52] F. Brémand, A. G., P. Doumalin, J.C. Dupré 2008, "Study of mechanical behavior of cancellous bone by Digital Volume Correlation and X-ray Micro-Computed Tomography " In: *Proceedings of the XIth International Congress and Exposition (Orlando, FL, USA)*.
- [53] Gillard, F., Boardman, R., Mavrogordato, M., Hollis, D., Sinclair, I., Pierron, F., and Browne, M., 2014, "The application of digital volume correlation (DVC) to study the microstructural behaviour of trabecular bone during compression," *Journal of the mechanical behavior of biomedical materials*, 29, pp. 480-499.
- [54] Liu, L., and Morgan, E. F., 2007, "Accuracy and precision of digital volume correlation in quantifying displacements and strains in trabecular bone," *J Biomech*, 40(15), pp. 3516-3520.
- [55] Zael, R., Yeni, Y. N., Bay, B. K., Dong, X. N., and Fyhrie, D. P., 2006, "Comparison of the linear finite element prediction of deformation and strain of human cancellous bone to 3D digital volume correlation measurements," *J Biomech Eng*, 128(1), pp. 1-6.

- [56] Christen, D., Levchuk, A., Schori, S., Schneider, P., Boyd, S. K., and Muller, R., 2012, "Deformable image registration and 3D strain mapping for the quantitative assessment of cortical bone microdamage," *Journal of Mechanical Behavior of Biomedical Materials*, 8, pp. 184-193.
- [57] Palanca, M., Tozzi, G., Cristofolini, L., Viceconti, M., and Dall'Ara, E., 2015, "Three-dimensional local measurements of bone strain and displacement: comparison of three digital volume correlation approaches," *J Biomech Eng*, 137(7).
- [58] Tozzi, G., Zhang, Q. H., and Tong, J., 2014, "Microdamage assessment of bone-cement interfaces under monotonic and cyclic compression," *J Biomech*, 47(14), pp. 3466 - 3474.
- [59] Hussein, A. I., Barbone, P. E., and Morgan, E. F., 2012, "Digital Volume Correlation for Study of the Mechanics of Whole Bones," *Procedia IUTAM*, 4, pp. 116-125.
- [60] Hussein, A. I., Mason, Z. D., and Morgan, E. F., 2013, "Presence of intervertebral discs alters observed stiffness and failure mechanisms in the vertebra," *J Biomech*, 46(10), pp. 1683-1688.
- [61] Tozzi Gianluca, D. V., Palanca Marco, Luca Cristofolini, SUBMITTED, "Elastic full-field strain analysis and microdamage progression in the vertebral body from digital volume correlation," *Strain*.
- [62] Freddi, A., Olmi, G., and Cristofolini, L., 2015, *Experimental Stress Analysis for Materials and Structures: Stress Analysis Models for Developing Design Methodologies*, Springer, Cham (Switzerland).
- [63] Palanca M., T. G., Dall'Ara E., Curto M., Innocente F., Danesi V., Cristofolini L., Submitted, "Strain uncertainties from two digital volume correlation approaches in natural and augmented vertebrae: an organ-level analysis " *Journal of the mechanical behavior of biomedical materials*.
- [64] Tozzi Gianluca, E. D. A., Marco Palanca, Marco Curto, Federica Innocente, Luca Cristofolini, submitted, "Strain uncertainties from two digital volume correlation approaches in prophylactically augmented vertebrae: local analysis on bone and cement-bone microstructures."
- [65] Ye, J., Coleman, J., Hunter, M. G., Craigon, J., Campbell, K. H., and Luck, M. R., 2007, "Physiological temperature variants and culture media modify meiotic progression and developmental potential of pig oocytes in vitro," *Reproduction (Cambridge, England)*, 133(5), pp. 877-886.
- [66] Reece, W. O., 2004, "Temperature Regulation and Thermal Environment, in *Dukes' Physiology of Domestic Animals*, 12th ed., Reece WO, Ed. Copyright 2004 by Cornell University.."
- [67] Hardisty, M. R., Akens, M., Yee, A. J., and Whyne, C. M., 2010, "Image registration demonstrates the growth plate has a variable affect on vertebral strain," *Ann Biomed Eng*, 38(9), pp. 2948-2955.
- [68] Danesi, V., Zani, L., Scheele, A., Berra, F., and Cristofolini, L., 2014, "Reproducible reference frame for in vitro testing of the human vertebrae," *Journal of biomechanics*, 47(1), pp. 313-318.
- [69] Madi, K., Tozzi, G., Zhang, Q. H., Tong, J., Cossey, A., Au, A., Hollis, D., and Hild, F., 2013, "Computation of full-field displacements in a scaffold implant using digital volume correlation and finite element analysis," *Med Eng Phys*, 35(9), pp. 1298-1312.

- [70] Hardisty, M. R., Akens, M. K., Hojjat, S. P., Yee, A., and Whyne, C. M., 2012, "Quantification of the effect of osteolytic metastases on bone strain within whole vertebrae using image registration," *J Orthop Res*, 30(7), pp. 1032-1039.
- [71] Hulme, P. A., Boyd, S. K., Heini, P. F., and Ferguson, S. J., 2009, "Differences in endplate deformation of the adjacent and augmented vertebra following cement augmentation," *Eur Spine J*, 18(5), pp. 614-623.
- [72] Farooq, N., Park, J. C., Pollintine, P., Annesley-Williams, D. J., and Dolan, P., 2005, "Can vertebroplasty restore normal load-bearing to fractured vertebrae?," *Spine (Phila Pa 1976)*, 30(15), pp. 1723-1730.
- [73] Grados, F., Depriester, C., Cayrolle, G., Hardy, N., Deramond, H., and Fardellone, P., 2000, "Long-term observations of vertebral osteoporotic fractures treated by percutaneous vertebroplasty," *Rheumatology (Oxford, England)*, 39(12), pp. 1410-1414.
- [74] Han, I. H., Chin, D. K., Kuh, S. U., Kim, K. S., Jin, B. H., Yoon, Y. S., and Cho, Y. E., 2009, "Magnetic resonance imaging findings of subsequent fractures after vertebroplasty," *Neurosurgery*, 64(4), pp. 740-744; discussion 744-745.
- [75] Kim, S. H., Kang, H. S., Choi, J. A., and Ahn, J. M., 2004, "Risk factors of new compression fractures in adjacent vertebrae after percutaneous vertebroplasty," *Acta radiologica (Stockholm, Sweden : 1987)*, 45(4), pp. 440-445.
- [76] Trout, A. T., Kallmes, D. F., and Kaufmann, T. J., 2006, "New fractures after vertebroplasty: adjacent fractures occur significantly sooner," *AJNR Am J Neuroradiol*, 27(1), pp. 217-223.
- [77] Tozzi, G., Zhang, Q. H., and Tong, J., 2012, "3D real-time micromechanical compressive behaviour of bone-cement interface: experimental and finite element studies," *J Biomech*, 45(2), pp. 356-363.
- [78] Brandolini, N., Cristofolini, L., and Viceconti, M., 2014, "Experimental methods for the biomechanical investigation of the human spine: a review " *Journal of Mechanics in Medicine and Biology*, 14(1), p. 1430002 (1430033 pages).
- [79] Furtado, N., Oakland, R. J., Wilcox, R. K., and Hall, R. M., 2007, "A Biomechanical Investigation of Vertebroplasty in Osteoporotic Compression Fractures and in Prophylactic Vertebral Reinforcement," *Spine*, 32(17), pp. E480-E487  
410.1097/BRS.1090b1013e31811ea31812ee.

# Conclusion

This study delivered a comprehensive *in vitro* investigation of the mechanical properties of the human thoraco-lumbar natural and prophylactic augmented vertebrae, through the experimental protocol developed. Moreover, the candidate provided a comprehensive biomechanical analysis to gain further insight on the mechanics of the failure process in augmented vertebrae as well as the performance of the treatments. To elucidate the mechanical properties of the natural (either healthy, or osteoporotic) and augmented vertebrae, an integrated approach is presented, which incorporates different experimental measurement methods (strain gauges and digital volume correlation).

1. To improve and make more reproducible *in vitro* biomechanical test of natural and treated vertebrae the following methods were validated and implemented by the candidate:

- Develop of a reproducible anatomical reference frame for the human vertebrae, suitable for *in vitro* and numerical applications
- Provide a comprehensive *in vitro* investigation on different boundary condition experienced by vertebrae, assessing the surface strain distribution between vertebra tested in physiological condition (i.e. through its adjacent discs and vertebrae) and the same vertebra tested as isolated vertebra body

2. The methods described above, were applied in the following applications. A set of main objectives were defined and completed to provide the presented investigation:

- Provide comprehensive *in vitro* investigation about prophylactic augmentation
- Develop an *in situ* testing protocol for use with natural and augmented vertebrae
- Provide for the first time experimental data on augmented vertebrae using DVC analysis
- Provide comprehensive investigation of the internal strain distribution, both in the elastic regime and up to failure in the natural and augmented vertebrae
- Evaluate biomechanical efficacy of prophylactic augmentation, using two different commercial biomaterials, in preventing fracture of non-fractured vertebral body.

## General Conclusion

Strong clinical interest is given to spinal fractures due to the high rate of morbidity and the increasing healthcare costs. Bone metastases, osteoporosis and trauma are the most common sources of vertebral fractures, which can lead to severe consequences and mortality. Spinal fractures are indeed one of the most serious problem in industrialized countries. More effective treatments are needed in order to improve patient's quality of life. The most promising approach to reduce the consequences of osteoporosis, is to diagnose the bone loss early and begin treatment strategies before fractures occur. In the last years prophylactic augmentation has been proposed as an alternative to pharmacological treatments in order to reduce the fracture risk of osteoporotic vertebrae or to prevent adjacent fractures after augmentation. This treatment is meant to increase the strength and the structural support of weak vertebrae, by injection of an augmentation material into the vertebral body. The associated risks (cement leakage and subsequent neural damage; tissue necrosis due to residual monomer and to the exothermal reaction; increased risk of fracture in the adjacent vertebrae) have raised questions about the efficacy and safety of the vertebroplasty in general. Furthermore, it is still debated whether prophylactic augmentation actually strengthens the treated vertebra. Therefore, there is a need for a clearer understanding on the cost-benefit trade-off. In the light of this debate, in-depth knowledge of the mechanical behaviour and failure of prophylactic-augmented vertebra is of fundamental importance to understand vertebral biomechanics and improve diagnosis and prophylactic treatments.

To overcome some limitations of the current *in vitro* methods, the first part of the presented thesis (chapter 2 and 3) was focused on improving and making more reproducible *in vitro* biomechanical test on natural and augmented vertebrae. From a biomechanical point of view, the spine is probably the most complex structure of the human musculoskeletal system and its investigation is an ongoing challenge. In the literature there are several studies on the mechanical behavior of the vertebrae, but results are fragmentary and incomplete with respect to some problems. While *in vitro* mechanical testing of the human vertebrae is regularly performed no clear definition has been proposed for an anatomical reference frame for *in vitro* purposes. This makes comparisons between various studies difficult, if not impossible. Moreover, none has demonstrated which boundary conditions better replicate the *in vivo* conditions.

The definition and adoption of an *in vitro* human vertebrae reference frame is found to be of extreme importance and usefulness, to perform experimental tests on the natural and augmented

vertebrae. Application of this anatomical reference frame to align specimens during tests provided more reproducible specimen alignment, making *in vitro* biomechanical tests more accurate. The use of this reference frame can also be useful *in silico* for the development of accurate numerical models, and for numerical-experimental comparison. Moreover, an anatomical reference frame for *in vitro* experiment was never formally defined and validated for the human vertebrae.

Different *in vitro* methods to characterize the mechanical behaviour of the vertebral body are present in the literature: the strength of natural and treated vertebrae can be assessed both on isolated vertebral bodies, and on sets of three-adjacent-vertebrae (where the central one, under investigation, is loaded through the adjacent intervertebral discs). In this thesis an investigation was developed to examine the effect of different experimental boundary conditions (with and without discs) in the human vertebra and to elucidate if testing a single-vertebra specimen (which provides a number of practical advantages) is an acceptable alternative to a three-adjacent-vertebrae-segment (which can be assumed closer to physiological), when measuring the principal strains (magnitude and direction) on the surface of the vertebral body, in the elastic regime. The investigation showed that the magnitude of the principal strains on the vertebral surface is significantly different between boundary condition (three-adjacent-vertebrae and single vertebra). Even if testing the single-vertebra is advantageous from several points of view, the strain distribution for this boundary condition presents some difference from the case where the vertebra is loaded through its adjacent discs, especially when axial compression is investigated. This lead to conclude that simplified boundary condition may limit the physiological relevance of results, therefore, when single vertebrae were tested, results on the bone surface should be taken with caution.

The methods described above, were applied in the following application (chapter 4, 5 and appendixes) to make investigation on the mechanical properties of natural and augmented vertebrae more accurate.

*In vitro* testing of the vertebral body has been extensively carried out in the past, but only in few cases the strain distribution has been measured. The strain in the vertebral body was investigated using different experimental techniques but mainly with strain gauges and digital image correlation. The strain gauges have been heavily used in biomechanics, and they are still considered the gold standard in bone strain measurements because their accuracy and high frequency response, however this measurement technique not provide any insight about the stress/strain distribution within the trabecular structure. As the internal trabecular bone of the

vertebral body plays a fundamental structural role, it would be extremely important to measure the internal strain distribution. An alternative tool for investigating internal strains is DVC. For this reason in this thesis, the mechanical properties of natural and treated vertebrae and the effect of prophylactic augmentation on the strength and toughness of the vertebrae were investigated both in terms of force-displacement plots, surface strain distribution (from standard testing with strain gauges), and internal strains and failure mechanism (from DVC). Application of DVC to whole porcine natural and augmented vertebrae has been able to capture and quantify internal microdamage initiation/evolution and the internal full-field strain distribution of the different components under loading. Findings showed that prophylactic augmentation increased the force required to induce damage only in some of the vertebrae and other specimens failed under a force that was lower than the one produced in the controls. This variability of the weakening/strengthening effect of prophylactic augmentation seems to support that the effect of augmentation depends on the quality of augmentation itself (amount, localization and distribution of the injected material). The positive/detrimental effect depends on a combination of factors describing the quality of augmentation. Results suggest that a proper strengthening is achieved when the cement is placed in the anterior region, and forms a unique mass bridging the endplates. Factors that deserve consideration to obtain a significant improvement of the strength and toughness of prophylactic-augmented vertebrae are: fill of the vertebral body (at least 25%), formation of a single cement mass (uni-pedicular access seems to be an advantage), endplate-to-endplate contact and cement mass placed in the anterior region. It is therefore reasonable to assume that to improve the outcomes of prophylactic augmentation, more attention should be dedicated to the quality of augmentation itself. Conversely, augmentation was not associated to an evident modification of the strain magnitude when compared to the control vertebrae, but rather to a different localization of highly strained regions due to the variable cement distribution. Such elevated strain concentration within the cement did not produce visible damage to the cement region itself, but affected the strength of the surrounded trabecular bone, resulting in an increased fracture risk at the cement-bone interdigitated region and of the surrounding trabecular bone regions just above or below the cement mass. The most critical region was the bone-cement interdigitated area where the onset of the fracture was recognizable. Starting from the bone-cement interdigitated area the microdamage gradually spread under load across the trabecular bone, which provided a lower stiffness than the cement injected. In the most of cases, the microdamage in the trabecular bone is mainly characterized by bending and buckling of the trabeculae in the transverse plane. There are some

limitations of this present study on DVC that must be considered. First of all, porcine specimens were used, which have a different anatomy and tissue properties than human ones. For this reason, the current results cannot be assumed in absolute terms as both the failure force and the strain magnitude might be different from the human ones. However, comparisons between the natural and augmented specimen were possible. All these limitations are compensated by the fact that, to the author's knowledge, this is the first time that the internal strain distribution (in the elastic regime) and the internal mechanism of failure are investigated in prophylactically-augmented vertebrae.

The present thesis underlined the importance to use an integrated approach, which combined different measurement methods (strain gauges and digital volume correlation) for the comprehensive investigation of the mechanical characterization of the human natural and treated thoraco-lumbar failure. It appears evident that no method is clearly superior to the others. Despite being old, strain gauges are still the gold standard when it comes to strain accuracy and measurement repeatability. They are recommended for accurate, discrete measurements in specific locations that can be a priori determined. Digital volume correlation can augment the knowledge in terms of internal strain distribution in bone in response to different loading conditions and when approaching yield. However, DVC is sensitive to noise in the obtained strain data. Such noise effects need to be controlled and measured in order to get a proper strain resolution. Moreover, the long acquisition time currently limits the usability to experiments where the real time strain response is not crucial.

Nonetheless, some tools could be developed further to better understand clinical needs and/or transferred to other projects. First at all, the DVC analysis conducted in this work were performed on porcine vertebrae, future work is necessary to implement and validate experimental protocol to human vertebrae. An additional next step is to test a spine segment in order to obtain strain distribution maps closest to physiological condition. Moreover the DVC results obtained could be combined with finite element analysis (FEA), to produce a more reliable predictive tools.

# **Appendix A: Strain distribution in the lumbar vertebrae under different loading configurations**

Luca Cristofolini, PhD<sup>1,2</sup>, Nicola Brandolini, MSc<sup>1</sup>, Valentina Danesi, MEng<sup>1,2</sup>, Mateusz M. Juszczak, PhD<sup>1,2</sup>, Paolo Erani, BEng<sup>1</sup>, Marco Viceconti, PhD<sup>1</sup>

<sup>1</sup> Laboratorio di Tecnologia Medica, Istituto Ortopedico Rizzoli, Bologna, Italy

<sup>2</sup> Facoltà di Ingegneria, Università di Bologna, Italy

*The candidate contributed to this study with the bibliography research and data elaboration. This work was published on the Spine Journal.*

## **Abstract**

**Background context** - The stress/strain distribution in the human vertebrae has seldom been measured, and only for a limited number of loading scenarios, at few locations on the bone surface.

**Purpose** – This *in vitro* study aimed at measuring how strain varies on the surface of the lumbar vertebral body, and how such strain pattern depends on the loading conditions.

**Methods** - Eight cadaveric specimens were instrumented with 8 triaxial strain gauges to measure the magnitude and direction of principal strains in the vertebral body. Each vertebra was tested in a three-adjacent-vertebrae-segment fashion. The loading configurations included a compressive force aligned with the vertebral body, but also tilted ( $15^\circ$ ) in each direction in the frontal and sagittal planes, a traction force, and torsion (both directions). Each loading configuration was tested 6 times on each specimen.

**Results** - The strain magnitude varied significantly between strain measurement locations. The strain distribution varied significantly when different loading conditions were applied (compression vs. torsion vs. traction). The strain distribution when the compressive force was tilted by  $15^\circ$  was also significantly different from the axial compression. Strains were minimal when the compressive force was applied coaxial with the vertebral body, compared to all other loading configurations. Also, strain was significantly more uniform for the axial compression, compared to all other loading configurations. Principal strains were aligned within  $19^\circ$  to the axis of the vertebral body for axial-compression and axial-traction. Conversely, when the applied force was tilted by  $15^\circ$ , the direction of principal strain varied by a much larger angle ( $15^\circ$ - $28^\circ$ ).

**Conclusions** - This is the first time that the strain distribution in the vertebral body is measured for such a variety of loading configurations, and a large number of strain sensors. The present findings suggest that the structure of the vertebral body is optimized to sustain compressive forces, whereas even a small tilt angle makes the vertebral structure work under sub-optimal conditions.

**Keywords:** Lumbar spine; strain distribution; principal strain and direction of principal strain; vertebral body; in vitro mechanical testing; structural optimization; axial compression; axial traction; anterior bending; torsion.

## Notation

AAL	strain gauge on the most anterior left side of the vertebral body
AL	strain gauge on the anterior left side of the vertebral body
AAR	strain gauge on the most anterior right side of the vertebral body
AR	strain gauge on the anterior right side of the vertebral body
BW	body weight
CV	coefficient of variation
CT	computed tomography
FE	Finite Element
L1	1 <sup>st</sup> lumbar vertebra
L3	3 <sup>rd</sup> lumbar vertebra
L5	5 <sup>th</sup> lumbar vertebra
LL	strain gauge on the lateral left side of the vertebra body
LR	strain gauge on the lateral right side of the vertebra body
PL	strain gauge on the posterior left side of the vertebra body
PR	strain gauge on the posterior right side of the vertebra body
$\epsilon_1$	maximum principal strain (typically tensile)
$\epsilon_2$	minimum principal strain (typically compressive)
$\theta_p$	angle of the principal planes (counterclockwise)

## 1. Introduction

Trauma, osteoporosis and bone metastases are the most common causes of vertebral fractures, which can lead to severe consequences and mortality [1-3]. Success of treatments such as fixation or augmentation can be jeopardized by limited understanding of spine biomechanics [4-7]. In-depth knowledge about the stress distribution in the vertebral body is fundamental to improve the understanding of spine biomechanics in health and disease, during ageing [8], and to improve surgical treatment [9]. Because of the difficulty of accessing *in vivo* the musculoskeletal loads in the spine, *in vitro* measurements of the load-strain relationship in the vertebral body can provide valuable indirect information about spine biomechanics.

*In vitro* biomechanical tests on the vertebral body often focus on fracture (e.g. [10-12]). In most such studies the strain distribution was not investigated. One of the first studies on the strain distribution in the vertebral body was carried out by means of brittle coating, photoelasticity [13] and 17 strain gauges [14], for different compressive loads. The effect of an inclined load (16°) has been investigated on functional spinal units using 3 to 4 strain gauges [15]. The contribution of the neural arch to load transfer was investigated by [16] with 11 triaxial strain gauges (8 on the vertebral body), with a compressive load. Strains induced by compression and shear loads were quantified with three triaxial strain gauges on the vertebral rim, and one on the endplate surface [17]. Fracture risk was assessed by [18], but the most stressed region could not be identified as only one gauge was applied on each vertebral body. Later, 3 triaxial strain gauges were used to assess the changes due to cement augmentation [19]. When uniaxial gauges are used (e.g. [20]) it is possible to determine neither the value of principal strains, nor their direction.

Axial compressive loading is probably the most frequent *in vitro* loading condition (e.g. [11, 21-25]). In some cases also eccentric compression [26-28] or anterior bending [10, 29] were simulated.

Finite element (FE) models can provide valuable insight in the stress/strain distribution [30-32]. Validation of FE models is mandatory to prove their accuracy and closeness to reality [33-35]. A combined numerical-experimental study was presented by [36], where 4 strain gauges were used to validate the FE predictions. A combination of experiments and FE modelling was used to estimate the elastic modulus of the cortical shell, based on the measured stiffness of the vertebral body [37].

The summary above highlights that the strain distribution in the vertebral body has been measured (i) with a limited number of strain gauges, (ii) for a limited set of loading configurations.

Aim of the present study was to explore the effect of different types of loading on the strain distribution in the vertebral body of the lumbar vertebrae.

## **2. Materials and Methods**

Non-destructive tests were performed on vertebral bodies of L1, L3, and L5 vertebrae. The strain distribution on the bone surface strain distribution was investigated by means of triaxial strain gauges. Different loading configurations were performed in order to obtain a comprehensive characterization of the strain distribution.

### **2.1 Bone Specimens**

Six thoraco-lumbar spines were obtained through an ethically-approved donation program from donors who did not suffer from musculoskeletal pathologies. Specimens were computed tomography (CT) scanned (BrightSpeed, General Electric, USA) to document bone quality and lack of abnormality or defects. Tests were performed on three-adjacent-vertebrae segments (8 specimens in total, Table 1), allowing physiological loading of the vertebral body through its adjacent intervertebral discs.

All the surrounding soft tissues were removed, including the ligaments. For each specimen the adjacent vertebrae were potted in acrylic cement (Restray, Salmoiraghi, Mulazzano, Italy) (Fig. 1). A 3-degrees-of-freedom clamp was used to hold the central vertebra in order to align its upper and lower vertebral rims parallel to the ground, fitting two parallel references. The spinous process was used to centre the specimen in the right/left direction, and align it about its vertical axis. In order to isolate the mechanical behaviour of the vertebral body from the surrounding structures, after potting the posterior arch was resected through the pedicles and removed.

**Table 1:** Details of the specimen investigated. In the first five columns, the details of the donors are listed. In the following three columns, the biomechanical dimensions are reported. The vertebral body height was measured between the centre of the upper endplate and the centre of the lower endplate. The antero-posterior length was measured between the most anterior and the most posterior point at mid-height of the vertebral body. The vertebral body width was measured between the most lateral points at mid-height of the vertebral body. In the last four columns the values of the applied loads are reported: the force (configurations: Axial-Compression, Axial-Traction, Anterior\_15-Compression, Posterior\_15-Compression, Left\_15-Compression, Right\_15-Compression), and the torque (Axial-Compression and Torsion-Clockwise). The average and standard deviation are summarized in the last two rows for the entire sample.

Specimen ID	Test vertebra	Donor's details					Vertebral body dimensions			Applied force		Applied torque	
		Gender	Age at death (years)	Height (cm)	Weight (kg)	Cause of death	Height (mm)	Antero-posterior length (mm)	Right-left width (mm)	(N)	(%BW)	(Nm)	(%BW*m)
L1a	L1	M	49	182	181	Pneumonia	25.7	23.7	37.2	781	44.0	5.10	0.287
L1b	L1	M	66	177	59	Infarct	25.7	27.0	37.4	1868	322	9.07	1.566
L3a	L3	M	49	182	181	Pneumonia	25.5	35.0	43.0	907	51.1	6.20	0.349
L3c	L3	F	78	171	64	Euthanasia	26.3	23.0	38.2	533	84.9	-	-
L3d	L5	M	88	180	77	Congestive heart failure	25.8	34.7	45.0	699	93	3.62	0.471
L3e	L5	M	70	168	86	Cardiac dysrhythmia	24.7	32.1	42.9	807	96	4.09	0.476
L5a	L5	M	49	182	181	Pneumonia	23.2	27.9	42.2	1406	79.2	5.67	0.319
L5f	L5	M	84	178	82	Dementia	28.8	31.9	43.1	1172	147	6.54	0.813
Average	-	-	67	178	114	-	25.7	29.4	41.4	1010	114.0	4.91	0.612
Standard deviation	-	-	16	5	56	-	1.5	4.4	2.8	499	90.0	2.72	0.456

During the tests, the specimens were kept hydrated with physiological saline solution. Specimens were stored sealed in bags at -24°C when not in use.

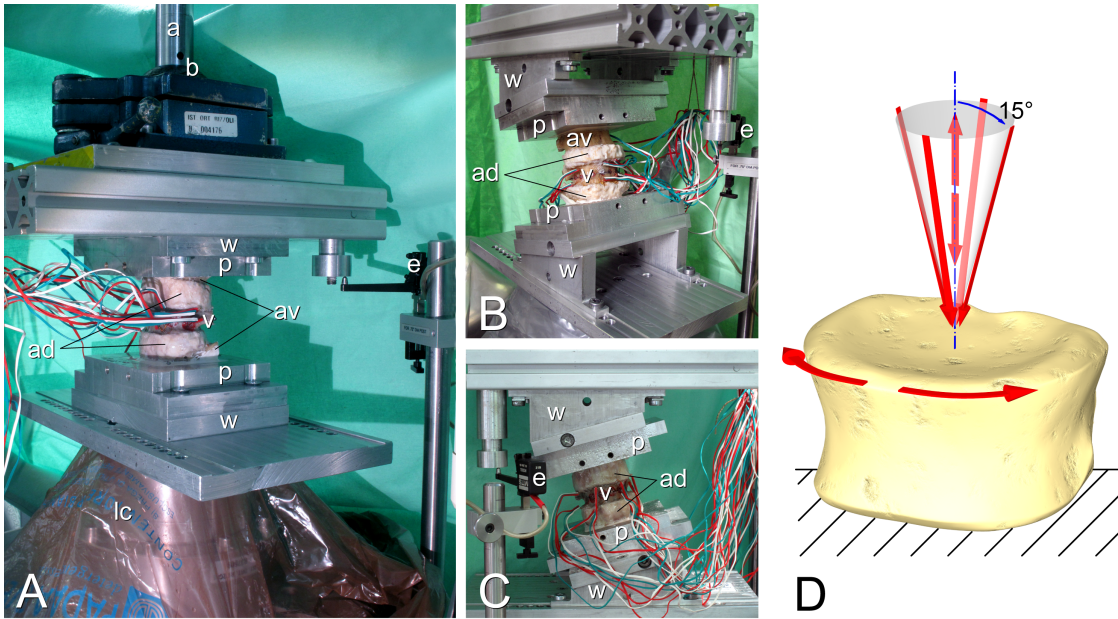


*Fig.1: Experimental setup for loading the three-adjacent-vertebrae specimens: (A) the specimen is loaded with a force aligned with the vertebral body (loading configuration “Axial-Compression”); (B) delivery of a force oblique (15°) towards anterior (configuration “Anterior\_15-Compression”) was achieved by tilting the specimen towards posterior; (C) delivery of a force oblique towards left (configuration “Left\_15-Compression”, with the specimen tilted towards right); (D) schematic showing the 8 loading configurations tested on each specimen. The vertebra under examination (v), instrumented with strain gauges, was loaded through its adjacent disks (ad) and vertebrae (av), which were embedded with acrylic cement in two aluminium pots (p). The specimen was mounted on top of the six-component load cell (lc, partially hidden by a polyethylene protection). Specimen alignment was obtained by means of wedges (w, either 0°, or 15° suitably oriented). Load was delivered to the specimen by the actuator of the testing machine (a), through a lockable ball-joint (b). Vertical displacement was measured by means of an additional extensometer (e).*

## 2.2 Strain measurement

Eight triaxial-stacked strain gauges were equally spaced around each vertebral body, at mid-height (Fig. 2). Both 1-mm grid (FRA-1-11-3L, TML Tokyo Sokki Kenkyujo, Tokyo, Japan) and 3-mm grid strain gauges (UFRA-3-350-11-3L, TML) were used, depending on the space available. Strain gauges were bonded following an established procedure for wet cadaveric specimens [38], which included:

- Accurate removal of soft tissues with a scalp and sandpaper (grade 400);
- Degreasing first with ethanol, then with a cocktail of acetone and 2-propanol;
- Bonding the strain gauges with cyanoacrylate glue (CN-Adhesive, TML);
- Waterproofing the strain gauges with polyurethane protection (M-COAT A, Vishay-MicroMeasurements, Raleigh, NC, USA).

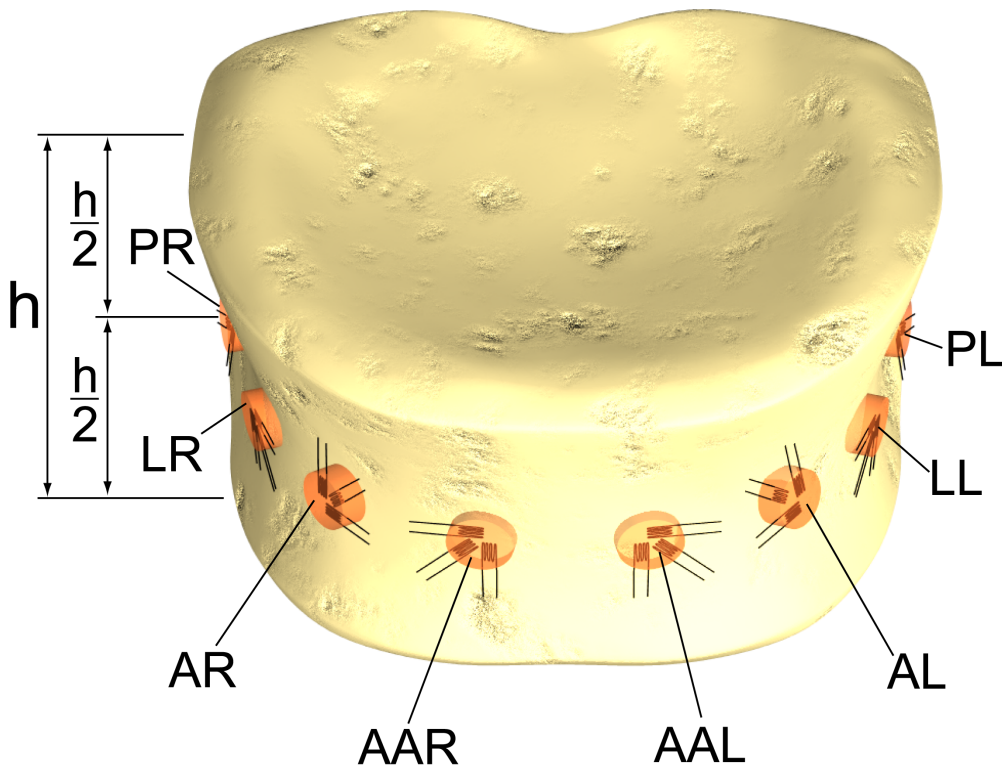


*Fig. 2 – Schematic of a vertebra with an indication of the position of the eight triaxial strain gauges around the vertebral body. One grid was aligned parallel to the vertical axis. The actual position was sometimes adjusted by up to 4 mm, when small defects (pores, ridges, or grooves) made the bone surface locally unsuitable for bonding a strain gauge.*

To avoid overheating, a grid excitation of 1 V was selected for the 1-mm gauges, whereas the 3-mm gauges were excited at 2 V. Strains were sampled at 5000 Hz using a multi channel data-logger (System 6000, Vishay-MicroMeasurements), together with the signals from the testing machine and all other transducers (see below). The principal strains  $e_1$  and  $e_2$  and the angle  $q_p$  of the principal planes were computed on the basis of the readout from the three grids of each strain gauge [39].

## 2.3 Analysis of the reinforcement caused by strain gauges

Strain gauges are known to cause reinforcement, especially on low-modulus materials and thin structures [40, 41]. This leads to an underestimation of the actual strain. As the cortical bone around the vertebral body is extremely thin, it was suspected that reinforcement would significantly bias strain measurements. The reinforcement caused by the strain gauge was estimated, assuming parallel loading between the bone thin shell and the strain gauge [40-42]. The thickness of the strain gauges used in this study was 0.085 mm, with an average Young modulus (estimated on the sandwich structure of the triaxial stacked strain gauges) of 6.4 GPa [43]. A typical Young's modulus of 15.0-18.0 GPa was assigned to the cortical bone based on the literature [44]. The thickness of the cortical shell was measured using a digital calliper (CD-15CP-500, Mitutoyo, Tokyo, Japan: precision 0.05mm). Only the contribution of the cortical shell was included in this estimate. As the contribution of the trabecular bone to structural stiffness was neglected, this analysis provides an overestimate of the reinforcing effect.

## 2.4 *In vitro* loading configurations

In order to explore the effect of a wide range of loading conditions on the strain distribution in the vertebral body, a set of simplified loading configuration was explored. Rather than replicating specific motor tasks, a selection of loading configurations was chosen that covered the physiological range of loading. To achieve better control on the testing conditions, load components were applied separately. Muscle forces were not simulated. The following eight loading configurations were tested (Fig. 1):

- To replicate a loading configuration frequently used in the literature (e.g. [16]), a compressive axial force was applied to the vertebral body (Axial-Compression).
- To understand if traction induces a symmetric strain distribution with respect to compression, a tensile axial force was similarly applied (Axial-Traction).
- To identify the range of direction of the force delivered to the vertebral body, a database available from telemeterized vertebral body replacements was interrogated [45, 46]. The force applied to the vertebral body during a variety of physiological activities (level walking, stair climbing, rising from a chair, elevation of both arms, traction of an elastic band, trunk flexion/extension and lateral bending while standing, trunk extension while

sitting, pelvis elevation from supine position) was found to fall within a cone of  $15^\circ$  around the vertical axis. Therefore, four extreme loading configurations were tested where the force was tilted by  $15^\circ$  in either direction in the frontal and sagittal planes (load configurations: Anterior\_15-Compression, Posterior\_15-Compression, Left\_15-Compression, Right\_15-Compression). This was achieved applying a vertical force to the vertebra which was tilted by  $15^\circ$  in each direction (Fig. 1).

- To test the strain distribution with torsional loading, a torque about the vertebral axis was applied in both opposite directions (Torsion-Clockwise and Torsion-Counterclockwise, with respect to the upper endplate). These loading configurations were not available for specimen L3b.

Tests were performed in over-constrained conditions: all components of rotation and translation were constrained at both the distal and proximal extremities. To monitor all components of loading during testing, a six-component load cell (FDC-011, Metior, Dongo, Italy) was used. The three-adjacent-vertebrae specimens were mounted on top of the six-components load cell, which was coaxial with the load cell of the testing machine (858-MiniBionix, MTS, Minneapolis, MN, USA). Wedges were used to tilt the specimens by the assigned angles ( $0^\circ$  for axial and torsion loading,  $15^\circ$  for the oblique loading, Fig. 1). A lockable ball-joint was placed between the actuator and the upper loading plate to ensure parallelism. During testing the ball-joint was locked, avoiding any further rotation, similar to [37, 47]. To provide a more accurate measurement, vertical displacement was measured by means of an additional extensometer (632.06H-20, MTS, Minneapolis, USA) (Fig. 1).

Specimens underwent a trapezoidal load ramp, for each loading configuration:

- For the Axial-Compression configuration the maximum force was tuned to induce 600 microstrain of strain (average over all strain gauges). Strain on the most stressed strain gauges did not exceed 1000 microstrain, which is considered as a physiological strain value [48], and it is approximately 10% of the failure strain for the cortical bone [49].
- For the compressive oblique ( $15^\circ$ ) and Axial-Traction configurations, the same force as for the Axial-Compression was applied.
- For Torsion-Clockwise and Torsion-Counterclockwise configurations, a torque inducing 600 microstrain of strain (average over all strain gauges).

- The load ramp was tuned so that the peak was reached in 0.2 seconds, which is comparable to the loading rate for many motor tasks [45, 46]. Thus, the strain rate was approximately  $0.005 \text{ s}^{-1}$  in the most stressed regions.
- The maximum displacement was held for 2 seconds to allow a constant time for a repeatable amount of creep to take place.
- To overcome variations due to viscoelasticity, strain readout was consistently averaged over the first 0.1 seconds of full-load application (500 points).

Each loading configuration was repeated six times for each specimen. The specimens were allowed to recover for 4 minutes between repetitions. This loading protocol is similar to previous works on bone specimens [50, 51].

## 2.5 Statistics

Linearity between force and strain was checked by linear regression separately for each strain gauge and each specimen.

To obtain a single output for each strain gauge and each specimen, the average over six load repetitions was calculated for the principal strains ( $\epsilon_1$ ,  $\epsilon_2$ ), and for the angle of the principal planes ( $\theta_p$ ). To estimate the measurement repeatability (intra-specimen variability) the standard deviation of the principal strains ( $\epsilon_1$ ,  $\epsilon_2$ ), and of the angle ( $\theta_p$ ) were computed between repetitions, for each strain gauge and each specimen. The coefficient of variation (CV: standard deviation expressed as a percentage of the average) was computed for the principal strain ( $\epsilon_1$ ,  $\epsilon_2$ ), for each measurement location. To avoid fictitiously increasing the CV with close-to-zero data, measurement locations where strains were lower than 100 microstrain were excluded.

Peirce's criterion was applied to exclude outliers [52]. First, for each specimen, each loading configuration and each strain gauge, suspect data were checked among repetitions: 7.1% of the data had to be excluded (mainly in association with strain gauges that had to be applied away from the standard position). Secondly, the entire sample was checked: none of the specimens had to be excluded.

To assess the significance of differences between strain values, non-parametric tests were performed (Kruskal-Wallis one-way analysis of variance) because of the limited sample size: (i) The significance of the difference between strain measurement locations was assessed separately for each loading configuration; (ii) The significance of the effect of the loading configurations on the value and direction of principal strain was assessed separately for each strain measurement location.

The difference between strain measurement locations depended on the loading configurations. To assess the significance of such load-related variation, we compared the variances (between measurement locations) computed for the different loading configurations (F-test for equality of variance).

To visualize the effect of opposite directions of loading (e.g. Axial-Compression vs. Axial-Traction, and Torsion-Clockwise vs. Torsion-Counterclockwise) on the strain distribution, the correlation between the strains measured with opposite directions of applied load was investigated by means of linear regression.

All statistical analyses were performed using dedicated software (IBM SPSS Statistics, v.14.0, SPSS Inc. Chicago, Illinois).

### **3. Results**

#### **3.1 Reinforcement caused by the strain gauges**

The cortical shell in some cases was as thin as 0.25 mm (range: 0.25-1.20mm). A similar thickness ( $0.44 \pm 0.24$  mm) has been reported for L1 [53]. The reinforcement associated with strain gauges was estimated to cause an underestimate of the actual strain by 3% to 9%, and varied from region to region and among specimens because of the uneven thickness of the cortical shell.

### 3.2 Intra-specimen and inter-specimen repeatability

Test repeatability (intra-specimen variability) was good:

- The Coefficient of Variation (CV) among replicates under the same conditions was on average 0.7% for the principal strains ( $\epsilon_1$ ,  $\epsilon_2$ ).
- The principal direction ( $\theta_p$ ) varied on average by  $0.3^\circ$  (standard deviation) among replicates for the same loading configuration.

Inter-specimen variability was obviously larger:

- To achieve the intended strain level (average 600 microstrain) the loading protocol involved different load values for each specimen (Table 1). Such differences were large both in absolute terms, and when normalized by the donors' body weight (BW). This might be explained by the fact that only the post-mortem BW was known: if the donors' BW changed significantly in the last months of their lives, it is possible that their vertebrae were “designed” for a different BW than that in Table 1.
- The principal direction ( $\theta_p$ ) varied by  $12^\circ$  to  $43^\circ$  between specimens, for the same loading configuration.

### 3.3 Linearity and viscoelasticity

Linearity between load and displacement was very high in all cases ( $R^2 \geq 0.98$ ). Also load-strain and displacement-strain linearity was excellent ( $R^2 \geq 0.98$ ) for each grid and each loading configuration, for all the cases where strains exceeded 100 microstrains. This confirms that the bone can be assumed to behave linearly with good approximation for the strain range and strain rate used in this study.

Strain readout was monitored during the holding phase of mechanical loading. The strain magnitude in the bone surface tended to decrease over 2 seconds by typically 1.5%–13% of the initial value (only in specimen L5d this decrease reached 22% of the initial value), because of relaxation in the adjacent discs. After unloading, bone strains returned rapidly to zero, with residual strain of 4% of the peak value 4 minutes after unloading.

### 3.4 Strain pattern

Tensile principal strains ( $\epsilon_1$ ) were similar to compressive ones ( $\epsilon_2$ ) in absolute value at all measurement locations. Only in Axial-Compression, compressive strain was slightly larger in absolute value than tensile strain, while in the Anterior\_15-Compression configuration tensile strain predominated.

The vertebral body exhibited a rather uniform distribution strain distribution (Fig. 3-4). Limited but statistically significant differences existed among strain measurement locations on both principal strains components, for some loading configurations (Table 2).

*Table 2: Significance of the difference between strain measurement locations for the maximum and minimum principal strain components ( $e_1$ ,  $e_2$ ), and for the direction of the principal planes ( $q_p$ ), for the 8 loading configurations. Significance is expressed in terms of p-value for the Kruskal-Wallis one-way analysis of variance.*

	Axial-Compression	Axial-Traction	Anterior_15-Compression	Posterior_15-Compression	Left_15-Compression	Right_15-Compression	Torsion-Clockwise	Torsion-Counter clockwise
$\epsilon_1$	p = 0.49	p = 0.23	p = 0.0001	p = 0.43	p = 0.081	p = 0.0094	p = 0.50	p = 0.25
$\epsilon_2$	p = 0.0004	p = 0.58	p = 0.0005	p = 0.0012	p < 0.0001	p = 0.0007	p = 0.92	p = 0.82
$\theta_p$	p = 0.31	p = 0.33	p < 0.0001	p < 0.0001	p = 0.0012	p = 0.0010	p = 0.20	p = 0.43

The variation of principal strain direction ( $\theta_p$ ) between measurement locations was limited (Fig. 5). However, because of the high measurement repeatability, such a variation was significant for most loading configurations (Table 2).

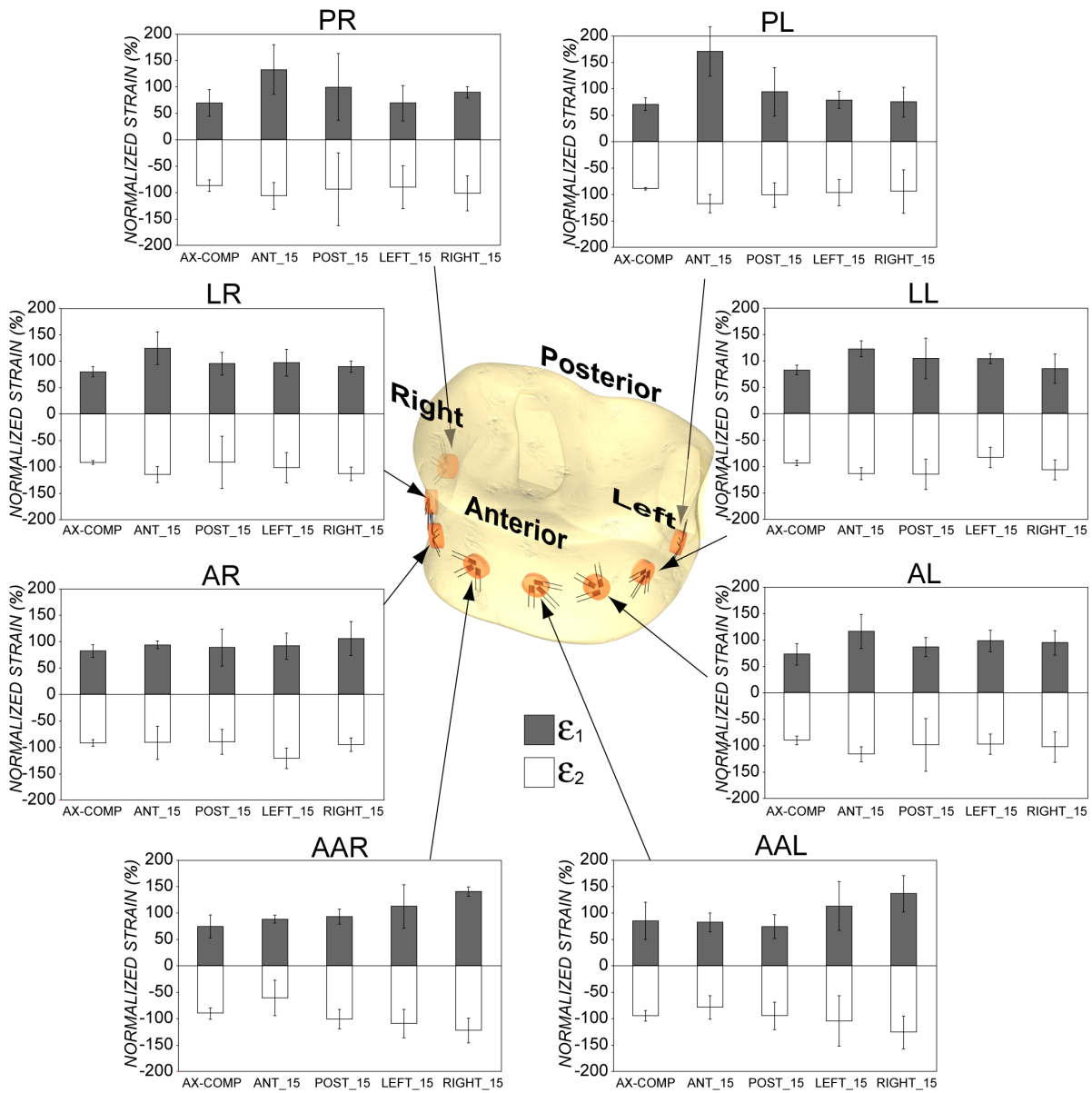


Fig. 3 – Maximum and minimum principal strains ( $\epsilon_1$ ,  $\epsilon_2$ ) on the surface of the vertebral body for the five compressive loading configurations: Axial-Compression (AXIAL), Anterior\_15-Compression (ANT), Posterior\_15-Compression (POST), Left\_15-Compression (LEFT) and Right\_15-Compression (RIGHT). To enable comparison between the different loading configurations, for each strain gauge, each strain component ( $\epsilon_1$  and  $\epsilon_2$ ) was normalized with respect to the average between the five loading configurations. The average and standard deviation of the six specimens is plotted.

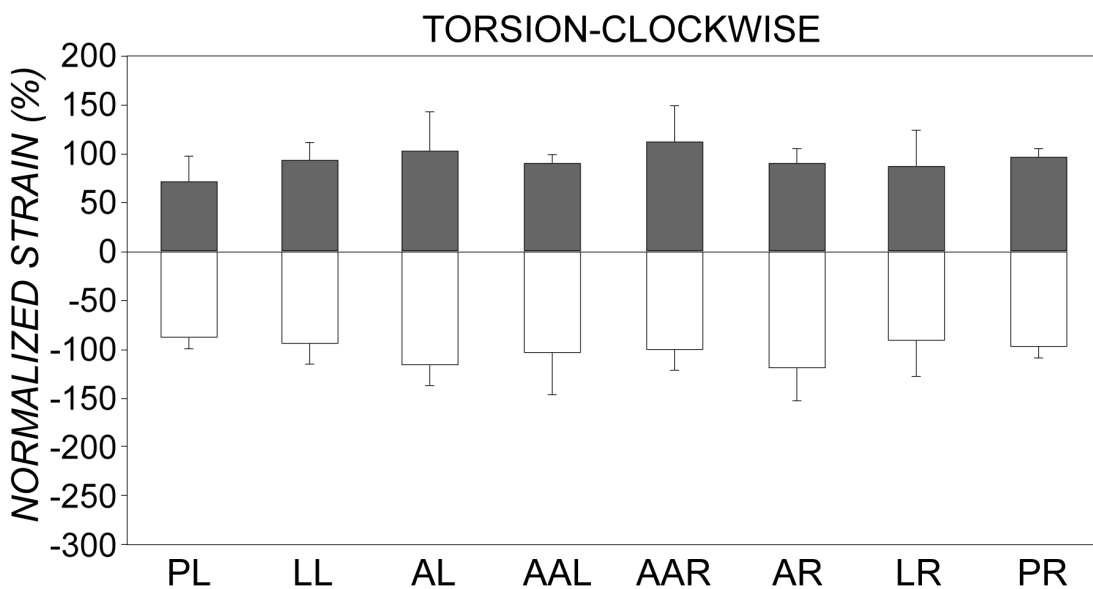
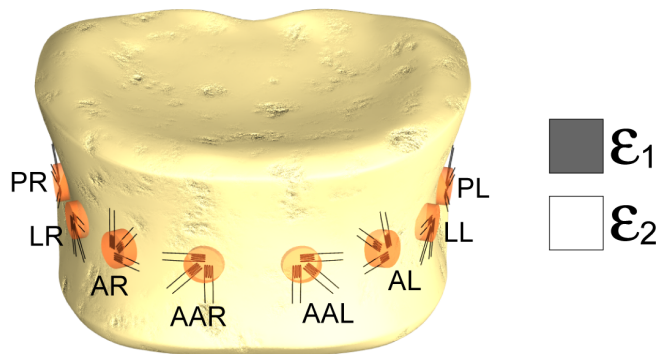
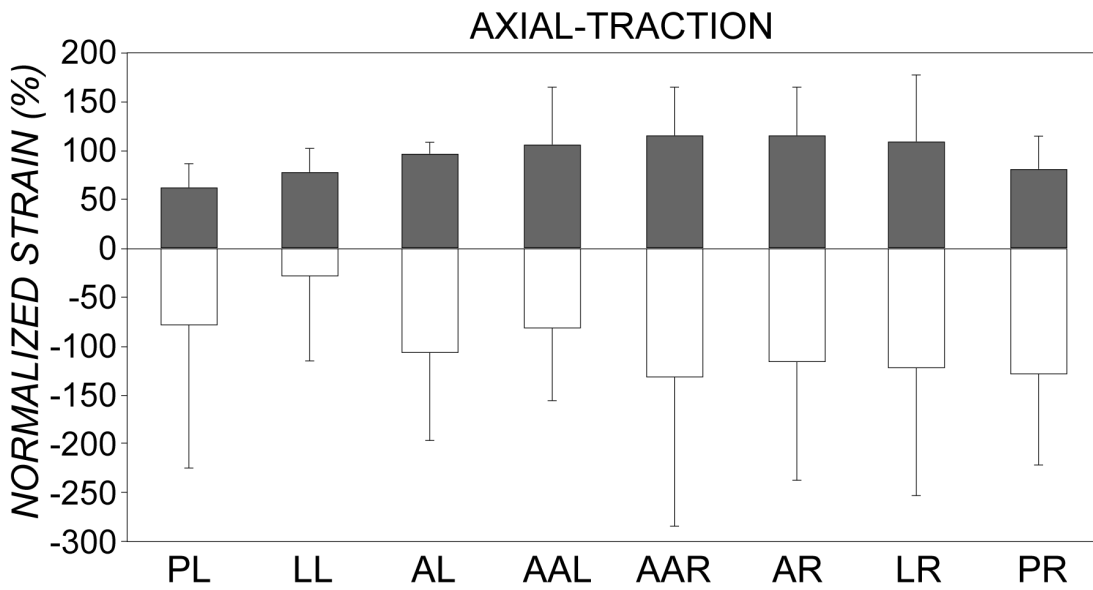


Fig. 4 – Maximum and minimum principal strains ( $\epsilon_1$ ,  $\epsilon_2$ ) on the surface of the vertebral body for Axial-Traction (top) and Torsion-Clockwise (bottom) loading configurations. Because of the large

inter-specimen variability, for each specimen, each strain component ( $\epsilon_1$  and  $\epsilon_2$ ) was normalized with respect to the average between measurement locations. The strain distribution for Torsion-Counterclockwise (not reported here for brevity) was similar to Torsion-Clockwise (see also Fig. 8). The average and standard deviation of the six specimens is plotted.

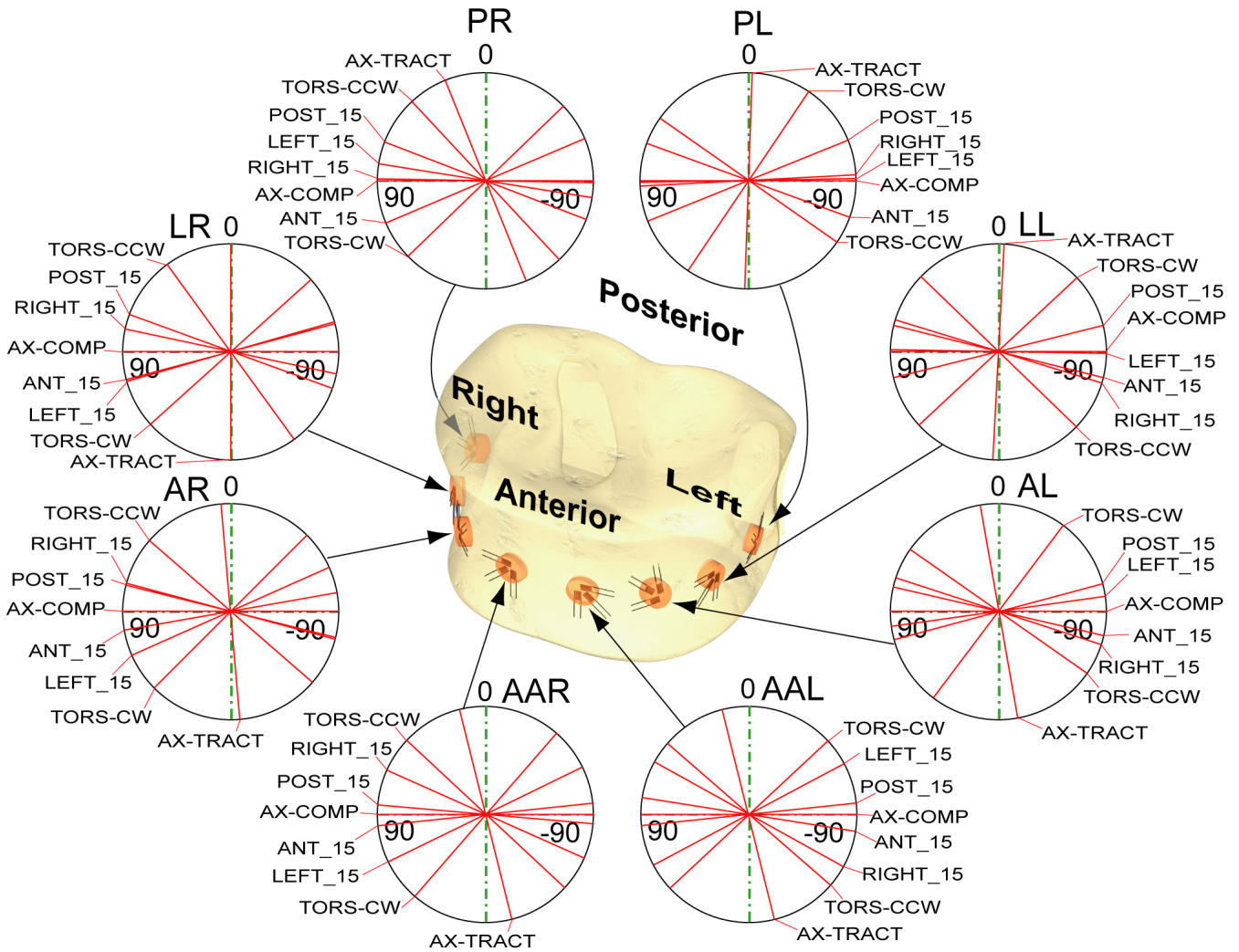


Fig. 5 – Direction of principal strains on the surface of the vertebral body for the eight loading configurations. The angle  $\theta_p$  of the maximum tensile principal strain  $\epsilon_1$  was measured with respect to the vertebral axis. The average of the six specimens is plotted.

### 3.5 Effect of the loading configurations

When the compressive force was applied in different directions, limited but statistically significant differences existed for both principal strains ( $\epsilon_1$ ,  $\epsilon_2$ : Fig. 3, Table 3). In general, the peak strain was lower when the force was aligned with the vertebral body (Axial-Compression), and larger when the force was tilted by  $15^\circ$  in any direction. The pattern for Axial-Traction, and for Torsion-Clockwise and Torsion-Counterclockwise differed from the compressive configurations (Fig. 4).

For the Axial-Compression configuration a rather uniform strain distribution was observed: the tensile principal strain ( $\epsilon_1$ , in the circumferential direction) varied by 5.1% (standard deviation between measurement locations), while the compressive principal strain ( $\epsilon_2$ , in the axial direction) varied by 2% (Fig. 6). Significantly larger variations between measurement locations were observed when the compressive force was tilted ( $15^\circ$ ), and in torsion. The variations between measurement locations were similar for all oblique loading configurations (Fig. 6).

*Table 3: Significance of the difference between the five compressive loading configurations (Axial-Compression, Anterior\_15-Compression, Posterior\_15-Compression, Left\_15-Compression, Right\_15-Compression) in the eight strain measurement locations. Significance is expressed in terms of p-value for the Kruskal-Wallis one-way analysis of variance for the maximum and minimum principal strain components ( $\epsilon_1$ ,  $\epsilon_2$ ), and for the direction of the principal planes ( $\theta_p$ ).*

	Axial-Compression	Axial-Traction	Anterior_15-Compression	Posterior_15-Compression	Left_15-Compression	Right_15-Compression	Torsion-Clockwise	Torsion-Counter clockwise
$\epsilon_1$	p = 0.49	p = 0.23	p = 0.0001	p = 0.43	p = 0.081	p = 0.0094	p = 0.50	p = 0.25
$\epsilon_2$	p = 0.0004	p = 0.58	p = 0.0005	p = 0.0012	p < 0.0001	p = 0.0007	p = 0.92	p = 0.82
$\theta_p$	p = 0.31	p = 0.33	p < 0.0001	p < 0.0001	p = 0.0012	p = 0.0010	p = 0.20	p = 0.43

The location of the largest strain changed in relation to the direction of the applied load (Fig. 3-4). The Anterior\_15-Compression configuration generally caused larger strains than any other loading configuration. Both the tensile and compressive principal strains in the anterior region (gauges AAR, AAL) exhibited a greater magnitude in the lateral configurations (Left\_15-Compression, Right\_15-Compression).

The principal direction ( $\theta_p$ ) varied greatly in relation to the direction of the applied force (Fig. 5). The principal tensile strain ( $\epsilon_1$ ) was nearly perpendicular to the vertebral body axis for the Axial-Compression, and roughly aligned with the vertebral body for Axial-Traction. The principal direction ( $\theta_p$ ) for Axial-Compression differed by 15°-28° from all other configurations tilted by 15° (Fig. 5). Principal strains were nearly at 45° to the vertebral body axis when torsion was applied. Such variations were statistically significant in all regions (Table 3).

When the two opposite directions of axial force were compared, the correlation was quite low, and the slope was quite different from 1.0: Axial-Traction generated larger strain (and with larger inter-specimen variations) than Axial-Compression, in absolute value (Fig. 7). Conversely, the two opposite direction of torsion (Clockwise and Counterclockwise) generated quite similar strain distribution (Fig. 8).

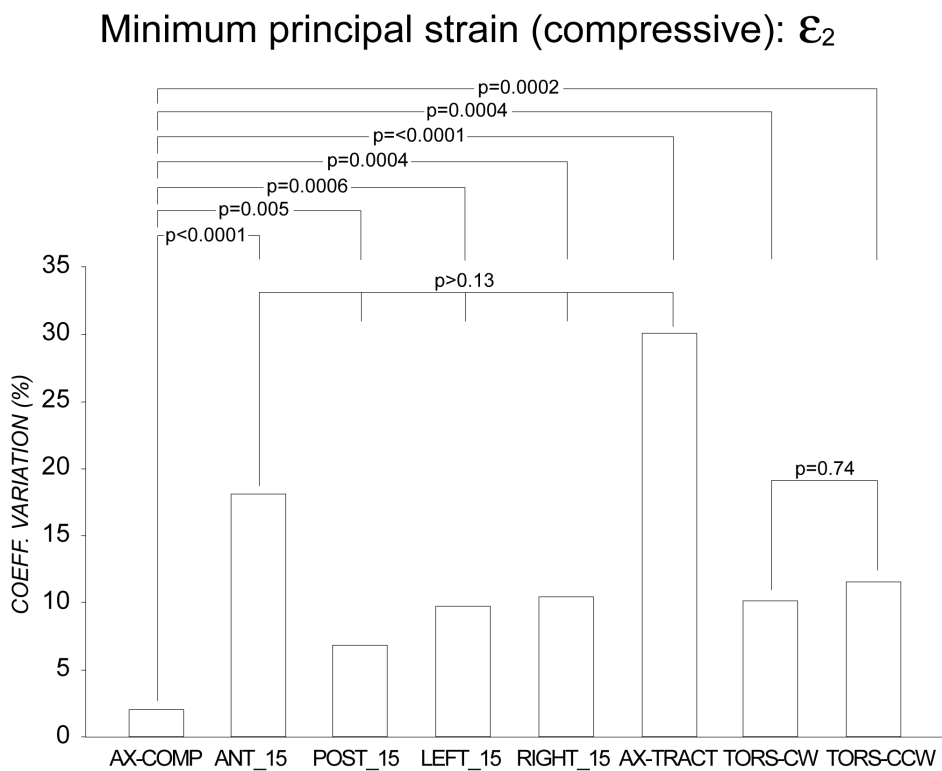
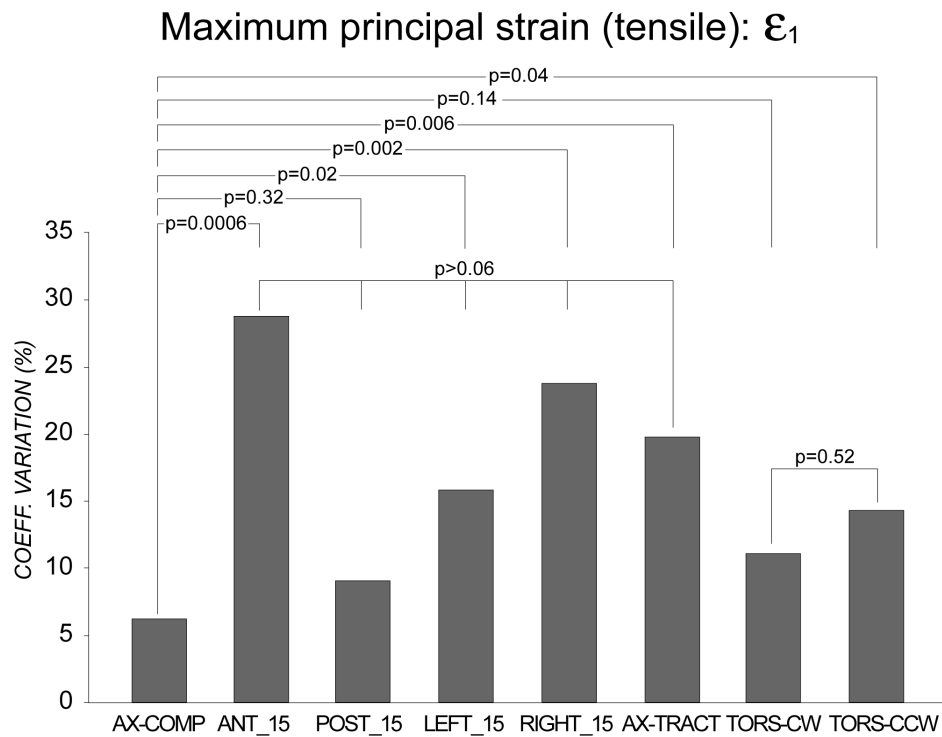


Fig. 6 – Strain inhomogeneity for the different loading configurations, computed as standard deviation between strain measurement locations, for the maximum ( $\epsilon_1$ ) and minimum ( $\epsilon_2$ ) principal

strain. The significance of the differences between loading configurations is indicated (F-test for equality of variance).

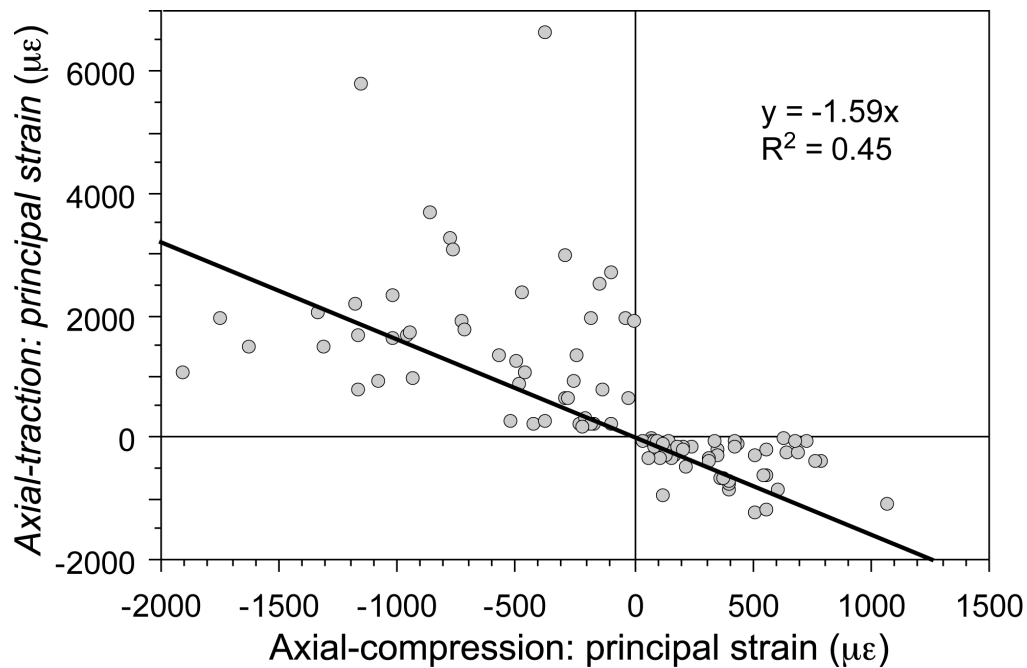


Fig. 7 – Correlation between strains when the vertebra was subjected to Axial-Compression and Axial-Traction loading configurations (same absolute value of the applied force, with opposite direction). All specimens and all strain measurement locations are pooled. A slope equal to -1.00 would indicate that strains in compression and traction had opposite sign and were equal in absolute value. The slope reported (larger than 1.00 in absolute value) indicates that strains in traction were larger (in absolute value) than in compression (i.e. the bone is more compliant in traction than compression). The low  $R^2$  value reported indicates a poor correlation between traction and compression.

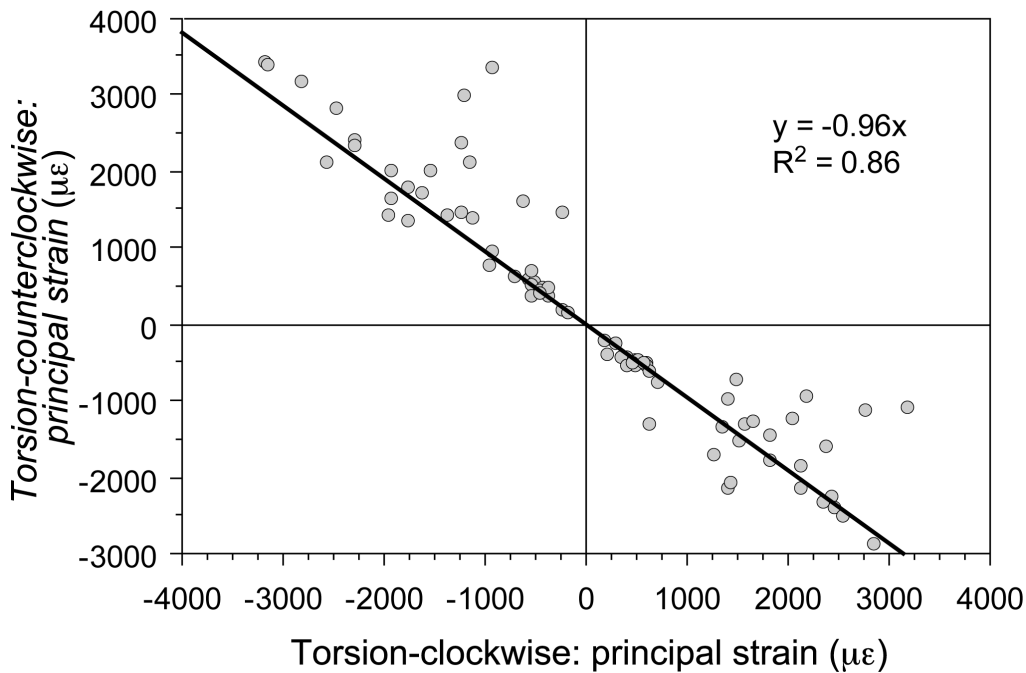


Fig. 8 – Correlation between strains when the vertebra was subjected to Torsion-Clockwise and Torsion-Counterclockwise loading configurations (same absolute value of the applied torque, with opposite direction). All specimens and all strain measurement locations are pooled. A slope equal to  $-1.00$  would indicate that strains for Torsion-Clockwise and Torsion-Counterclockwise had opposite sign and were equal in absolute value. The slope reported (lower than  $1.00$  in absolute value) indicates that strains in Torsion-Counterclockwise were slightly lower (in absolute value) than in Torsion-Clockwise. The  $R^2$  value reported indicates a good correlation between opposite directions of torsion.

#### 4. Discussion

This study aimed at assessing the effect of different loading configurations on the strain distribution in the lumbar vertebral body.

The strain distribution was measured in the vertebral body of eight lumbar vertebrae, under a variety of loading configurations that included the cone spanned by the resultant force during physiological motor tasks, but also other load components such as torsion and traction. The maximum principal strain ( $\epsilon_1$ ) was generally aligned as expected: circumferentially for all loading configurations implying a compressive force, axially for a tensile force, and roughly at  $45^\circ$  for

torsion (Fig. 6). The strain pattern was significantly affected by the loading configuration. In fact, when the same compressive force was applied, significantly lower strain were observed for the Axial-Compression configuration compared to all other configurations tilted by 15° (Fig. 3). A remarkably uniform strain distribution was generally observed for the Axial-Compression configuration. Conversely, significantly larger differences between measurement locations existed for all the other configurations (Fig. 5).

The strain distribution was quite different when the same force was applied in compression (Axial-Compression) as opposed to tension (Axial-Traction) (Fig. 7). Part of such a difference could be explained by the different response of the intervertebral disc in compression (physiologically generating a rather uniform pressure over the entire endplate) and traction (the nucleus pulposus has limited response in traction and most of the tensile force is transferred by the annulus fibrosus). In fact, for Axial-Compression the three-adjacent-vertebra specimens were 69% to 186% stiffer than for Axial-Traction. Conversely, quite similar strains were observed for the two opposite directions of torsion (Fig. 8). The torsional stiffness of the three-adjacent-vertebra specimens differed by 3% to 33% for opposite directions of torsion.

The loads applied in the present study were designed to generate a strain range (average: 600 microstrain) compatible with the physiological range in the literature, which ranges from 300 (for light activity) to 2500 microstrain (most severe tasks) [54-56]. In fact, the physiological strain (to prevent bone remodelling and resorption) is assumed to be in the range of 1000 microstrain [48]. For the compressive loading configuration, a force of 0.4-3.2BW was required (Table 1). This is compatible with the forces measured *in vivo* for physiological motor tasks (0.2-1.2BW [45, 46]).

Comparison is possible with a few studies where strain has been measured in the vertebral body. Strains of the order of 500-1500 microstrains were found for a 1470N compressive force [14]. Strains of 200-700 microstrains were reported for a 490 compressive force [16], and 100-300 microstrains for a 500 N compressive force [17]. A compressive strain of 650 microstrains was measured on the anterior surface of the vertebra when a force (2800 N) was applied tilted anteriorly at 16° [15]. Such strain ranges are compatible with those reported here, if scaled by the applied load.

There are some limitations of this study that must be considered. First of all, the strain measurement was affected by systematic error: the actual strain was underestimated by 3-9%

because of the reinforcement effect of the strain gauges. While the absolute strain values are affected by such an error, such an artefact is eliminated when different loading configurations are compared for the same strain measurement location.

A second limitation relates to the limited sample size (eight specimens), caused by the large effort required to instrument and test the specimens. It must be noted that the amount of strain data (8 triaxial strain gauges on each specimen, for a total of 192 strain sensors), and the variety of physiological and non-physiological loading (8 scenarios in total) in this study is unequalled in the literature.

The loading configurations were based on measurements from telemeterized vertebral body replacements [45, 46]. It is possible that such patients did not load their spines in the most physiological way. However, this is the only source of directly measured *in vivo* loads in the literature.

In our experiment, the posterior arch was removed to ensure a better control of the loading conditions applied to the vertebral body, similar to [22, 29, 57]. In fact, this way the vertebral body was loaded uniquely through its adjacent discs, while it would have been extremely difficult to measure the additional load components applied through the facets. This operation modifies the spinal kinematics [58]. However, an *in vitro* study on 21 strain-gauged specimens has shown that removal of the posterior arch has a limited effect on the strain distribution in the anterior and central region of the vertebral body (while differences were larger near the insertion of the posterior processes) [16]. A similar trend was demonstrated with an FE model of the lumbar vertebrae [59].

Finally, similarly to most studies based on cadaver specimens, there was some uncertainty about the actual BW of the donors, which was measured only post-mortem. For this reason, it is difficult to relate the *in vitro* loads to the actual BW of the donors.

The results from the present study seem to indicate that the structure of the vertebral body is optimized for a compressive force aligned with the vertebral body. In fact:

- The strain distribution was significantly more uniform for Axial-Compression than for any other configuration (uniform stress/strain is an optimization criterion in structural engineering).

- Strain was lower when the compressive force was perpendicular to the vertebral body, as opposed to all the oblique configurations.
- When the force was tilted by 15° in any plane, the direction of principal strains varied by a wider angle (15°-28°) compared to the Axial-Compression configuration. As bone (especially trabecular bone) is known to be significantly weaker when loaded oblique to its structure [60], this seems to suggest that the structure of the vertebra is optimized (in terms of local tissue arrangement, and anisotropy) for a specific loading direction.

Such an observation is in agreement with the fact that the resultant force delivered *in vitro* to the vertebral body spans a narrow angle [45, 46]. This supports the hypothesis that the vertebral body is loaded between two ball-joint-like structures (the intervertebral disks). Such a hypothesis underlies many numerical models of the spine [61, 62]. Most disk replacements are designed consistently with such a ball-joint-like assumption [63].

To the authors' knowledge, this is the first time that the strain distribution was measured in the vertebral body for a variety of loading configurations. The information provided in this study (strain gradients, and dependence from loading scenario) can help improve the understanding of spine biomechanics, and can also serve to improve validation of numerical models of the spine.

## References

- [1] Ferrar, L., Jiang, G., Adams, J., and Eastell, R., 2005, "Identification of vertebral fractures: An update," *Osteoporosis International*, 16(7), pp. 717-728.
- [2] WHO, 1994, "Assessment of fracture risk and its application to screening for postmenopausal osteoporosis. Report of a WHO study group. WHO Technical Report Series, World Health Organization, Geneva, Switzerland, 843: 1-130."
- [3] Tancioni, F., Lorenzetti, M. A., Navarra, P., Pessina, F., Draghi, R., Pedrazzoli, P., Scorsetti, M., Alloisio, M., Santoro, A., and Rodriguez y Baena, R., 2011, "Percutaneous vertebral augmentation in metastatic disease: state of the art," *J Support Oncol*, 9(1), pp. 4-10.
- [4] Wilcox, R. K., 2004, "The biomechanics of vertebroplasty: a review," *Proc Inst Mech Eng H*, 218(1), pp. 1-10.
- [5] Kandziora, F., Pflugmacher, R., Schafer, J., Born, C., Duda, G., Haas, N. P., and Mittlmeier, T., 2001, "Biomechanical comparison of cervical spine interbody fusion cages," *Spine (Phila Pa 1976)*, 26(17), pp. 1850-1857.
- [6] Paik, H., Dmitriev, A. E., Lehman, R. A., Jr., Gaume, R. E., Ambati, D. V., Kang, D. G., and Lenke, L. G., 2012, "The biomechanical effect of pedicle screw hubbing on pullout resistance in the thoracic spine," *Spine J*, 12(5), pp. 417-424.
- [7] Tseng, Y. Y., Yang, T. C., Tu, P. H., Lo, Y. L., and Yang, S. T., 2009, "Repeated and multiple new vertebral compression fractures after percutaneous transpedicular vertebroplasty," *Spine (Phila Pa 1976)*, 34(18), pp. 1917-1922.
- [8] Pollintine, P., van Tunen, M. S., Luo, J., Brown, M. D., Dolan, P., and Adams, M. A., 2010, "Time-dependent compressive deformation of the ageing spine: relevance to spinal stenosis," *Spine (Phila Pa 1976)*, 35(4), pp. 386-394.
- [9] Goel, V. K., Panjabi, M. M., Patwardhan, A. G., Dooris, A. P., and Serhan, H., 2006, "Test Protocols for Evaluation of Spinal Implants," *Journal of Bone and Joint Surgery*, 88(suppl\_2), pp. 103-109.
- [10] Granhed, H., Jonson, R., and Hansson, T., 1989, "Mineral content and strength of lumbar vertebrae. A cadaver study," *Acta orthopaedica Scandinavica*, 60(1), pp. 105-109.
- [11] Moro, M., Hecker, A. T., Bouxsein, M. L., and Myers, E. R., 1995, "Failure load of thoracic vertebrae correlates with lumbar bone mineral density measured by DXA," *Calcif Tissue Int*, 56(3), pp. 206-209.
- [12] Ebbesen, E. N., Thomsen, J. S., Beck-Nielsen, H., Nepper-Rasmussen, H. J., and Mosekilde, L., 1999, "Lumbar vertebral body compressive strength evaluated by dual-energy X-ray absorptiometry, quantitative computed tomography, and ashing," *Bone*, 25(6), pp. 713-724.
- [13] Shah, J. S., Coggins, J., Rogers, R., Jayson, M. I., and Hampson, W. G., 1976, "Surface strain distribution in isolated single lumbar vertebrae," *Ann Rheum Dis*, 35(1), pp. 51-55.
- [14] Shah, J., Hampson, W., and Jayson, M., 1978, "The distribution of surface strain in the cadaveric lumbar spine," *J Bone Joint Surg Br*, 60-B(2), pp. 246-251.

- [15] Lin, H. S., Liu, Y. K., and Adams, K. H., 1978, "Mechanical response of the lumbar intervertebral joint under physiological (complex) loading," *J Bone Joint Surg Am*, 60(1), pp. 41-55.
- [16] Hongo, M., Abe, E., Shimada, Y., Murai, H., Ishikawa, N., and Sato, K., 1999, "Surface Strain Distribution on Thoracic and Lumbar Vertebrae Under Axial Compression: The Role in Burst Fractures," *Spine*, 24(12), p. 1197.
- [17] Frei, H., Oxland, T. R., and Nolte, L. P., 2002, "Thoracolumbar spine mechanics contrasted under compression and shear loading," *J Orthop Res.*, 20(6), pp. 1333-1338.
- [18] Kayanja, M. M., Ferrara, L. A., and Lieberman, I. H., 2004, "Distribution of anterior cortical shear strain after a thoracic wedge compression fracture," *The Spine Journal*, 4(1), pp. 76-87.
- [19] Kayanja, M. M., Togawa, D., and Lieberman, I. H., 2005, "Biomechanical changes after the augmentation of experimental osteoporotic vertebral compression fractures in the cadaveric thoracic spine," *The Spine Journal*, 5(1), pp. 55-63.
- [20] Pintar, F. A., Yoganandan, N., Pesigan, M., Reinartz, J., Sances, J. A., and Cusick, J. F., 1995, "Cervical Vertebral Strain Measurements Under Axial and Eccentric Loading," *Journal of Biomechanical Engineering*, 117(4), pp. 474-478.
- [21] Jiang, G., Luo, J., Pollintine, P., Dolan, P., Adams, M. A., and Eastell, R., 2010, "Vertebral fractures in the elderly may not always be "osteoporotic"," *Bone*, 47(1), pp. 111-116.
- [22] Lochmüller, E. M., Poschl, K., Wurstlin, L., Matsuura, M., Muller, R., Link, T. M., and Eckstein, F., 2008, "Does thoracic or lumbar spine bone architecture predict vertebral failure strength more accurately than density?," *Osteoporos Int*, 19, pp. 537-545.
- [23] Bürklein, D., Lochmüller, E. M., Kuhn, V., Grimm, J., Barkmann, R., Müller, R., and Eckstein, F., 2001, "Correlation of thoracic and lumbar vertebral failure loads with in situ vs. ex situ dual energy X-ray absorptiometry," *Journal of Biomechanics*, 34(5), pp. 579-587.
- [24] Luo, J., Bertram, W., Sangar, D., Adams, M. A., Annesley-Williams, D. J., and Dolan, P., 2010, "Is kyphoplasty better than vertebroplasty in restoring normal mechanical function to an injured spine?," *Bone*, 46(4), pp. 1050-1057.
- [25] Fields, A. J., Lee, G. L., Liu, X. S., Jekir, M. G., Guo, X. E., and Keaveny, T. M., 2011, "Influence of vertical trabeculae on the compressive strength of the human vertebra," *Journal of Bone & Mineral Research*, 26(2), pp. 263-269.
- [26] Teo, E. C., Paul, J. P., Evans, J. H., and Ng, H. W., 2001, "Experimental investigation of failure load and fracture patterns of C2 (axis)," *J Biomech*, 34(8), pp. 1005-1010.
- [27] Furtado, N., Oakland, R. J., Wilcox, R. K., and Hall, R. M., 2007, "A Biomechanical Investigation of Vertebroplasty in Osteoporotic Compression Fractures and in Prophylactic Vertebral Reinforcement," *Spine*, 32(17), pp. E480-E487  
410.1097/BRS.1090b1013e31811ea31812ee.
- [28] Oakland, R. J., Furtado, N. R., Wilcox, R. K., Timothy, J., and Hall, R. M., 2009, "Preliminary biomechanical evaluation of prophylactic vertebral reinforcement adjacent to vertebroplasty under cyclic loading," *The Spine Journal*, 9(2), pp. 174-181.
- [29] Buckley, J. M., Cheng, L., Loo, K., Slyfield, C., and Xu, Z., 2007, "Quantitative Computed Tomography-Based Predictions of Vertebral Strength in Anterior Bending," *Spine*, 32(9), pp. 1019-1027.

- [30] Jones, A. C., and Wilcox, R. K., 2007, "Assessment of factors influencing finite element vertebral model predictions," *J Biomech Eng.*, 129(6), pp. 898-903.
- [31] Dall'Ara, E., Schmidt, R., Pahr, D., Varga, P., Chevalier, Y., Patsch, J., Kainberger, F., and Zysset, P., 2010, "A nonlinear finite element model validation study based on a novel experimental technique for inducing anterior wedge-shape fractures in human vertebral bodies in vitro," *Journal of Biomechanics*, 43(12), pp. 2374-2380.
- [32] Chevalier, Y., Pahr, D., and Zysset, P. K., 2009, "The role of cortical shell and trabecular fabric in finite element analysis of the human vertebral body," *J Biomech Eng*, 131(11), p. 111003.
- [33] Henninger, H. B., Reese, S. P., Anderson, A. E., and Weiss, J. A., 2010, "Validation of computational models in biomechanics," *Proc Inst Mech Eng H*, 224(7), pp. 801-812.
- [34] Cristofolini, L., Schileo, E., Juszczyk, M., Taddei, F., Martelli, S., and Viceconti, M., 2010, "Mechanical testing of bones: the positive synergy of FE models and in vitro experiments," *Philos Transact A Math Phys Eng Sci*, 368, pp. 2725-2763.
- [35] Dolan, P., and Adams, M. A., 2001, "Recent advances in lumbar spinal mechanics and their significance for modelling," *Clin Biomech (Bristol, Avon)*, 16 Suppl 1, pp. S8-S16.
- [36] Imai, K., Ohnishi, I., Bessho, M., and Nakamura, K., 2006, "Nonlinear finite element model predicts vertebral bone strength and fracture site," *Spine (Phila Pa 1976)*, 31(16), pp. 1789-1794.
- [37] Liebschner, M. A., Kopperdahl, D. L., Rosenberg, W. S., and Keaveny, T. M., 2003, "Finite element modeling of the human thoracolumbar spine," *Spine (Phila Pa 1976)*, 28(6), pp. 559-565.
- [38] Viceconti, M., Toni, A., and Giunti, A., 1992, "Strain gauge analysis of hard tissues: factors influencing measurements," *Experimental mechanics. Technology transfer between high tech engineering and biomechanics.*, E. G. Little, ed., Elsevier, Amsterdam, pp. 177-184.
- [39] Dally, J. W., and Riley, W. F., 2005, *Experimental stress analysis*, College House Enterprises, Knoxville.
- [40] Ajovalasit, A., and Zuccarello, B., 2005, "Local Reinforcement Effect of a Strain Gauge Installation on Low Modulus Materials," *The Journal of Strain Analysis for Engineering Design*, 40(7), pp. 643-653.
- [41] Little, E. G., Tocher, D., and O'Donnell, P., 1990, "Strain gauge reinforcement of plastics," *Strain*, 26(3), pp. 91-98.
- [42] Perry, C. C., 1985, "Strain-gage reinforcement effects on low-modulus materials," *Experimental techniques*, 9, pp. 25-27.
- [43] Cristofolini, L., IN PRESS, "Applications in Orthopaedics," *UNESCO Encyclopedia, Encyclopedia of Life Support Systems*, Section 6.161A. Biomechanics, M. Doblaré, and J. Merodio, eds., EOLSS, Paris, France.
- [44] Fung, Y. C., 1980, "Bone and cartilage," *Biomechanics - Mechanical properties of living tissues*, Springer Verlag, New York, pp. 383-415.
- [45] Bergmann, G., 2011, " (ed.), Charite – Universitaetsmedizin Berlin "OrthoLoad". Retrieved July 1, 2011. <<http://www.OrthoLoad.com>>."
- [46] Rohlmann, A., Graichen, F., Kayser, R., Bender, A., and Bergmann, G., 2008, "Loads on a Telemeterized Vertebral Body Replacement Measured in Two Patients," *Spine*, 33(11), pp. 1170-1179.

- [47] Kopperdahl, D. L., Pearlman, J. L., and Keaveny, T. M., 2000, "Biomechanical consequences of an isolated overload on the human vertebral body," *Journal of Orthopaedic Research*, 18(5), pp. 685-690.
- [48] Lanyon, I. E., 1980, "Bone remodelling, mechanical stress, and osteoporosis," *Osteoporosis*, H. F. De Luca, ed., University Park Press, Baltimore, pp. 129-138.
- [49] Bayraktar, H. H., Morgan, E. F., Niebur, G. L., Morris, G. E., Wong, E. K., and Keaveny, T. M., 2004, "Comparison of the elastic and yield properties of human femoral trabecular and cortical bone tissue," *J Biomech*, 37(1), pp. 27-35.
- [50] Cristofolini, L., Conti, G., Juszczuk, M., Cremonini, S., Van Sint Jan, S., and Viceconti, M., 2010, "Structural behaviour and strain distribution of the long bones of the human lower limbs," *J Biomech*, 43(5), pp. 826-835.
- [51] Juszczuk, M. M., Cristofolini, L., and Viceconti, M., 2011, "The human proximal femur behaves linearly elastic up to failure under physiological loading conditions," *J Biomech*, 44(12), pp. 2259-2266.
- [52] Ross, S. M., 2003, "Peirce's criterion for the elimination of suspect experimental data," *J. Engineering Technology*, 2003(Fall), pp. 1-12.
- [53] Silva, M. J., Wang, C., Keaveny, T. M., and Hayes, W. C., 1994, "Direct and computed tomography thickness measurements of the human, lumbar vertebral shell and endplate," *Bone*, 15(4), pp. 409-414.
- [54] Aamodt, A., Lund-Larsen, J., Eine, J., Andersen, E., Benum, P., and Husby, O. S., 1997, "In vivo measurements show tensile axial strain in the proximal lateral aspect of the human femur," *J Orthop Res.*, 15(6), pp. 927-931.
- [55] Caler, W. E., Carter, D. R., Vasu, R., McCarthy, J. C., and Harris, W. H., 1982, "In vivo intracortical loading histories calculated from bone strain telemetry," *Biomechanics - Principles and applications*, R. Huiskes, D. H. van Campen, and J. R. de Wijn, eds., Martinus Nijhoff Publishers, The Hague, pp. 241-245.
- [56] Konieczynski, D. D., Truty, M. J., and Biewener, A. A., 1998, "Evaluation of a bone's in-vivo 24-hour loading history for physical exercise compared with background loading," *J Orthop Res.*, 16, pp. 29-37.
- [57] Hulme, P. A., Ferguson, S. J., and Boyd, S. K., 2008, "Determination of vertebral endplate deformation under load using micro-computed tomography," *J Biomech*, 41(1), pp. 78-85.
- [58] Wilke, H. J., Schmidt, H., Werner, K., Schmolz, W., and Drumm, J., 2006, "Biomechanical evaluation of a new total posterior-element replacement system," *Spine (Phila Pa 1976)*, 31(24), pp. 2790-2796; discussion 2797.
- [59] Whyne, C. M., Hu, S. S., Klisch, S., and Lotz, J. C., 1998, "Effect of the pedicle and posterior arch on vertebral body strength predictions in finite element modeling," *Spine (Phila Pa 1976)*, 23(8), pp. 899-907.
- [60] Öhman, C., Baleani, M., Perilli, E., Dall'Ara, E., Tassani, S., Baruffaldi, F., and Viceconti, M., 2007, "Mechanical testing of cancellous bone from the femoral head: Experimental errors due to off-axis measurements," *Journal of Biomechanics*, 40(11), pp. 2426-2433.
- [61] de Zee, M., Hansen, L., Wong, C., Rasmussen, J., and Simonsen, E. B., 2007, "A generic detailed rigid-body lumbar spine model," *J Biomech*, 40(6), pp. 1219-1227.

- [62] Han, K. S., Zander, T., Taylor, W. R., and Rohlmann, A., 2011, "An enhanced and validated generic thoraco-lumbar spine model for prediction of muscle forces," *Med Eng Phys*, 34(6), pp. 709-716.
- [63] Taksali, S., Grauer, J. N., and Vaccaro, A. R., 2004, "Material considerations for intervertebral disc replacement implants," *Spine J*, 4(6 Suppl), pp. 231S-238S.

# **Appendix B: A preliminary *in vitro* biomechanical evaluation of prophylactic cement augmentation of the thoracolumbar vertebrae**

Luca Cristofolini, Ph.D. <sup>1</sup>, Nicola Brandolini M.Eng <sup>2</sup>, Valentina Danesi, M.Eng. <sup>1</sup>,  
Paolo Erani, B.Eng. <sup>2</sup>, Marco Viceconti, Ph.D. <sup>3</sup>, Stephen J Ferguson Ph.D. <sup>4</sup>

<sup>1</sup> Department of Industrial Engineering, School of Engineering and Architecture, Viale  
Risorgimento 2, University of Bologna, Italy

<sup>2</sup> Laboratorio di Tecnologia Medica, Istituto Ortopedico Rizzoli, Via di Barbiano 1/10, Bologna,  
Italy

<sup>3</sup> Department of Mechanical Engineering and Insigneo Institute for in Silico Medicine, The  
University of Sheffield, Mappin St, Sheffield, S1 3JD, United Kingdom

<sup>4</sup> Institute for Biomechanics, ETH Zurich, Zurich, Switzerland

*The candidate contributed to this study with the bibliography research and data elaboration. This work is in press on Proceedings of the Institution of Mechanical Engineers, Part H, Journal of Engineering in Medicine.*

## Abstract

The biomechanical effectiveness of prophylactic augmentation in preventing fracture was investigated. *In vitro* biomechanical tests were performed to assess which factors make prophylactic augmentation effective/ineffective in reducing fracture risk. Non-destructive and destructive *in vitro* tests were performed on isolated osteoporotic vertebrae. Five sets of three-adjacent-vertebrae were tested. The central vertebra of each triplet was tested in the natural condition (control) non-destructively (axial-compression, torsion) and destructively (axial-compression). The two adjacent vertebrae were first tested non-destructively (axial-compression, torsion) pre-augmentation; prophylactic augmentation (uni- or bi-pedicular access) was then performed delivering 5.04 to 8.44 ml of acrylic cement by means of a customized device; quality of augmentation was CT-assessed; the augmented vertebrae were re-tested non-destructively (axial-compression, torsion), and eventually loaded to failure (axial-compression). Vertebral stiffness was correlated with the first-failure, but not with ultimate failure. The force and work to ultimate failure in prophylactic-augmented vertebrae was consistently larger than in the controls. However, in some cases the first-failure force and work in the augmented vertebrae were lower than for the controls. To investigate the reasons for such unpredictable results, the correlation with augmentation quality was analyzed. Some augmentation parameters seemed more correlated with mechanical outcome (statistically not-significant due to the limited sample size): uni-pedicular access resulted in a single cement mass, which tended to increase the force and work to first- and ultimate failure. The specimens with the highest strength and toughness had also: at least 25% cement filling, cement mass shifted anteriorly, and cement-endplate contact. These findings seem to confirm that prophylactic augmentation may aid reducing the risk of fracture. However, inadequate augmentation may have detrimental consequences. This study suggests that to improve the strength of the augmented vertebrae, more attention should be dedicated to the quality of augmentation in terms of amount and position of the injected cement.

**Keywords:** Prophylactic augmentation; vertebral body; *in vitro* mechanical testing; strength; work to failure; strain distribution.

## LIST OF ACRONYMS AND ABBREVIATIONS

AAL	strain-gauge on the most anterior left side of the vertebral body
AL	strain-gauge on the anterior left side of the vertebral body
AAR	strain-gauge on the most anterior right side of the vertebral body
AR	strain-gauge on the anterior right side of the vertebral body
BMD	bone mineral density
BW	body weight
CV	coefficient of variation
CT	computed tomography
LL	strain-gauge on the lateral left side of the vertebra body
LR	strain-gauge on the lateral right side of the vertebra body
PMMA	polymethylmethacrylate
PL	strain-gauge on the posterior left side of the vertebra body
PR	strain-gauge on the posterior right side of the vertebra body
$\varepsilon_1$	maximum principal strain
$\varepsilon_2$	minimum principal strain
$\theta_p$	angle of the principal planes (counterclockwise)

## 1. Introduction

Pathological conditions, such as osteoporosis [1] or metastatic infiltration [2], weaken the vertebra by compromising its micro- and/or macro-structure. If untreated, such vertebrae may fracture, causing severe pain and morbidity. Moreover, a high incidence of fracture of the adjacent vertebrae is reported for patients who have undergone vertebroplasty/kyphoplasty [3-5]. Therefore, there is a need for strategies to promptly reduce the fracture risk, or prevent further fractures from occurring. Prophylactic augmentation has been recently proposed as an option to reduce the fracture risk through mechanical reinforcement of the vertebral body by injection of a synthetic material. Thus, the prophylactic augmentation aims at strengthening selected weaker vertebrae [6-10]. Augmentation has also been associated with retention of the original vertebral body height, and preservation of spinal alignment [11]. In addition, prophylactic augmentation is associated with a lower risk of para-vertebral cement leakage, compared to augmentation in fractured vertebrae (where the cortical shell is compromised) [12].

While many studies have investigated the biomechanical effects of vertebroplasty on fractured single vertebral bodies [13-17] or spine segments [7, 11, 18, 19], very little data exist regarding the efficacy of prophylactic augmentation on non-fractured vertebrae.

In an *in vitro* study [20], an increase in strength was found in 10 out of 12 *in vitro* augmented lumbar vertebrae, while the remaining samples showed a controversial decrease. Other *in vitro* studies [16, 21] showed that failure strength in prophylactic augmentation with polymethylmethacrylate (PMMA) or calcium phosphate cement was on average greater than that of non-augmented vertebrae. In a different *in vitro* study [12], prophylactic augmentation increased the failure strength (normalized to bone mineral density and dimensions of the vertebral body), and restored vertebral stiffness more effectively when compared to post-fracture vertebroplasty. The failure load of prophylactic-augmented vertebrae has been reported to increase [15, 21, 22], to remain unchanged [7], or even to decrease [19] in comparison to untreated controls. Similarly, the stiffness has been reported to increase [12, 21-23] or to remain unchanged [15, 19] after prophylactic augmentation. It must be noted that most studies focused on the overall behavior of the treated vertebral body, without analyzing the strain distribution.

A possible explanation to the variability of the reinforcement effect of prophylactic augmentation can be sought in the bone quality, and in some details of treatment. The effects of

cement volume and BMD on the mechanics of prophylactic-augmented lumbar vertebrae were investigated [15]: a 20% fill resulted in a significant increase in the compressive strength of the vertebrae, while the localization of the cement mass did not appear to affect the resultant mechanical properties. In a different study, prophylactic augmentation resulted in a significant increase in stiffness and strength in osteoporotic specimens, but not in specimens with normal BMD [23]. Greater stiffening and strengthening has been found when the injected cement was in contact with both endplates than for the cases where cement reached only one endplate, both *in vitro* [24] and *in silico* [25-27].

Despite the potential advantage of augmentation in preventing fracture, prophylactic augmentation has several drawbacks, similar to post-fracture vertebroplasty. Clinical studies have shown that excessive cement fill is associated with increased complications such as para-vertebral leakage (which in many cases is associated with neural damage), and pulmonary embolism [28-30]. It has been shown that cement leakage is conditioned by factors such as cement viscosity, and placement of the injected cement [26, 31, 32]. Other potential problems of using PMMA include necrosis of the surrounding tissues due to the high polymerization temperature and monomer toxicity. Furthermore, when PMMA is used, it remains as a foreign body within the vertebra, with no chances of osteointegration [33]. The vertebrae next to the prophylactic-augmented one(s) are exposed to a higher risk of fracture, due to the greater stiffness of the treated vertebra [11, 34].

Therefore, treatment of a non-fractured vertebra exposes the patient to additional risks. At the same time, it is not quite clear whether prophylactic augmentation provides a biomechanical benefit. For this reason, there is a need for a clearer understanding on of the cost-benefit trade-off.

The aim of the present study was to investigate the biomechanical efficacy of prophylactic augmentation in preventing fracture of intact vertebral bodies. More specifically, it has been hypothesized that the effect of augmentation depends on the quality of augmentation itself. Therefore, we aimed at identifying which surgical factors make prophylactic augmentation effective/ineffective in reducing the risk of fracture. For this reason we measured *in vitro* both the structural properties (stiffness, strength, toughness) and the strain distribution of the intact and augmented vertebrae.

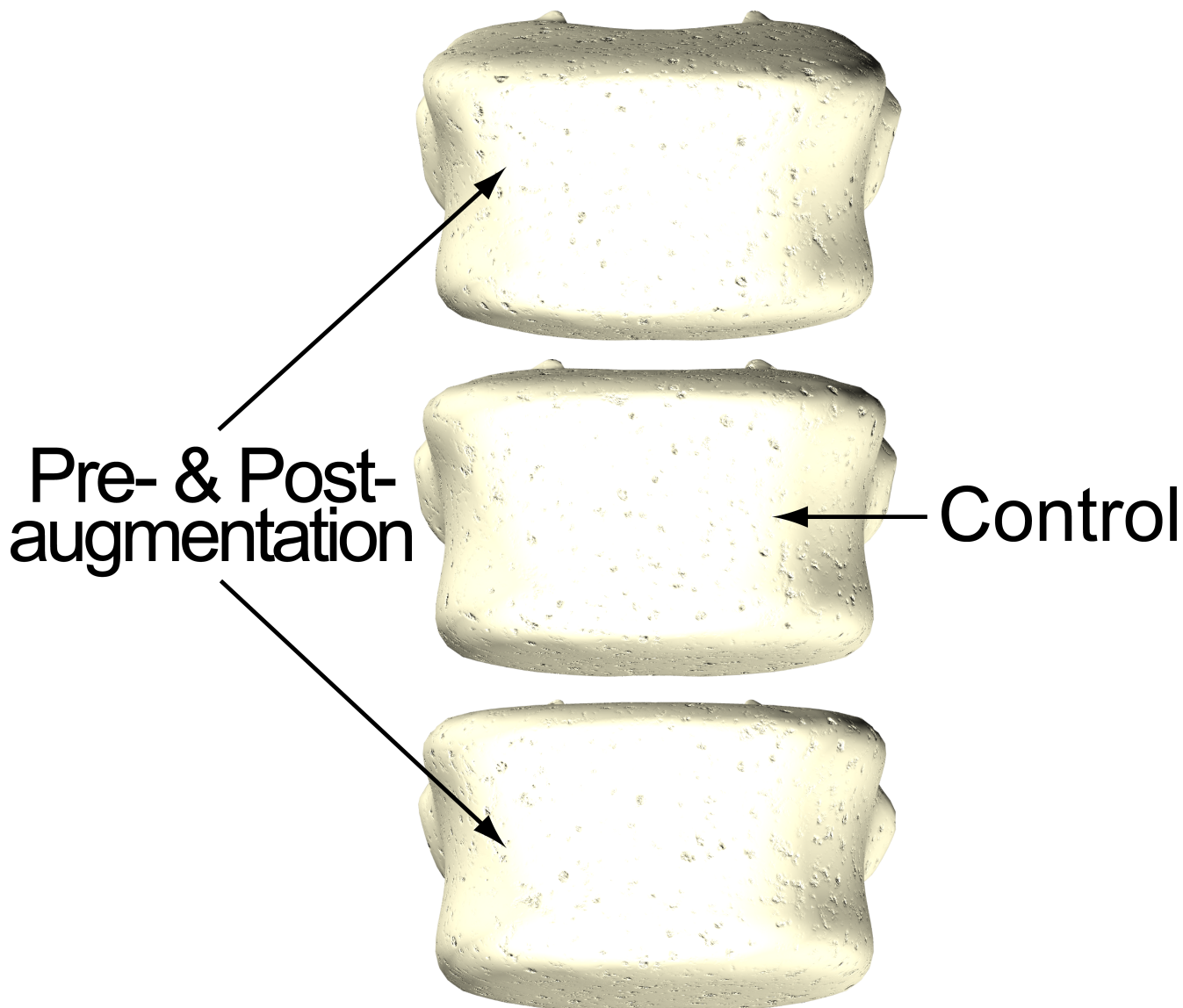
## 2. Material and methods

Non-destructive and destructive tests were carried out on non-treated and prophylactic-augmented isolated vertebral bodies, under axial compression and torsional loading. Groups of three adjacent vertebrae were used to allow comparison between prophylactic-augmented vertebrae and controls. Strain on the bone surface was measured on selected specimens by means of strain-gauges.

### 2.1 Bone Specimens

Four fresh thoraco-lumbar spines were obtained through ethically-approved donation programs (IIAM, <http://www.iiam.org>) from donors who did not suffer from musculoskeletal pathologies or cancer. The specimens were computed-tomography (CT) scanned (multislice BrightSpeed, General-Electric Medical System, Waukesha, USA) with a voxel size of 0.20 mm to document lack of defects and bone quality (all specimens were osteoporotic). Tests were performed on five series of three adjacent vertebrae, to allow comparison between matching vertebrae (either prophylactic-augmented or non-treated control: Figure 1).

The T11-T12-L1 segment was available for all four donors; in addition, the L4-L5-S1 segment was available for one donor (Table 1). The central vertebra of each set served as control and was tested non-destructively and destructively in the non-augmented condition. The two adjacent vertebrae were subjected to prophylactic augmentation and tested non-destructively both pre- and post-augmentation, while destructive test was carried out in the post-augmentation condition.



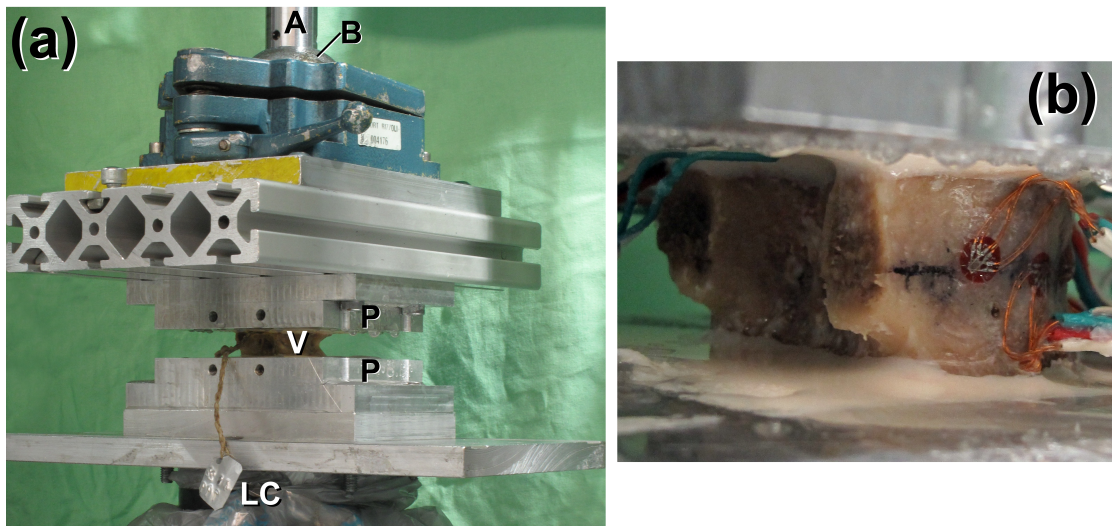
*Fig. 1. Schematic of the use of the vertebrae of each set of three: the central vertebra was used as a control (non-augmented, tested non-destructively and destructively), while the two adjacent ones were tested in the natural (non-destructively) and prophylactic-augmented condition (non-destructive and destructive). Within each set of three vertebrae, one of the two prophylactic-augmented vertebrae was randomly assigned for a uni-pedicular access, while the other one had a bi-pedicular access.*

Table 1. Details of the specimens investigated. In the first 6 columns, the details of the donors are listed. In the following columns, the biomechanical dimensions are reported for each vertebra. The vertebral body height was measured between the centre of the upper endplate and the centre of the lower endplate. The antero-posterior length was measured between the most anterior and the most posterior point at mid-height of the vertebral body. The vertebral body width was measured between the most lateral points at mid-height of the vertebral body. Indication of the presence of the strain-gauges is reported for each vertebra. The last two columns report the testing conditions of the augmented and of the control vertebrae.

Donor	Gender	Age at death (years)	Height (cm)	Body Weight BW (kg)	Cause of death	Test vertebra	Height (mm)	Antero-posterior length (mm)	Right-left width	Strain gauges	Non-destructive testing (Axial-compression & Torsion)	Destructive testing (Axial-compression)
#1	M	88	180	77	Electrical storm Congestive heart failure	T11	24	29.7	38.2	-	pre- & post-augmentation	post-augmentation
						T12	27	35.0	35.4	-	control (non-augmented)	control (non-augmented)
						L1	27.5	35.5	37.9	-	pre- & post-augmentation	post-augmentation
#2	M	88	165	59	Respiratory failure	T11	19.8	30.1	35.6	-	pre- & post-augmentation	post-augmentation
						T12	19.9	32.5	34.8	-	control (non-augmented)	control (non-augmented)
						L1	23.3	29.7	38.2	-	pre- & post-augmentation	post-augmentation
#3	M	84	178	82	Dementia	T11	22.7	38.0	42.9	-	pre- & post-augmentation	post-augmentation
						T12	26	33.8	44.4	-	control (non-augmented)	control (non-augmented)
						L1	25	38.7	44.8	-	pre- & post-augmentation	post-augmentation
#3	M	84	178	82	Dementia	L4	22.8	32.9	49.9	-	control (non-augmented)	control (non-augmented)
						L5	23.6	36.1	49.8	8	pre- & post-augmentation	post-augmentation
						S1	No treatment nor test was performed, as augmentation is not performed on S1 in clinical practice					
#4	M	70	168	86	Cardiac dysrhythmia	T11	24.5	33.5	37.0	8	pre- & post-augmentation	post-augmentation
						T12	23.9	35.1	39.7	8	control (non-augmented)	control (non-augmented)
						L1	25.7	27.9	42.9	8	pre- & post-augmentation	post-augmentation

All the surrounding soft tissues were removed, ligaments included. Alignment was performed using a 6-degrees-of-freedom clamp similar to Danesi et al.[35]. The endplates of each vertebra were potted in PMMA to a depth of 2 mm to embed the endplate rim (Figure 2). The

neural arch was subsequently excised through resection of the pedicles. During the preparation and tests (typically 3-4 days altogether), the specimens were kept hydrated with physiological saline solution. When not in use they were sealed in bags at  $-24^{\circ}\text{C}$ .



*Fig. 2. In vitro loading setup. (a) Overview with a vertebra, V, without strain-gauges. The superior and inferior endplates of the vertebra were potted with acrylic cement in two aluminum pots, P. The specimen was mounted on top of the six-component load cell, LC (partially hidden by a polyethylene protection). Load (axial-compression or torsion) was delivered to the specimen by the actuator of the testing machine, A, through a lockable ball-joint, B. (b) Posterior-lateral detailed view of a vertebra with strain-gauges. On the posterior side the resected posterior processes can be seen.*

## 2.2 Prophylactic Augmentation

Augmentation was performed on 9 vertebrae (Table 1) after the non-destructive mechanical testing in the natural condition. Room-temperature bowl-mixed acrylic bone cement (Simplex-P, Stryker, Mahwah, NC, USA) was used. A customized formulation was adopted to reduce viscosity (to better match the specifications of the injection device [36, 37]) and enhance radiopacity (as part of a different study [38]): 10 gr Simplex-P powder, 10 ml liquid, 1 gr additional  $\text{BaSO}_4$ .

Augmentation was performed by means of a custom delivery device that enabled control of injection speed (hence volumetric flow rate), while simultaneously recording plunger displacement

and injection force [36, 37] (Figure 3). The flow rate and injection force data can be used to estimate the cement viscosity. Either a uni-pedicular or bi-pedicular access was randomly assigned to one vertebra of each set of three.

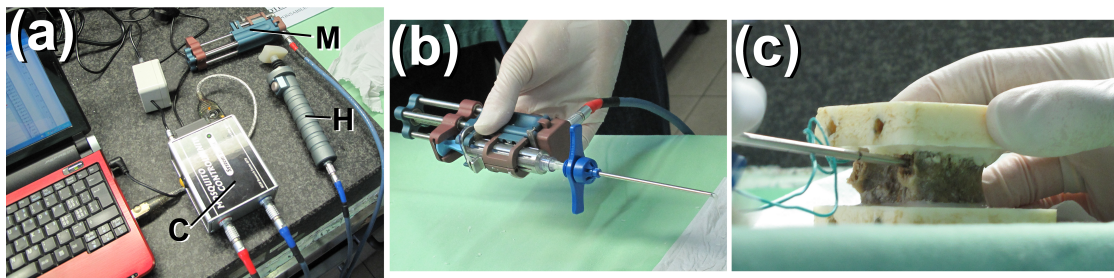


*Fig. 3. Device to perform augmentation while controlling flow rate and injection force 37,38. (a) Overview of the system with the laptop (for data logging), controller box (C), the hand-held haptic command to control injection speed and pressure (H), and the motorized injection device (M). (b) Detail of the motorized instrumented injection device with the cement syringe and needle in place. (c) Detail of a vertebra with a needle ready for uni-pedicular in vitro prophylactic augmentation.*

Between 5.04 and 8.44 ml of cement were injected in each vertebra (injection was stopped at the first visible sign of para-vertebral leakage). The specimens were CT-scanned again post-augmentation (voxel size: 0.20 mm) to assess the distribution of cement inside the vertebral body. The following indicators were obtained from the augmentation files, and from visual examination of the post-augmentation CT-scans (Table 2):

- Access: uni-pedicular, bi-pedicular;
- Volume of cement injected (measured by the injection device);
- Degree of filling of the vertebral body: injected volume (measured by the injection device) / volume of the vertebral body (estimated based on its height and cross-section, approximated with an ellipse);
- Para-vertebral leakage: yes, no;
- Placement in the sagittal plane: centered, or in contact with the anterior cortical shell;
- Distribution in the transverse plane: one-mass or two-masses;
- Sphericity of fill: sphere, ellipsoid (typically cranial-caudal due to the preferential trabecular direction), or diffuse;
- Achievement of endplate contact: none, one, or both;

Table 2. For each augmented vertebra the parameters defined during the injection (uni- or bi-pedicular access, injected volume of cement, degree of filling as a % of the volume of the vertebral body, para-vertebral leakage) are reported in the first columns. The volume of the vertebral body was estimated based on its cross-section (approximated with an ellipse) and its height. In the following 4 columns the parameters measured from the CT images are reported: placement in the sagittal plane (centered vs. in contact with the anterior cortical wall), and in the transverse plane (one-mass, two-masses), sphericity of the cement mass, and achievement of endplate contact. In the last five columns the type of failure, and the force and displacement at first and ultimate failure are indicated for the Axial-compression destructive test (with reference to Figure 4)

Donor	Test vertebra	Access	Volume of cement injected (ml)	Degree of filling (%)	Leakage	Placement in sagittal plane	Distribution in transverse plane	Sphericity of fill	Endplate contact	Type of failure	First-failure force N (%BW)	First-failure displacement (mm)	Ultimate failure force N (%BW)	Ultimate failure displacement (mm)
#1	T11	Uni-pedicular	6.21	29.1	No	Anterior	One-mass	Ellipsoid	Both	B'	5084 (673)	0.76	12486 (1654)	5.93
	L1	Bi-pedicular	6.29	21.7	No	Middle	Two-masses	Ellipsoid	One	B	4309 (571)	0.61	11893 (1575)	6.54
#2	T11	Uni-pedicular	8.25	49.5	Yes	Middle	One-mass	Ellipsoid	Both	B	11202 (1935)	1.04	15313 (2645)	3.80
	L1	Bi-pedicular	6.78	32.7	No	Middle	Two-masses	Sphere	One	C	7861 (1358)	0.93	11510 (1988)	5.54
#3	T11	Bi-pedicular	6.04	20.8	Yes	Anterior	Two-masses	Diffuse	One	B	8111 (1009)	0.85	8635 (1074)	5.98
	L1	Uni-pedicular	6.35	18.6	No	Anterior	One-mass	Sphere	Both	C	5959 (741)	0.87	11893 (1479)	6.54
#3	L5	Uni-pedicular	8.44	25.4	No	Anterior	One-mass	Sphere	One	B	12431 (1546)	1.12	14111 (1755)	5.56
	S1	-	-	-	-	-	-	-	-	-	-	-	-	-
#4	T11	Bi-pedicular	5.04	21.1	No	Anterior	Two-masses	Sphere	None	C	7842 (930)	0.86	11926 (1415)	5.06
	L1	Uni-pedicular	6.39	26.6	No	Anterior	One-mass	Sphere	Both	C	7468 (886)	0.90	14643 (1737)	6.21

## 2.3 Non-destructive testing

In order to explore the effect of augmentation under different conditions two types of loading configurations were applied to each vertebra (Figure 2). A compressive axial force was applied to the vertebral body (Axial-compression), to replicate a scenario close to physiological loading, as frequently found in the literature [39]. In addition, to gather information about a completely different (yet physiological) loading scenario, a torque about the vertebral axis was applied in both opposite directions (Torsion-clockwise and Torsion-counterclockwise), similar to Cristofolini et al. [40]. To enable an estimation of the measurement precision, and obtain more reliable data from each specimen, each loading configuration was repeated six times for each vertebra pre- and post-augmentation. The specimens were allowed to recover for 4 minutes between repetitions.

Tests were performed on an axial-torsional testing machine (858-MiniBionix, MTS, Minneapolis, MN, USA, Figure 2). The specimens were over-constrained: all components of rotation and translation were constrained at both extremities. A lockable ball-joint was placed between the actuator and the upper loading plate to ensure correct alignment. During the test, the ball-joint was locked, avoiding any further rotation [41, 42]. To monitor all components of loading during testing, an additional six-component load cell (FDC-011, Metior, Dongo, Italy) was used.

The loading protocol was similar to previous works on bone specimens [40, 43]. The testing machine operated in position control (axial displacement/rotation). A trapezoidal ramp was used, where the full-load was reached in 0.2 seconds, which is comparable to the rate for many physiological motor tasks [44, 45]. The maximum displacement was held for 2 seconds to allow a repeatable amount of viscoelasticity to take place. To overcome variations due to viscoelasticity, strain readout was consistently averaged over the first 0.1 seconds of full-load application (500 data points). The actuator displacement was adjusted for each specimen based on a preliminary test, to achieve on average 600 microstrain (calculated on the specimen free length, and verified from the strain-gauges where available). Strain on the most stressed strain-gauges did not exceed 1000 microstrain, which is considered a physiological value [46], and is approximately 10% of the failure strain for cortical bone [47]. This resulted in different load magnitudes for each specimen. In axial-compression the applied force was on average 501 N (range: 297-769 N), which corresponded to 67% of the donor's body weight (BW) (range: 51-96% BW). In torsion the applied torque was on

average 6.22 Nm (range: 4.95-8.20 Nm), which corresponded to 0.83% BW\*m (range: 0.66-1.02% BW\*m).

## 2.4 Destructive testings

All vertebrae eventually underwent destructive testing, either post-augmentation or non-augmented (control, Table 1). The same axial-compression loading configuration as for the non-destructive testing was used, with the same actuator speed, down to a compression equal to 20% of the height of the vertebral body, such as [48].

## 2.5 Strain distribution and structural properties

Four vertebrae (both from the augmentation and the control group, Table 1) were instrumented with eight strain-gauges each, equally spaced around the vertebral body, at mid-height (Figure 2). Triaxial-stacked 1-mm rosettes strain-gauges (FRA-1-11-3L, TML, Tokyo, Japan) were bonded following an established procedure for wet cadaveric specimens [43], which included removal of soft tissues with a scalpel and sandpaper, degreasing first with ethanol, then with a cocktail of acetone and 2-propanol, bonding the strain-gauges with cyanoacrylate glue (CN-Adhesive, TML), and waterproofing the strain-gauges with polyurethane (M-COAT A, Vishay-MicroMeasurements, Raleigh, NC, USA).

To avoid overheating, a grid excitation of 0.5 V was selected. Strains were sampled at 5000 Hz using a multi channel data-logger (System6000, Vishay-MicroMeasurements), together with force and displacement signals from the testing machine. The principal strains ( $\epsilon_1$ ,  $\epsilon_2$ ) and the angle ( $\theta_p$ ) of the principal planes were computed from the readout of each strain-gauge.

To assess the effect of augmentation, the stiffness was determined during the non-destructive testing as the slope of the force/displacement (or torque/rotation) curve for each vertebra pre- and post-augmentation.

The force-displacement curves of the destructive tests differed between specimens, according to the augmentation quality (Figure 4).

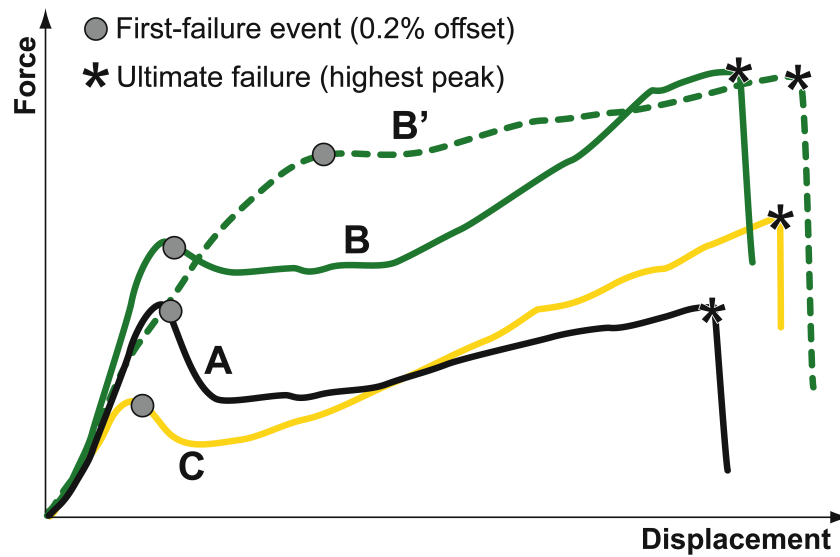


Fig. 4. Typical force-displacement plots obtained during destructive testing. TYPE A: all the non-augmented vertebrae showed a first force peak, a significant force decrease followed by plateau until ultimate failure, which occurred at a lower force than the first peak. TYPE B: for some augmented vertebrae the first peak was higher than the control, and was followed by a steady increase of force until ultimate failure (for one of such augmented vertebrae, B', the first-failure event could hardly be detected as the ramp was roughly monotonic). TYPE C: for other augmented vertebrae the first force peak was lower than the control, and was followed by a significant load recovery until ultimate failure, which occurred at a higher force than the first peak. The actual First-failure and ultimate failure forces of each specimen are reported in Table 2.

The following data were extracted:

1. To have a robust and consistent identification of the first-failure event, we adopted the 0.2% offset criterion for the force-displacement curve (in most cases this point was immediately followed by a load drop). We chose the offset strategy, which is more robust than a generic “first peak” when the force-displacement curves exhibit local fluctuations and/or progressive yield. This criterion is often used to determine the failure initiation both in mechanics [49] and in bone biomechanics [50]. This identifies the point where the vertebra starts being damaged.
2. The ultimate failure was defined as the highest peak of the force-displacement curve after the first-failure event (typically, after this point the force dropped by at least 20%). This identifies the point where the integrity of the vertebra is seriously compromised.

3. To quantify the toughness, the work required to reach the first-failure event and the ultimate failure was computed as the integral of the force-displacement curve;
4. The force, displacement and the work required by the post-augmented vertebrae were expressed as a fraction of the value of the corresponding control vertebrae.

Similarly, the post-augmentation principal strains ( $\varepsilon_1$ ,  $\varepsilon_2$ ) were expressed as a fraction of the pre-augmentation strain, while the variation of the angle ( $\theta_p$ ) of principal strain was computed between the pre- and post-augmentation condition.

## 2.6 Statistics

Test repeatability (intra-specimen variability) was good. For Axial-compression, the Coefficient of Variation (CV) among repetitions was on average 2.4% for the stiffness, and 2.2% for the principal strains ( $\varepsilon_1$ ,  $\varepsilon_2$ ). The principal direction ( $\theta_p$ ) varied on average by  $0.8^\circ$  (standard deviation) among repetitions. In Torsion, the CV was 5.2% for the stiffness, and 1.6% for the principal strains ( $\varepsilon_1$ ,  $\varepsilon_2$ ). The principal direction ( $\theta_p$ ) varied on average by  $0.2^\circ$ . The Peirce's criterion was applied to exclude outliers [51]. First, for each specimen, each loading configuration and each strain-gauge, suspect data were checked among repetitions: 7% of the repetitions were excluded. To obtain a single output for each specimen, the average over six load repetitions was calculated for the stiffness, the principal strains ( $\varepsilon_1$ ,  $\varepsilon_2$ ), and the angle ( $\theta_p$ ) of the principal strain. To enable comparisons between repetitions (the actual force slightly varied among repetitions) and between specimens, the strain readouts were normalized respectively to the same reference force (100% BW) and moment (1.00% BW\*m), similar to a previous study[40].

The entire sample was then checked with the Peirce's criterion: none of the specimens had to be excluded.

To ensure that the two groups (control and augmentation) were comparable, their stiffness in the pre-augmentation condition was compared (Wilcoxon-signed-rank-test for paired samples).

The significance of the effect of augmentation on the mechanical outcome was assessed using Wilcoxon-signed-rank-test for paired samples: the strain distribution and stiffness were compared for the same specimen pre- and post-augmentation; the first-failure and ultimate force and work were compared between the augmented specimens and the respective controls.

The effect of the factors describing the quality of augmentation (Table 2) on the mechanical outcome was assessed with Mann-Whitney-Wilcoxon (factors with 2 levels) and Kruskal-Wallis (factors with 3 levels) non-parametric tests.

All statistical analyses were performed with StatView-5.0.1 (SAS-Institute, Cary, NC, USA).

### **3. Results**

#### **3.1 Augmentation group versus control group**

The stiffness (measured during the non-destructive test) of the vertebrae in the pre-augmented condition was similar to the control group. For axial-compression the control group was on average 16% stiffer (range -8% to +71%). This difference was statistically not significant (Wilcoxon-signed-rank-test for paired samples,  $p=0.06$ ). In torsion the control group was on average 1% less stiff (range -38% to +22%). This difference was not significant (Wilcoxon-signed-rank-test for paired samples,  $p=0.68$ ).

#### **3.2 Stiffness before and after prophylactic augmentation**

When the stiffness measured during the non-destructive testing was compared for the same vertebra pre- and post-augmentation, very small differences were found (Figure 5).

For axial-compression, the prophylactic-augmented vertebrae were on average 1% less stiff than in the pre-augmented condition (range -35% to +32%: only 5 vertebrae out of 9 were stiffer). Such a difference was not statistically significant (Wilcoxon-signed-rank-test for paired samples,  $p=0.86$ ). In torsion, the prophylactic-augmented vertebrae were on average only 9% stiffer (range -19% to +39%: 7 vertebrae out of 9 were stiffer) than in the pre-augmented condition (not statistically significant: Wilcoxon-signed-rank-test for paired samples,  $p=0.17$ ).

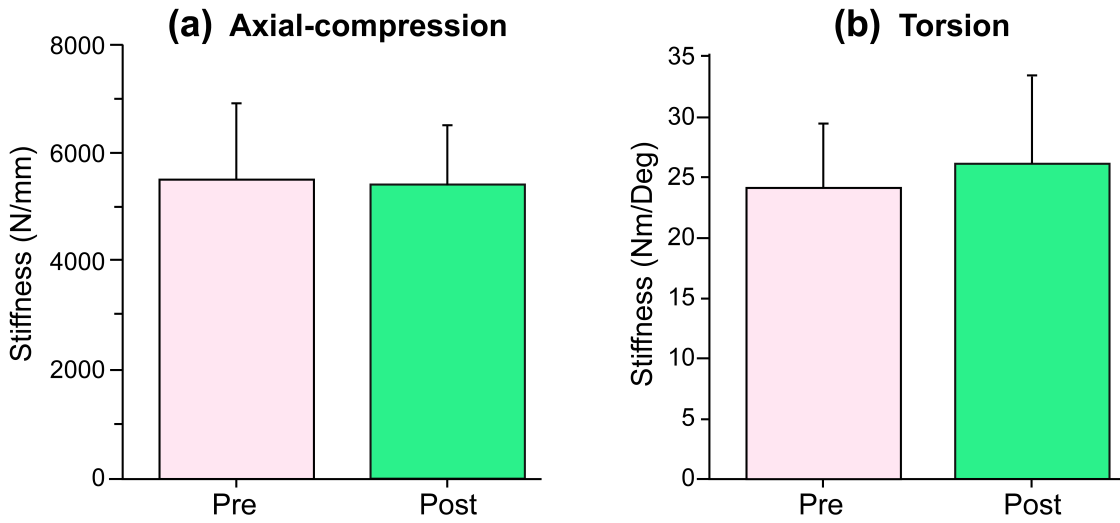


Fig. 5. Comparison of the stiffness of the 9 test specimens (average and standard deviation), in the pre-augmentation and post-augmentation conditions for axial-compression (a) and torsion (b).

### 3.3 Strain distribution

The magnitude of the principal strains measured during the non-destructive testing in the same vertebra post-augmentation was on average lower than pre-augmentation (Figure 6).

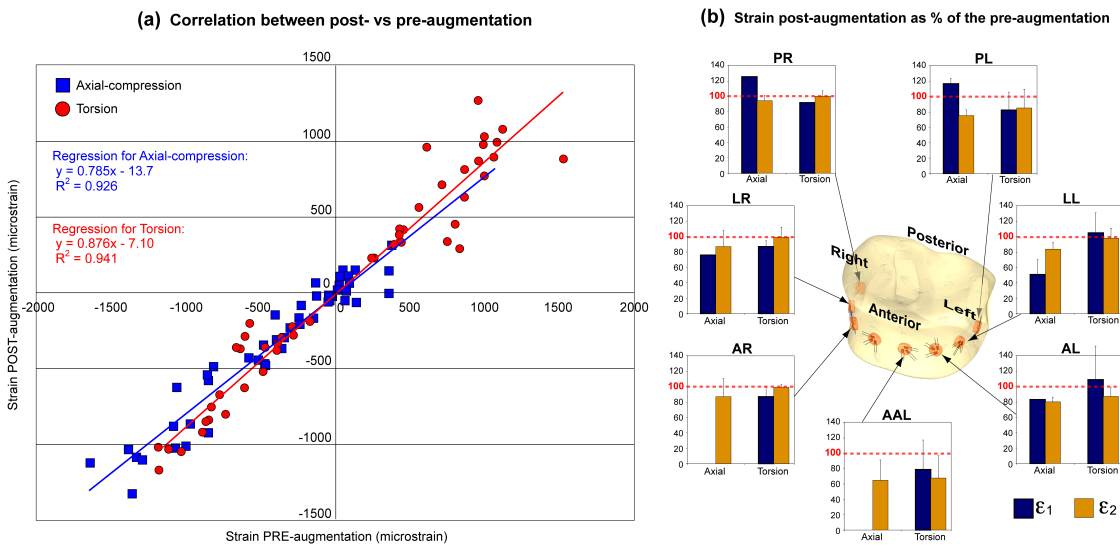


Fig. 6. (a) Strains in the post-augmentation condition are plotted versus the corresponding values in the pre-augmentation condition for the axial-compression and torsion tests. A value of the regression slope equal to 1.000 indicates no effect of augmentation on the strain magnitude; a

value lower than 1.000 indicates that strains were lower post-augmentation. (b) Schematic of a vertebra with an indication of the position of the eight triaxial strain-gauges around the vertebral body. The plots depict the effect of prophylactic augmentation on the maximum and minimum principal strains, for axial-compression and torsion. Strains in the post-augmentation condition are reported as a percentage of the corresponding strain in the pre-augmentation condition: a value of 100% means no variation due to prophylactic augmentation, a value lower than 100% indicates that prophylactic augmentation caused a reduction of bone strain. Bars are missing for those locations where strains were lower than 100 microstrain.

For axial-compression, the principal compressive strain (longitudinal) decreased on average by 18% due to prophylactic augmentation (Wilcoxon-signed-rank-test for paired samples,  $p=0.0002$ ). The principal tensile strain (circumferential) decreased on average by 59% ( $p=0.75$ ). In torsion, both principal strain components decreased on average by 12% due to prophylactic augmentation (Wilcoxon-signed-rank-test for paired samples,  $p<0.01$ ).

For axial-compression, principal strains were nearly aligned with the axes of the vertebral body; the direction of principal strains varied very little due to prophylactic augmentation (average variation  $6^\circ$ , maximum  $25^\circ$ ; Wilcoxon-signed-rank-test for paired samples,  $p=0.73$ ). In torsion, principal strains were close to  $\pm 45^\circ$  from the anatomical axis; the variation of the direction of principal strains due to prophylactic augmentation was small (average variation  $6^\circ$ , maximum  $15^\circ$ ; Wilcoxon-signed-rank-test for paired samples,  $p=0.0007$ ).

The effect of augmentation on the magnitude and direction of principal strains did not vary among measurement locations (Kruskal-Wallis,  $p>0.1$ ).

### **3.4 Strength and toughness**

During the axial-compression destructive tests the effect of prophylactic augmentation was visible (Figure 7):

1. For the prophylactic-augmented vertebrae the first-failure event occurred at a force that was on average 121% of the controls (Wilcoxon-signed-rank-test for paired samples,  $p=0.37$ ). In 5 vertebrae out of 9, failure started with a force that was larger (119% up to 237% of the

- controls). However, 4 vertebrae started failing with a force that was slightly lower (77% to 91% of the controls).
- The work required by the prophylactic-augmented vertebrae to reach the first-failure event was on average 155% of the controls (Wilcoxon-signed-rank-test for paired samples,  $p=0.26$ ). In 7 vertebrae out of 9, failure started with a work that was larger (104% to 399% of the controls). However, two vertebrae required less work to start failing (75% to 98% of the controls).
  - The ultimate force of the prophylactic-augmented vertebrae was on average 295% of the controls (consistently higher for all specimens, range: 169% to 541%, Wilcoxon-signed-rank-test for paired samples,  $p=0.008$ ).
  - The work taken by the prophylactic-augmented vertebrae to reach ultimate failure was on average 280% of the controls (consistently higher for all specimen, range: 156% to 598%, Wilcoxon-signed-rank-test for paired samples,  $p=0.008$ ).

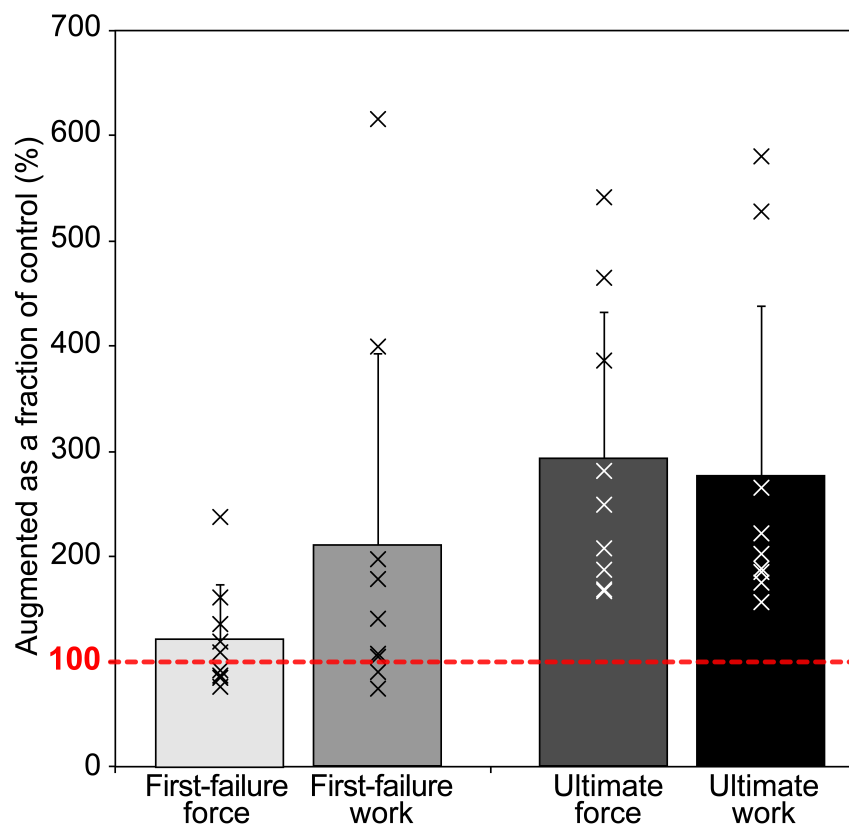


*Fig. 7. Mechanical outcome of prophylactic augmentation: the values of the force and work to the first-failure event and to ultimate failure are plotted for the augmented vertebrae as a fraction of the adjacent control. The average and standard deviation (all specimens pooled together) are*

*represented, together with the individual data points. A value of 100% indicates no variation with respect to the control; a value larger than 100% indicates that prophylactic augmentation increased the strength/toughness of the vertebral body.*

In an attempt to understand the reason(s) for the large variability of the mechanical outcome of prophylactic augmentation, correlation between the quality of augmentation and the mechanical outcome was assessed (Figure 8):

1. Access: the vertebrae prepared with a uni-pedicular access had higher first-failure force and work, as well as higher ultimate force and work than those prepared with a bi-pedicular access (not statistically significant: Mann-Whitney-Wilcoxon,  $p>0.1$ ).
2. Degree of filling: the median value of cement filling was 25.4% of the vertebral body volume. The vertebrae filled by more than 25% had higher first-failure and ultimate force and work than those filled by less than 25% (not statistically significant: Mann-Whitney-Wilcoxon,  $p>0.1$ ).
3. Para-vertebral cement leakage: the vertebrae with leakage had lower first-failure and ultimate force and work than those without leakage (not statistically significant: Mann-Whitney-Wilcoxon,  $p>0.1$ ).
4. Placement in the sagittal plane: the vertebrae in which the cement mass was in contact with the anterior cortical shell had higher first-failure and ultimate force and work than those in which the cement mass was central (not statistically significant: Mann-Whitney-Wilcoxon,  $p>0.1$ ).
5. Distribution in a transverse plane: the cases where the cement formed a unique mass had higher first-failure and ultimate force and work than when the cement formed two separate masses (not statistically significant: Mann-Whitney-Wilcoxon,  $p>0.1$ ).
6. Sphericity of fill: an ellipsoid-shaped cement mass was associated with higher first-failure force, and ultimate force and work; a spherical-shaped cement mass was associated with the highest first-failure work (not statistically significant: Kruskal-Wallis,  $p>0.1$ ).
7. Endplate contact: achievement of contact with both endplates was associated with an increase of all magnitudes, except the first-failure force (not statistically significant: Kruskal-Wallis,  $p>0.1$ ).

8. The correlation between mechanical properties of the augmented vertebrae was assessed by means of the Pearson's correlation coefficient ( $R^2$ ). The stiffness was correlated with the first-failure force ( $R^2=0.90$ ) and work ( $R^2=0.84$ ), but poorly correlated with the ultimate failure force ( $R^2=0.66$ ) and work ( $R^2=0.75$ ). The first-failure force and work were highly correlated with each other ( $R^2=0.99$ ), but respectively poorly correlated with the ultimate failure force ( $R^2=0.66$ ,  $R^2=0.61$ ) and work ( $R^2=0.79$ ,  $R^2=0.74$ ). The ultimate force and work were highly correlated with each other ( $R^2=0.93$ ).

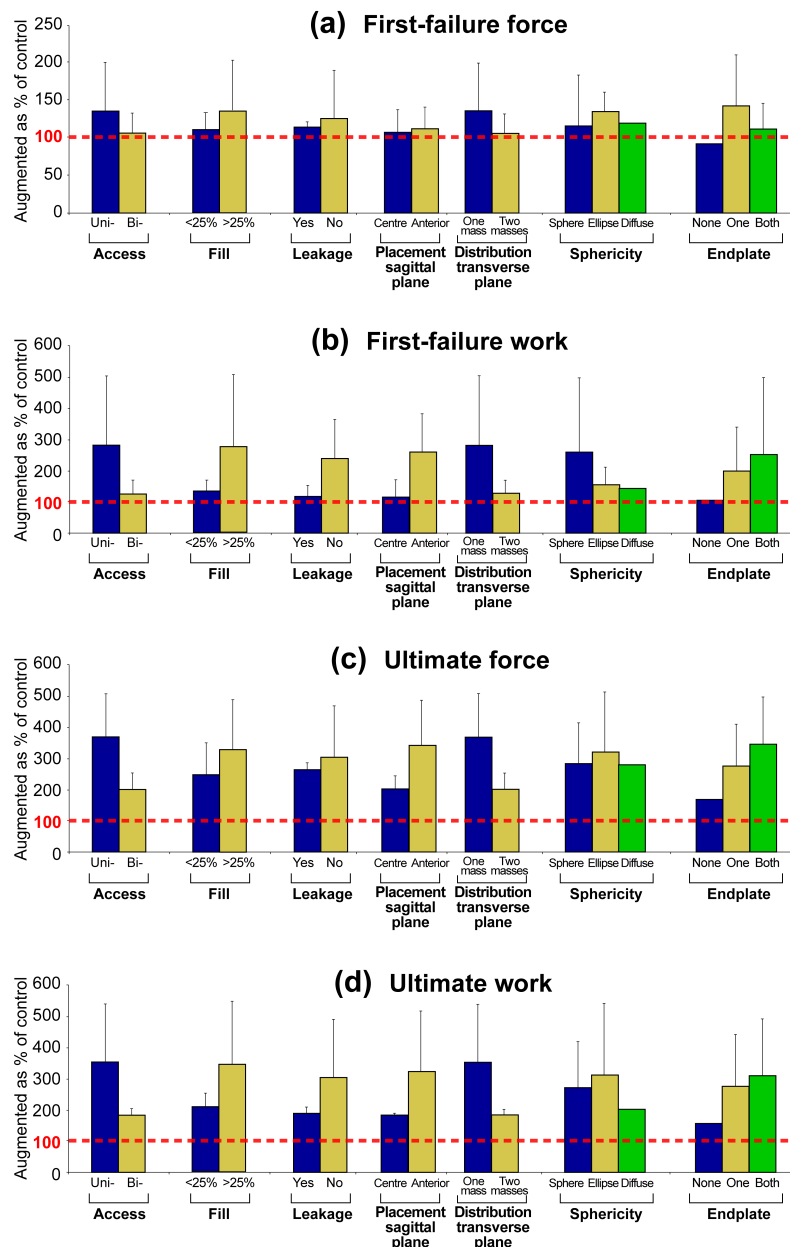


Fig. 8. Effect of the prophylactic augmentation parameters on the mechanical outcome: the values of first-failure force (a) and work (b), and ultimate force (c) and work (d) are plotted for the prophylactic-augmented vertebrae as a fraction of the adjacent control. A value of 100% indicates no variation with respect to the control; a value larger than 100% indicates that prophylactic augmentation increased the strength/toughness of the vertebral body. Legend: Access (uni-pedicular or bi-pedicular); degree of filling (lower or greater than 25% of the vertebral body volume); para-vertebral leakage (yes/no); placement in the sagittal plane (centered vs. in contact with the anterior cortical wall); distribution in the transverse plane (one-mass, two-masses), sphericity of the cement mass (sphere, ellipsoid, diffuse); endplate contact (none, one or both).

## 4. Discussion

While the biomechanical effects of vertebroplasty on fractured vertebrae have been thoroughly investigated in the past, very little data exist regarding the effects of prophylactic augmentation on non-fractured vertebrae. The aim of the present study was to investigate the biomechanical effectiveness of prophylactic augmentation in preventing fractures. It has been hypothesized that the effect of augmentation depends on the quality of augmentation itself; therefore we aimed at identifying which factors influence the suitability of prophylactic augmentation in reducing the risk of fracture.

Our findings suggest that augmentation is associated with a marked (although not uniform) decrease of the strain in the cortical shell when compared to pre-augmentation conditions. Such strain alterations were two orders of magnitude larger than the errors possibly associated with strain measurement. This suggests an alteration of the load sharing, where most of the load is transferred through the (augmented) core of the vertebral body. This may result in an altered load transfer to the endplates [52] and discs [53], which is widely supposed to contribute to the onset of adjacent fractures [3-5, 54, 55].

Even with a limited sample size, our findings suggest that, on average, prophylactic augmentation tends to increase the strength and toughness of the vertebral body. In particular, prophylactic augmentation significantly increased in all vertebrae the force and work required to achieve ultimate failure (which is associated with serious loss of integrity of the vertebral body). However, the first-failure event (which is associated with a first degree of structural damage) in some prophylactic-augmented vertebrae occurred with a force and work lower than in the controls. Therefore, while in all specimens prophylactic augmentation reduced the risk of reaching ultimate failure, in some cases it increased the risk of partial failure. Our results suggest that the stiffness itself is a poor predictor of the strength of the vertebra: while the stiffness was somehow correlated with the first-failure event, it was poorly correlated with ultimate failure. The first-failure and ultimate failure events were poorly correlated with each other.

Even if a limited sample was available, we tried to investigate the causes of such a variability of results by examining the augmentation details of each specimen. We focused on the parameters defined during the injection, and on the cement distribution inside the vertebral body.

As a trend (although not statistically significant), an association was found between some indicators of the quality of augmentation, and the strengthening/weakening effect with respect.

The different types of force-displacement curves we found for the prophylactic-augmented and control vertebrae (Figure 4) were similar to those reported by previous studies [20, 23]. Our findings concerning an insignificant increase of the stiffness due to augmentation are in agreement with other studies where no significant stiffening was found [12, 15, 19, 21]. Therefore, we do not support the idea that prophylactic augmentation would significantly stiffen the vertebral body as reported elsewhere [9, 22, 23]. However, other studies reported lower stiffness after prophylactic augmentation [7].

We found that the first-failure force was on average higher after prophylactic augmentation. Our findings are in agreement with other studies [12, 16], which reported that first-failure force of prophylactic-augmented vertebrae were on average greater than the controls (without specifying if they found cases where the augmented vertebra was weaker). However, in our study, 4 out of 9 augmented vertebrae showed a first-failure force lower than that in the untreated controls. This is consistent with a previous study [20], which reported an increase of the first-failure force in 10 out of 12 treated specimens. At the same time, the study [20] reported an increase of the ultimate failure load in all the prophylactic-augmented vertebrae with respect to the control, which is consistent with our findings. Similarly, Lim et al. [21] reported that the maximum force (apparently defined as our “ultimate failure”) of prophylactic-augmented vertebrae was greater than the control. A different study [19] reported a reduction of 19% of the first-failure force in prophylactic-augmented spinal segments.

In our specimens, the type of access seemed to affect (but with no statistical significance) both the first- and ultimate failure event: the uni-pedicular access provided better results. This is possibly explained because the cement formed a single mass, more suitably placed within the vertebral body, and achieved better contact with the endplates. Our results are not in agreement with a previous study [56], which reported no difference in the strength of bi-pedicular and uni-pedicular vertebroplasty in fractured vertebrae.

Although no statistical significance was found, a better mechanical effect of prophylactic augmentation was found for a cement fill greater than 25% of the vertebral volume. Similarly, previous studies [15, 57], reported a better outcome when cement fill exceeded 20-30% of the

vertebral body volume. Only a study on vertebroplasty of fractured vertebral body [32] reported that the fill ratio was not a significant factor in the effectiveness of augmentation.

We found that the amount of cement injected was not the only factor affecting the strengthening/weakening effect, as also the cement distribution within the vertebral body played a role. In our study, the augmented vertebrae had larger (but not statistically significant) first-failure force and work than the controls when the cement mass was: anterior in the sagittal plane, formed a single mass in the transverse plane, and was in contact with both endplates. The shape of the cement mass had very marginal effect on the resultant strength. Although slightly better results were obtained when the cement mass was ellipsoid-shaped (stretched in the cranial-caudal direction), little difference was found between sphere-shaped and diffuse cement mass. Such findings are in agreement with other *in vitro* [20, 24] and *in silico* [25-27] studies that demonstrated the importance of cement distribution over the simple amount of cement injected. Only Higgins et al. [15] reported that cement distribution was not to a significant factor.

There are some limitations of this study that must be considered. First of all, the limited sample size may not be sufficient to allow a generalization of our findings. Furthermore, due to budget and time constraints, only a limited sub-sample could be instrumented with strain gauges. The low statistical power in some cases permitted only to deduce conclusions from trends that were indicative of the actual behavior. At the same time, this is the first time that prophylactic-augmented vertebrae are tested for multiple loading configurations, while measuring several parameters and indicators of the quality of augmentation.

One may suspect that the results of the destructive tests may have been affected by previous non-destructive tests. However, the possibility that specimens were pre-damaged was very low because they were loaded in the elastic range (maximum recorded strain: 1000 microstrain). In fact, the failure force actually recorded during the destructive tests exceeded by a factor 15 (average) the force applied in the non-destructive tests.

Due to the destructive nature of the last part of our tests, the strength and toughness of the augmented vertebrae could only be compared against the adjacent control (non-augmented) vertebrae. Adjacent vertebrae were compared as augmented and control specimens. This strategy was chosen (rather than comparing matched vertebrae from different donors) because even if the specimens compared were not equal from an anatomical point of view, during donor's life they

experienced the same physiological load, lifestyle etc. It must be noticed that differences between neighboring vertebrae are more pronounced in the posterior arch and processes (which were not included in this study) and less in the vertebral body (more or less cylindrical). In fact, no statistical differences were found when we compared the stiffness of the control sample and that of the augmentation sample (measured pre-augmentation) for different loading configurations.

The over-constrained axial loading we applied could not promote wedge-shaped fractures; hence our test might not be very sensitive to the position of the cement. Furthermore, we did not include load transmission through the posterior elements. Previous studies [58, 59] have shown that in physiological conditions only a small fraction of the load is carried by the posterior elements.

Another concern is the non-physiological loading of the vertebra through the endplates potted in PMMA, although frequently adopted [9, 22, 23]. Since we compared the pre- and post-augmentation as paired specimens, variations due to augmentation were reliably detected whilst compensating the effect of endplate embedding (conversely, our stiffness and strength data might be biased by such boundary conditions).

The strain measurement was affected by systematic error: the actual strain was underestimated by 3-9% because of the local reinforcement effect of the strain-gauges; which becomes negligible at a structural level, when the entire vertebral body is considered [40]. While the absolute strain values are affected by such error, the artifact is compensated when comparing same strain measurement locations between pre- and post-augmentation. Strain-gauged vertebrae were present in both the augmentation and control group (Table 1). Therefore, also the structural reinforcement effect -if any- was balanced.

This study identified failure from the force-displacement curves, and measured strain on the outer bone surface. It might be interesting to measure internal strains, so as to identify the region where failure initiates (e.g. in the cement mass, in the cancellous bone, at the cement-bone interface). The recent developments of digital volume correlation (DVC) would possibly be able to gather this additional piece of information [60-62].

In summary, this study confirmed that prophylactic augmentation might be able to reduce the risk of macroscopic loss of integrity of the vertebral body, since in all cases an increase of the force and work required to reach ultimate failure was detected. However, in some cases inadequate

augmentation seemed to increase the risk of partial fractures. The positive/detrimental effect of prophylactic augmentation seemed to depend on a combination of factors describing the quality of augmentation. Although no statistical significance was found, our results seem to suggest that an adequate strengthening can be achieved when the cement is placed in the anterior region, and forms a unique mass bridging the endplates. Factors that would deserve further consideration to improve the strength and toughness of prophylactic-augmented vertebrae are: degree of fill of the vertebral body (at least 25%); formation of a single cement mass (uni-pedicular access seems to be an advantage); achievement of endplate-to-endplate contact; placement of the cement mass in the anterior region.

## References

- [1] WHO, 1994, "Assessment of fracture risk and its application to screening for postmenopausal osteoporosis. Report of a WHO study group. WHO Technical Report Series, World Health Organization, Geneva, Switzerland, 843: 1-130."
- [2] Sutcliffe, P., Connock, M., Shyangdan, D., Court, R., Kandala, N. B., and Clarke, A., 2013, "A systematic review of evidence on malignant spinal metastases: natural history and technologies for identifying patients at high risk of vertebral fracture and spinal cord compression," *Health technology assessment (Winchester, England)*, 17(42), pp. 1-274.
- [3] Grados, F., Depriester, C., Cayrolle, G., Hardy, N., Deramond, H., and Fardellone, P., 2000, "Long-term observations of vertebral osteoporotic fractures treated by percutaneous vertebroplasty," *Rheumatology (Oxford, England)*, 39(12), pp. 1410-1414.
- [4] Han, I. H., Chin, D. K., Kuh, S. U., Kim, K. S., Jin, B. H., Yoon, Y. S., and Cho, Y. E., 2009, "Magnetic resonance imaging findings of subsequent fractures after vertebroplasty," *Neurosurgery*, 64(4), pp. 740-744; discussion 744-745.
- [5] Uppin, A. A., Hirsch, J. A., Centenera, L. V., Pfiefer, B. A., Pazianos, A. G., and Choi, I. S., 2003, "Occurrence of new vertebral body fracture after percutaneous vertebroplasty in patients with osteoporosis," *Radiology*, 226(1), pp. 119-124.
- [6] Chiang, C. K., Wang, Y. H., Yang, C. Y., Yang, B. D., and Wang, J. L., 2009, "Prophylactic vertebroplasty may reduce the risk of adjacent intact vertebra from fatigue injury: an ex vivo biomechanical study," *Spine (Phila Pa 1976)*, 34(4), pp. 356-364.
- [7] Kayanja, M. M., Togawa, D., and Lieberman, I. H., 2005, "Biomechanical changes after the augmentation of experimental osteoporotic vertebral compression fractures in the cadaveric thoracic spine," *The Spine Journal*, 5(1), pp. 55-63.
- [8] Langdon, J., Way, A., Heaton, S., Bernard, J., and Molloy, S., 2009, "The management of spinal metastases from renal cell carcinoma," *Annals of the Royal College of Surgeons of England*, 91(8), pp. 649-652.

- [9] Sun, K., and Liebschner, M. A., 2004, "Biomechanics of prophylactic vertebral reinforcement," *Spine (Phila Pa 1976)*, 29(13), pp. 1428-1435; discussion 1435.
- [10] Tancioni, F., Lorenzetti, M. A., Navarra, P., Pessina, F., Draghi, R., Pedrazzoli, P., Scorsetti, M., Alloisio, M., Santoro, A., and Rodriguez y Baena, R., 2011, "Percutaneous vertebral augmentation in metastatic disease: state of the art," *J Support Oncol*, 9(1), pp. 4-10.
- [11] Oakland, R. J., Furtado, N. R., Wilcox, R. K., Timothy, J., and Hall, R. M., 2008, "The biomechanical effectiveness of prophylactic vertebroplasty: a dynamic cadaveric study," *J Neurosurg Spine*, 8(5), pp. 442-449.
- [12] Furtado, N., Oakland, R. J., Wilcox, R. K., and Hall, R. M., 2007, "A Biomechanical Investigation of Vertebroplasty in Osteoporotic Compression Fractures and in Prophylactic Vertebral Reinforcement," *Spine*, 32(17), pp. E480-E487  
410.1097/BRS.1090b1013e31811ea31812ee.
- [13] Brandolini, N., Cristofolini, L., and Viceconti, M., 2014, "Experimental methods for the biomechanical investigation of the human spine: a review " *Journal of Mechanics in Medicine and Biology*, 14(1), p. 1430002 (1430033 pages).
- [14] Belkoff, S. M., Mathis, J. M., Fenton, D. C., Scribner, R. M., Reiley, M. E., and Talmadge, K., 2001, "An ex vivo biomechanical evaluation of an inflatable bone tamp used in the treatment of compression fracture," *Spine (Phila Pa 1976)*, 26(2), pp. 151-156.
- [15] Higgins, K. B., Harten, R. D., Langrana, N. A., and Reiter, M. F., 2003, "Biomechanical effects of unipedicular vertebroplasty on intact vertebrae," *Spine (Phila Pa 1976)*, 28(14), pp. 1540-1547; discussion 1548.
- [16] Ikeuchi, M., Yamamoto, H., Shibata, T., and Otani, M., 2001, "Mechanical augmentation of the vertebral body by calcium phosphate cement injection," *Journal of orthopaedic science : official journal of the Japanese Orthopaedic Association*, 6(1), pp. 39-45.
- [17] Luo, J., Daines, L., Charalambous, A., Adams, M. A., Annesley-Williams, D. J., and Dolan, P., 2009, "Vertebroplasty: only small cement volumes are required to normalize stress distributions on the vertebral bodies," *Spine (Phila Pa 1976)*, 34(26), pp. 2865-2873.
- [18] Ananthakrishnan, D., Berven, S., Deviren, V., Cheng, K., Lotz, J. C., Xu, Z., and Puttlitz, C. M., 2005, "The effect on anterior column loading due to different vertebral augmentation techniques," *Clin Biomech (Bristol, Avon)*, 20(1), pp. 25-31.
- [19] Berlemann, U., Ferguson, S. J., Nolte, L. P., and Heini, P. F., 2002, "Adjacent vertebral failure after vertebroplasty. A biomechanical investigation," *J Bone Joint Surg Br*, 84(5), pp. 748-752.
- [20] Dean, J. R., Ison, K. T., and Gishen, P., 2000, "The strengthening effect of percutaneous vertebroplasty," *Clinical radiology*, 55(6), pp. 471-476.
- [21] Lim, T. H., Brebach, G. T., Renner, S. M., Kim, W. J., Kim, J. G., Lee, R. E., Andersson, G. B., and An, H. S., 2002, "Biomechanical evaluation of an injectable calcium phosphate cement for vertebroplasty," *Spine (Phila Pa 1976)*, 27(12), pp. 1297-1302.
- [22] Bai, B., Jazrawi, L., Kummer, F., and Spivak, J., 1999, "The use of an injectable, biodegradable calcium phosphate bone substitute for the prophylactic augmentation of osteoporotic vertebrae and the management of vertebral compression fracture," *Spine*, 24(15), pp. 1521-1526.

- [23] Heini, P. F., Berlemann, U., Kaufmann, M., Lippuner, K., Fankhauser, C., and van Landuyt, P., 2001, "Augmentation of mechanical properties in osteoporotic vertebral bones--a biomechanical investigation of vertebroplasty efficacy with different bone cements," *Eur Spine J*, 10(2), pp. 164-171.
- [24] Steens, J., Verdonshot, N., Aalsma, A. M., and Hosman, A. J., 2007, "The influence of endplate-to-endplate cement augmentation on vertebral strength and stiffness in vertebroplasty," *Spine (Phila Pa 1976)*, 32(15), pp. E419-422.
- [25] Chevalier, Y., Pahr, D., Charlebois, M., Heini, P., Schneider, E., and Zysset, P., 2008, "Cement distribution, volume, and compliance in vertebroplasty: some answers from an anatomy-based nonlinear finite element study," *Spine (Phila Pa 1976)*, 33(16), pp. 1722-1730.
- [26] Liebschner, M. A., Rosenberg, W. S., and Keaveny, T. M., 2001, "Effects of bone cement volume and distribution on vertebral stiffness after vertebroplasty," *Spine (Phila Pa 1976)*, 26(14), pp. 1547-1554.
- [27] Tschirhart, C. E., Finkelstein, J. A., and Whyne, C. M., 2006, "Optimization of tumor volume reduction and cement augmentation in percutaneous vertebroplasty for prophylactic treatment of spinal metastases," *Journal of spinal disorders & techniques*, 19(8), pp. 584-590.
- [28] Laredo, J. D., and Hamze, B., 2005, "Complications of percutaneous vertebroplasty and their prevention," *Seminars in ultrasound, CT, and MR*, 26(2), pp. 65-80.
- [29] Legroux-Gerot, I., Lormeau, C., Boutry, N., Cotten, A., Duquesnoy, B., and Cortet, B., 2004, "Long-term follow-up of vertebral osteoporotic fractures treated by percutaneous vertebroplasty," *Clinical rheumatology*, 23(4), pp. 310-317.
- [30] Ryu, K. S., and Park, C. K., 2009, "The prognostic factors influencing on the therapeutic effect of percutaneous vertebroplasty in treating osteoporotic vertebral compression fractures," *Journal of Korean Neurosurgical Society*, 45(1), pp. 16-23.
- [31] Baroud, G., and Bohner, M., 2006, "Biomechanical impact of vertebroplasty. Postoperative biomechanics of vertebroplasty," *Joint Bone Spine*, 73(2), pp. 144-150.
- [32] Molloy, S., Mathis, J. M., and Belkoff, S. M., 2003, "The effect of vertebral body percentage fill on mechanical behavior during percutaneous vertebroplasty," *Spine (Phila Pa 1976)*, 28(14), pp. 1549-1554.
- [33] Lieberman, I. H., Togawa, D., and Kayanja, M. M., 2005, "Vertebroplasty and kyphoplasty: filler materials," *Spine J*, 5(6 Suppl), pp. 305s-316s.
- [34] Polikeit, A., Nolte, L. P., and Ferguson, S. J., 2003, "The effect of cement augmentation on the load transfer in an osteoporotic functional spinal unit: finite-element analysis," *Spine (Phila Pa 1976)*, 28(10), pp. 991-996.
- [35] Danesi, V., Zani, L., Scheele, A., Berra, F., and Cristofolini, L., 2014, "Reproducible reference frame for in vitro testing of the human vertebrae," *Journal of biomechanics*, 47(1), pp. 313-318.
- [36] Loeffel, M., Heini, P. F., Bouduban, N., Burger, J., Nolte, L. P., and Kowal, J., 2007, "Development of a computer-assisted high-pressure Injection device for vertebroplasty," *IEEE Trans Biomed Eng*, 54(11), pp. 2051-2056.

- [37] Loeffel, M., Ferguson, S. J., Nolte, L. P., and Kowal, J. H., 2008, "Vertebroplasty: experimental characterization of polymethylmethacrylate bone cement spreading as a function of viscosity, bone porosity, and flow rate," *Spine*, 33(12), pp. 1352-1359.
- [38] Widmer Soyka, R. P., Lopez, A., Persson, C., Cristofolini, L., and Ferguson, S. J., 2013, "Numerical description and experimental validation of a rheology model for non-Newtonian fluid flow in cancellous bone," *Journal of the mechanical behavior of biomedical materials*, 27, pp. 43-53.
- [39] Hongo, M., Abe, E., Shimada, Y., Murai, H., Ishikawa, N., and Sato, K., 1999, "Surface Strain Distribution on Thoracic and Lumbar Vertebrae Under Axial Compression: The Role in Burst Fractures," *Spine*, 24(12), p. 1197.
- [40] Cristofolini, L., Brandolini, N., Danesi, V., Juszczuk, M. M., Erani, P., and Viceconti, M., 2013, "Strain distribution in the lumbar vertebrae under different loading configurations," *The Spine Journal*, 13(10), pp. 1281-1292.
- [41] Liebschner, M. A., Kopperdahl, D. L., Rosenberg, W. S., and Keaveny, T. M., 2003, "Finite element modeling of the human thoracolumbar spine," *Spine (Phila Pa 1976)*, 28(6), pp. 559-565.
- [42] Kopperdahl, D. L., Pearlman, J. L., and Keaveny, T. M., 2000, "Biomechanical consequences of an isolated overload on the human vertebral body," *Journal of Orthopaedic Research*, 18(5), pp. 685-690.
- [43] Cristofolini, L., Conti, G., Juszczuk, M., Cremonini, S., Van Sint Jan, S., and Viceconti, M., 2010, "Structural behaviour and strain distribution of the long bones of the human lower limbs," *J Biomech*, 43(5), pp. 826-835.
- [44] Rohlmann, A., Graichen, F., Kayser, R., Bender, A., and Bergmann, G., 2008, "Loads on a Telemeterized Vertebral Body Replacement Measured in Two Patients," *Spine*, 33(11), pp. 1170-1179.
- [45] Bergmann, G., 2011, " (ed.), Charite – Universitaetsmedizin Berlin "OrthoLoad". Retrieved July 1, 2011. <<http://www.OrthoLoad.com>>."
- [46] Lanyon, I. E., 1980, "Bone remodelling, mechanical stress, and osteoporosis," *Osteoporosis*, H. F. De Luca, ed., University Park Press, Baltimore, pp. 129-138.
- [47] Bayraktar, H. H., Morgan, E. F., Niebur, G. L., Morris, G. E., Wong, E. K., and Keaveny, T. M., 2004, "Comparison of the elastic and yield properties of human femoral trabecular and cortical bone tissue," *J Biomech*, 37(1), pp. 27-35.
- [48] Nazarian, A., and Muller, R., 2004, "Time-lapsed microstructural imaging of bone failure behavior," *J Biomech*, 37(1), pp. 55-65.
- [49] Anonymous, 2015, "Yield (Engineering)," Wikipedia, [https://en.wikipedia.org/wiki/Yield\\_%28engineering%29](https://en.wikipedia.org/wiki/Yield_%28engineering%29), accessed 31 August 2015.
- [50] Hardisty, M. R., Zael, R., Stover, S. M., and Fyhrie, D. P., 2013, "The importance of intrinsic damage properties to bone fragility: a finite element study," *J Biomech Eng*, 135(1), p. 011004.
- [51] Ross, S. M., 2003, "Peirce's criterion for the elimination of suspect experimental data," *J. Engineering Technology*, 2003(Fall), pp. 1-12.

- [52] Hulme, P. A., Boyd, S. K., Heini, P. F., and Ferguson, S. J., 2009, "Differences in endplate deformation of the adjacent and augmented vertebra following cement augmentation," *Eur Spine J*, 18(5), pp. 614-623.
- [53] Farooq, N., Park, J. C., Pollintine, P., Annesley-Williams, D. J., and Dolan, P., 2005, "Can vertebroplasty restore normal load-bearing to fractured vertebrae?," *Spine (Phila Pa 1976)*, 30(15), pp. 1723-1730.
- [54] Kim, S. H., Kang, H. S., Choi, J. A., and Ahn, J. M., 2004, "Risk factors of new compression fractures in adjacent vertebrae after percutaneous vertebroplasty," *Acta radiologica (Stockholm, Sweden : 1987)*, 45(4), pp. 440-445.
- [55] Trout, A. T., Kallmes, D. F., and Kaufmann, T. J., 2006, "New fractures after vertebroplasty: adjacent fractures occur significantly sooner," *AJNR Am J Neuroradiol*, 27(1), pp. 217-223.
- [56] Tohmeh, A. G., Mathis, J. M., Fenton, D. C., Levine, A. M., and Belkoff, S. M., 1999, "Biomechanical efficacy of unipedicular versus bipedicular vertebroplasty for the management of osteoporotic compression fractures," *Spine (Phila Pa 1976)*, 24(17), pp. 1772-1776.
- [57] Lee, S., Jun, B., and Tack, G., 2002, "Prediction and assessment of optimal volume for PMMA injection in percutaneous vertebroplasty using image and biomechanical analyses. ," *Proceedings of the 48th Annual Meeting of the Orthopaedic Research Society, Dallas*, p. 786.
- [58] Hulme, P. A., Boyd, S. K., and Ferguson, S. J., 2007, "Regional variation in vertebral bone morphology and its contribution to vertebral fracture strength," *Bone*, 41(6), pp. 946-957.
- [59] Pollintine, P., Przybyla, A. S., Dolan, P., and Adams, M. A., 2004, "Neural arch load-bearing in old and degenerated spines," *Journal of Biomechanics*, 37(2), pp. 197-204.
- [60] Palanca, M., Tozzi, G., Cristofolini, L., Viceconti, M., and Dall'Ara, E., 2015, "Three-dimensional local measurements of bone strain and displacement: comparison of three digital volume correlation approaches," *J Biomech Eng*, 137(7).
- [61] Roberts, B. C., Perilli, E., and Reynolds, K. J., 2014, "Application of the digital volume correlation technique for the measurement of displacement and strain fields in bone: a literature review," *J Biomech*, 47(5), pp. 923-934.
- [62] Tozzi, G., Zhang, Q. H., and Tong, J., 2014, "Microdamage assessment of bone-cement interfaces under monotonic and cyclic compression," *J Biomech*, 47(14), pp. 3466 - 3474.

# **Appendix C: Strain uncertainties from two Digital Volume Correlation approach in natural and augmented vertebrae**

Marco Palanca, MSc<sup>1</sup>, Gianluca Tozzi, PhD<sup>2</sup>, Enrico Dall'Ara, PhD<sup>3</sup>, Marco Curto, MSc<sup>2</sup>, Federica Innocente, BEng<sup>1</sup>, Valentina Danesi, MSc<sup>1</sup>, Luca Cristofolini, PhD<sup>1</sup>

<sup>1</sup> Department of Industrial Engineering, University of Bologna, Italy

<sup>2</sup> School of Engineering, University of Portsmouth, UK

<sup>3</sup> Department of Oncology and Metabolism and INSIGNEO Institute for In Silico Medicine, University of Sheffield, UK

*The candidate contributed to this study taking care of micro-CT acquisition. This work has been submitted to Journal of the Mechanical Behavior of Biomedical Materials (JMBBM)*

## Abstract

Digital Volume Correlation (DVC) is becoming popular for measuring the strain distribution inside bone structures. There are a number of methodological questions still not satisfactorily addressed: as the reliability of DVC to investigate augmented bone tissue, the magnitude of errors on different specimens, the distribution of measurement errors inside a bone, the presence of preferential directions. To address these issues, five augmented and five natural porcine vertebrae were subjected to repeated micro-CT scan (~39 micrometers voxel size) in a zero-strain condition. The acquired images were processed with a local (DaVis-DC) and a global (ShIRT-FE) DVC approaches. Different computation sub-volumes were considered ranging from 16 voxel (624 micrometers) to 128 voxel (4992 micrometers). The deviation from the ideal zero-strain value was analyzed to quantify systematic and random error. The local approach produced very large errors in the entire image, mainly due to the saline solution surrounding the vertebrae, whereas the global approach was more robust in this case and insensitive to saline environment. When a volume-of-interest was cropped inside the vertebra errors were significantly lower. The systematic error was generally within the range -100 to 100 microstrain and did not depend on the computation sub-volume. The random error was higher than 1000 microstrain for the smallest sub-volume (16 voxels) and rapidly decreased: with a sub-volume of 64 or larger the random errors were within 200 microstrain for both approaches. The errors did not show any preferential direction inside the vertebra nor respect to the micro-CT acquisition geometry. While these trends were rather consistent within the sample, two individual specimens yielded unpredictably larger errors. For this reason, a zero-strain check on each specimen should always be performed before any in-situ micro-CT testing campaign is conducted. This study clearly shows that, when sufficient care is dedicated to preliminary methodological work, different DVC computation approaches allow measuring the strain with a reduced overall error (i.e. ~200 microstrain), which makes it a viable technique also to investigate strain in more physiological conditions.

**Keywords:** Digital Volume Correlation (DVC), micro-CT, measurement uncertainties, augmented and natural vertebrae.

## 1. Introduction

Digital Volume Correlation (DVC) is a novel measurement technique able to explore the full field three-dimensional (3D) displacement and strain distribution inside specimens from 3D images [1-3]. Potential applications include investigation of the strain distribution and the failure mechanism in bony structures, such as augmented vertebrae. Since the introduction of DVC, several studies were performed to evaluate its reliability (measurement error). As no other experimental method allows measuring internal displacements and strains, validation experiments must be designed where the field of displacement and/or strain are known a priori. Tests in a zero-strain condition have been performed, from the tissue-level (trabecular or cortical bone [1, 4-8]), to the organ-level (vertebral bodies [9, 10]). Depending on the nature of the tissue under investigation and voxel size of the input images, the accuracy of strain measurements can range between 300 microstrain and 794 microstrain, while the precision between 69 microstrain and 630 microstrain [2]. However, direct comparison between different studies is often difficult, as images with different voxel sizes are typically produced (i.e. ranging from 9.96 micrometers to 36 micrometers). In any case, all these studies showed how the performance of the methods depends on the features available in the specimen (i.e. hystomorphometric parameters in trabecular bone) and how DVC was suitable to examine the pre- and post-yield deformation in bone [4].

Although the above-mentioned studies allowed a deep knowledge about the reliability and main benefits/limitations of the DVC applied to bone, only one paper [4] performed an evaluation on more bone types (2 specimens for each type), considering the intrinsic variability in different biological tissues. Another open issue relates to the reliability of DVC in bone specimens and their inter-digitation with biomaterials, such as cement-bone composites. In fact, in the last decades, vertebroplasty has become increasingly popular to treat and/or prevent vertebral fractures [11]. Because of the potential clinical implications of investigations on augmented bone, the reliability of DVC on augmented bone must be investigated. To the authors' knowledge, a wide validation, comparing different DVC approaches (i.e. local and global), at the organ-level, on specimens including different materials such as an augmented vertebra is currently missing.

The aims of this work were to:

- Quantify the reliability (in terms of systematic and random error) of DVC when applied to natural and augmented bones;

- Assess the effect of the variability between different specimens;
- Investigate the spatial distribution of the errors, and the presence of any preferential direction;
- Compare the output of global and local DVC approaches;

To extend the robustness of our study, repeated scans of natural and augmented vertebrae were elaborated with two DVC approaches (a local and a global approach) to compute the apparent strains (the specimens were in a zero-strain condition) and quantify the systematic and random error.

## **2. Materials and Methods**

### **2.4 Specimens and Images**

Ten thoracic vertebrae specimens were collected from six fresh porcine spines, dispatched from alimentary purposes. Soft tissues, intervertebral disks and growth plates were removed, without damaging the vertebral body or alter the morphological features. A sample of five vertebrae was used for augmentation (hereafter referred to as “augmented”). Acrylic cement (Mendec Spine, Tecres, Italy), which contains BaSO<sub>4</sub> pellets with an average size of 300 micrometers, was injected in the vertebral body with a custom made device, until the cement started leaking from the bone (typically ~1 ml of cement). The vertebrae were heated, before and after the augmentation, in a circulating bath at 40°C, which represents the physiologic temperature in pigs [12], to facilitate injection, flow and consolidation of the cement. Another sample of five vertebrae was used as natural specimens, without augmentation (hereafter referred to as “natural”). Sampling was arranged so that the augmented and natural samples were well distributed within the thoracic spine segment (T1-T3). The posterior processes were removed for both samples and endplates of each vertebra were potted in poly-methyl-methacrylate (PMMA) support through a custom-made setup, to allow alignment [13] within the micro-CT.

In order to evaluate the reliability of DVC approaches, each specimen was scanned twice in a zero-strain condition, without any repositioning between the scans, such as in the Repeated-Scan-Test [7]. Micro-CT (XTH225, Nikon Metrology, UK) scans of the entire vertebrae were performed using the following settings: voltage: 88kV; current: 110-115 micro-A; voxel size: 39.0-39.9 micrometers; exposure: 2s; rotation step: 0.23 degree; total rotation 360 degree. The samples were placed in the environmental chamber of a loading device (CT5000, Deben Ltd, UK) and immersed in saline-solution throughout the duration of the test, in order to closely simulate in situ loading conditions that are typically being applied to such vertebral bodies.

Volumes of interest (VOIs) were obtained (MeVisLab, Me Vis Medical Solution AG, <http://www.mevislab.de/>) to reduce the dimension of the images, cropping only the whole vertebral body (VOI-0) or cropping only the largest possible region inscribed to the vertebral body (VOI-1) and consistently with all the samples dimensions (Fig. 1). VOI-0 was a parallelepiped inscribing the contour in the transversal plane of the vertebra, including 432 slices and with slice dimensions ranging from 548 pixels to 812 pixels, in x-axis and from 525 pixels to 825 pixels, in y-axis. This was prepared to study the strain error inside the vertebra and in surrounding or border areas. VOI-1 was a parallelepiped inscribed inside the transversal plane of the vertebra with 300x300x432 voxel and was prepared to study the error only inside the vertebra.

In order to allow comparison between the results obtained from different DVC approaches, the image datasets used in the present study will be made available to the interested researchers by contacting us.

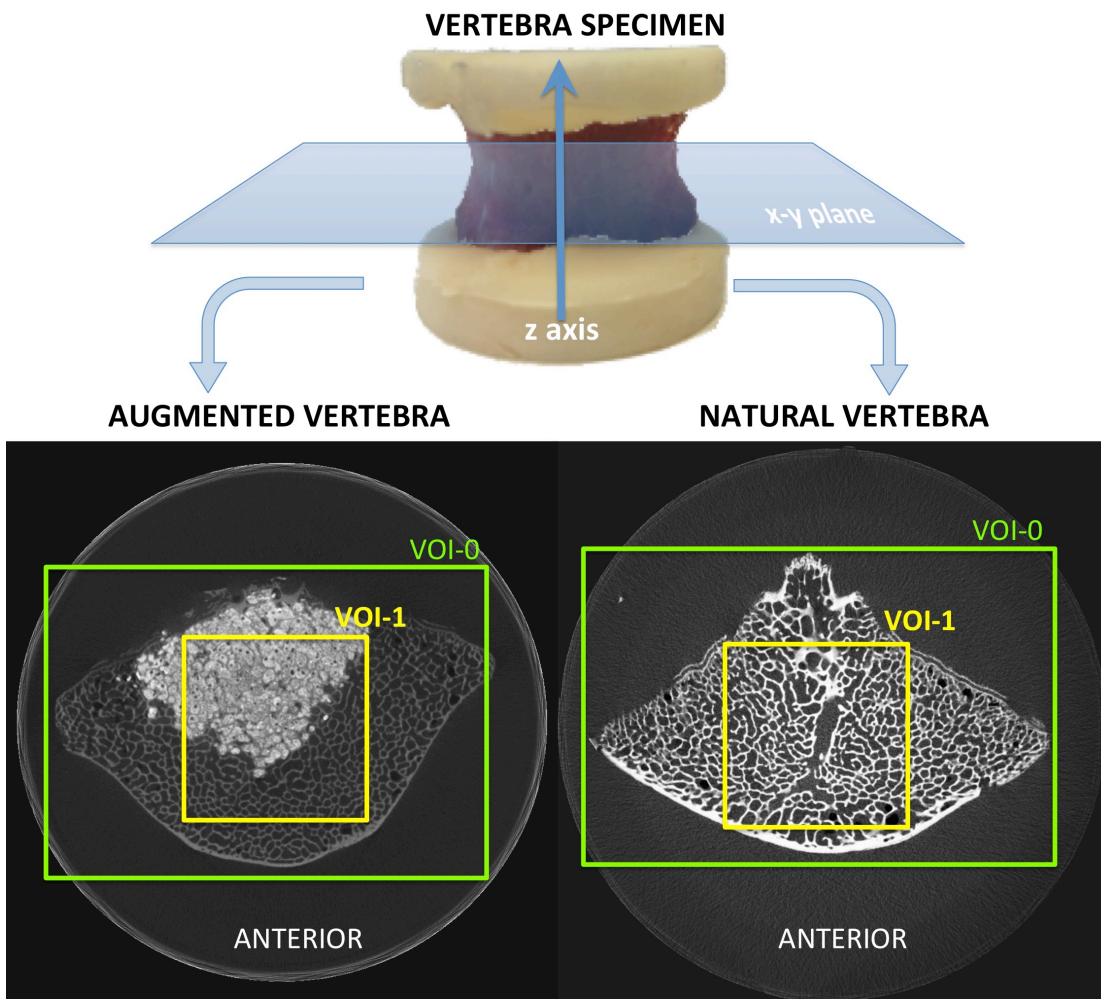


*Fig. 1 – The vertebra was aligned and potted in a PMMA support and then scanned with a micro-CT. In order to show the differences between VOIs, only the slice in the mid-height of each vertebra sample was reported. The larger box represents VOI-0: the entire vertebra with the surrounding saline solution. The smaller box represents VOI-1: the inside of the vertebra.*

## 2.5 Local approach vs. global approach

Two DVC software packages, using either a local or a global approach, were compared in this work, similarly to [7]. The local approach is implemented in a commercial package (DaVis 8.2.1, LaVision, Germany) later referred to as “DaVis-DC”. The global approach is a combination of an home-written elastic registration software ShIRT (Sheffield Image Registration Toolkit)[14] [15, 16] and a Finite Element (FE) software package (Ansys Mechanical Apdl v.14.0, ANSYS, Inc., Canonsburg, PA), later referred to as “ShIRT-FE”. The operating principles of the two DVC

approaches were described in detail in [7]. Briefly, DaVis-DC starts in dividing the 3D images into smaller sub-volumes, which have the ability to be independently correlated as a discrete function of grey-levels. The matching between the sub-volumes is done via direct correlation (DC), which was found to provide better results compared to other correlation functions such as FFT [7] for bone. A piece-wise linear shape function and a cross-correlation function are employed to quantify the similarity between the reference and deformed image. The displacement field was evaluated at the centre of each sub-volume. Finally, the strain field is computed using the centred finite differences (CFD) scheme. ShIRT-FE focuses on the recognition of identical features in the whole 3D images by superimposing a grid with selectable nodal spacing (sub-volume) to the images. The approach solves the elastic equations at the nodes of the grid to evaluate the displacement field. The grid is then converted into an eight-noded hexahedrons mesh and the displacements computed by ShIRT at each node are imposed as boundary conditions. The strain field was obtained differentiating the displacement field obtained with ShIRT by using the FE software package.

In order to compute the measurement errors related to a specific sub-volume for these specimens, a group of eight sub-volume sizes (from 16 to 128 voxels, in steps of 16 voxels) was investigated (Table 1). Moreover, to avoid misinterpretation of the results, the percentage of the correlated volume for each sub-volume size was computed as the ratio between the number of the correlated voxels and the total number of voxels (Table 1).

*Table 1: Comparison of the correlated volume for the different approaches evaluated for both vertebrae sample (augmented and natural) and both VOI for each sub-volume size. The values reported for the sample were obtained as the median on the five augmented vertebrae and the five natural vertebrae.*

VOI	SAMPLE	SUB-VOLUME SIZE	DaVis-DC	ShIRT-FE
VOI-0	Augmented	16	100%	100%
		32	100%	
		48	100%	
		64	98%	
		80	99%	
		96	100%	
		112	97%	
		128	100%	
	Natural	16	100%	
		32	100%	
		48	100%	
		64	99%	
		80	98%	
		96	98%	
		112	94%	
		128	97%	
VOI-1	Augmented	16	100%	
		32	100%	
		48	100%	
		64	94%	
		80	94%	
		96	97%	
		112	79%	
		128	100%	
	Natural	16	99%	

		32	100%	
		48	100%	
		64	94%	
		80	94%	
		96	97%	
		112	80%	
		128	100%	

For the local approach it was essential, being the correlation of each sub-volume independent from each other. For the global approach, instead, on the entire volume was imposed a grid and the displacement and strain were computed only on the nodes of the grid; so no regions were excluded. Finally, a multipass scheme with final sub-volume size of 48 voxels (mp(48), Table 2), available only on DaVis-DC and described in (Palanca et al., 2015), was tested to explore the potentialities of the local approach.

*Table 2: Series of steps implemented in the multipass approach, mp(48), without any overlap. This feature is available only on DaVis-DC.*

<b>STEP</b>	<b>SUB-VOLUME SIZE</b>	<b>NUMBER OF ITERATIONS</b>
1	128	1
2	112	2
3	96	2
4	80	2
5	64	2
6	48	2

## 2.6 Quantification of the errors (error metrics)

Given the zero-strain condition, any strain value different from zero was considered to be an error. Strain values were extracted for each component of strain from both DVC approaches, and both VOIs. The following analyses were carried-out:

- Strain component comparison: for each specimen, the systematic and random errors were quantified as the average and standard deviation, separately, for each component of strain. This analysis was repeated for VOI-0 and VOI-1 for the different sub-volume sizes.
- Strain distribution: in order to identify the areas with larger errors, a qualitative analysis of the apparent strain distribution was performed on the slice at mid-height, for both DVC approaches, both in the natural and augmented samples, in the z-direction, for sub-volume size of 48 voxels.
- Variability: the variability of the systematic and random errors between specimens was investigated. The errors for each component of strain in VOI-1 were reported for each specimen (both augmented and natural) for a sub-volume size of 48 voxels. The bone volume fraction (BV/TV: bone volume, divided by the total volume) for the natural vertebrae or the solid volume fraction (SV/TV: the sum of the volume of the cement and of the bone, divided by the total volume) for the augmented vertebrae were computed in order to investigate if a link existed between the magnitude of the error and the intrinsic morphology of each specimen. Both BV/TV and SV/TV were calculated using a voxel-based method implemented in ImageJ (Rasband, W.S., ImageJ, U. S. National Institutes of Health, Bethesda, Maryland, USA, <http://imagej.nih.gov/ij/>, 1997-2015) (BoneJ plugin (Doubé et al., 2010)). The images were segmented by using a single level threshold, chosen in the valley between the first and second peak of the frequency distribution of the greyscale (histograms). The threshold value was adapted by visual comparison of the segmented and greyscale image in order to separate bone (or bone and cement) from the background values for natural (or augmented) vertebrae.

All the elaborations of the results were processed with a home-written script in MatLab 2014a (MathWorks, US). Data were screened for outliers applying the criterion of Peirce (Ross, 2003).

### 3. Results

#### 3.1 Errors over VOI-0

VOI-0 included the entire vertebra and some surrounding saline solution. Apart from the initial peak for the smallest sub-volume size, the systematic errors fluctuated around zero microstrain (Fig. 2).

A large difference existed between the two approaches, especially for small sub-volume size. Only with sub-volume size larger than 96 voxels the systematic errors were comparable (generally within 100 microstrain). Otherwise DaVis-DC had errors up to two orders of magnitude larger than the ones in ShIRT-FE.

The random errors showed a clear decreasing trend towards larger sub-volume sizes (Fig. 3). The differences between the approaches were as high as two orders of magnitude.

The multipass scheme (Table 2) on DaVis-DC was able to reduce both the systematic and random errors by up to a factor ten, with respect to the ones provided with equivalent sub-volume size (48 voxels). Nevertheless, the two DVC approaches were still incomparable: for multipass scheme DaVis-DC showed systematic errors in the order of hundreds microstrain, and random errors of thousands microstrain, while ShIRT-FE showed errors respectively below hundred microstrain and around thousand microstrain for sub-volume size of 48 voxels.

Generally speaking, no evident and consistent differences between the components of strain were found in terms of systematic or random error. Systematically, the errors on augmented vertebrae were larger, up to 50%, than the ones on natural vertebrae.

The distribution of apparent strain within VOI-0 (Fig. 4) showed that most of the errors for DaVis-DC were due to the regions outside the vertebral body (the saline solution offers less clearly recognisable features to the local correlation algorithm). Similarly, even though the maximal errors for ShIRT-FE were three orders of magnitude lower than the ones for DaVis-DC, the highest values were as well localized in the corner of the image, outside the bone.

## VOI-0

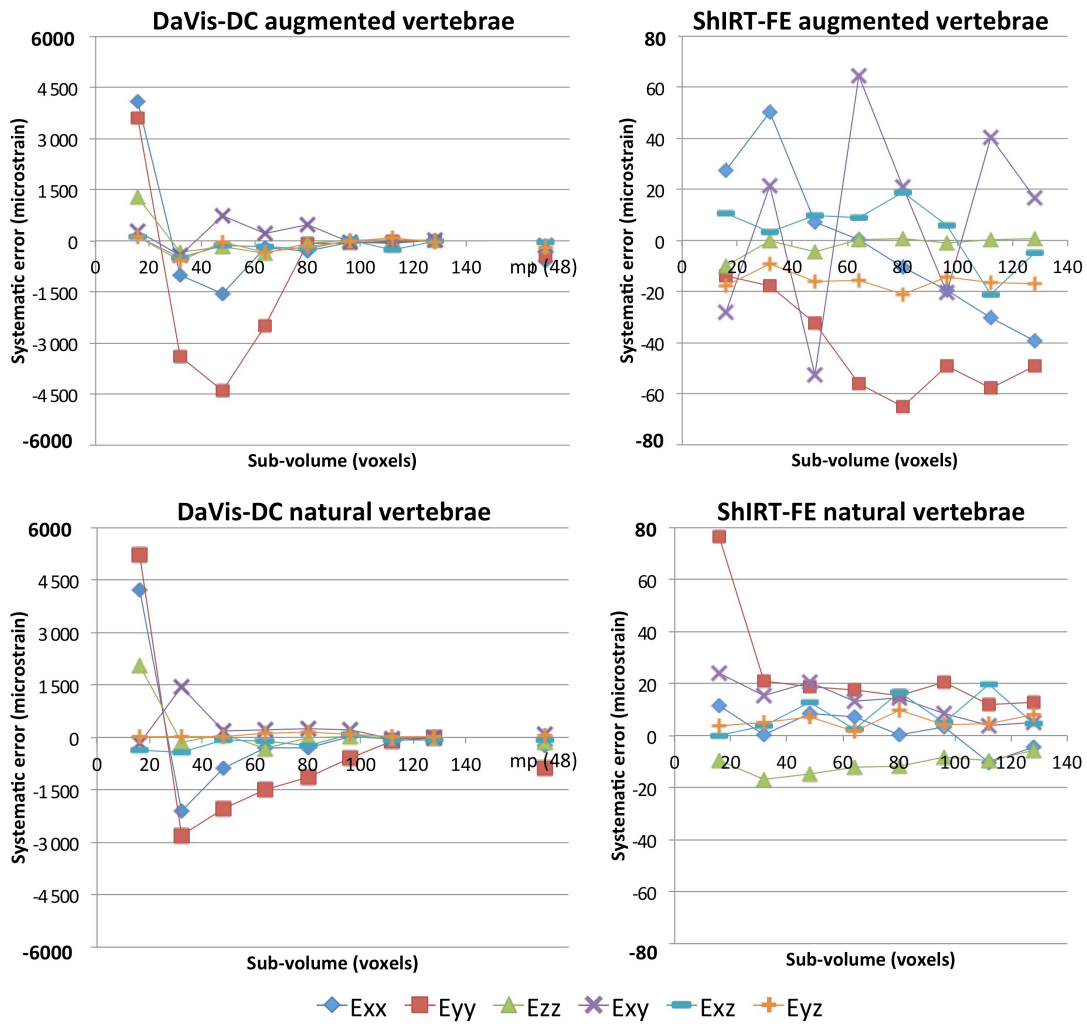
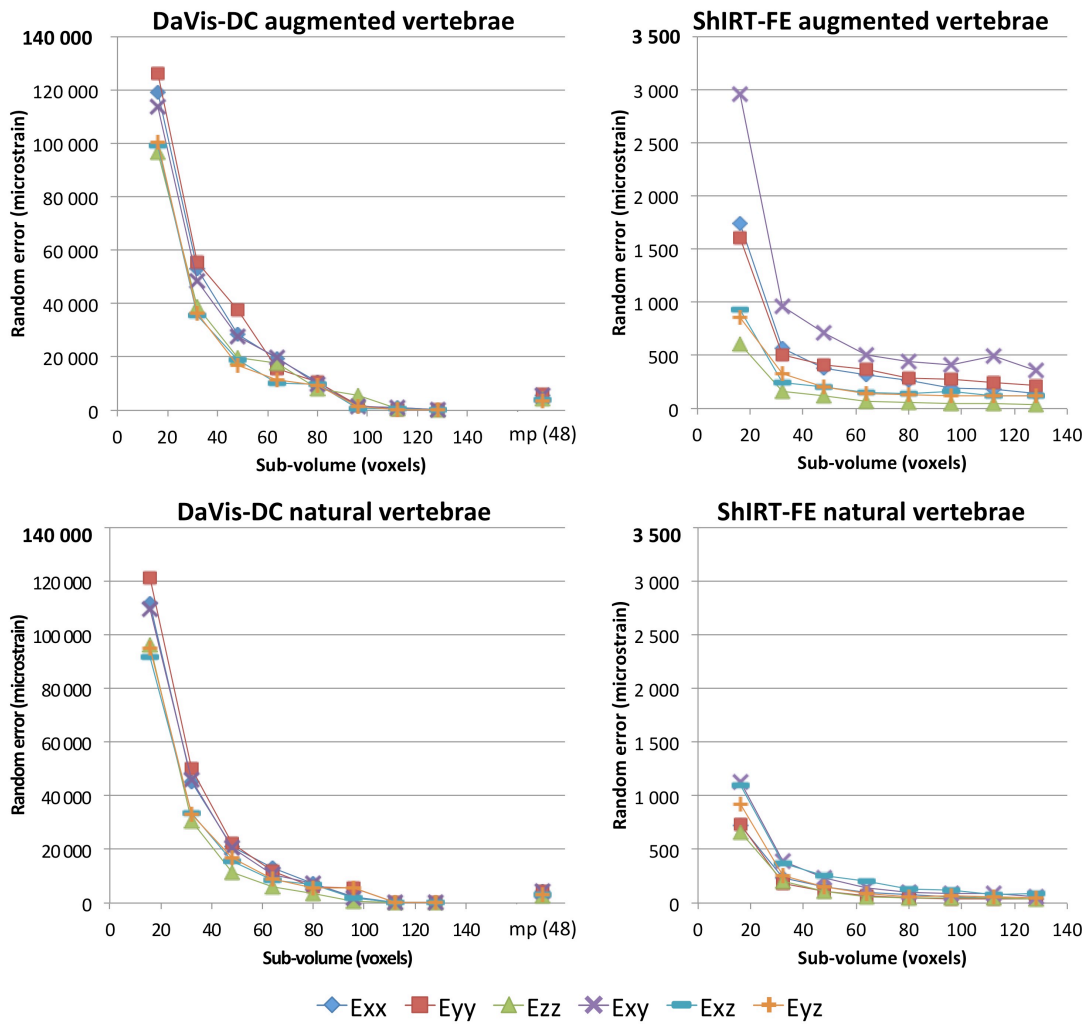


Fig. 2: Systematic errors for the local (DaVis-DC) and global (ShIRT-FE) DVC approaches, evaluated for VOI-0 in the augmented and natural vertebrae, for sub-volume sizes ranging from 16 to 128 voxels. A multipass computation for DaVis-DC (mp(48); 6 passes, from 128 to 48 voxels) is also reported. The median over the five augmented and five natural specimens is plotted.

## VOI-0



**Fig. 3:** Random errors for the local (DaVis-DC) and global (ShIRT-FE) DVC approaches, evaluated for VOI-0 in the augmented and natural vertebrae, for sub-volume sizes ranging from 16 to 128 voxels. A multipass computation for DaVis-DC (mp(48); 6 passes, from 128 to 48 voxels) is also reported. The median over the five augmented and five natural specimens is plotted.

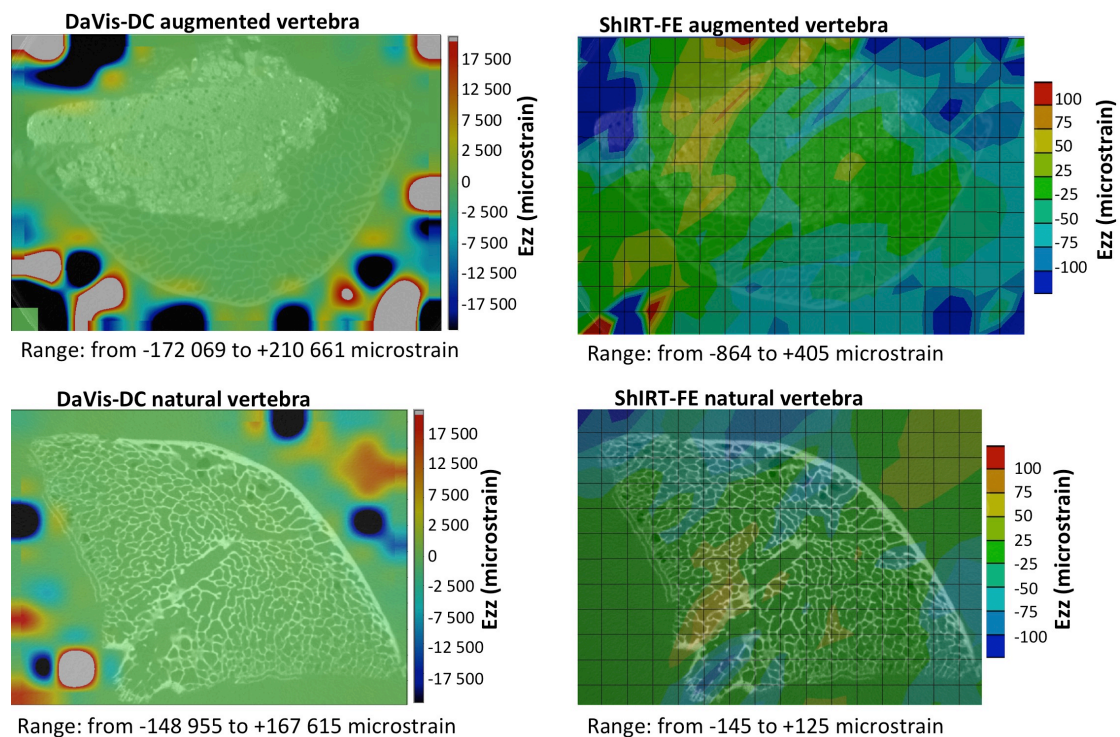
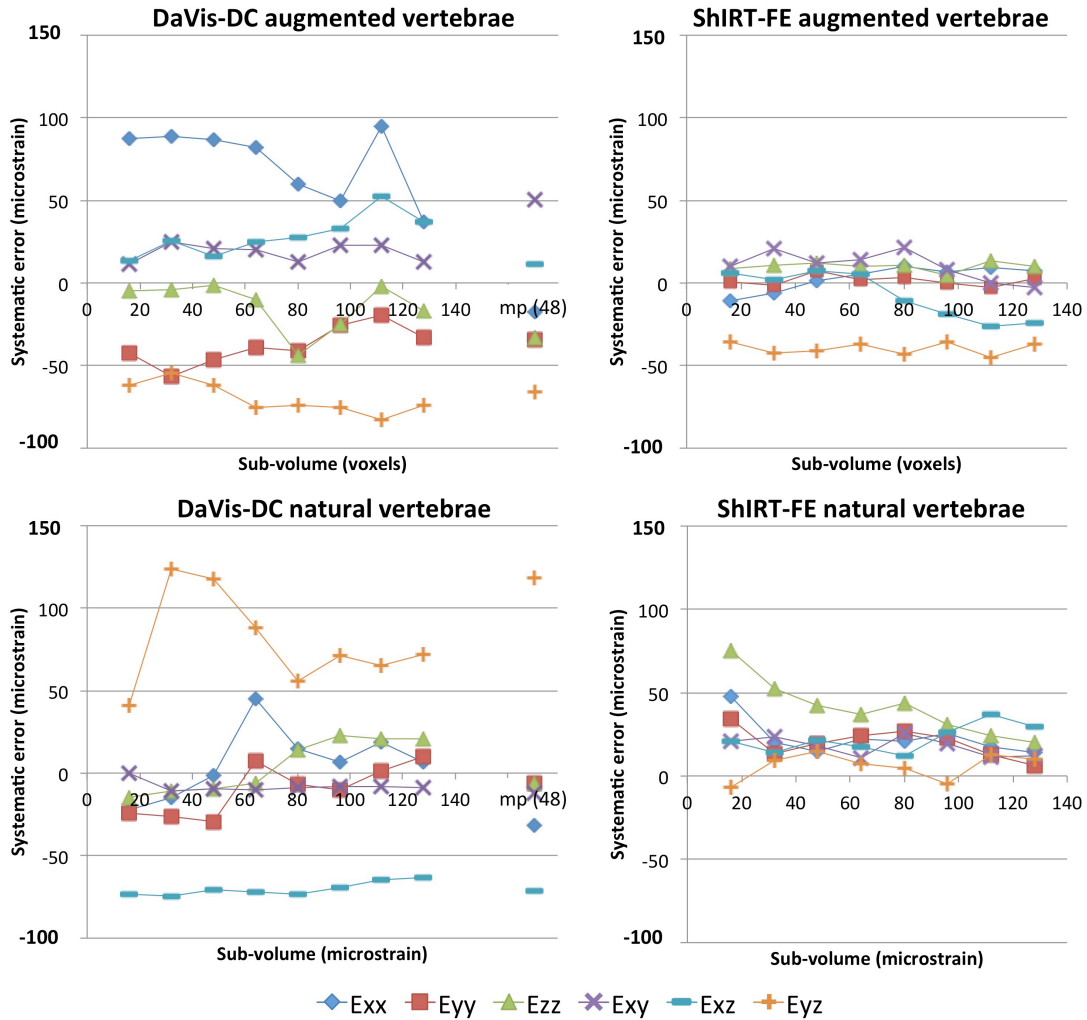


Fig. 4: Strain distribution in the z-direction with a sub-volume size of 48 voxels on a mid-height cross section of typical augmented and natural specimens, for, on the left the local approach (DaVis-DC) and, on the right, the global approach (ShIRT-FE). The scales on the right of each plot were selected to allow visualization of the strain distribution in the region of interest. The maximum ranges recorded are reported under each strain map.

### 3.2 Error over VOI-1

In order to evaluate the errors of the DVC for regions of effective interest (i.e. within the specimen), VOI-1 was analysed. In this case, the systematic and random errors were of the same order of magnitude and showed similar trends for both DVC approaches (Fig. 5 and 6).

## VOI-1



**Fig. 5:** Systematic errors for the local (DaVis-DC) and global (ShIRT-FE) DVC approaches, evaluated for VOI-1 in the augmented and natural vertebrae for sub-volume sizes ranging from 16 to 128 voxels. A multipass computation for DaVis-DC (mp(48)); 6 passes from 128 to 48 voxels) is also reported. The median over the five augmented and five natural specimens is plotted.

For DaVis-DC the systematic and random errors were drastically lower than for VOI-0. For ShIRT-FE the difference between the errors for VOI-0 and VOI-1 was minimal. Comparing the two approaches, DaVis-DC was affected by slightly larger (tens microstrains) systematic and random errors compared to ShIRT-FE.

The effect of sub-volume size on the systematic error was negligible (Fig. 5).

The random error had a decreasing trend towards larger sub-volume sizes, for both DVC approaches (Fig. 6). For the smallest sub-volume (16 voxels) the random errors for DaVis-DC were in the range 960 - 1517 microstrain for the augmented vertebrae, and 807 - 1279 microstrain for the natural vertebrae. The maximum random error for DaVis-DC on VOI-1 was two orders of magnitude lower than VOI-0. Random errors with DaVis-DC were generally lower than 200 microstrain with sub-volume size equal or larger than 48. The benefit of the multipass scheme for VOI-1 was less pronounced than for VOI-0, and similar results were obtained with and without multipass scheme.

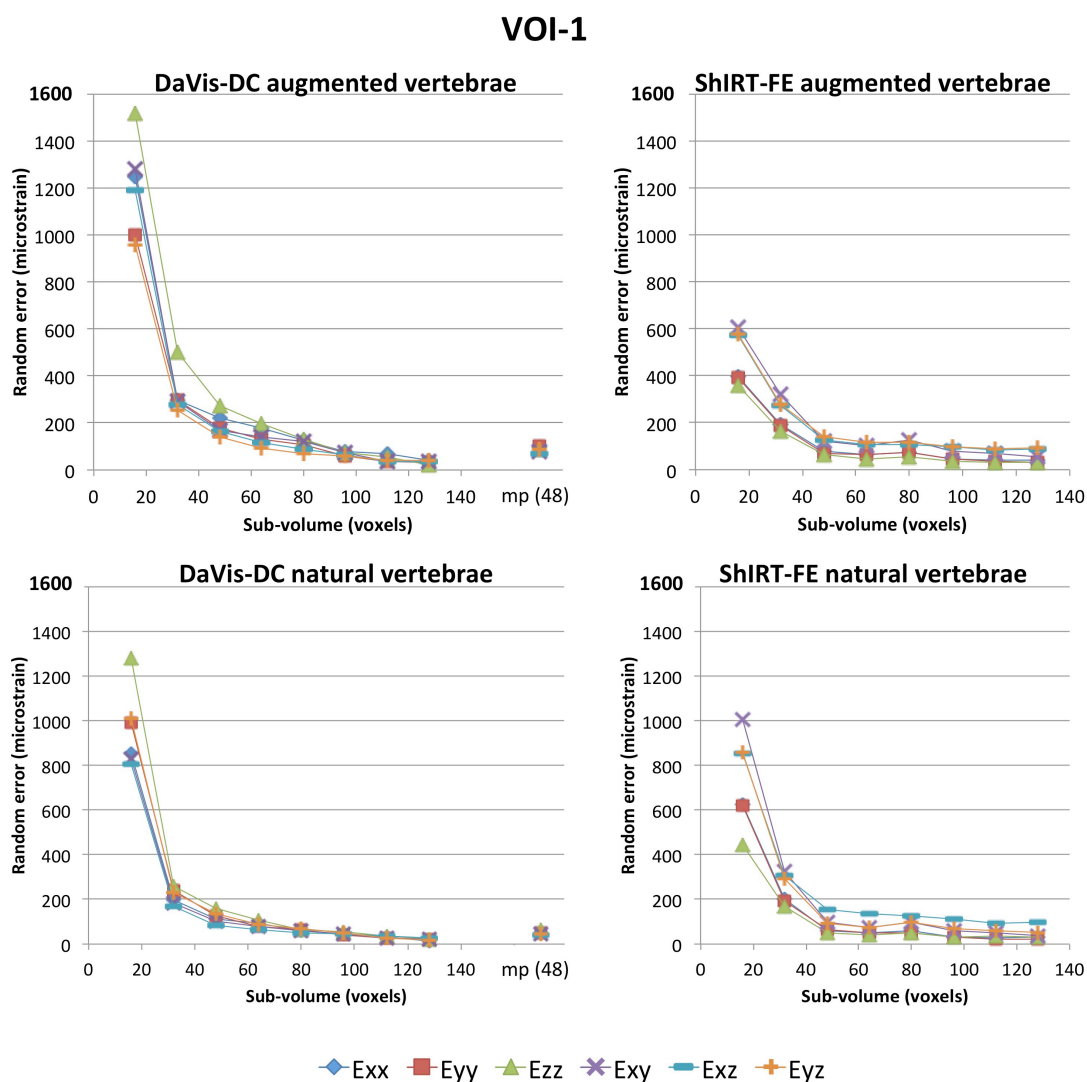


Fig. 6: Random errors for the local (DaVis-DC) and global (ShIRT-FE) DVC approaches, evaluated for VOI-1 in augmented and natural vertebrae for sub-volume sizes ranging from 16 to

*128 voxels. A multipass computation for DaVis-DC (mp(48); 6 passes from 128 to 48 voxels) is also reported. The median over the five augmented and five natural specimens is plotted.*

ShIRT-FE confirmed for VOI-1 the same trend and order of magnitude of the random errors found in VOI-0. The highest random errors (corresponding to the smallest sub-volume, 16 voxels) for ShIRT-FE were in the range 359 - 606 microstrain for the augmented vertebrae, and 445 - 1003 microstrain for the natural vertebrae. For larger sub-volumes random errors for ShIRT-FE were consistently smaller than 200 microstrain.

The two DVC approaches provided comparable random errors (both for the augmented and natural samples) for sub-volume size larger than 48 voxels, and were stably lower than 200 microstrain above 64 voxels.

A systematic difference was observed between the augmented and the natural vertebrae for DaVis-DC, with lower random errors for the natural vertebrae for all the sub-volume sizes. ShIRT-DC, instead, had comparable errors for the augmented and natural samples.

No significant differences were found between the components of strain for both ShIRT-FE and DaVis-DC.

Random and systematic errors showed large inter-specimen differences (Fig. 7). In particular, within the augmented sample, considerably higher errors were found for specimen-1, with both DVC approaches. Similarly, specimen-3 was associated with the largest error in the natural sample. However, the reason is not clear, as the error was not associated with the highest/lowest values of solid volume fraction, or bone volume fraction (Table 3). The Peirce's criterion identified these two specimens as outliers in terms of error values, but not in terms of volume fraction.

### VOI-1

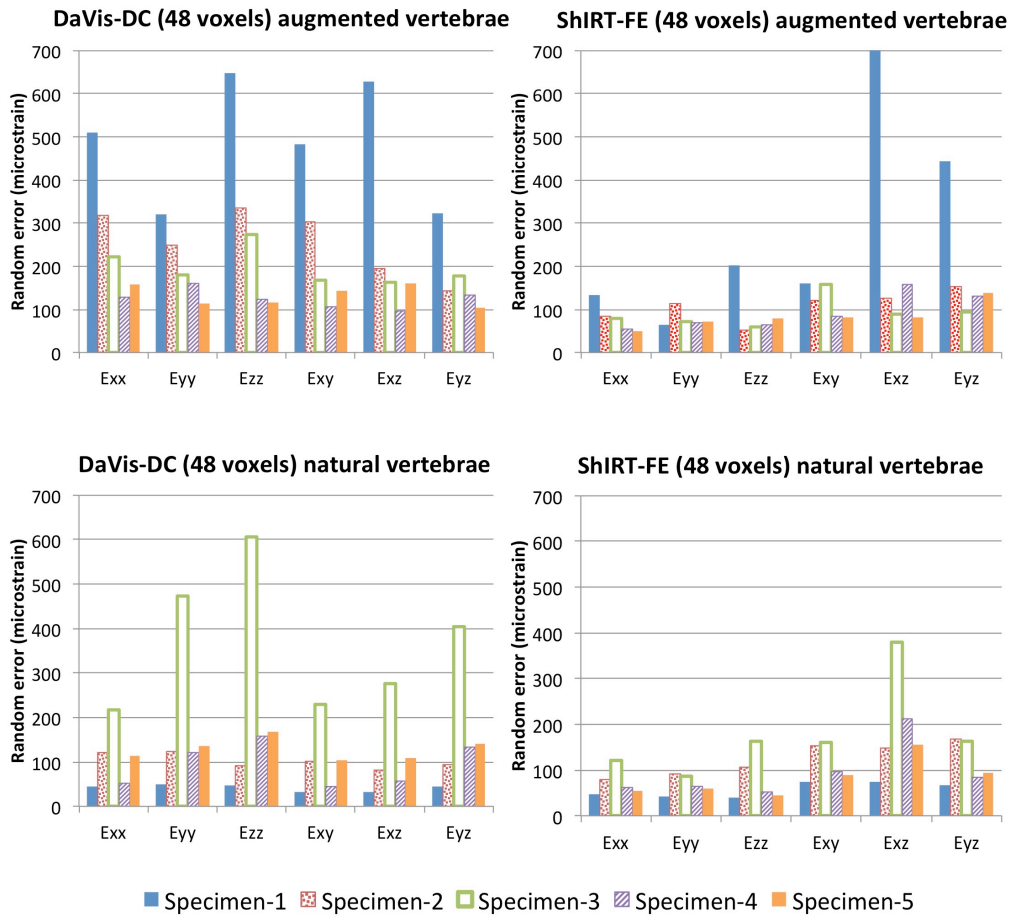


Fig. 7: Variability of the random error inside the augmented and natural vertebrae, for VOI-1, for a sub-volume size of 48 voxels. Similar trends were found for the systematic error.

Table 3: Solid Volume Fraction (SV/TV) evaluated as the ratio between the sum of the volume of the cement and the bone, and the total volume for augmented vertebrae and Bone Volume Fraction (BV/TV) evaluated as the ratio between the bone volume and the total volume for natural vertebrae.

Augmented	SV/TV (%)
1	44.4
2	72.2
3	50.1
4	63.6
5	57.1

<b>Natural</b>	<b>BV/TV (%)</b>
1	29.5
2	32.0
3	29.0
4	30.4
5	27.7

#### **4. Discussion**

The aims of this work were to quantify the measurement uncertainties of different DVC approaches applied to augmented bones at the organ-level. More specifically, we intended to investigate how such uncertainties vary between specimens and if there is any anisotropy-related directionality in the measurement error.

Two DVC approaches were investigated: a local correlation algorithm (DaVis-DC) and a global strategy (ShiRT-FE). As no robust alternative reference method is available for measuring internal strains, repeated scans (zero-strain condition) of natural and augmented vertebrae were shared between our institutions in a sort of round-Robin test.

Our results showed that applying a local approach directly on images with limited pre-processing (bone including the surrounding saline solution, VOI-0) yielded significantly larger systematic and random errors compared to the same images cropped to include only bone (VOI-1). This is possibly explained by the lack of features provided by the saline solution to the correlation algorithm. The analysis of the spatial distribution of the errors (Fig. 4) confirmed this hypothesis: the areas that acted as noise source were mainly the outer boundaries of the bone and the saline solution; the areas where errors were substantially lower were all inside the specimen (which are typically the areas of interest). Therefore, average measurements over a volume including regions with lack of features should be used with care if a local algorithm is applied. This effect could be an issue for low BV/TV samples such as osteoporotic human vertebrae where a few features are present. A marked improvement was obtained with a multipass approach applied to VOI-0, as it

allows a more robust tracking of areas poor of features as it initially relies on larger sub-volumes and only in the later iterations refines down to smaller sub-volumes. Conversely, the global approach was insensitive to the surrounding saline solution. This suggests that a global approach may be more accurate for strain measurements at the border of specimen. This is particularly important for the vertebrae where the cortical shell is thin.

For VOI-1 the errors had the same order of magnitude for the local and global approaches inside the specimens. For both approaches the bias (systematic error) fluctuated generally within 100 microstrain, meaning that the average of the strain components were close to zero, independently of the selected sub-volume size. Both approaches showed a decreasing trend of the random error with larger sub-volumes, and comparable results above the sub-volume size of 48 voxels (approximately 100-200 microstrain).

However, a larger sub-volume implies a reduction of the spatial resolution in the measurement [5]. The errors for the local approach consistently decreased for each subsequent sub-volume. The effect of the multipass scheme was limited, compared to VOI-0, because a single pass was sufficient to recognize and track the feature of interest.

While for the local approach the random error had continuously decreasing trend for the range of computation sub-volumes explored, the global approach reached a plateau after 48 voxels.

The comparison between augmented and natural vertebrae at the organ-level showed small differences in terms of systematic and random error, and of the respective trends. This confirms the strength of both DVC approaches on different biomaterial interdigitation, as it is confirmed in tissue-level study [17]. It must be noted that the present results were obtained with cement with pellets of BaSO<sub>4</sub> (300 micrometers), which could have provided suitable features to the correlation algorithms.

For both DVC approaches, the systematic and random errors were similar in all directions, independently of the preferential direction of trabecular bone, and of the rotation axis of the micro-CT (Fig. 2,3,5,6).

The findings reported above applied quite consistently on the sample of five augmented and five natural vertebrae. While the trend was extremely consistent, some differences existed between specimens in absolute terms. To the authors' best knowledge inter-specimen variations and

potential outliers have not been considered before at organ level. In a sample of five specimens it is questionable to perform an outlier analysis, such as the Peirce's criterion [18]. However, two specimens (Specimen-1 for augmented vertebrae and Specimen-3 for natural vertebrae, Fig. 7) showed clear outlier behaviour for both approaches. The small differences existing in terms of morphometric characteristics (similar dimensions, same species, same age, etc.), quality of the images (grayscale distribution), solid/bone volume fraction (for augmented vertebrae, specimen-1 had a SV/TV of 44.4%, while the average was 60.8%; for natural vertebrae, specimen-3 had a BV/TV of 29%, while the average was 29.9%), did not correlate with the different behaviour in terms of errors in DVC-computed strains. As no *a-priori* indicator suggested that some of the specimens could cause larger errors, it would not be fair to exclude *a-posteriori* such specimens from the analysis. In fact, if one were to perform a DVC-based strain measurement, would not be able to detect *a-priori* a potentially critical specimen. This can be a warning for future works, because a sequence of apparently high-quality images can unexpectedly result in this kind of problem. A question left open with this work is whether some robust parameters exist and whether these are able to avoid such errors and their consequences. Therefore, when the application requires a high precision of the DVC, the authors always recommend a zero-strain test, as described above, before loading the specimen. Unfortunately this kind of methodological analysis is frequently missing [9].

A similar zero-strain study on human, bovine and rabbit trabecular bone was performed by [4]. They analyzed 4.3 mm cubes with a voxel size of 36 micrometers. They explored a range of computation sub-volume of 20, 30, 40 and 50 with three DVC methods (based on home-written algorithm of digital particle image velocimetry and ultrasound elastography). In that paper the individual components of error were not reported. Conversely, a scalar indicator (which contains less information) was computed: accuracy and precision were quantified for the first time as average and standard deviation of the average of the absolute values of the six components of strain for each sub-volume. They reported [4] a similar trend with smaller errors for larger computation sub-volumes. For the human vertebrae and a 40 voxels sub-volume they found an accuracy in the order 500 microstrain, and a precision of 150-200 microstrain. They found slightly lower errors for the bovine distal femur. The smallest total error they found was 345 microstrain. To allow comparisons, we computed the same scalar indicators for the augmented and natural sample for VOI-1 (Fig. 8). Also with this representation of our results the errors of accuracy and precision decreased increasing the sub-volume size, with a simultaneous loss in terms of resolution, as it was

proved in previous works [4, 5, 7]. In order to compare the results, interpolated power laws were evaluated and used to compute the errors of accuracy and precision. DaVis-DC showed an accuracy of 275 microstrain for the augmented vertebrae and 215 microstrain for the natural vertebrae; while ShIRT-FE had an accuracy of 159 microstrain for the augmented vertebrae and 139 for the natural vertebrae. The errors of precision were 116 microstrain for the augmented vertebrae and 68 microstrain for the natural vertebrae, evaluated with DaVis-DC. Instead, error of 68 microstrain for the augmented vertebrae and 61 microstrain for the natural vertebrae, were obtained using ShIRT-FE.

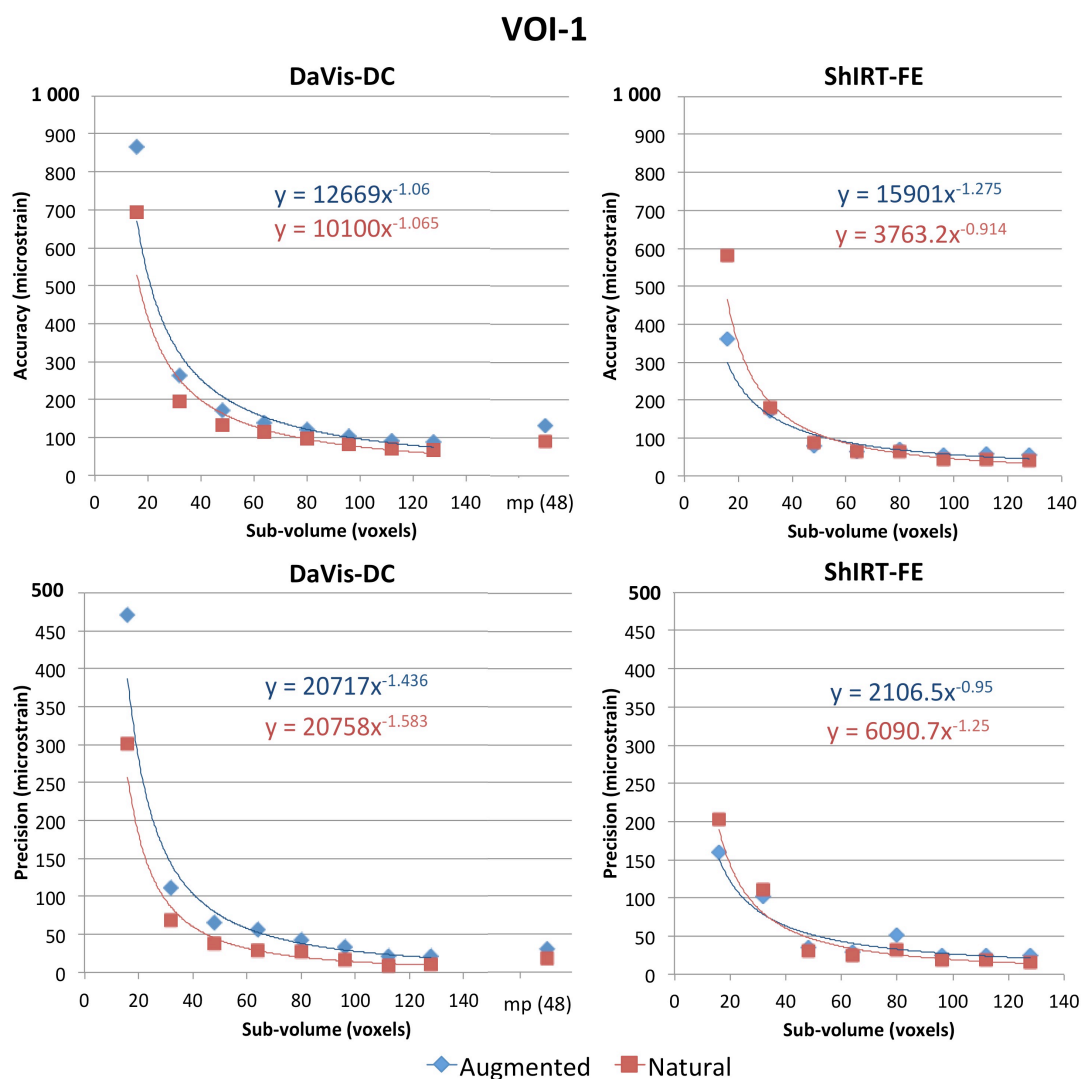


Fig. 8: Accuracy and precision (with interpolated power laws) for the local (DaVis-DC) and global (ShIRT-FE) DVC approaches, evaluated for VOI-1 in augmented and natural vertebrae for sub-volume sizes ranging from 16 to 128 voxels, in step of 16 voxels. A multipass computation for

*DaVis-DC (mp(48); 6 passes from 128 to 48 voxels) is also reported. The median between the five augmented and the five natural specimens is plotted.*

An evaluation of the mean and standard deviation error of strain in a zero-strain condition was provided for human natural vertebrae in [10]. The voxel size (37 micrometers) was similar to the present work. They analyzed a single sub-volume size of 4.8 mm, which corresponds to approximately 130 voxels. They reported larger errors than in the present study: accuracy of 740 microstrain, precision of 630 microstrain and the analysis was performed as a preliminary check before the actual compression test.

The current study has shown that, when sufficient care is dedicated to a preliminary methodological optimization, both DVC approaches allow measuring strain with an overall error of better than 200 microstrain. This may be sufficient to investigate the strain distribution for physiological (in terms of magnitude) loads (1000-2000 microstrain) [19, 20], and definitely adequate to investigate failure (7000-10000 microstrain) [21, 22]. Of course, an issue related to the time-consuming of the micro-CT scans is still open. Moreover, while DVC methods have been used to quantitatively validate the outputs of micro finite element models of trabecular bone samples [23, 24] or to qualitatively compare the outputs of computational and DVC measurements for whole vertebrae [10], and to the authors' knowledge there is no quantitative comparison performed at the organ level. The results of this study suggest that for whole vertebrae the DVC methods are accurate enough for proper validation of the strain predictions from computational models only when sub-volumes equal or larger than 48 voxels (equivalent to approximately 2mm in side length) are used. However, in order to validate the strain at spatial resolutions of 10-30 micrometers, typical of micro finite element models [25], the accuracy of the current DVC approaches should be improved.

A limitation of the present work is the use of porcine vertebrae instead of human ones. This was an ethical choice, in order to perform such an extensive methodological work. While the present results might not directly translate to human specimens in absolute terms, the trends and the general observation will certainly apply also to human trabecular bone.

Another study focused on smaller volumes of interest, to investigate if measurement error depends on the type of tissue (trabecular vs cortical) or material (bone vs cement) interdigitation [17].

## 5. Conclusion

This study demonstrated the suitability of local and global DVC approaches to investigate both natural and augmented bone, confirming that the most crucial issue is the presence of suitable features in the imaged specimen. Systematic and random errors were rather isotropic, with no relation to bone anisotropy or micro-CT scanning planes. While the errors were rather consistent between specimens, some specimens caused unpredictably and inexplicably larger errors: for this reason, it is highly recommended to perform a preliminary zero-strain check on each specimen being tested.

With the accuracy and precision measured in this study for a reasonable high sub-volume size (i.e. 100-200 microstrain for sub-volume equal to 48 voxels), the DVC becomes an attractive tool not only for the detection of local failure, but also for the measurement of local properties (displacements and strain) in the elastic range. This could be useful per se, to investigate bone micromechanics, but also to reliably validate predictions of computational models at the tissue level for spatial resolutions of approximately 2mm.

## References

- [1] Bay, B. K., Smith, T. S., Fyhrie, D. P., and Saad, M., 1999, "Digital Volume Correlation: Three-dimensional Strain Mapping Using X-ray Tomography," *Experimental Mechanics*, 39(3), pp. 217 - 226.
- [2] Roberts, B. C., Perilli, E., and Reynolds, K. J., 2014, "Application of the digital volume correlation technique for the measurement of displacement and strain fields in bone: A literature review," *Journal of biomechanics*, 47(5), pp. 923-934.
- [3] Grassi, L., and Isaksson, H., 2015, "Extracting accurate strain measurements in bone mechanics: A critical review of current methods," *J Mech Behav Biomed Mater*, 50, pp. 43-54.
- [4] Liu, L., and Morgan, E. F., 2007, "Accuracy and precision of digital volume correlation in quantifying displacements and strains in trabecular bone," *Journal of biomechanics*, 40(15), pp. 3516-3520.
- [5] Dall'Ara, E., Barber, D., and Viceconti, M., 2014, "About the inevitable compromise between spatial resolution and accuracy of strain measurement for bone tissue: A 3D zero-strain study," *Journal of biomechanics*, 47(12), pp. 2956 - 2963.
- [6] Gillard, F., Boardman, R., Mavrogordato, M., Hollis, D., Sinclair, I., Pierron, F., and Browne, M., 2014, "The application of digital volume correlation (DVC) to study the microstructural behaviour of trabecular bone during compression," *J Mech Behav Biomed Mater*, 29, pp. 480-499.
- [7] Palanca, M., Tozzi, G., Cristofolini, L., Viceconti, M., and Dall'Ara, E., 2015, "3D Local Measurements of Bone Strain and Displacement: Comparison of Three Digital Volume Correlation Approaches," *J. Biomech Eng. (ASME)*, 137(7), pp. 071006-071001/071006-071014.
- [8] Zhu, M. L., Zhang, Q. H., Lupton, C., and Tong, J., 2015, "Spatial resolution and measurement uncertainty of strains in bone and bone-cement interface using digital volume correlation," *J Mech Behav Biomed Mater*, 57, pp. 269-279.
- [9] Hardisty, M. R., and Whyne, C. M., 2009, "Whole bone strain quantification by image registration: a validation study," *Journal of biomechanical engineering*, 131(6), p. 064502.
- [10] Hussein, A. I., Barbone, P. E., and Morgan, E. F., 2012, "Digital Volume Correlation for Study of the Mechanics of Whole Bones," *Procedia IUTAM*, 4, pp. 116-125.
- [11] Wilcox, R. K., 2004, "The biomechanics of vertebroplasty: a review," *Proc Inst Mech Eng H.*, 218(1), pp. 1-10.
- [12] Ye, J., Coleman, J., Hunter, M. G., Craighan, J., Campbell, K. H. S., and Luck, M. R., 2007, "Physiological temperature variants and culture media modify meiotic progression and developmental potential of pig oocytes *in vitro*," *Reproduction*, 133(5), pp. 877 - 886.
- [13] Danesi, V., Zani, L., Scheele, A., Berra, F., and Cristofolini, L., 2014, "Reproducible reference frame for in vitro testing of the human vertebrae," *Journal of biomechanics*, 47(1), pp. 313-318.

- [14] Barber, D. C., Oubel, E., Frangi, A. F., and Hose, D. R., 2007, "Efficient computational fluid dynamics mesh generation by image registration," *Med Image Anal*, 11(6), pp. 648-662.
- [15] Barber, D. C., and Hose, D. R., 2005, "Automatic segmentation of medical images using image registration: diagnostic and simulation applications," *J Med Eng&Tech*, 29(2), pp. 53-63.
- [16] Khodabakhshi, G., Walker, D., Scutt, A., Way, L., Cowie, R. M., and Hose, D. R., 2013, "Measuring three-dimensional strain distribution in tendon," *J Microsc*, 249(3), pp. 195-205.
- [17] Tozzi, G., Dall'Ara, E., Palanca, M., Curto, M., Innocente, F., and Cristofolini, L., 2016, "Strain uncertainties from two DVC approaches in prophylactically augmented vertebrae: local analysis on bone and bone-cement microstructures," *Journal of the Mechanical Behavior of Biomedical Materials*, Submitted.
- [18] Ross, S. M., 2003, "Peirce's criterion for the elimination of suspect experimental data," *J. Engineering Technology*, 2003(Fall), pp. 1-12.
- [19] Aamodt, A., Lund-Larsen, J., Eine, J., Andersen, E., Benum, P., and Husby, O. S., 1997, "In vivo measurements show tensile axial strain in the proximal lateral aspect of the human femur," *J Orthop Res.*, 15(6), pp. 927-931.
- [20] Cristofolini, L., 2015, "In vitro evidence of the structural optimization of the human skeletal bones," *Journal of biomechanics*, 48(5), pp. 787-796.
- [21] de Bakker, P. M., Manske, S. L., Ebacher, V., Oxland, T. R., Cripton, P. A., and Guy, P., 2009, "During sideways falls proximal femur fractures initiate in the superolateral cortex: evidence from high-speed video of simulated fractures," *Journal of biomechanics*, 42(12), pp. 1917-1925.
- [22] Bayraktar, H. H., Morgan, E. F., Niebur, G. L., Morris, G. E., Wong, E. K., and Keaveny, T. M., 2004, "Comparison of the elastic and yield properties of human femoral trabecular and cortical bone tissue," *Journal of biomechanics*, 37(1), pp. 27-35.
- [23] Zael, R., Yeni, Y. N., Bay, B. K., Dong, X. N., and Fyhrie, D. P., 2006, "Comparison of the linear finite element prediction of deformation and strain of human cancellous bone to 3D digital volume correlation measurements," *Journal of biomechanical engineering*, 128(1), pp. 1-6.
- [24] Chen, Y., Dall'Ara, E., Sales, E., Manda, K., Wallace, R., Pankaj, P., and Viceconti, M., 2016, "Micro-CT based finite element models of cancellous bone predict accurately displacement computed by elastic registration: a validation study," *Journal of Mechanical Behavior of Biomedical Materials*, Unpublished Results - Submitted.
- [25] Van Rietbergen, B., Weinans, H., Huiskes, R., and Odgaard, A., 1995, "A New Method to Determine Trabecular Bone Elastic Properties and Loading Using Micromechanical Finite-Element Models," *Journal of biomechanics*, 28(1), pp. 69-81.